Multiscale body maps in the human brain

THÈSE N^O 7543 (2017)

PRÉSENTÉE LE 9 JUIN 2017
À LA FACULTÉ DES SCIENCES DE LA VIE
CHAIRE FONDATION BERTARELLI DE NEUROPROSTHÉTIQUE COGNITIVE
PROGRAMME DOCTORAL EN NEUROSCIENCES

ÉCOLE POLYTECHNIQUE FÉDÉRALE DE LAUSANNE

POUR L'OBTENTION DU GRADE DE DOCTEUR ÈS SCIENCES

PAR

Michel AKSELROD

acceptée sur proposition du jury:

Prof. S. Micera, président du jury
Prof. O. Blanke, Prof. R. Gassert, directeurs de thèse
Prof. N. Wenderoth, rapporteuse
Prof. H. Flor, rapporteuse
Prof. D. Van De Ville, rapporteur

EPFL

ÉCOLE POLYTECHNIQUE
FÉDÉRALE DE LAUSANNE

Suisse
2017

Abstract

A large number of brain regions are dedicated to processing information from the body in order to enable interactions with the environment. During my thesis, I studied the functional organization of brain networks involved in processing bodily information. From the processing of unimodal low-level features to the unique experience of being a unified entity residing in a physical body, the brain processes and integrates bodily information at many different stages.

Using ultra high-field functional Magnetic Resonance Imaging (fMRI), I conducted four studies to map and characterize multiscale body representations in the human brain. The goals of my thesis were first to extend the actual knowledge about primary sensorimotor representations, and second to develop novel approaches to investigate more complex and integrated forms of body representations.

In studies I and II, I first investigated how natural touch was represented in the three first cortical areas processing tactile information. I applied a mapping procedure to identify in each of these three areas the somatosensory representations of 24 different body parts on hands, feet and legs at the level of single subjects. Using fMRI and resting-state data, I combined classical statistical analyses with modern methods of network analysis to describe the functional properties of the formed network.

In study III, I applied these methods to investigate primary somatosensory and motor representations in a rare population of patients. Following limb loss, the targeted muscle and sensory reinnervation (TMSR) procedure enables the intuitive control of a myoelectric prosthesis and creates an artificial map of referred touch on the reinnervated skin. I mapped the primary somatosensory and motor representations of phantom sensations and phantom movements in TMSR patients. I investigated whether sensorimotor training enabled via TMSR was associated with preserved somatosensory and motor representations compared to healthy controls and amputee patients without TMSR.

Finally in study IV, I studied brain regions involved in the subjective body experience. Following specific manipulations of sensorimotor information, it is possible to let participants experience a fake or virtual hand as their own and to give

them the sensation of being in control of this hand. Using MR-compatible robotics and virtual reality, I investigated the brain regions associated with the alteration of the sense of hand ownership and the sense of hand agency.

The present work provides important findings and promising tools regarding the understanding of brain networks processing bodily information. In particular, understanding the functional interactions between primary unimodal cortices and networks contributing to subjective body experience is a necessity to promote modern approaches in the fields of neuroprosthetic and human-machine interactions.

Résumé

De nombreuses régions du cerveau sont dédiées au traitement de l'information relative au corps pour lui permettre d'intéragir avec son environnement. Durant ma thèse, j'ai étudié l'organisation fonctionnelle des réseaux cérébraux impliqués dans le traitement de l'information corporelle. Du traitement des composantes unimodales de bas-niveau jusqu'à l'unique expérience d'être une entité unifiée habitant dans un corps physique, le cerveau traite et intègre l'information corporelle à des nombreux niveaux différents.

Par la méthode de l'Imagerie par Résonance Magnétique fonctionnelle à champ ultra élevé (IRMf), j'ai conduit quatre études dans le but de cartographier et caractériser à de multiples échelles les représentations du corps dans le cerveau humain. Les objectifs de ma thèse sont premièrement d'étendre les connaissances actuelles à propos des représentations corporelles primaires et deuxièmement de développer de nouvelles approches pour étudier des représentations corporelles plus complexes et intégrées.

Pour les études I et II, j'ai tout d'abord étudié la façon dont le toucher naturel est représenté dans les trois premières zones corticales qui traitent l'information tactile. J'ai appliqué une procédure de cartographie pour identifier dans chacune de ces zones les représentations somatosensorielles de 24 régions du corps sur les mains, les pieds et les jambes de façon individuelle pour chaque sujet. En utilisant des données IRMf de stimulation tactile et d'état de repos, j'ai combiné des méthodes classiques d'analyse statistique et des méthodes modernes d'analyse de réseaux pour décrire les propriétés fonctionnelles du réseau formé.

Pour l'étude III, j'ai appliqué ces méthodes pour étudier les représentations somatosensorielles et motrices dans une population rare de patients. Après la perte d'un membre, la procédure de réinervation ciblée musculaire et sensorielle (TMSR) permet de contrôler une prothèse myoéléctrique de façon intuitive et crée une carte artificielle de toucher référé sur la peau réinnervée. J'ai cartographié les représentations somatosensorielles et motrices primaires associées avec les sensations fantômes et mouvements fantômes chez ces patients. J'ai étudié si l'entraînement sensoriel et moteur rendu possible par la TMSR est associé à des représentations

somatosensorielles et motrices préservées en comparaison à des sujets contrôles et des patients amputés sans TMSR.

Finalement pour l'étude IV, j'ai étudié les régions cérébrales impliquées dans l'expérience subjective du corps. Suite à des manipulations spécifiques de l'information sensorielle et motrice, il est possible de donner l'impression à un sujet qu'une fausse main ou une main virtuelle est la sienne et qu'il en a le contrôle. En combinant la robotique IRM-compatible et la réalité virtuelle, j'ai étudié les régions cérébrales dont l'activité est associée à l'altération du sentiment d'appartenance pour une main et du sentiment d'agentivité pour une main.

Le travail proposé dans cette thèse fournit des éléments importants et des outils prometteurs pour la compréhension des réseaux cérébraux qui traitent l'information corporelle. En particulier, comprendre les intéractions fonctionnelles entre les zones cérébrales primaires et les réseaux contribuant à notre perception du corps est une nécessité pour promouvoir des approches modernes dans les domaines de la neuroprosthétique et des intéractions homme-machine.

Mots-clés: représentations corporelles, parties du corps, cartographie du corps, IRMf, connectivité fonctionnelle au repos, cortex somatosensoriel primaire, cortex moteur primaire, traitement multisensoriel.

Table of content

8

9

1 - General Introduction

The perceptual experience that we have of our body is amazingly rich. We can feel gentle touch, pain, itching or tinkling, and we can even have bodily feelings, such as goose bumps. Somatosensory signals from the body, including touch, temperature, pain and proprioception, are relayed to the brain by the peripheral nervous system. The primary somatosensory cortex is the first cortical area processing somatosensory information and is crucial for perceiving somatosensations (**Gallace and Spence, 2010**). Beyond feeling our body, we have the unique experience of being a unified entity residing in a physical body and being in control of this body, termed bodily self-consciousness (BSC). BSC is a multisensory construct of the brain, which is permanently being updated by the continuous integration of bodily information (**Blanke et al. 2012**). Unsurprisingly, a large number of cortical areas are involved in the processing of bodily information. Starting with the processing of unimodal low-level features in primary somatosensory cortex and up to the subjective body experience, the brain processes and integrates bodily information across large-scale functional networks (**Blanke et al. 2015**).

The present thesis aimed at investigating the functional networks processing bodily information in the human brain. In particular, the goals of the thesis were two-folds. The first goal was to extend the actual knowledge about body representations within primary sensorimotor cortices. The second goal was to develop novel approaches to investigate more complex and integrated forms of body representations associated with BSC. The thesis is presented as a collection of scientific articles divided into 4 major brain-imaging studies.

1.1 Neuroimaging

During the last decades, functional Magnetic Resonance Imaging (fMRI) has become one of the most employed non-invasive neuroimaging modalities to study the functional organization of the human brain. fMRI relies on local changes of brain hemodynamics as a measure of neuronal activity, known as the Blood-Oxygen-Level-Dependent signal (BOLD). Perceptual and cognitive tasks can be compared across healthy and clinical populations to study the associated brain activity (**Glover, 2011**). Compared to electroencephalography or intracortical recordings, the three-

dimensional and large coverage of fMRI allows studying the distributed contributions of distant brain areas with unprecedented spatial resolution. In particular, ultra high-field 7T fMRI allows improving the spatial resolution to the millimeter scale (**van der Zwaag et al. 2009**) and has been shown to closely match the activity of small neuronal populations (**Siero et al. 2014**). Thus, 7T fMRI is well suited to study the precise organization of sensory areas and has already been applied to study primary visual (**Olman et al. 2010**), auditory (**Da Costa et al. 2014**) and somatosensory areas (**Martuzzi et al. 2014**).

It is well established that human brain functions are supported by functional networks rather than by isolated and independent functional units. Investigating how information is shared and transferred across brain regions is a crucial point for the understanding of functions supported by brain networks. The functional interactions between brain regions can be investigated using fMRI and resting-state data. Indeed, at rest, regions belonging to the same functional network exhibit synchronous low-frequency fluctuations of the BOLD signal (**Biswal et al. 1995**). Resting-state functional connectivity (rs-FC) relies on the coupling of these spontaneous BOLD fluctuations to assess functional relations between brain regions (**Fox and Raichle, 2007, Lee et al. 2013, van den Heuvel and Pol, 2010**). For example, rs-FC has been used to parcellate and to identify distinct functional brain networks of the human brain, such as the default mode network or the attentional network (**Beckmann et al. 2005; Damoiseaux et al. 2006**), and has also been applied to investigate short-scale connectivity within unimodal sensory cortices (**Eckert et al. 2008; Li et al. 2015**). In addition, graph theory and graph optimization approaches are complementary analytical tools to study the topographical and computational properties of brain networks (**Bullmore and Sporns, 2009**).

1.2 Body representations in primary somatosensory cortex

Some brain regions are specialized to topographically represent different features of the body and are organized somatotopically to form cortical body maps. The most well known depictions of body maps in the human brain are the so-called motor and somatosensory homunculi, which were inspired by the seminal work of Rasmussen and Penfield (**1947**). In particular, the primary somatosensory cortex, S1, has the most precise somatotopic organization with each body part being represented at a precise

location along the postcentral gyrus. S1 is composed of 4 anatomical subregions corresponding to Brodmann areas (BAs) 3a, 3b, 1 and 2, which are specialized in the early processing of somatosensory information. In particular, BAs 3b, 1 and 2 are the three first cortical areas processing tactile information. Studies in non-human primates showed that each of these three S1 subregions contains a complete representation of the body surface (**Kaas et al. 1979**) and suggested that the different BAs forming S1 also represent functional subregions (**Iwamura, 1998**). Recent 7T neuroimaging studies allowed to extend such investigations to human S1 and centered on the representations of single fingers within S1 subregions (**Martuzzi et al. 2014, 2015; Sanchez-Panchuelo et al. 2010, 2012, 2014; Stringer et al. 2011, 2014**). However, such somatotopic descriptions of human S1 are limited to finger representations with few existing studies focusing on other important S1 representations such as the foot and the leg. In addition, little is known about the functional interactions between body part representations within S1.

The goal of the first study presented in this thesis (study I) was to precisely map the cortical representations of six body regions on the right and on the left lower limbs within BAs 3b, 1, and 2 using ultra high-field 7T fMRI, and to achieve this at the level of single subjects. Analyzing the BOLD responses associated with tactile stimulations of 12 different leg/foot regions (big toe, small toe, heel, calf, thigh and hip bilaterally), I quantified their somatotopic location, their extent and strength of activation, as well as their specificity.

In my second study (study II), I investigated patterns of rs-FC across multiple body representations using 7T fMRI. Considering the tactile representations of 24 body parts within BAs 3b, 1 and 2, leading to 72 separate S1 representations, I analyzed the low-frequency BOLD fluctuations across these regions. I investigated the modular and topographical organization of the formed network, as well as the local functional organization across neighboring representations highlighting important differences between hand, foot and leg representations.

In study III, I investigated in a rare population of patients (Targeted Muscle and Sensory Reinnervation, TMSR, **Kuiken, et al. 2004; Kuiken et al. 2007**) the effect of sensorimotor training enabled via TMSR on primary somatosensory and motor representations using 7T fMRI. TMSR consists in rerouting motor and sensory nerves

from the residual limb towards intact muscle groups and skin regions. Movement of a myoelectric prosthesis is enabled via decoded EMG activity from reinnervated muscles and touch sensation on the missing limb is enabled by stimulation of the reinnervated skin areas. The goal of study III was to investigate whether the TMSR procedure in amputees is associated with preserved primary somatosensory and motor representations. I recruited 3 TMSR patients and mapped the primary somatosensory (S1) and primary motor (M1) representations of their missing limb and compared them with a group a normal upper limb amputees and a group of healthy controls. I assessed the presence of cortical reorganization within primary somatosensory and motor areas in terms of extent, strength and location of BOLD activations associated with phantom sensations and phantom movements of the missing limb. In addition, I analyzed the rs-FC to assess interactions between somatosensory and motor representations, as well as their respective interactions with parietal multisensory areas.

1.3 Bodily self-consciousness and higher-tier body representations

Beyond primary somatosensory and motor areas, recent studies showed that body maps are also found in other brain areas including the posterior parietal cortex, the premotor cortex, the supplementary motor areas, the secondary somatosensory cortex, the insula, the cingulate cortex and subcortical areas such as the putamen, the globus pallidus or the thalamus (**Hong et al. 2011; Huang et al. 2012; Kiss et al. 1994; Saadon-Grosman et al. 2015; Sereno and Huang, 2014; Zeharia et al. 2015**). Body maps are commonly found across these areas, starting from primary unisensory areas to higher-tier multisensory areas. Interestingly, the brain regions containing body maps are also believed to be involved in the brain mechanisms underlying BSC (**Blanke, 2012; Blanke and Metzinger, 2006; Tsakiris et al. 2007**). It is possible that the common presence of body maps in areas processing primary somatosensory information and in areas involved in BSC is an important feature for their functional interactions.

Body ownership for body parts, agency for bodily actions, self-identification with the full-body and self-location in space are the major and most studied components of BSC (**Blanke et al. 2015**). Neurological studies showed that distinct components of BSC can be specifically impaired, suggesting that they rely on distinct brain

mechanisms. For example, somatoparaphrenia is a disorder in which the patient denies recognizing his hand as his own, showing that specific brain lesions can abolish the sense of hand ownership (**Vallar and Ronchi, 2009**). Similarly, the alien hand syndrome is associated with unintentional and uncontrolled hand movements of the patient leading to a loss of the sense of hand agency (**Biran and Chatterjee 2004; Hassan and Josephs, 2016**). Furthermore, out-of-body experiences induced by the stimulation of specific brain areas show that self-location can be modulated by brain activity and can be dissociated from the physical body (**Blanke et al. 2004**).

Studies showed that the experimental manipulation of multisensory signals can induce altered states of BSC (**Botvinick and Cohen, 1998; Ehrsson et al. 2005; Tsakiris et al. 2006; Lenggenhager et al. 2007; Kannape et al. 2010; Aspell et al. 2013; Klackert et al. 2014**), suggesting that the underlying mechanisms rely on the integration of multisensory and motor signals (**Blanke et al. 2015**). Neurological and neuroimaging studies showed that the alteration of BSC is associated with activity in fronto-parietal and temporo-parietal areas (**Berkater-Bodman et al. 2014; Blanke et al. 2004; Ehrsson et al. 2004; Gentile et al. 2013; Guterstam et al. 2013; Ionta et al., 2011; Petkova et al. 2011; Tsakiris et al. 2010, Vallar and Ronchi, 2009**).

The goal of study IV was to investigate the neural correlates of two intriguingly linked components of BSC: the subjective experience of having and owning our hands termed sense of hand ownership (SO) and the subjective experience of controlling our hands, termed sense of hand agency (SA) (**Schwabe and Blanke 2007; Tsakiris 2010**). Previous studies showed that it is possible to extend SO and SA towards fake or virtual hands (**Asai et al. 2016; Braun et al. 2014; Caspar et al. 2015; Dummer et al. 2009; Hara et al. 2016; Jenkinson and Preston, 2015; Klackert and Ehrsson, 2012, 2014; Ma and Hommel, 2015; Shibuya et al. 2016; Tsakiris et al. 2006**). Importantly, neuroimaging studies investigating the neural correlates of either SO or SA showed that they are both associated with activity in fronto-parietal and temporo-parietal areas (**Berkater-Bodman et al. 2012, 2014; Brozzoli et al. 2012; Ehrsson et al. 2004, 2005; Gentile et al. 2013; Guterstam et al. 2013; Limanowski et al. 2014, 2015, 2016; Petkova et al. 2011; Tsakiris et al. 2007** for SO and **David et al. 2006; Farrer and Frith 2002; Farrer et al. 2003, 2008; Fink et al. 1999; Leube et al. 2003** for SA). However, few studies were able to

study the interplay between SO and SA. In study IV of my thesis, a novel setup combining advanced MR-compatible robotics and virtual reality was developed to induce altered states of SO and SA. During the acquisition of 3T fMRI data allowing whole brain coverage, subjects performed a robotically controlled pinching movement with their right hand, while observing a virtual hand performing a pinching movement in different experimental conditions. We manipulated the synchrony and the congruency between visual and sensorimotor information, as well as the nature of the movements produced i.e. comparing passive and active movements. After each trial, subjects rated their subjective feelings of hand ownership and of hand agency towards the virtual hand. Representational similarity analysis (**Kriegeskorte et al. 2008**) was used to identify brain networks sensitive to subjective changes in body ownership and agency, allowing the mapping and the comparison of hand specific fronto-parietal and temporo-parietal networks associated with both aspects of BSC.

To summarize, the present thesis aimed at studying multiscale body representations in the human brain and proposed 4 fMRI studies. Study I investigated at ultra high-field (7T) the functional properties of lower limb representations within subregions of human S1. Study II described the functional interactions (rs-FC) between hand, foot and leg representations within subregions of human S1 using 7T fMRI. Study III investigates the link between sensorimotor training enabled by modern neuroprosthetic approaches in a rare population of amputees (TMSR) and cortical plasticity within primary somatosensory and motor cortices using 7T fMRI. Study IV proposed an innovative approach combining MR-compatible robotics and virtual reality to map the neural correlates of the sense of hand ownership and the sense of hand agency.

2 - Study I: anatomical and functional properties of the foot and leg representations in areas 3b, 1 and 2 of primary somatosensory cortex in humans: a 7T fMRI study

Michel Akselrod, Roberto Martuzzi, Andrea Serino, Wietske van der Zwaag, Roger Gassert and Olaf Blanke

Abstract

Primary somatosensory cortex (S1) processes somatosensory information and is composed of multiple subregions. In particular, tactile information from the skin is processed in three subregions, namely Brodmann areas (BAs) 3b, 1 and 2, with each area representing a complete map of the contralateral hemi-body. The anatomico-functional organization of these multiple S1 maps in humans has been extensively studied for the hand. In addition, previous studies provided important knowledge about the organization of foot and leg representations in S1, reporting a latero-medial organization when moving from proximal to distal leg regions. However, there is no study investigating such aspects within different subregions of S1. Using ultra-high field MRI (7T), we mapped six cortical representations of the lower limbs (from toes to hip) at the single subject level and in BAs 3b, 1 and 2. Analyzing the BOLD responses associated with tactile stimulations of six foot and leg regions on each side, we quantified their somatotopic location, strength and extent of activation, as well as their response selectivity. We show somatotopy for the leg, but not the foot in all BAs and in all participants, with large inter-subject variability. We found greater strength/extent of S1 activation for the big toe representation (compared to the other mapped representations) within all BAs, suggesting a possible homology between the first digit of foot and hand in humans. Finally, we observed drastically different patterns of selectivity in the foot representations (lower selectivity) compared to other leg representations (greater selectivity), likely related to different functional properties of these S1 representations and the nature of tactile stimulation in everyday life. The present data describe the detailed anatomical and functional organization of the lower limbs within three subregions of S1 using a single-subject approach. We discuss our data with respect to neurophysiological data in S1 of non-human primates

and previous neuroimaging work in humans, as well as their relevance for future S1 work in cognitive, social, and clinical research.

Detailed contributions: I was in charge of the project. I prepared the paradigms, collected and analyzed the data, wrote the initial manuscript and created the figures.

2.1 Introduction

Magnetic Resonance Imaging (MRI) is one of the major non-invasive neuroimaging modalities. Compared to the widely established 3T MRI, the increased signal-to-noise ratio of ultra-high field MRI (7T) improves spatial resolution to the millimeter or even sub-millimeter scale (**van der Zwaag et al. 2009**). This has allowed studying brain responses without the need of averaging across participants, avoiding concerns related to inter-subject variability. Ultra-high field fMRI has already been applied to the study of the retinotopic organization of the human primary visual cortex (**Hoffman et al. 2009; Olman et al. 2010**), the tonotopical organization of the human primary auditory cortex (**Da Costa et al. 2011, 2014**), as well as the somatotopic organization in primary somatosensory cortex (S1) (**Besle et al. 2014; Martuzzi et al. 2014, 2015; Sanchez-Panchuelo et al. 2010, 2012, 2014; Stringer et al. 2011, 2014**). However, such somatotopic descriptions of human S1 were so far limited to the representations of single fingers with only few neuroimaging studies targeting important S1 representations of body parts other than the hand, such as the foot and the leg (**Bao et al. 2012; Nakagoshi et al. 2005; Saadon-Grosman et al. 2015**).

Primate S1 is located along the postcentral gyrus and contains three different cytoarchitectonic regions involved in the processing of tactile information, namely Brodmann Areas (BAs) 3b, 1, and 2 (**Jones et al. 1978; Powell and Mountcastle, 1959**). Previous studies described the anatomical location of the 3 BAs processing tactile information within human S1: BA 3b is located on the anterior wall, BA 1 on the crown, and BA 2 on the posterior wall (**Geyer et al. 1999, 2000; Grefkes et al. 2001**). Studies conducted in non-human primates showed that each of these BAs is somatotopically organized, with each body part being represented at a precise cortical position (**Kaas et al. 1979; Merzenich et al. 1978; Nelson et al. 1980**). Concerning tactile processing in S1, research in non-human primates showed that moving from BA 3b to BA 1 and BA 2, neurons progressively have larger receptive fields, become less specific for the represented portion of the skin (i.e. they respond to tactile information coming from larger portions of the skin), and also encode more complex tactile features, such as stimulus orientation and direction (**Costanzo and Gardner, 1980; Gardner, 1988; Hyvarinen and Poranen, 1978**), suggesting that tactile

18

information is hierarchically processed in the different BAs (**Iwamura, 1998**). Recent work using 7T fMRI has shown – consistently with what has been observed in non-human primates – that human BA 3b shows highly selective activations in response to single finger stimulation, while BA 1 and BA 2 are less selective, responding to the stimulation of multiple digits (**Besle et al. 2014; Martuzzi et al. 2014; Stringer et al. 2014**). Regarding differences across BAs with respect to their sensitivity to the nature of stimulation, a recent 7T study showed that mechanical stimulation induces lower BOLD responses over the entire S1 (in particular in BA 2) compared to stroking (**van der Zwaag et al. 2015**). This explains the difficulty of recruiting BA 2 representations in studies using mechanical stimulation (**Besle et al. 2014; Sanchez-Panchuelo et al. 2010; Stringer et al. 2011, 2014**). Contrastingly, it was demonstrated that manual stroking (as used in the present study) is able to induce reliable BOLD responses in BAs 3b, 1 and 2 (**Martuzzi et al. 2014, 2015**), although the mapped representations were smaller in BA 2.

Most previous S1 studies have centered on the investigation of the somatotopical representations in the hand area of S1 because of its large cortical representation and its important role in tactile perception (**Gelnar et al. 1998; Kurth et al. 1998, 2000; Maldjian et al. 1999; Martuzzi et al. 2014; Moore et al. 2000; Nelson and Chen, 2008; Overduin and Servos, 2004; Sanchez-Panchuelo et al. 2010, 2012, 2014; Schweizer et al. 2008; Schweisfurth et al. 2014; Stringer et al. 2011, 2014; van Westen et al. 2004; Weibull et al. 2008**). Considering the importance of legs and feet for stance, balance and locomotion, surprisingly few imaging studies focused on the representations of the lower limbs in human S1 (**Bao et al. 2012; Nakagoshi et al. 2005; Saadon-Grosman et al. 2015**). More specifically, Nakagoshi and colleagues (**2005**) mapped the knee region and a region located on the foot (below the ankle) and reported a lateral to medial organization when moving from the proximal to the distal skin region. Similarly, Bao and colleagues (**2012**) reported a lateral to medial organization of four cutaneous points located below the knee and above the ankle when moving from proximal to more distal skin regions. Both studies reported the organization of the leg representation in S1 only at the group level (i.e. not for each subject individually). Remarkably, Saadon-Grosman and colleagues (**2015**) were recently able to define whole-body somatotopic maps in individual subjects using 3T fMRI and reported whole-body gradients along the postcentral gyrus, replicating the

well-known findings from the work of Penfield and Rasmussen (**Penfield and Boldrey, 1937; Rasmussen and Penfield, 1947**). In particular, they reported a latero-medial gradient along S1 when moving from the buttocks to the toes. However, none of these studies investigated separately the different subregions of S1.

The aim of the present study was to precisely map the cortical representations of six skin regions of the right lower limb and of the left lower limb in S1, in Brodmann regions 3b, 1, and 2, and to do this at the level of single subject. To this aim, we first applied the mapping procedure proposed in Martuzzi et al. (**2014**) to three regions on the foot (big toe, small toe, heel) and three regions on the leg (calf, thigh and hip), separately for the right and the left lower extremities using ultra-high field 7T fMRI. Based on the seminal work by Penfield and Rasmussen (**Penfield and Boldrey, 1937; Rasmussen and Penfield, 1947**) and more recent neuroimaging work (**Bao et al. 2012; Nakagoshi et al. 2005; Saadon-Grosman et al. 2015**), we expected the toes to be located in the most medial and superior portion of the postcentral gyrus, and the more proximal foot and leg representations more laterally and dorsally on the postcentral gyrus. By homology to finger somatotopy with respect to the location of arm representation in S1, we speculated that the big toe would be located more medially compared to the small toe. However, considering that there are no existing data to support this hypothesis, we also considered an alternative ordering in which the small toe would be located most medially. We also quantified the strength and extent of BOLD responses of each mapped foot and leg representation in the different BAs of each individual subject, and investigated the selectivity of each mapped representation across the different BAs. These metrics were analyzed to investigate differences across body regions, across BA and across hemispheres. We expected that the representation of big toe (digit I) would be dominant in terms of strength and extent compared to small toe (digit V), in line with what was previously shown for the corresponding digits of the hand (**Martuzzi et al. 2014**). Furthermore, we also expected that the size of representations within BA 2 would be smaller in comparison to BA 3b and BA 1 as previously reported for finger representations (**Martuzzi et al. 2014**). In addition, we hypothesized that human BA 2, which has the largest receptive fields in non-human primates (**Costanzo and Gardner, 1980; Gardner, 1988; Hyvarinen and Poranen, 1978**), would show less selectivity in response to tactile stimulation of different body regions compared to other BAs, as already shown for

finger representations in human S1 by recent work from several laboratories (**Besle et al. 2014; Martuzzi et al. 2014; Stringer et al. 2014**).

2.2 Methods

2.2.1 Subjects

15 healthy subjects (5 females) aged between 18 and 39 years old (mean ± std: 24.3 ± 5.2 years) participated in the study. One participant was excluded due to excessive motion during MRI acquisition (up to 5mm of movement in the z-direction for this particular subject). All participants were right handed and had a right foot preference, as assessed during an oral interview adapted from the Edinburgh Handedness Inventory (**Oldfield, 1971**) (Tab.2.S1).

All subjects gave written informed consent, all procedures were approved by the Ethics Committee of the Faculty of Biology and Medicine of the University of Lausanne, and the study was conducted in accordance with the Declaration of Helsinki.

2.2.2 Experimental procedure

Subjects were scanned in supine position while tactile stimulation was delivered to the selected body parts on the lower limbs. Tactile stimulation consisted of a gentle manual stroking performed by an experimenter with his index finger, as a previous study showed that this stimulus induces more reliable BOLD signal responses over the different BAs (BA 3b, BA 1 and BA 2) forming S1, compared to vibrations or tapping (**van der Zwaag et al. 2015**). The experimenter was standing at the entrance of the bore to provide the stimulation and received instructions by means of MR compatible earphones. Six regions on both legs (big toe, small toe, heel, calf, thigh and hip) were repeatedly stimulated. During one run, the six regions of the same limb were stroked in a fixed order (thigh – big toe – calf – heel – hip – small toe) and the sequence was repeated 4 times. The order of the lower limb being stimulated was randomized across participants. Stimulation periods of 20 s were interleaved with periods of 10 s of rest. The skin regions were repeatedly stroked on the same portion of naked skin at the constant rate of 1 Hz, corresponding to a surface of about 3 cm^2,

with the exception of the small toe, which was stroked on its entire length. To reduce the variability of the tactile stimulation across participants and to guarantee that a reliable and constant pressure was exerted, the stroking was always performed by the same researcher, which received extensive training prior to data acquisition. To ensure the subjective quality of the stimulation, the subjects were verbally asked between each run whether they could adequately feel the stimulation, if it was not the case the run would be repeated (this happened on 7 occasions).

2.2.3 Data acquisition

MR images were acquired using a short-bore head-only 7 Tesla scanner (Siemens Medical, Germany) equipped with a 32-channel Tx/Rx RF-coil (Nova Medical, USA) (**Salomon et al. 2014**). Functional images were acquired using a sinusoidal readout EPI sequence (**Speck et al. 2008**) and comprised 28 axial slices placed approximately orthogonal to the postcentral gyrus (in-plane resolution=$1.3 \times 1.3 mm^2$, slice thickness=1.3mm, no gap, TR=2s, TE=27ms, flip angle=75°, matrix size=160x160, FOV=210mm, GRAPPA factor=2). The mapping sequence included 361 volumes for each of the lower limbs.

For each subject, a set of anatomical images was acquired using an MP2RAGE sequence (**Marques et al. 2010**) in order to facilitate the separation of Brodmann areas (BAs) and for display purposes (resolution=$1 \times 1 \times 1 mm^2$, TE = 2.63ms, TR = 7.2ms, TI1 = 0.9sec, TI2 = 3.2sec, TR_{mprage} = 5sec). To aid coregistration between the functional and the anatomical images, a whole brain EPI volume was also acquired with the same inclination used in the functional runs (81 slices, in-plane resolution=$1.3 \times 1.3 mm^2$, slice thickness=1.3mm, no gap, TE=27ms, flip angle=75°, FOV=210mm, GRAPPA factor=2).

2.2.4 Data processing

All images were analyzed using the SPM8 software (Wellcome Department of Cognitive Neurology, London, UK). The MRIcron software was used for visualizing results in 3D space (McCausland Center for Brain Imaging, University of South Carolina, US, http://www.mccauslandcenter.sc.edu/mricro/mricron) and

BrainVoyager QX [version 2.8] was used for surface visualization (Brain Innovation, Maastricht, Netherlands).

Preprocessing of fMRI data included slice timing correction, spatial realignment, and smoothing (FWHM=2mm). A GLM analysis was carried out to estimate the response induced by the stimulation of the different body regions. The model included 6 regressors (one for each stroked region) convoluted with the hemodynamic response and with the corresponding first-order time derivatives, as well as the 6 rigid-body motion parameters as nuisance regressors. For each limb separately, a F-contrast across all conditions was computed to identify all the voxels activated by the stroking of at least one region. A t-contrast (against rest) was also computed for each stimulated region.

2.2.5 Separation of S1 into BAs 3b, 1 and 2

Probabilistic maps for the separation of the postcentral gyrus into BAs 3b, 1 and 2 (**Geyer et al. 1999, 2000; Grefkes et al. 2001**) were used to separate the 3 homologous representations of each region. For each subject, the probabilistic maps were back-projected onto their native space using standard procedures implemented in SPM8.

We note that the complete analysis described below was replicated with manually designed separations into BA 3b, BA 1 and BA 2 following the procedure described in Martuzzi et al. (**2014**), where BA 3b is manually defined as the anterior wall of the postcentral gyrus, BA 1 as the crown of the postcentral gyrus and BA 2 as the posterior wall of the postcentral gyrus. This analysis replicated the results described using the published probabilistic maps (**Geyer et al. 1999, 2000; Grefkes et al. 2001**).

2.2.6 Definition of somatosensory representations

Independently for each limb, the clusters corresponding to the representations of each stimulated body region were delimited using an approach previously presented in Martuzzi et al. (**2014**). First, the active voxels in the F-contrast ($p<0.0001$ uncorrected) located within the contralateral postcentral gyrus were used as a S1 mask

to identify all voxels responding to at least the stimulation of one body part. Then, based on a "winner takes all" approach, each voxel within the S1 mask was labeled as representing the body region demonstrating the highest t-score (against rest) for that particular voxel. The identified clusters were further divided into BAs 3b, 1 and 2 using the probabilistic maps described above.

This approach has the advantage of producing continuous and non-overlapping body maps, similarly to the approach of phase encoding used in retinotopic mapping studies (**Hoffman et al. 2009; Olman et al. 2010; Serono et al. 1995**), as well as in studies focusing on the somatosensory system (**Sanchez-Panchuelo et al. 2012; Saadon-Grosman et al. 2015**) or the motor system (**Zeharia et al. 2015**). One of the drawbacks of this approach is that it is possible that one or more body regions are not associated to any voxel, because the stimulation of other body parts elicited higher activity in all considered voxels, leading to missing representations. Across all subjects, only 2.4 representations on average (± std: ± 3.3, range 0-9) were missing out of a total of 36 representations per subject. Small toe, calf and thigh representations accounted for 94% of these missing representations.

2.2.7 Single subject data

To emphasize the importance and relevance of single subject analysis, we report in details the identified body maps for 4 individuals. In addition, we report the cortical volumes and response selectivity of body representations for these individual subjects. The cortical volume is measured as the number of voxels within each representation normalized by the total number of voxels of the corresponding BA of the same hemisphere to account for inter-subject and inter-areal volumetric differences. The response selectivity is measured as the average BOLD response (beta values) within each representation during the stimulation of the different body regions, which allows to investigate whether the stimulation of a given body region also elicits activity in other representations.

2.2.8 Analysis of somatotopic sequence

Within each identified body representation, the coordinates of the peak activation (maximum t-value) were extracted and transformed into MNI coordinates using SPM8. In case of missing body representation, we considered the original t-contrast

of that body part (against rest) used to define somatosensory representations (see above) and extracted the coordinates of the peak activation located in the corresponding BA, which were transformed into MNI coordinates. The average MNI coordinates of peak activations of each representation were calculated by averaging across subjects. To assess the presence of somatotopic ordering, a Principal Component Analysis was first computed to determine the main axis of orientation (corresponding to the 1st principal component) along the MNI coordinates of peak activations of the 6 representations (big toe - small toe - heel - calf - thigh - hip) within each BA and for each individual subject. The distribution across participants of these transformed coordinates of peak activations is reported for each BA.

To statistically evaluate the ordering, we computed Page's trend tests (**Page, 1963**) on the transformed coordinates for each BA. We assessed ordering based on the following sequence as hypothesized in the introduction: "big toe - small toe - heel - calf - thigh - hip". In addition, we tested an alternative ordering: "small toe - big toe - heel - calf - thigh - hip". The statistical significance of the calculated L statistic was assessed using the tabulated values reported by Page (**1963**) for 6 variables and a sample size of 14: L=1078 for p=0.05, L=1098 for p=0.01 and L=1121 for p=0.001. In addition, we report the average value of L-statistics for 1000 random permutations of our data. We note that we also investigated the second principal component of the PCA. As a confirmatory analysis, we computed the Euclidean distances between the representations to qualitatively assess whether the distance was increasing between representations as expected by the proposed ordering: "big toe - small toe - heel - calf - thigh - hip".

2.2.9 Analysis of strength and extent of BOLD activations

To investigate differences across body representations, BAs and hemispheres in terms of strength and extent of BOLD activations associated with the stimulation of the different body parts, we conducted the following analyses.

First, we investigated the strength of BOLD activations using the peak activation within each representation as dependent variable. In case of missing body representation, the peak activation located in the corresponding BA was extracted from the original t-contrast (against rest) of that body part. We computed a three-way

repeated-measures ANOVA with body regions (6 levels), BA (3 levels) and hemisphere (2 levels) as within-subject factors.

Second, we analyzed the extent of BOLD activations using the size of each cortical representation as dependent variable. The volume in mm^3 of each representation was computed, and normalized by the total volume of the corresponding BA of the same hemisphere to account for inter-subject and inter-areal volumetric differences. In case of missing body representation, the cortical volume was set to 0. Similarly to the previous analyses, we computed a three-way repeated-measures ANOVA with body regions (6 levels), BA (3 levels) and hemisphere (2 levels) as within-subject factors.

For both analyses, post-hoc Bonferroni corrected pair-wise comparisons were used to assess differences between levels of significant factors. The significance level was set to α=0.05 for both ANOVAs and post-hoc tests. We also assessed the sphericity and the normality of the data. In case of violation of sphericity, we conducted a Greenhouse-Geisser correction on the ANOVA (**Geisser and Greenhouse, 1958**). In case of violation of normality, we computed a confirmatory analysis using linear mixed models with the ranked data as dependent variable (**Cnaan et al. 1997**). Both analyses of strength and extent of BOLD activations were conducted in the native space of individual subjects.

2.2.10 Analysis of somatotopic selectivity

To investigate the somatotopic selectivity of the mapped representations, we computed the average BOLD response (beta values) within each representation during the stimulation of the different body regions. This measures whether body representations can be co-activated by the stimulation of other body regions than the one represented. We computed one-sample t-tests to assess whether the stimulation of other body regions could induce significant BOLD response within the mapped S1 representations. To account for multiple comparisons and find an appropriate statistical threshold, we used permutation tests. The beta values were randomly permuted and one-sample t-tests were computed. This procedure was repeated 1000 times. The resulting t-values were then sorted and the 95th percentile was selected as the statistical threshold, corresponding to α=0.05 corrected (t-value = 3.17). In case of

missing body representations, data from that body representation were excluded from the analysis. This analysis was conducted in the native space of individual subjects.

To further investigate whether the observed patterns of somatotopic selectivity could be simply explained by the cortical distance between representations, we conducted an additional analysis based on univariate regressions. We considered 3 different fitting functions: 1) a decaying linear function to describe a constant decrease in strength of co-activation with increased cortical distance, 2) a decaying exponential function to describe that co-activation decreases faster with increased cortical distance compared to the linear function (i.e. penalizing distant interactions), 3) a sigmoidal function to describe a functional clustering with local co-activations and a drastic decrease in strength of co-activation for distant interactions. Separately for each stimulated body region, each BA and each subject, we fitted the linear, exponential and sigmoidal functions to the data using the co-activations as the dependent variable and the cortical distance as the independent variable. Each of the fitting functions included 2 free parameters (slope and offset), which were optimized using a least-square approach. The best fitting function was determined by comparing the coefficient of determination R^2 using non-parametric Wilcoxon signed-rank tests with a Bonferroni correction (**Wilcoxon, 1946**). Unreliable regressions ($R^2 < 0.3$) were excluded from the pairwise comparisons. We note that the fitting parameters of the best fitting function were further analyzed to investigate possible differences across body representations, BAs and hemispheres using linear mixed models on the ranked data.

2.3 Results

A total of 12 body regions (6 on each body side) were stimulated during the acquisition of functional data, allowing the mapping of the cortical representations of these body regions within 3 different BAs (BA 3b, BA 1 and BA 2) as defined by published probabilistic maps (**Geyer et al. 1999, 2000; Grefkes et al. 2001**) leading to a total of 36 mapped representations in S1 per subject (see Methods).

2.3.1 Single subject data

We first present individual data regarding 4 representative subjects. The somatotopic maps are shown in Fig.2.1. Additional data regarding the properties of

these maps are shown in Fig.2.S1-S2. The aim of presenting these data is to highlight the robustness and reproducibility of the somatotopic maps across participants and to show that metrics such as the relative size of cortical representations or the response selectivity of cortical representations can be retrieved at the level of single subjects and separately for the different subregions of S1.

For subject 1 (Fig.2.1 and Fig.2.S1A), hip, thigh and calf representations appear in an ordered manner from lateral to medial positions in all BAs. In BA 1 and BA 2, heel representations are located medially compared to leg representations and laterally compared to toes representations. Big and small toes representations are located most medially, but do not appear organized along the latero-medial axis. Larger representations are found for big toe, heel and hip, while small toe representations are smaller. The analysis of somatotopic selectivity shows that representations located closer to each other are co-activated by the tactile stimulation, while more distant representations are not. This effect seems stronger within foot representations (more co-activations) compared to leg representations. This suggests less selective BOLD responses for foot representations compared to leg representations.

For subject 2 (Fig.2.1 and Fig.2.S1B) and similarly to subject 1, hip, thigh and calf representations appear in an ordered manner from lateral to medial positions in all BAs. In BA 1 and BA 2, heel representations are located medially compared to leg representations and laterally compared to toes representations. Big and small toes are located most medially, but are not aligned along the latero-medial axis. Calf representations are smaller compare to other representations. As for subject 1, representations located closer to each other are co-activated by the tactile stimulation, but not distant ones. Strong co-activations are found for foot representations (especially in the right hemisphere). For leg representations, more selective responses are observed.

For subject 3 (Fig.2.1 and Fig.2.S2A) and similarly to subjects 1 and 2, hip, thigh and calf representations appear in an ordered manner from lateral to medial positions in all BAs. Heel and toes representations are located medially compared to leg representations, but do not appear organized along the latero-medial axis. Larger representations are found for big toe and hip, while small toe representations are smaller. Representations located closer to each other are co-activated by the tactile
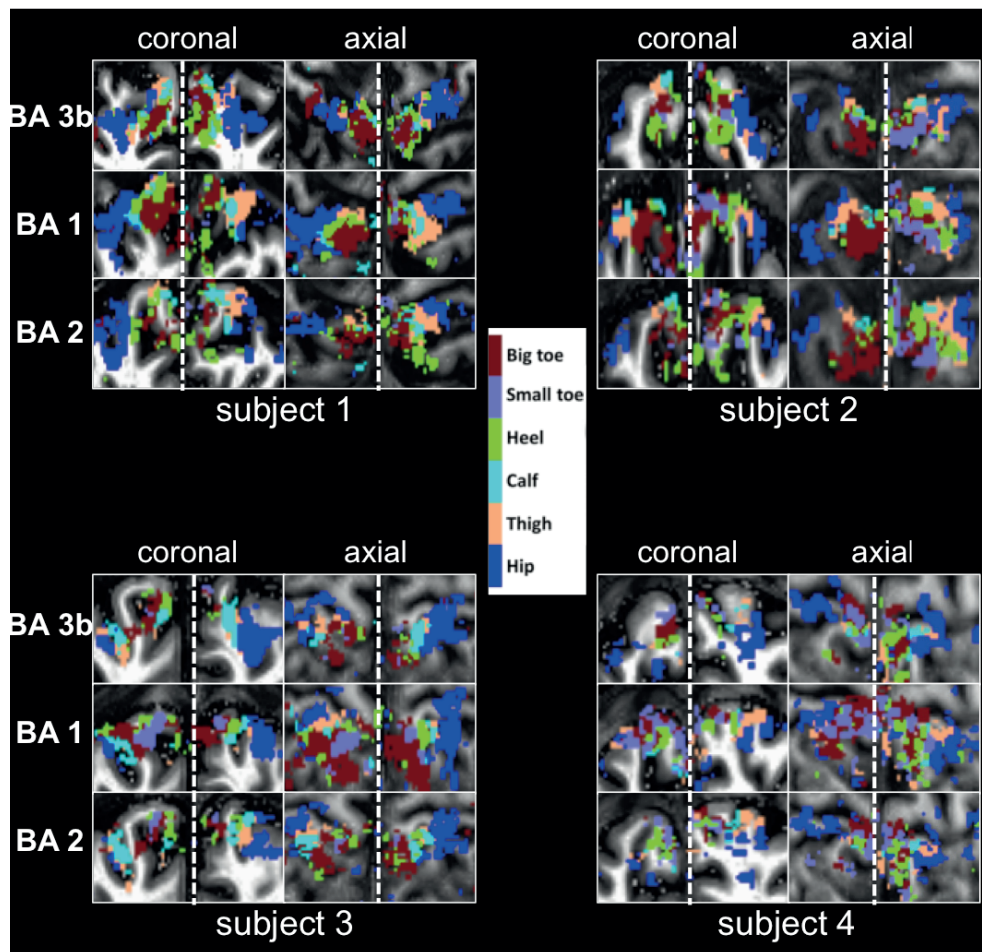
Fig.2.1 Somatotopic maps. Somatosensory representations within BA 3b, BA 1 and BA 2 of right and left big toe, small toe, heel, calf, thigh and hip of 4 individual subjects. The maps are color coded and represented on coronal and axial projections in native space of individual subjects (the projection of the maps lead to the apparent spatial overlap across BA's). Individual metrics (cortical volume and somatotopic selectivity between representations) are presented in supplementary materials.

stimulation, except in BA 1 and BA 2 of the right hemisphere where responses are very selective. Strong co-activations are found within foot representations in all BAs of the left hemisphere and in BA 3b of the right hemisphere. Overall, there are less co-activation compared to subjects 1 and 2.

For subject 4 (Fig.2.1 and Fig.2.S2B), hip, thigh and calf representations appear in an ordered manner from lateral to medial positions, in particular in BA 3b and BA 2. Heel and toes representations are located medially compared to leg representations, but do not appear organized along the latero-medial axis. Larger volumes are found for hip representations, while calf and thigh representations are smaller. Less co-

29

activation is observed compared to other subjects, in particular for the left hemisphere.

To summarize, we were able to identify somatotopic maps within all investigated BAs and for all subjects. The somatotopic ordering was present in all of these 4 participants and in all BAs, although the precise sequence of toes ordering could not be determined. In particular, hip, thigh and calf representations consistently appeared in an ordered manner along the latero-medial axis. Foot representations were located medially with respect to leg representations, but the ordering along the latero-medial axis of heel and toes representations was not consistent across participants. Larger volumes are found for big toe and hip representations. The somatotopic selectivity shows that representations located closer to each other are co-activated by tactile stimulation, while more distant representations are not. Co-activations are more frequently observed for foot representations compared to leg representations. Similar results were found in the rest of the participants.

2.3.2 Somatotopic sequence

The MNI locations of peak activations of the mapped representations are reported in Tab.2.1 and represented in Fig.2.2. Similarly to what was described for individual subjects, the foot representations were located in the medial region of the postcentral gyrus in the hemisphere contralateral to the stimulated foot and located more medially with respect to leg representations. There was no consistent ordering of foot representations. The calf, thigh and hip representations were located most laterally and appeared in an orderly manner moving from medial to lateral positions, respectively (all representations were lateral with respect to the foot representations).

To statistically quantify the somatotopic ordering for each BA, we used non-parametric Page's trend tests (**Page, 1963**). First, we computed a PCA separately for each BA and each participant to identify the main axis of orientation of the peak activations. The spatial distributions across participants of locations of peak activations within each BA along the first principal component are shown in Fig.2.S3. There is substantial overlap across the distributions, suggesting a large degree of inter-subject variability. However, there is a clear somatotopic ordering for leg representations. Although foot representations are consistently located medially
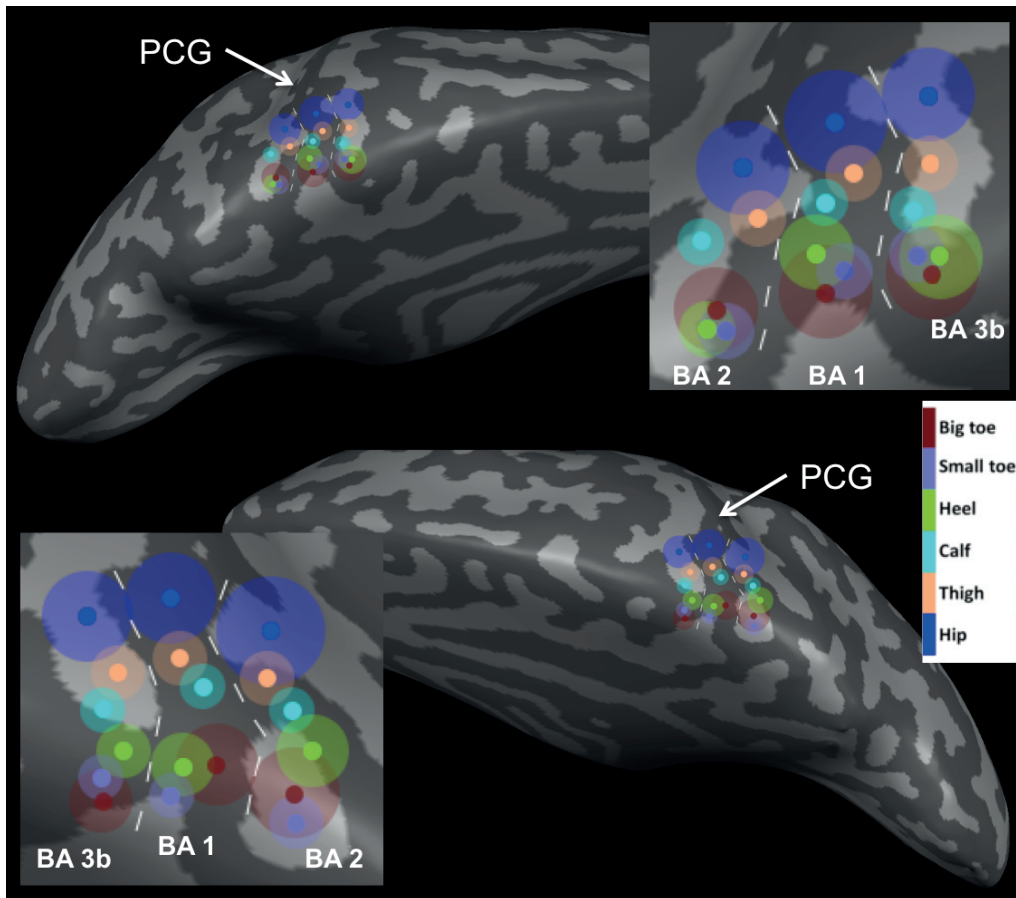
Fig.2.2 Locations of lower limb representations. Average MNI locations of peak activations are depicted on an inflated brain. The somatosensory representations of right (top) and left (bottom) lower limbs within BAs 3b, 1 and 2 (big toe, small toe, heel, calf, thigh and hip) are shown with color-coded circles. The transparent circles represent the respective size of each representation. The postcentral gyrus (PCG) is indicated by the white arrows.

compared to leg representations, there was no apparent ordering along the first principal component. Using these transformed coordinates as dependent variable for Page's trend tests, we found that the following somatotopic sequence: "big toe - small toe - heel - calf - thigh - hip" led to statistically significant ordering in all tested BAs (all $p<0.001$). The alternate somatotopic sequence (small toe - big toe - heel - calf - thigh - hip) also led to significant ordering (all $p<0.001$). This result suggests that the ordering of the big and small toes cannot be determined with the present data (see discussion). The same tests performed with random permutations of our data led to non-significant results (5% of the permuted data led to significant ordering as expected). The statistical results are presented in Tab.2.2. We note that we also performed the same analysis with the 2nd principal component, but there was no consistent ordering across foot or leg representations.

left hemisphere

	BA3b			BA1			BA2		
	x	y	z	x	y	z	x	y	z
big toe	-8.2±0.7	-42.0±1.3	65.7±1.2	-8.8±1.4	-39.9±1.5	67.0±1.5	-9.4±1.1	-41.2±1.4	66.9±1.1
small toe	-8.8±1.0	-42.2±1.4	65.0±1.3	-9.2±2.1	-37.8±1.9	65.9±1.7	-7.2±1.2	-41.4±1.7	65.2±1.4
heel	-8.6±0.8	-42.6±1.5	64.4±1.2	-10.0±1.7	-41.9±1.5	68.6±1.7	-8.7±1.3	-42.4±1.4	64.5±1.3
calf	-12.5±2.1	-41.8±1.6	62.3±2.3	-14.5±1.6	-39.5±1.2	68.8±1.5	-13.1±2.5	-43.9±2.3	62.5±4.0
thigh	-14.2±1.6	-38.7±1.5	64.8±1.6	-17.4±1.1	-37.9±1.1	69.0±1.5	-15.4±1.8	-38.3±1.6	66.3±1.7
hip	-22.3±1.6	-37.7±1.1	57.1±1.5	-21.1±1.1	-38.8±1.0	64.3±1.9	-20.3±1.6	-39.3±1.0	60.0±1.7

right hemisphere

	BA3b			BA1			BA2		
	x	y	z	x	y	z	x	y	z
big toe	8.2±1.0	-39.8±2.1	67.8±1.0	11.7±2.0	-42.1±2.3	70.9±1.0	9.9±1.4	-39.3±1.5	70.1±0.8
small toe	9.2±2.5	-39.1±2.0	65.4±2.7	8.0±1.7	-37.9±1.2	70.7±1.8	6.6±1.3	-39.1±1.4	68.2±1.6
heel	10.1±1.5	-42.1±1.4	67.0±1.3	10.2±1.8	-39.6±1.6	68.5±1.5	11.2±1.9	-41.5±1.7	67.6±1.6
calf	12.7±2.2	-38.1±2.0	66.0±2.9	15.1±1.5	-42.4±2.4	69.1±1.2	15.1±2.8	-40.4±2.1	64.7±3.2
thigh	15.2±2.2	-40.5±1.8	62.9±1.3	18.1±1.1	-39.3±1.4	68.9±1.4	17.6±1.1	-38.0±1.2	67.1±1.2
hip	20.7±1.5	-37.0±1.7	59.5±1.8	22.6±1.2	-39.2±1.2	66.1±1.6	20.9±1.2	-38.4±1.1	61.5±1.7

Tab.2.1 MNI Locations of peak activations. The location in MNI stereotaxic space of the average peak activations (mean ± std) of the mapped representations in different BAs are reported for right body regions (top) and left body regions (bottom).

	ordering 1		ordering 2		random	
	L statistic	p-value	L statistic	p-value	L statistic	p-value
left BA 3b	1193	p<0.001	1191	p<0.001	1030	p>0.05
left BA 1	1128	p<0.001	1129	p<0.001	1029	p>0.05
left BA 2	1189	p<0.001	1198	p<0.001	1029	p>0.05
right BA 3b	1187	p<0.001	1187	p<0.001	1029	p>0.05
right BA 1	1180	p<0.001	1175	p<0.001	1028	p>0.05
right BA 2	1168	p<0.001	1163	p<0.001	1030	p>0.05

Tab.2.2 Summary of Page's Trend tests. L statistics and corresponding p-values are reported for the tested orderings. Ordering 1 corresponds to "big toe – small toe – heel – calf – thigh – hip". Ordering 2 corresponds to "small toe – big toe – heel – calf – thigh – hip". In addition, we report the average L statistics for random permutations of our data. Values for statistical significance were derived from Page (1963) for data with 6 variables and 14 samples (L=1078 for p=0.05, L=1098 for p=0.01 and L=1121 for p=0.05).

Finally, we computed the Euclidean distances between the different body representations, which are shown in Fig.2.S4. Qualitatively, the results confirmed the previously reported somatotopic ordering showing increased distances when moving from foot representations to calf, thigh and hip representations respectively. Distances between calf, thigh and hip representations are also in accordance with their somatotopic arrangement. As reported in previous analyses, we did not observe consistent ordering across BAs based on distances between big toe, small toe and heel.

Importantly, there was substantial inter-subject variability with respect to the exact spatial layout of the mapped body representations in MNI space, as suggested by the distributions of peak activations. In addition, we found that on average only 2.15 out of 14 subjects (6 at best) shared the same representation at a given voxel.

To summarize, we were able to quantify somatotopy for each BA, in particular for calf, thigh and hip representations, which appeared highly somatotopically organized along S1. The foot representations were located more medially compared to leg representations, but did not appear in a consistent ordering along S1. Interestingly, the exact spatial layout of somatotopy strongly differed across subjects.

2.3.3 Strength and extent of BOLD activations

Here we analyzed the strength and extent of BOLD activations within the cortical representation of each of the 6 mapped body regions within the different BAs in right and left S1. To this aim, the peak activations and cortical volume within each of the 36 mapped body representations were analyzed by means of three-way repeated measures ANOVAs with body region (big toe, small toe, heel, calf, thigh and hip), BA (BA 3b, BA 1 and BA 2), and hemisphere (left and right) as within subject factors.

For the analysis of peak activations, The ANOVA showed a significant main effect of body region ($F_{5,65}$=23.7, p<0.001, Fig.2.3A). Post-hoc pairwise comparisons (Bonferroni corrected) revealed that the big toe representations (independent of BA or hemisphere) had significantly greater peak activations than those of the small toe, calf and the thigh (all p<0.001). Furthermore, we found that the hip representation had a significantly larger volume than small toe, calf and thigh (p<0.001, p<0.001 and p=0.01 respectively). This analysis also revealed that the heel representation had a significantly larger volume than small toe, calf and thigh (p=0.002 and p<0.001 and p=0.02 respectively). Overall, this shows that certain body parts, especially big toe, heel and hip, were associated with greater peak activations compared to other body parts, and this effect was present in all tested BA and in both hemispheres. We also found a main effect of BA ($F_{2,26}$=6.3, p=0.01, Fig.2.3B) indicating that peak activations within body representations differed across BAs independently from the body part represented and independently from the hemisphere. Post-hoc pairwise
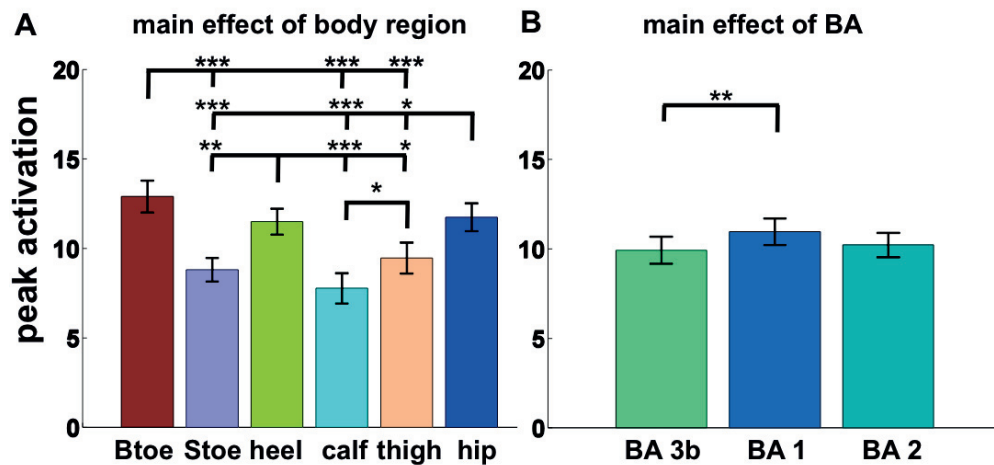
Fig.2.3 Strength of BOLD activations. A) Main effect of body regions for the analysis of peak activations ($F_{5,65}=23.7$, $p<0.001$). **B)** Main effect of BA for the analysis of peak activations ($F_{2,26}=6.3$, $p=0.01$). In addition, a two-way interaction between body region and side, as well as between BA and side (see ISM.6). The results are presented in the color-coded bar plot. Error bars represent standard errors of the mean. Significant post-hoc comparisons between the respective peak activations within the different body representations are shown with asterisks (* $p<0.05$, ** $p<0.01$, *** $p<0.001$).

comparisons (Bonferroni corrected) showed that peak activations within BA 3b were smaller compared to BA 1 (p=0.005). In addition to those main effects, we also found interactions between the investigated factors. In particular, a significant two-way interaction between body region and side was found ($F_{5,65}=4.5$, p=0.006; Fig.2.S5A). Post-hoc pairwise comparisons (Bonferroni corrected) showed that in the left hemisphere peak activations of foot representations are stronger compared to leg representations. Finally, a two-way interaction between BA and side was also found ($F_{2,26}=4.9$, p=0.03; Fig.2.S5B). Post-hoc pairwise comparisons (Bonferroni corrected) showed that differences reported for the main effect of BA are mainly driven by differences in the left hemisphere (i.e. no differences between peak activations across BAs in the right hemisphere).

For the analysis of cortical volume, the ANOVA showed a significant main effect of body region ($F_{5,65}=25.3$, p<0.001, Fig.2.4A). Post-hoc Tukey HSD comparisons revealed that the big toe representation (independent of BA or hemisphere) had a significantly larger volume than those of the small toe, calf and the thigh (all p<0.001). Furthermore, we found that the hip representation had a significantly larger volume than small toe, heel, calf and thigh (all p<0.001). This analysis also revealed that the heel representation had a significantly larger volume than those of the small toe and the calf (p=0.02 and p=0.002 respectively). We also found a main effect of
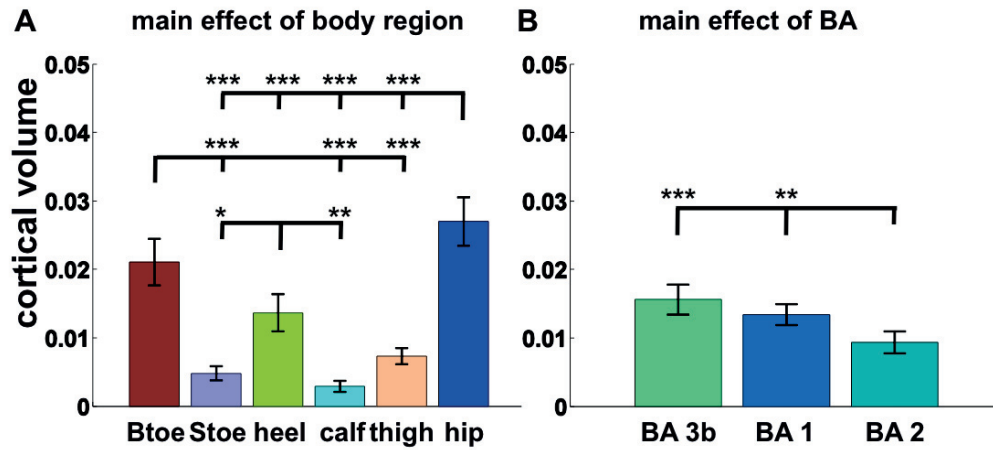
Fig.2.4 Extent of BOLD activations. A) Main effect of body regions for the analysis of cortical volumes ($F_{5,65}$=25.3, p < 0.001). **B)** Main effect of BA for the analysis of cortical volumes ($F_{2,26}$=13.2, p < 0.001). The results are presented in the color-coded bar plot. Error bars represent standard errors of the mean. Significant post-hoc comparisons between the respective volumes of body representations are shown with asterisks (* p<0.05, ** p<0.01, *** p<0.001).

BA ($F_{2,26}$=13.2, p<0.001, Fig.2.4B) indicating that the volume of body representations differed across BAs. Post-hoc Tukey HSD comparisons showed that the volumes of representations within BA 2 were smaller compared to BA 3b and BA 1 (p<0.001 and p=0.008 respectively). We note that the normality of cortical volume data was not fully satisfied. Therefore, we replicated the analysis using linear mixed models (**Cnaan et al. 1997**) on the ranked data and confirmed the presented results.

To summarize, our results indicate that in right-footed individuals overall big toe representation is associated with stronger and larger BOLD responses than small toe representation. This was also the case for hip representations compared to other leg representations. Interestingly, we found different effects across BAs regarding the strength and extent of BOLD responses. Strength of BOLD responses within BA 3b are weaker compared to BA 1, while extent of BOLD responses within BA 2 are smaller compared to BA 3b and BA 1.

2.3.4 Somatotopic selectivity

The aim of this analysis was to further investigate how these S1 responses are tuned to tactile stimulation across certain body regions within the different BAs and hemispheres. To this aim, we investigated how the 36 mapped representations respond to the stimulation of the body region that they were classified as representing, and whether the included voxels within each body representation also respond to the

stimulation of other body regions (i.e. whether the big toe representation in left BA 1 also responds to stimulation of the small toe or the calf).

In particular, we tested for each stimulated body region whether the tactile stimulation led to statistically significant positive BOLD responses within any of the other mapped representations (corrected for multiple comparisons, see Methods), thus determining somatotopic selectivity *within* limbs. Results concerning the somatotopic selectivity are presented in Fig.2.5. We observed patterns of co-activation for the 3 representations of the 3 body regions of the foot (big toe, small toe, and heel). Stimulation of toes strongly activated other foot regions (small toe, heel), but not the leg regions that we tested; this was the case for both hemispheres. Concerning the stimulation of the heel, which strongly activated other foot regions (as for big and small toes), the activations were not restricted to the foot-toe regions and also involved tested leg regions (broader *within* limb selectivity). Within limb somatotopic selectivity was reduced for calf, thigh and hip stimulation. In particular, calf stimulation (right and left) either co-activated exclusively thigh representations or did not elicit co-activation depending on the BA. Thigh stimulation either co-activated calf and hip representations or did not induce co-activations depending on the BA. Finally, hip stimulation either exclusively co-activated thigh representations or did not elicit co-activation depending on the BA. We note that toes representations never co-activated with leg representations (calf - thigh - hip). In addition, there was no evidence of qualitative differences in somatotopic selectivity across BAs.

To further investigate whether the lack of functional interactions between foot and leg representations could be explained by the factor of cortical distance, we conducted a regression analysis to characterize the relationship between co-activations and cortical distance. Separately for each stimulated body region, each BA and each participant, we considered 3 different fitting functions: 1) a decaying linear function corresponding to a constant decrease in co-activation with increased distance, 2) a decaying exponential function corresponding to a faster decrease in co-activations for distant representations compared to the linear function, 3) a sigmoidal function corresponding to a spatial clustering and drastic decrease in co-activation outside of
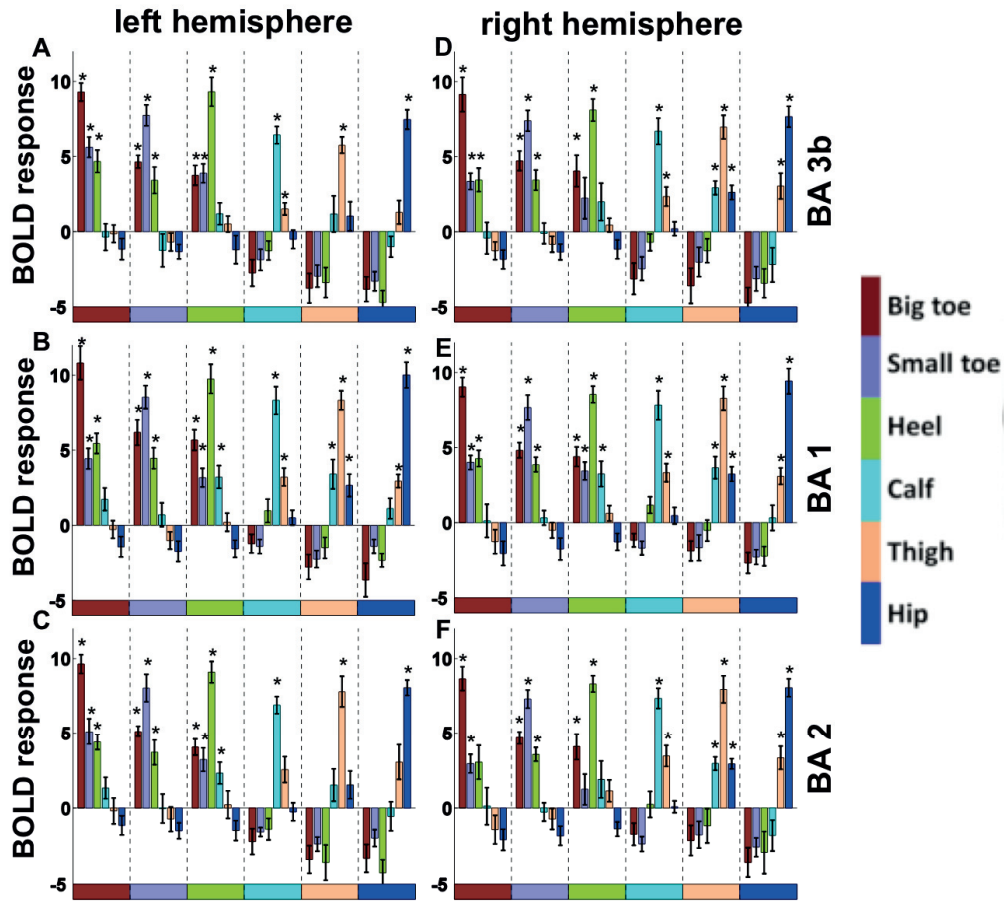
Fig.2.5 *Within* **limb somatotopic selectivity in lower limb representations in different BAs and hemispheres**. The mean BOLD activations within the mapped representations are plotted and color-coded. On the horizontal axis, data are grouped by stimulated body regions. Panels **A** and **D** show the representations within BA 3b for left and right hemisphere respectively. Panels **B** and **E** show the representations within BA 1 for left and right hemisphere, respectively. Panels **C** and **F** show the representations within BA 2 for left and right hemisphere, respectively. Error bars represent standard errors of the mean. Asterisks represent significant BOLD activations as defined by permutation tests.

the cluster. We then compared the resulting coefficients of determination R^2 for the 3 different fitting functions to determine which of them best describes the relationship between co-activations and cortical distance. We computed pairwise Wilcoxon signed-rank tests (Bonferroni corrected) (**Wilcoxon, 1945**) and found that the sigmoidal function performed better compared to the linear and exponential functions (mean ± std: linear fit $R^2 = 0.64 ± 0.18$, exponential fit $R^2 = 0.69 ± .019$, sigmoidal fit R2=0.74 ± 0.19; linear vs sigmoidal: $Z_{366}=12.8$, p<0.001; exponential vs sigmoidal: $Z_{378}=4.7$, p<0.001). We analyzed further the parameters (slope and offset) of the sigmoidal regression, but found no differences with respect to body regions, BAs or side.

We also tested *between* limbs somatotopic selectivity. For this we inspected whether the stimulation of a body region could lead to significant BOLD responses in the representations of the other limb, i.e. in the hemisphere ipsilateral to the stimulated body region. We note that the stimulation of all body region (except the hip) induced no or a negative BOLD response in representations of the contralateral limb in all BAs (i.e. *between* limbs selectivity). Hip representations were co-activated bilaterally during tactile stimulation of the hip (right and left). The results for *between* limbs somatotopic selectivity are shown in supplementary materials (Fig.2.S6).

To summarize, this analysis revealed that *within* limb somatotopic selectivity was weaker for the 3 tested leg regions compared to the 3 tested foot regions. In addition, there was no co-activation between foot and leg representations, and this effect could not be simply attributed to the factor of cortical distance, but was rather associated with a functional clustering. Interestingly, the hip is the only body region, which elicited significant interhemispheric activations following tactile stimulation (bilaterally and in all BA's) (see discussion). We note that we did not find any evidence in favor of differences between BAs for somatotopic selectivity.

2.4. Discussion

The present work investigated the foot and leg representation in human S1. By stimulating 12 different body regions (6 on each body side) during the acquisition of functional data at ultra-high field MRI (7T), we were able to identify separate representations of the stroked body regions within three BAs of human S1, namely BA 3b, 1 and 2. A total of 36 (6 body regions, 3 BA and 2 hemispheres) separate S1 body region representations were identified, revealing a somatotopic organization in each participant, the sequence of which showed strong inter-subject variability. To the best of our knowledge, this is the first study characterizing the anatomical and functional properties of the representations of foot and leg in 3 different BAs in human S1, analyzing the somatotopic sequence, the strength and extent of BOLD responses, and the somatotopic selectivity for the lower limb.

2.4.1 Anatomical location of S1 representations and inter-subject variability in the somatotopic sequence

We report that the S1 sequence for foot and leg representations follows a medial-to-lateral gradient (when moving the stimulation from distal to proximal parts of the lower limb) along the postcentral sulcus in BAs 3b, 1 and 2, partly reminiscent of the classic homunculus described in S1 **(Bao et al. 2012; Nakagoshi et al. 2005; Penfield and Boldrey, 1937; Rasmussen and Penfield, 1947; Saadon-Grosman et al. 2015)**. We found that calf, thigh and hip representations consistently follow a medial to lateral gradient along S1 in all investigated BAs, but this was not the case for foot representations. These data are thus compatible with a difference in toe versus finger representations in S1, with the different fingers ordered along the latero-medial axis (**Martuzzi et al. 2014**) and the toes possibly ordered along the rostral-caudal axis in the postcentral gyrus. Such difference is comparable with previous studies in non-human primates reporting differences regarding the organization of the digits of lower and upper limbs. Indeed, in monkey BA 3b, the lower limb digits have been reported to be organized along the latero-medial axis, while in monkey BA 1, they are rather organized along the rostro-caudal axis within a strip of the postcentral gyrus. Upper limb digits are somatotopically organized along the latero-medial axis of the postcentral gyrus in both monkey BA 3b and BA 1, similarly to humans (**Merzenich et al. 1978; Kaas et al. 1979; Nelson et al. 1980, Martuzzi et al. 2014**). Future studies will be necessary to investigate the representations of all 5 toes for more accurate mapping of toe somatotopy (not investigated in the present study). Here, we rather focused on the entire leg and foot, preventing us from more clearly determining a potential rostro-caudal somatotopic toe sequence for BAs in S1. A similar argument holds for the location of the heel with respect to the toes. In non-human primates, the sole representation lies adjacent to the toes along the rostro-caudal axis in both BA 3b and BA 1 (**Merzenich et al. 1978; Kaas et al. 1979; Nelson et al. 1980**).

Despite the evidence for somatotopy at the individual level (except for foot representations), we observed substantial inter-subject variability with respect to the exact sequence and location of each of the 12 mapped representations within S1. Such strong inter-individual variability was already reported for non-human primates (**Merzenich et al. 1978),** showing that a given body region is not at the same position in different individuals, and highlights the importance of studies focusing on single

subject analyses to recover the detailed functional organization of human S1. In particular, small cortical representations might not overlap at all across individuals, suggesting that generalizations based on group analysis should be regarded with caution. This likely explains the rather low number of publications describing lower limb somatotopy in S1 (using group-level analysis and lower spatial resolution) (**Bao et al. 2012; Nakagoshi et al. 2005**). This is different for the hand, where the respective representations are larger and thus more likely to overlap across subjects, compatible with previously described somatotopic S1 organization of the upper limb at the group level (**Gelnar et al. 1998; Kurth et al. 1998, 2000; Maldjian et al. 1999; Moore et al. 2000; Nelson and Chen, 2008; Overduin and Servos, 2004; van Westen et al. 2004).** These data highlight the importance of single subject analysis to characterize the functional properties of human S1, and are of relevance for the study of plasticity-dependent changes in S1 (**Muret et al. 2016; Pleger et al. 2003**), as well as for clinical research in amputees or spinal cord injury related to potential S1 changes in chronic pain (**Freund et al. 2011; Henderson et al. 2014**) and phantom limb pain (**Flor et al. 1995; Makin et al. 2013**).

2.4.2 Dominant representation of digit 1 of the foot

Concerning the different body part representations, big toe stimulation was associated with greater strength and extent of BOLD responses compared to other foot (and leg) representations, suggesting a possible homology with the representation of the thumb, whose larger cortical representation in S1 has already been demonstrated in a recent ultra-high resolution study (**Martuzzi et al. 2014**) using a similar approach. Human thumb magnification was also hinted at in the classical work of Penfield (**1937**). One possible explanation for the over-representation of the thumb in humans is its extensive solicitation compared to other digits. This could also account for the importance of the big toe representation due to its greater mobility and control (and hence its respective larger and more frequent somatosensory input) as well as its greater importance for stance, balance and locomotion (**Chou et al. 2009; Hughes et al. 1990**). We note, however, that there is no evidence for magnification in non-human primates for digit 1 of the upper or lower limb (**Merzenich et al. 1978; Kaas et al. 1979; Nelson et al. 1980**), although this aspect was not directly investigated in these studies.

Interestingly, we also found greater strength and extent of BOLD responses for hip representation, which is compatible with findings reported from neurophysiological studies in primates (**Taoka et al. 2000**). A possible interpretation of such result is that the tactile stimulation of the hip also activated adjacent body regions of the trunk. Indeed in the present study, the hip is the only stimulated body region located above the physical separation of legs, which would be compatible with its inclusion in a potentially larger trunk representation. In addition, the trunk and hip are known to have tactile receptive fields with different receptive field properties, compared to hands and feet, and are known to be functionally relevant for tactile stimuli to generate whole-body percepts (i.e. **Blanke et al. 2015**). Unilateral hip (and trunk) stimulations are also more likely to activate bilateral S1 regions (**Taoka et al. 1998, 2000**) and here we also found that from all stimulated body regions only hip stimulation leads to ipsilateral activations in the contralateral hip representations, suggesting the presence of large and bilateral tactile S1 hip representations. However, it is also possible that the described over-representation of the hip was simply induced by the lack of competing neighboring representations located more laterally on the postcentral gyrus, since we did not stimulate higher portions of the trunk or the chest. Other factors could also be associated to this result, such as more difficult access to this region during tactile stimulation in the 7T scanner, possibly leading to larger stimulated skin portions or less regular applied stroking patterns.

2.4.3 Lower selectivity in foot representations

Another interesting finding is that the stimulation of all foot regions (toes and heel) consistently elicited positive activity in the other representations of the same foot, but not in the mapped regions of the leg (calf, thigh and hip). This was found across all BAs, suggesting that information is broadly processed in all S1 foot representations, while still preferentially processed in the specific map. In addition, this effect was associated with a functional clustering of foot representations rather than simply explained by the cortical distance between representations. This may be the case as most tactile stimulation at the level of the foot will likely stimulate many toes, the sole and heel simultaneously (especially during upright stance and walking), which differs from tactile stimulation at the hand that more commonly involves single fingers. Compatible with this account, tactile stimulation of the leg (of calf, thigh and

hip) elicited more specific activations compared to foot stimulation, and did not elicit any activation in the foot areas, compatible with the absence of co-stimulation of calf, thigh, hip and foot in everyday behavior. Our data thus suggest that the prominent role of tactile processing from the foot in standing and locomotion and its related tactile co-activation, are associated with very broad tactile specificity even when stimulated in isolation. This finding differs from leg (present study) and from hand/finger representations (**Martuzzi et al. 2014**). Our findings are compatible with, and lend further support (for the case of the lower limbs) accounts of plasticity in S1 representations, whereby single body part maps are formed and maintained by the continuous competition and interaction between inputs from different body regions during activities of daily living (**Buonomano et al. 1998; Serino and Haggard 2010**).

Interestingly, we observed no activation in ipsilateral S1 in response to tactile stimulation (except for hip stimulation) and this was the case in all BAs and for all stimulated body regions. This finding is in accordance with previous studies reporting BOLD deactivation in ipsilateral S1 using median nerve stimulation (**Nihashi et al. 2005**) or tactile stimulation of fingers (**Hlushchuk et al. 2006**). We here report for the first time a similar effect for the lower limbs in S1. Accordingly, a previous study reported similar effects regarding the lack of interhemispheric interactions for motor representations of the lower limb (**Ruddy et al. 2016**)

2.4.4 Differences across Brodmann areas

Regarding differences across BAs with respect to the strength of BOLD responses, we observed weaker responses in BA 3b compared to BA 1. In addition, the extent of BOLD responses was greater in BA 3b and BA 1 compared to BA 2, which is compatible with what has been described for finger representations (**Martuzzi et al. 2014**). This suggests that the size/extent of body representation is reduced in BA 2 compared to BA 3b and BA 1, at least as demonstrated in Martuzzi et al. (**2014**) and in the present study with the use of a natural tactile stimulation. We note that the activity induced by tactile stimulation across the different BAs is highly dependent on the modality of stimulation (**van der Zwaag et al. 2015**), in particular in BA 2.

We note that we did not find any apparent difference across BAs with respect to somatotopic selectivity, which was expected based on the known reduced selectivity in BA 2, as shown for finger representations (**Besle et al. 2014; Martuzzi et al. 2014; Stringer et al. 2014**). It is possible that such an effect is less present for lower limbs compared to fingers and/or that the present study lacks the sensitivity to highlight its presence. However, it is also possible that the respective roles of the different BAs with respect to tactile processing are not the same for the different body parts, such as foot, leg or fingers. Further studies directly comparing such aspects between lower and upper limbs are necessary. The present study does not provide sufficient evidence to argue for the presence or absence of such organizational principle for the lower limbs.

2.4.5 Interhemispheric differences

Our data generally reveal very few interhemispheric differences between left and right S1 with respect to the strength and extent of BOLD responses within somatosensory representations and with respect to the somatotopic tuning of BOLD responses in our right-footed participants. This overall lack of hemispheric specialization with respect to foot/leg preference could be linked to the relatively low degree of specialization of foot and leg compared to hands when considering the shared role of both legs for stance, balance and locomotion. Moreover, even for the hand, there is little or no evidence supporting hemispheric differences between the S1 representations of the left and right hands in right-handed subjects. Accordingly, several neuroimaging studies reported no differences between right and left hand representations **(Boakye et al. 2000; Park et al. 2007; White et al. 1997)**. In particular, studies investigating morphological differences between right and left sensory-motor hand areas, both at the cellular scale using cytoarchitectonic measurements **(White et al. 1997)** and at the macroscopic scale using computed tomography imaging **(Park et al. 2007)**, found no evidence for any asymmetries. In addition, Boakye and colleagues **(2000)** explicitly examined this issue, but did not report any interhemispheric differences between the BOLD activations observed in S1 during right and left median nerve stimulation.

2.4.6 Limitations of the study

We would like to acknowledge that the present study suffers from several limitations. First, it was not possible to precisely determine the arrangement of toes in the different subregions of S1. A design including the stimulation of the five toes would be more appropriate to distinguish between a latero-medial and a rostro-caudal arrangement of toes. In addition, the investigation of the S1 representation of the five toes could potentially be more sensitive to highlight changes in selectivity across BAs, as it was demonstrated for fingers. Finally, the complex and variable shape of the postcentral gyrus leads to non-linear arrangements of body representation, which can be difficult to investigate in volumetric space. Although we agree that surface-based approaches can partially address this issue, they suffer from other limitations including the necessity of adequately coregistering and segmenting structural images and the difficulty to preserve small ROIs.

2.5 Conclusions

The present study investigates the non-invasive and precise mapping of the representation of lower limbs in different subregions S1 (BAs 3b, 1 and 2) at the individual subject level, based on high-resolution fMRI. These data are of great interest scientifically because as compared to other sensory modalities (vision, audition), much less is known about the organization of the human somatosensory system. By analyzing the localization, the strength, the extent and the somatotopic selectivity of the different representations, we describe here the functional properties of different lower limb representations. In particular, we showed that certain body regions (i.e. big toe, hip and heel) of the lower limbs have stronger and larger cortical representations in S1, and that different sectors of the lower limb, namely the foot and the leg, have a different degree of selectivity in response to tactile stimulation. These results were discussed in the context of a possible link between the functional properties of S1 representations and the respective functions of different regions of the lower limbs.

These data might have important implications for clinical and translational research in order to study plasticity in lower limb representations following different experimental manipulations (i.e. **Muret et al. 2016; Pleger et al. 2003**) as well as

certain pathologies affecting the lower limb, such as amputation, vascular disease, diabetes, and spinal cord injury, in which the lower limbs are much more frequently affected than the upper limbs (**Flor et al. 1995; Freund et al. 2011; Henderson et al. 2014; Makin et al. 2013**).

2.6 Supplementary materials

Do you practice an activity requiring a particular level of dexterity with hands ? (i.e. play an instrument)
With which hand do you write?
With which hand would you punch?
With which hand do you brush your teeth?
Do you practice an activity requiring a particular level of dexterity with feet? (i.e. play soccer or drum)
With which foot would you kick a soccer ball?
With which foot would you burst a door open?
Which foot would be in the back if you were to do skateboarding or snowboarding?
if foot preference remains unclear, subjects would be instructed to close their eyes and would be pushed backward to identify which foot is used to catch up their balance (i.e. the dominant foot)

Tab.2.S1 Questionnaire used to determine hand and foot preference of participants.

Fig.2.S1 Individual data from subjects 1 and 2. The cortical volume and somatotopic selectivity of body representations are shown for subjects 1 and 2.

Fig.2.S2 Individual data from subjects 3 and 4. The cortical volume and somatotopic selectivity of body representations are shown for subjects 3 and 4.

47
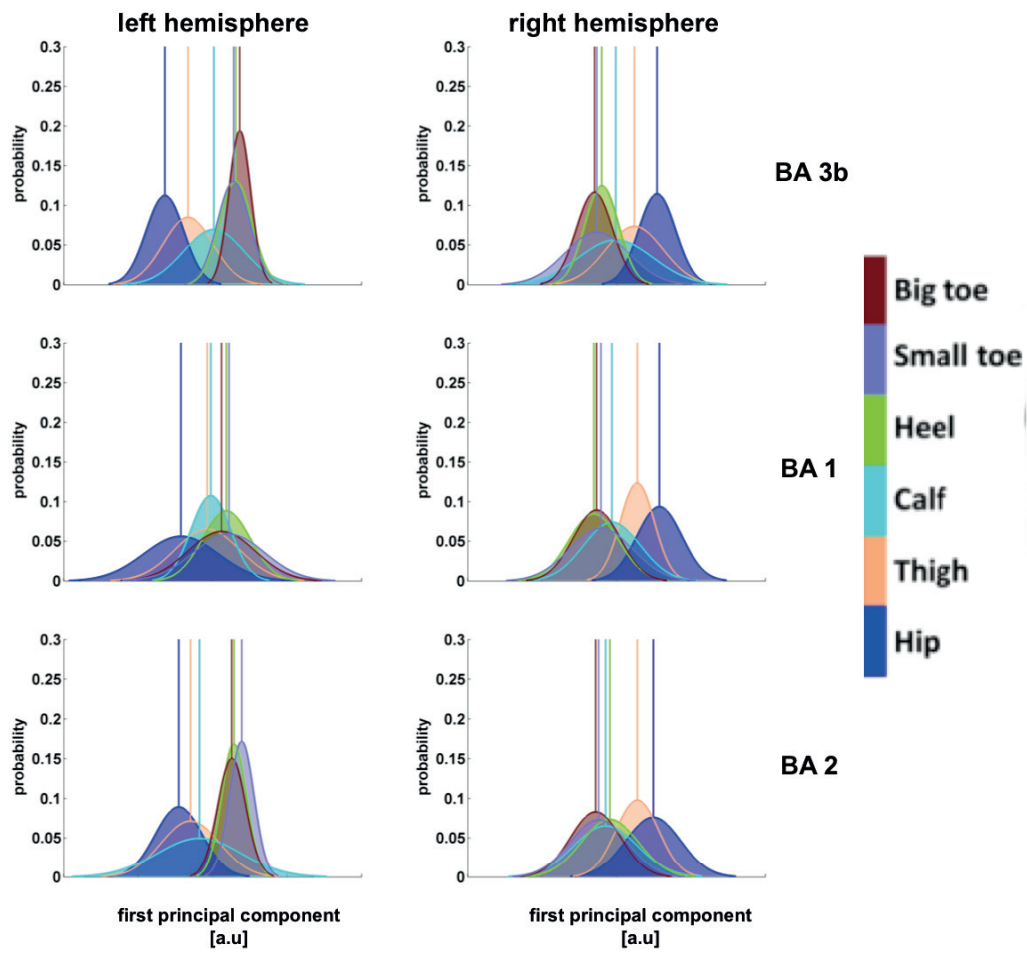
Fig.2.S3 Spatial distributions of peak activations. The spatial distribution of peak activations along the first principal component are shown. Hip, thigh and calf distributions are well distinguished on all BAs, but this is not the case for foot representations.
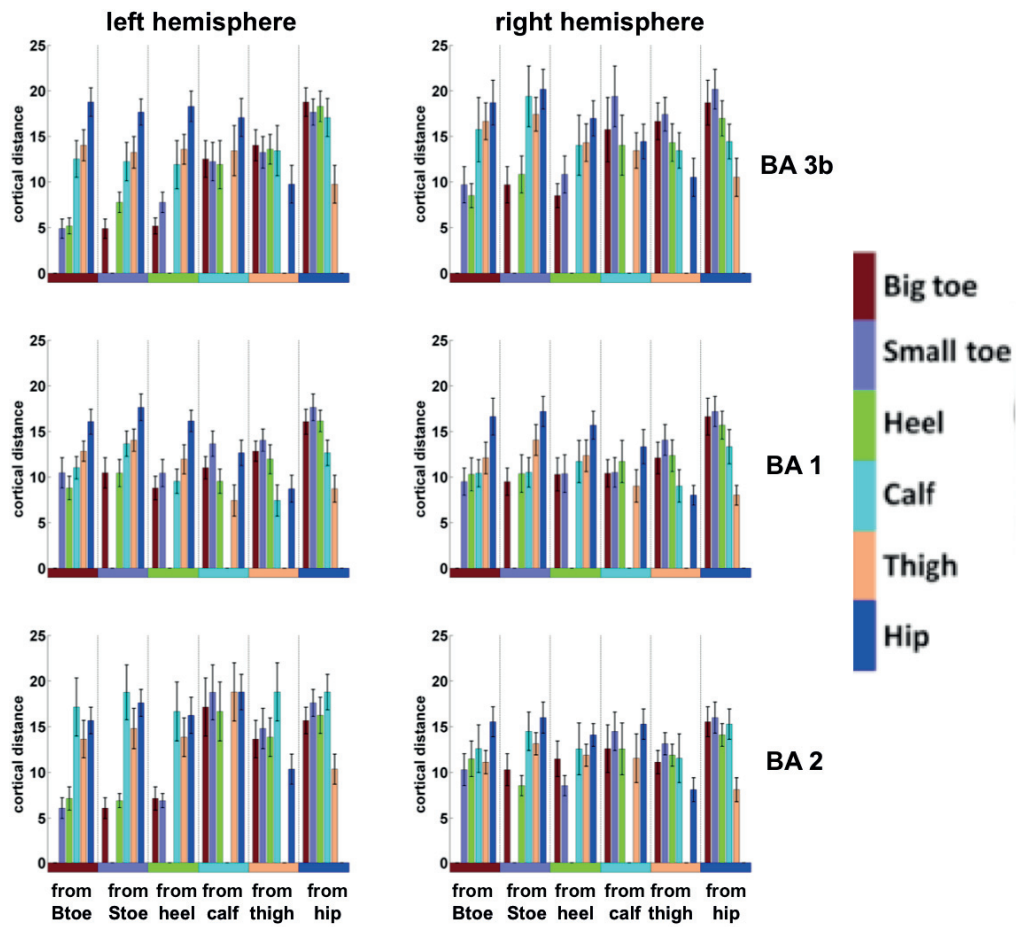
Fig.2.S4 Average peak to peak distances. The Euclidean distance between body representations are averaged across subjects. In all BAs, the distances are increasing when moving from foot representations to leg representations compatible with a somatotopic ordering. Distances between calf, thigh and hip representations are also in accordance with their somatotopic arrangement. There is no consistent ordering across BAs based on distances for big toe, small toe and heel.
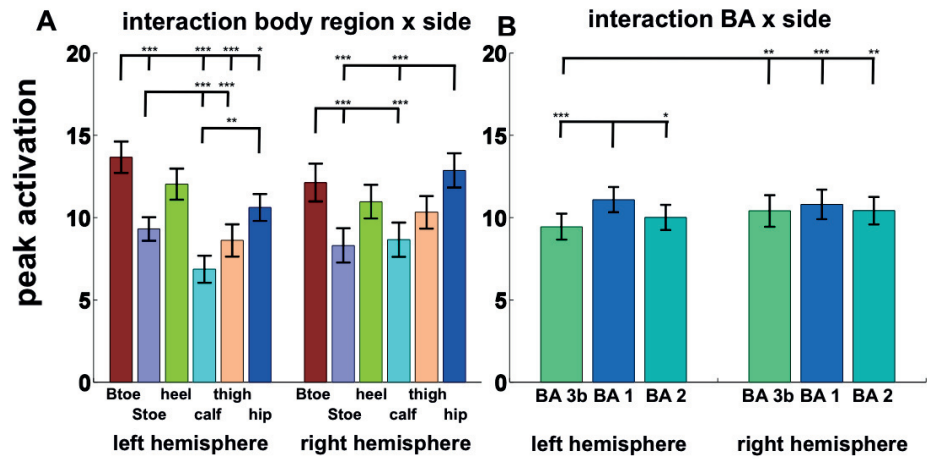
Fig.2.S5 Strength of BOLD activations (interactions). A) Interaction between body region and side for the analysis of peak activations ($F_{2,26}$=4.5, p = 0.006), the interaction is driven by greater peak activations within foot representations compared to leg representations in the left hemisphere. **B)** Interaction between BA and side for the analysis of peak activations($F_{2,26}$=4.9, p = 0.03), the interaction is driven the presence of differences across BAs in the left hemisphere, but in the right hemisphere. The results are presented in the color coded bar plot. Error bars represent standard errors of the mean. Significant post-hoc comparisons between the respective peak activations of body representations are shown with asterisks (* p<0.05, ** p<0.01, *** p<0.001).
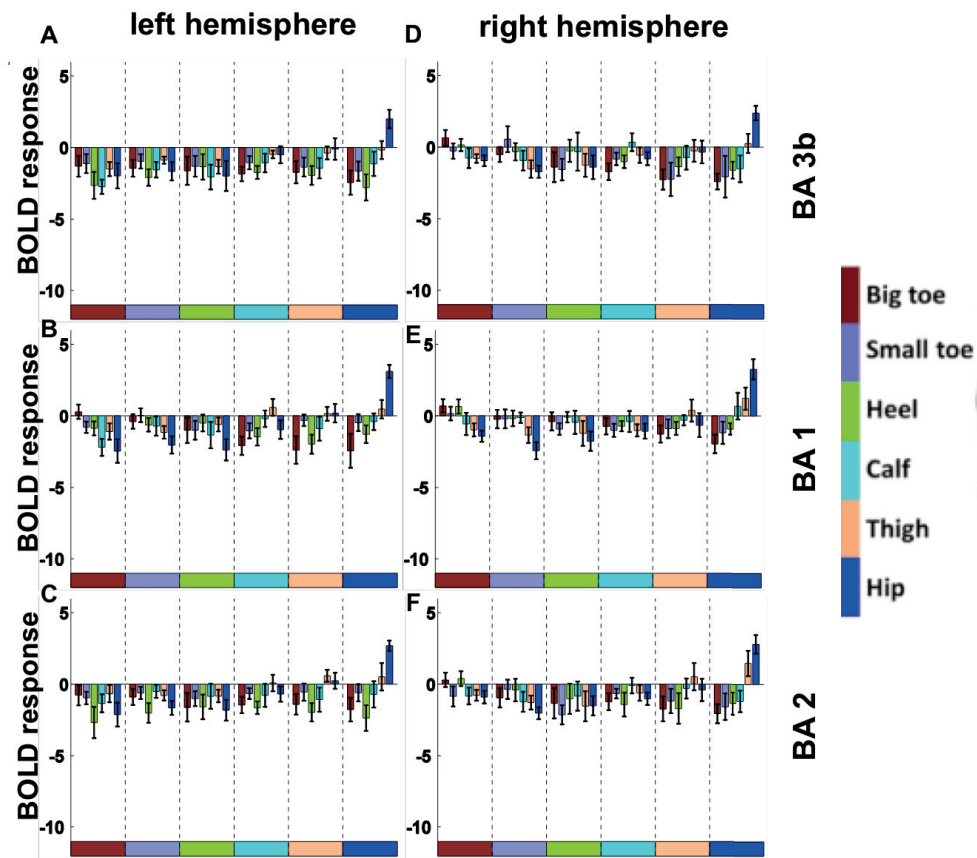
Fig.2.S6 *Between* **limb somatotopic selectivity in lower limb representations in different BAs and hemispheres.** The mean BOLD activations within the mapped representations are plotted and color-coded. On the horizontal axis, data are grouped by stimulated body regions. Panels **A** and **D** show the BOLD responses within BA 3b in left and right hemisphere following stimulation of left and right body regions, respectively. Panels **B** and **E** show the BOLD responses within BA 1 in left and right hemispheres following stimulation of left and right body regions, respectively. Panels **C** and **F** show the BOLD responses within BA 2 in left and right hemispheres following stimulation of left and right body regions, respectively. Error bars represent standard errors of the mean.

2.7 References

Bao, R., Wei, P., Li, K., Lu, J., Zhao, C., Wang, Y., Zhang, T., 2012. Within-limb somatotopic organization in human SI and parietal operculum for the leg: an fMRI study. Brain research 1445, 30–9. doi:10.1016/j.brainres.2012.01.029

Besle, J., Sanchez-Panchuelo, R.-M., Bowtell, R., Francis, S., Schluppeck, D., 2014. Event-Related fMRI at 7T Reveals Overlapping Cortical Representations for Adjacent Fingertips in S1 of Individual Subjects. Human brain mapping 2043, 2027–2043. doi:10.1002/hbm.22310

Blanke, O., Slater, M., Serino, A., 2015. Behavioral, Neural, and Computational Principles of Bodily Self-Consciousness. Neuron. doi:10.1016/j.neuron.2015.09.029

Boakye, M., Huckins, S.C., Szeverenyi, N.M., Taskey, B.I., Hodge, C.J., 2000. Functional magnetic resonance imaging of somatosensory cortex activity produced by electrical stimulation of the median nerve or tactile stimulation of the index finger. Journal of neurosurgery 93, 774–83. doi:10.3171/jns.2000.93.5.0774

Buonomano, D. V, Merzenich, M.M., 1998. Cortical plasticity: from synapses to maps. Annual review of neuroscience 21, 149–186. doi:10.1146/annurev.neuro.21.1.149

Chou, S.W., Cheng, H.Y.K., Chen, J.H., Ju, Y.Y., Lin, Y.C., Wong, M.K. a, 2009. The role of the great toe in balance performance. Journal of Orthopaedic Research 27, 549–554. doi:10.1002/jor.20661

Cnaan, A., Laird, N.M., Slasor, P., 1997. Using the general linear mixed model to analyse unbalanced repeated measures and longitudinal data. Statistics in Medicine 16, 2349–2380. doi:10.1002/(SICI)1097-0258(19971030)16:20

Constanzo, R., Gardner, E., 1980. A Quantitative Analysis of Responses of Direction-Sensitive Neurons in Somatosensory Cortex of Awake Monkeys 43.

Da Costa, S., Saenz, M., Clarke, S., van der Zwaag, W., 2014. Tonotopic Gradients in Human Primary Auditory Cortex: Concurring Evidence From High-Resolution 7 T and 3 T fMRI. Brain topography 0–3. doi:10.1007/s10548-014-0388-0

Da Costa, S., van der Zwaag, W., Marques, J.P., Frackowiak, R.S.J., Clarke, S., Saenz, M., 2011. Human primary auditory cortex follows the shape of Heschl's gyrus. The Journal of neuroscience : the official journal of the Society for Neuroscience 31, 14067–75. doi:10.1523/JNEUROSCI.2000-11.2011

Flor, H., Elbert, T., Knecht, S., Wienbruch, C., 1995. Phantom-limb pain as a perceptual correlate of cortical reorganization following arm amputation. Science 375, 482–484.

Freund, P., Weiskopf, N., Ashburner, J., Wolf, K., Sutter, R., Altmann, D.R., Friston, K., Thompson, A., Curt, A., 2013. MRI investigation of the sensorimotor cortex and the corticospinal tract after acute spinal cord injury: a prospective longitudinal study. The Lancet. Neurology 12, 873–81. doi:10.1016/S1474-4422(13)70146-7

Gardner, E.P., 1988. Somatosensory cortical mechanisms of feature detection in tactile and kinesthetic discrimination. Canadian journal of physiology and pharmacology 66, 439–54. doi:10.1139/y88-074

Geisser, S., Greenhouse, S.W., 1958. An Extension of Box's Results on the Use of the F Distribution in Multivariate Analysis. The Annals of Mathematical Statistics 29, 885–891. doi:10.2307/2237272

Gelnar, P.A., Krauss, B.R., Szeverenyi, N.M., Apkarian, A. V, 1998. Fingertip representation in the human somatosensory cortex: an fMRI study. NeuroImage 7, 261–283. doi:10.1006/nimg.1998.0341

Geyer, S., Schleicher, a, Zilles, K., 1999. Areas 3a, 3b, and 1 of human primary somatosensory cortex. NeuroImage 10, 63–83. doi:10.1006/nimg.1999.0440

Geyer, S., Schormann, T., Mohlberg, H., Zilles, K., 2000. Areas 3a, 3b, and 1 of human primary somatosensory cortex. Part 2. Spatial normalization to standard anatomical space. NeuroImage 11, 684–96. doi:10.1006/nimg.2000.0548

Grefkes, C., Geyer, S., Schormann, T., Roland, P., Zilles, K., 2001. Human somatosensory area 2: observer-independent cytoarchitectonic mapping, interindividual variability, and population map. NeuroImage 14, 617–31. doi:10.1006/nimg.2001.0858

Henderson, L. a, Gustin, S.M., Macey, P.M., Wrigley, P.J., Siddall, P.J., 2011. Functional reorganization of the brain in humans following spinal cord injury: evidence for underlying changes in cortical anatomy. The Journal of neuroscience : the official journal of the Society for Neuroscience 31, 2630–7. doi:10.1523/JNEUROSCI.2717-10.2011

Hlushchuk, Y., Hari, R., 2006. Transient Suppression of Ipsilateral Primary Somatosensory Cortex during Tactile Finger Stimulation. Journal of Neuroscience 26, 5819–5824. doi:10.1523/JNEUROSCI.5536-05.2006

Hoffmann, M.B., Stadler, J., Kanowski, M., Speck, O., 2009. Retinotopic mapping of the human visual cortex at a magnetic field strength of 7T. Clinical neurophysiology : official journal of the International Federation of Clinical Neurophysiology 120, 108–16. doi:10.1016/j.clinph.2008.10.153

Hughes, J., Clark, P., Klenerman, L., 1990. The importance of the toes in walking. The Journal of bone and joint surgery. British volume 72, 245–251.

Hyvarinen, B.Y.J., Poranent, A., 1978. Orientation-Selective Cutaneous Receptive Fields In The Hand Area Of The Post-Central Gyrus In Monkeys. Journal of Physiology 523–537.

Iwamura, Y., 1998. Hierarchical somatosensory processing. Current opinion in neurobiology 8, 522–8.

Jones, E.G., Coulter, J.D., Hendry, S.H., 1978. Intracortical connectivity of architectonic fields in the somatic sensory, motor and parietal cortex of monkeys. The Journal of comparative neurology 181, 291–347. doi:10.1002/cne.901810206

Kaas, J., Nelson, R., Sur, M., Lin, C., Merzenich, M., 1979. Multiple representations of the body within the primary somatosensory cortex of primates. Science 204, 1977–1979.

Kurth, R., Villringer, K., Curio, G., Wolf, K.J., Krause, T., Repenthin, J., Schwiemann, J., Deuchert, M., Villringer, A., 2005. fMRI shows multiple somatotopic digit representations in human primary somatosensory cortex. Neuroreport 11, 1–5. doi:10.1097/00001756-200005150-00025

Kurth, R., Villringer, K., Mackert, B.M., Schwiemann, J., Braun, J., Curio, G., Villringer, a, Wolf, K.J., 1998. fMRI assessment of somatotopy in human Brodmann area 3b by electrical finger stimulation. Neuroreport 9, 207–12.

Makin, T.R., Scholz, J., Filippini, N., Slater, D.H., Tracey, I., Johansen-berg, H., Henderson Slater, D., 2013. Phantom pain is associated with preserved structure and function in the former hand area. Nature communications 4, 1570. doi:10.1038/ncomms2571

Maldjian, J. a, Gottschalk, a, Patel, R.S., Detre, J. a, Alsop, D.C., 1999. The sensory somatotopic map of the human hand demonstrated at 4 Tesla. NeuroImage 10, 55–62. doi:10.1006/nimg.1999.0448

Marques, J., Kober, T., van der Zwaag, W., Kruegger, G., Gruetter, R., 2008. MP2RAGE, a self-bias field corrected sequence for improved segmentation at high field. Proceedings 16th Scientific Meeting, International Society for Magnetic Resonance in Medicine Toronto, 1393.

Martuzzi, R., van der Zwaag, W., Dieguez, S., Serino, a., Gruetter, R., Blanke, O., 2015. Distinct contributions of Brodmann areas 1 and 2 to body ownership. Social Cognitive and Affective Neuroscience 1–11. doi:10.1093/scan/nsv031

Martuzzi, R., van der Zwaag, W., Farthouat, J., Gruetter, R., Blanke, O., 2014. Human finger somatotopy in areas 3b, 1, and 2: A 7T fMRI study using a natural stimulus. Human brain mapping 35, 213–226. doi:10.1002/hbm.22172

Merzenich, M.M., Kaas, J.H., Sur, M., Lin, C.S., 1978. Double representation of the body surface within cytoarchitectonic areas 3b and 1 in "SI" in the owl monkey (Aotus trivirgatus). The Journal of comparative neurology 181, 41–73. doi:10.1002/cne.901810104

Moore, C.I., Stern, C.E., Corkin, S., Fischl, B., Gray, a C., Rosen, B.R., Dale, a M., 2000. Segregation of somatosensory activation in the human rolandic cortex using fMRI. Journal of Neurophysiology 84, 558–569.

Muret, D., Daligault, S., Dinse, H.R., Delpuech, C., Mattout, J., Reilly, K.T., Farnè, A., Farne, A., 2016. Neuromagnetic correlates of adaptive plasticity across the hand-face border in human primary somatosensory cortex. Journal of Neurophysiology 2095–2104. doi:10.1152/jn.00628.2015

Nakagoshi, A., Fukunaga, M., Umeda, M., Mori, Y., Higuchi, T., Tanaka, C., 2005. Somatotopic representation of acupoints in human primary somatosensory cortex: an FMRI study. Magnetic resonance in medical sciences : MRMS : an official journal of Japan Society of Magnetic Resonance in Medicine 4, 187–9.

Nelson, A.J., Chen, R., 2008. Digit somatotopy within cortical areas of the postcentral gyrus in humans. Cerebral Cortex 18, 2341–2351. doi:10.1093/cercor/bhm257

Nelson, R.J., Sur, M., Felleman, D.J., Kaas, J.H., 1980. Representations of the body surface in postcentral parietal cortex of Macaca fascicularis. The Journal of comparative neurology 192, 611–43. doi:10.1002/cne.901920402

Nihashi, T., Naganawa, S., Sato, C., Kawai, H., Nakamura, T., Fukatsu, H., Ishigaki, T., Aoki, I., 2005. Contralateral and ipsilateral responses in primary somatosensory cortex following electrical median nerve stimulation--an fMRI study. Clinical neurophysiology : official journal of the International Federation of Clinical Neurophysiology 116, 842–848. doi:10.1016/j.clinph.2004.10.011

Oldfield, R.C., 1971. The assessment and analysis of handedness: The Edinburgh inventory. Neuropsychologia 9, 97–113. doi:10.1016/0028-3932(71)90067-4

Olman, C. a, Van de Moortele, P.-F., Schumacher, J.F., Guy, J.R., Uğurbil, K., Yacoub, E., 2010. Retinotopic mapping with spin echo BOLD at 7T. Magnetic resonance imaging 28, 1258–69. doi:10.1016/j.mri.2010.06.001

Overduin, S.A., Servos, P., 2004. Distributed digit somatotopy in primary somatosensory cortex. NeuroImage 23, 462–472. doi:10.1016/j.neuroimage.2004.06.024

Page, E., 1963. Ordered hypotheses for multiple treatments: a significance test for linear ranks. Journal of the American Statistical Association 58, 216–230. doi:10.1080/01621459.1963.10500843

Park, M.C., Goldman, M.A., Park, M.J., Friehs, G.M., 2007. Neuroanatomical localization of the "precentral knob" with computed tomography imaging. Stereotactic and Functional Neurosurgery 85, 158–161. doi:10.1159/000099074

Penfield, W., Boldrey, E., 1937. Somatic motor and sensory representation in the cerebral cortex of man as studied by electrical stimulation. Brain.

Pleger, B., Dinse, H.R., Ragert, P., Schwenkreis, P., Malin, J.P., Tegenthoff, M., 2001. Shifts in cortical representations predict human discrimination improvement. Proceedings of the National Academy of Sciences of the United States of America 98, 12255–60. doi:10.1073/pnas.191176298

Powell, T.P.S., Mountcastle, V.B., 1959. The cytoarchitecture of the postcentral gyrus of the monkey macaca mulatta. Bulletin Johns Hopkins Hospital 105, 108–130.

Rasmussen, T., Penfield, W., 1947. Further studies of the sensory and motor cerebral cortex of man. Federation proceedings 6, 452–460.

Ruddy, K.L., Jaspers, E., Keller, M., Wenderoth, N., 2016. Interhemispheric sensorimotor integration; an upper limb phenomenon? Neuroscience 333, 104–113. doi:10.1016/j.neuroscience.2016.07.014

Saadon-Grosman, N., Tal, Z., Itshayek, E., Amedi, A., Arzy, S., 2015. Discontinuity of cortical gradients reflects sensory impairment. Proceedings of the National Academy of Sciences of the United States of America 112, 16024–9. doi:10.1073/pnas.1506214112

Salomon, R., Darulova, J., Narsude, M., van der Zwaag, W., 2014. Comparison of an 8-channel and a 32-channel coil for high-resolution FMRI at 7 T. Brain topography 27, 209–12. doi:10.1007/s10548-013-0298-6

Sanchez-Panchuelo, R.M., Besle, J., Beckett, A., Bowtell, R., Schluppeck, D., Francis, S., 2012. Within-digit functional parcellation of Brodmann areas of the human primary somatosensory cortex using functional magnetic resonance imaging at 7 tesla. Journal of Neuroscience 32, 15815–22. doi:10.1523/JNEUROSCI.2501-12.2012

Sanchez-Panchuelo, R.M., Francis, S., Bowtell, R., Schluppeck, D., 2010. Mapping Human Somatosensory Cortex in Individual Subjects With 7T Functional MRI. J. neurophysiol 2544–2556. doi:10.1152/jn.01017.2009.

Sánchez-Panchuelo, R.-M., Besle, J., Mougin, O., Gowland, P., Bowtell, R., Schluppeck, D., Francis, S., 2014. Regional structural differences across functionally parcellated Brodmann areas of human primary somatosensory cortex. NeuroImage 93 Pt 2, 221–30. doi:10.1016/j.neuroimage.2013.03.044

Schweisfurth, M. a., Frahm, J., Schweizer, R., 2014. Individual fMRI maps of all phalanges and digit bases of all fingers in human primary somatosensory cortex. Frontiers in Human Neuroscience 8, 1–14. doi:10.3389/fnhum.2014.00658

Schweizer, R., Voit, D., Frahm, J., 2008. Finger representations in human primary somatosensory cortex as revealed by high-resolution functional MRI of tactile stimulation. NeuroImage 42, 28–35. doi:10.1016/j.neuroimage.2008.04.184

Sereno, M.I., Dale, a M., Reppas, J.B., Kwong, K.K., Belliveau, J.W., Brady, T.J., Rosen, B.R., Tootell, R.B., 1995. Borders of multiple visual areas in humans revealed by functional magnetic resonance imaging. Science (New York, N.Y.) 268, 889–93.

Serino, A., Haggard, P., 2010. Touch and the body. Neuroscience and Biobehavioral Reviews. doi:10.1016/j.neubiorev.2009.04.004

Speck, O., Stadler, J., Zaitsev, M., 2008. High resolution single-shot EPI at 7T. Magnetic Resonance Materials in Physics, Biology and Medicine 21, 73–86. doi:10.1007/s10334-007-0087-x

Stringer, E.A., Chen, L.M., Friedman, R.M., Gatenby, C., Gore, J.C., 2011. Differentiation of somatosensory cortices by high-resolution fMRI at 7 T. NeuroImage 54, 1012–20. doi:10.1016/j.neuroimage.2010.09.058

Stringer, E., Qiao, P.-G., Friedman, R.M., Holroyd, L., Newton, A.T., Gore, J.C., Min Chen, L., 2014. Distinct fine-scale fMRI activation patterns of contra- and ipsilateral somatosensory areas 3b and 1 in humans. Human Brain Mapping 35, 4841–4857. doi:10.1002/hbm.22517

Taoka, M., Toda, T., Iwamura, Y., 1998. Representation of the midline trunk, bilateral arms, and shoulders in the monkey postcentral somatosensory cortex. Experimental brain research. Experimentelle Hirnforschung. Expérimentation cérébrale 123, 315–22. doi:10.1007/s002210050574

Taoka, M., Toda, T., Iriki, A., Tanaka, M., Iwamura, Y., 2000. Bilateral receptive field neurons in the hindlimb region of the postcentral somatosensory cortex in awake macaque monkeys. Experimental Brain Research 134, 139–146. doi:10.1007/s002210000464

van der Zwaag, W., Francis, S., Head, K., Peters, A., Gowland, P., Morris, P., Bowtell, R., 2009. NeuroImage fMRI at 1 . 5 , 3 and 7 T : Characterising BOLD signal changes. NeuroImage 47, 1425–1434. doi:10.1016/j.neuroimage.2009.05.015

van der Zwaag, W., Gruetter, R., Martuzzi, R., 2015. Stroking or Buzzing? A Comparison of Somatosensory Touch Stimuli Using 7 Tesla fMRI. PloS one 10, e0134610. doi:10.1371/journal.pone.0134610

van Westen, D., Fransson, P., Olsrud, J., Rosén, B., Lundborg, G., Larsson, E.-M., Westen, D. Van, 2004. Finger somatotopy in area 3b: an fMRI-study. BMC neuroscience 5, 28. doi:10.1186/1471-2202-5-28

Weibull, A., Björkman, A., Hall, H., Rosén, B., Lundborg, G., Svensson, J., 2008. Optimizing the mapping of finger areas in primary somatosensory cortex using functional MRI. Magnetic Resonance Imaging 26, 1342–1351. doi:10.1016/j.mri.2008.04.007

White, L.E., Andrews, T.J., Hulette, C., Richards, A., Groelle, M., Paydarfar, J., Purves, D., 1997. Structure of the human sensorimotor system. II: Lateral symmetry. Cerebral Cortex 7, 31–47. doi:10.1093/cercor/7.1.31

Wilcoxon, F., 1946. Individual comparisons of grouped data by ranking methods. Journal of economic entomology 39, 269. doi:10.2307/3001968

Zeharia, N., Hertz, U., Flash, T., Amedi, A., 2015. New whole-body sensory-motor gradients revealed using phase-locked analysis and verified using multivoxel pattern analysis and functional connectivity. The Journal of neuroscience : the official journal of the Society for Neuroscience 35, 2845–59. doi:10.1523/JNEUROSCI.4246-14.2015

3 - Study II: properties of the functional connectivity network of hands, feet and legs representations in three areas of primary somatosensory cortex in humans: a 7T study

Michel Akselrod, Roberto Martuzzi, Andrea Serino, Wietske van der Zwaag,

Roger Gassert and Olaf Blanke

Abstract

A large number of recent ultra-high field (7T) fMRI studies focused on the mapping of multiple body parts representations within subregions of the human primary somatosensory cortex (S1). Here, we extend these mapping results to investigate the resting-state functional connectivity (rs-FC) between multiple S1 representations at ultra high-field fMRI. First, we applied a mapping procedure to identify at the single subject level the tactile representations of 12 bilateral skin regions of hands, feet and legs within Brodmann areas (BAs) 3b, 1 and 2, leading to 72 separate S1 representations. Second, using resting-state data we analyzed the correlation between low-frequency spontaneous BOLD fluctuations across these regions. Using graph theory metrics and graph visualization approaches, we investigated whether the formed network was functionally organized in terms of interhemispheric, interareal and intersomatic interactions and whether this organization differed for hands and lower limbs. We also investigated the local patterns of rs-FC between neighboring representations across BAs and across body part. Finally, we investigated the overall relationship between rs-FC and cortical distance. The results showed that the patterns of rs-FC within primary somatosensory cortices are highly constrained by anatomical factors such as cortical distance, but the fine functional organization largely differed between hands, feet and legs, which we linked to the functional role of these different body parts and their functional interactions during everyday activities.

Detailed contributions: I was in charge of the project. I prepared the paradigms, collected and analyzed the data, wrote the initial manuscript and created the figures.

3.1 Introduction

One of the most relevant methods to investigate brain connectivity in humans (**Friston et al. 1993; Cradock et al. 2013)** is based on the evidence that, at rest, regions belonging to the same functional network exhibit synchronous low-frequency (<0.1 Hz) fluctuations of the BOLD signal (**Biswal et al. 1995**). The analysis of these spontaneous BOLD fluctuations at rest, which is now known as resting state functional connectivity (rs-FC, **Fox and Raichle, 2007**), has allowed mapping the functional networks of the brain. In particular, rs-FC has been widely applied to parcellate the brain and to identify large-scale functional brain networks like for example the default mode network or the attentional network **(Beckmann et al. 2005; Damoiseaux et al. 2006; Greicius et al. 2003; Harrison et al. 2015; Yeo et al. 2011, van den Ven et al. 2004)**. On the other hand, rs-FC has also been used to study the short-scale connectivity within unimodal sensory cortices (**Burton et al. 2015; Cha et al. 2016; Eckert et al. 2008; Li et al. 2015; Long et al. 2014; Maudoux et al. 2012; Striem-Amit et al. 2015**). For example, it was demonstrated that rs-FC reflects the retinotopic organization of primary visual cortices (**Raemaekers et al. 2016; Striem-Amit et al. 2015**) and also reflects the tonotopic organization of primary auditory cortices (**Cha et al. 2016**). In addition, rs-FC within unimodal areas was shown to be altered in many clinical conditions, and could potentially be used as biomarker to quantify impairments and recovery (**Burton et al. 2015; Maudoux et al. 2012; Striem-Amit et al. 2015**). The present study investigates the rs-FC of somatosensory representations of 24 body parts across three subregions of the human primary somatosensory cortex.

The human primary somatosensory cortex, S1, is located along the postcentral gyrus and is composed of four different Brodmann Areas (BAs 3a, 3b, 1, and 2, **Jones et al. 1978; Powell and Mountcastle, 1959**). Previous studies described the anatomical location of the different BAs forming human S1: BA 3a is anatomically located on the fundus of the postcentral gyrus, BA 3b on the anterior wall, BA 1 on the crown, and BA 2 on the posterior wall (**Geyer et al. 1999; Geyer et al. 2000; Grefkes et al. 2001**). In particular, BAs 3b, 1 and 2 are involved in tactile processing and as shown by studies conducted in non-human primates and in humans, and each of these BAs is somatotopically organized, with each body part being represented in a

precise cortical position (**Kaas et al. 1979; Merzenich et al. 1978; Nelson et al. 1980, Martuzzi et al. 2014, 2015; Sanchez-Panchuelo et al. 2010, 2012, 2014; Stringer et al. 2011, 2014, Akselrod et al. in revision**). Recent ultra-highfield (7T) MRI studies mapped the representations of single fingers in three subregions of S1 processing tactile information (BA 3b, BA 1 and BA 2) and in individual subjects (**Martuzzi et al. 2014, 2015; Sanchez-Panchuelo et al. 2010, 2012, 2014; Stringer et al. 2011, 2014**). Even more recently, the anatomical and functional properties of feet and leg representations within these three subregions of S1 have been described (**Akselrod et al. in revision**). However, little is known about the interactions between representations of multiple body parts within different subregions of S1.

In non-human primates, the anatomical connectivity among BA 3a, 3b, 1, and 2 has been previously investigated using tracing methods and showing bidirectional connections among them, however the strength of these connections was not quantified (**Jones et al. 1978; Shanks et al. 1985; Felleman & van Essen 1991**). More recently, it has been shown that within BA3b, finger representations are functionally and anatomically connected among each other (**Wang et al. 2013**), and that the functional and anatomical connectivity between BA 3b and BA 1 is stronger between representations of the same finger (**Ashaber et al. 2014; Wang et al. 2013; Chen et al. 2011**).

In humans, only few studies investigated rs-FC within somatosensory cortices (**Li et al. 2015; Long et al. 2014**). In particular, Long and colleagues (**2014**) considered a global "sensorimotor" cortex (lacking the distinction between S1 and M1) and showed that, based on rs-FC data, the sensorimotor cortex could be parcellated (along the latero-medial axis) into three regions corresponding to upper, middle and lower body parts. Similarly, Li and colleagues (**2015**) targeted the primary somatosensory cortex (lacking the distinction between different BAs) and proposed a parcellation of S1 into two regions (upper and lower body parts) based on rs-FC data. To date, there are no studies in humans directly investigating the rs-FC between independently mapped primary somatosensory representations of multiple body parts in different BAs and hemispheres.

The aim of the present study was to investigate the rs-FC between different body part representations within the three BAs (3b, 1 and 2) of S1 using 7T MRI. We first

applied a mapping procedure previously described in Martuzzi et al. **(2014, 2015)** or in Akselrod et al. (**in revision**). This method was used to localize, at the single subject level, the S1 representations of the right and left hands (each finger and the palm), as well as of the right and left lower limbs (big toe, small toe, heel, calf, thigh and hip), separately for BAs 3b, 1, and 2. We then analyzed the rs-FC between each pair of mapped S1 representations. We investigated whether the rs-FC network of S1 representations was functionally organized and structured according to the interhemispheric (left versus right hemisphere), interareal (BAs 3b, 1 and 2) and intersomatic (across somatotopic representations) organization of S1. First, we described at a macroscopic level how the different body representations are interconnected. Second, we tested whether the formed network was organized into functional modules by assessing the modularity of the network (**Sporns and Zwi, 2004; Bassett and Bullmore, 2006; Van den Heuvel and Sporns, 2011**). Third, we used graph visualization approaches to inspect the topographical organization of the network (**Kamada and Kawai, 1989; Six and Tollis, 2006**). In addition, we analyzed locally the rs-FC between neighboring representations across different BAs (interareal) and across different body part (intersomatic). Similarly to what was proposed by Wang and colleagues **(2013)**, we expect that the connectivity between homologous representations would be stronger than between non-homologous representations, and that the connectivity between adjacent representations within the same BA would be stronger compared to distant ones. Finally, we investigated the relationship between rs-FC and cortical distance, which is believed to be an important factor shaping the patterns of rs-FC between brain regions. As proposed in previous studies, we expect that rs-FC will decrease with increased cortical distance (**Salvador et al. 2005; Ercsey-Ravasz et al. 2013; Alexander-Bloch et al. 2013**).

3.2 Methods

3.2.1 Subjects

15 healthy subjects (5 females) aged between 18 and 39 years old (mean ± std: 24.3 ± 5.2 years) participated in the study. One participant was excluded due to excessive motion during MRI acquisition (up to 5mm of movement in the z-direction for this particular subject). All participants were right handed and had a right foot

preference, as assessed during an oral interview covering a subset (see Supp. Materials, table S1) of the Edinburgh Handedness Inventory (**Oldfield, 1971**). All subjects gave written informed consent, all procedures were approved by the Ethics Committee of the Faculty of Biology and Medicine of the University of Lausanne, and the study was conducted in accordance with the Declaration of Helsinki.

3.2.2 Mapping of somatosensory representations of hands, feet and legs

The detailed description of the procedure to map somatosensory representations has been described in previous publications (**Martuzzi et al. 2014, 2015; Akselrod et al. in revision**). Subjects were scanned while tactile stimulation was delivered to different regions on the body surface. Tactile stimulation consisted of a gentle manual stroking performed by an experimenter with his index finger and was delivered on a skin area of 3 cm^2. Six regions on both hands (thumb, index, middle, ring, small, palm) and 6 regions on both lower limbs (big toe, small toe, heel, calf, thigh and hip) were repeatedly stimulated. Four functional runs of approximately 12 min were acquired in pseudo-randomized order. The 6 regions of the same hand or lower limb were stimulated during the same functional run in a fixed order during 30 s each and with 4 repetitions. Rest periods of 10 s were interleaved between periods of tactile stimulation. All images were analyzed using the SPM8 software (Wellcome Department of Cognitive Neurology, London, UK). Preprocessing of fMRI data included slice timing correction, spatial realignment, and smoothing (FWHM=2mm). A GLM analysis was carried out to estimate the response induced by the stimulation of the different body parts. Independently for each limb, the somatotopic representations of each stimulated region were delimited as follow. The active voxels in the F-contrast (p<0.0001 uncorrected) located within the contralateral postcentral gyrus were used as a S1 mask. Then, based on a "winner takes all" approach, each voxel within the S1 mask was labeled as representing the body part demonstrating the highest t-score (vs. rest) for that particular voxel. In addition, probabilistic maps containing the separation of the postcentral gyrus into BAs 3b, 1 and 2 (**Geyer et al. 2000; Grefkes et al. 2001**) were used to separate the 3 homologous representations of each region. On rare occasions, the stimulation of a given body part did not elicit sufficient BOLD activity in one or more BAs to survive the "winner takes all" competition" leading to missing data. On average there was 2.64 ± 3.32 (mean ± std)

missing representations per subject. Data from missing representations were excluded from the subsequent analyses.

3.2.3 Data acquisition

Subjects were scanned in supine position. MR images were acquired using a short-bore head-only 7 Tesla scanner (Siemens Medical, Germany) equipped with a 32-channel Tx/Rx RF-coil (Nova Medical, USA). Functional images were acquired using a sinusoidal readout EPI sequence (**Speck et al. 2008**) and comprised 28 axial slices placed approximately orthogonal to the postcentral gyrus (in-plane resolution=1.3×1.3mm^2, slice thickness=1.3mm, no gap, TR=2s, TE=27ms, flip angle=75°, matrix size=160x160, FOV=210mm, GRAPPA factor=2). Following the mapping procedure for all four limbs (described above and in **Martuzzi et al. 2014, 2015; Akselrod et al. in revision)**, a 5 minutes (150 volumes) resting scan was acquired, during which subjects were asked to relax with the eyes closed and to refrain from performing any goal-oriented mental activity. During the resting run, cardiac and respiratory signals were acquired using the plethysmograph and the respiratory belt provided by the MR scanner manufacturer. These data were used for the rs-FC analysis.

For each subject, a set of anatomical images was acquired using an MP2RAGE sequence (**Marques et al. 2010**) in order to allow the separation of BAs (transformation of BAs probabilistic maps to native space) and for display purposes (TE = 2.63ms, TR = 7.2ms, TI1 = 0.9sec, TI2 = 3.2sec, TRmprage = 5sec). To aid coregistration between the functional and the anatomical images, a whole brain EPI volume was also acquired with the same inclination used in the functional runs (81 slices, in-plane resolution=1.3×1.3mm^2, slice thickness=1.3mm, no gap, TE=27ms, flip angle=75°, FOV=210mm, GRAPPA factor=2).

3.2.4 Functional connectivity data processing

rs-FC between all mapped representations, namely 72 Regions of Interest (ROIs; 12 body parts x 3 BAs x 2 hemispheres), was analyzed using the Conn toolbox (**Withfield-Gabrieli et al. 2012**). Images were first preprocessed using SPM8 (Wellcome Department of Cognitive Neurology, London, UK) by applying slice-

timing correction, realignment, smoothing (FWHM=2mm) and coregistration with the functional images of the previous runs (used to obtain the S1 maps). At each voxel, the BOLD signal was band-pass filtered (0.008-0.09 Hz). The cardiac and respiratory related components of the BOLD signal were estimated using the RETROICOR algorithm (**Glover et al. 2000**) and regressed out from the data. The average BOLD signal of white matter and cerebrospinal fluid (CSF) and the six estimated motion parameters were also included as nuisance regressors in the model. The bivariate temporal correlations between all combinations of pairs of ROI were calculated from the preprocessed BOLD time-courses of the resting state run. The obtained correlation coefficients were transformed into gaussian values by applying the Fisher transform (**Fisher, 1915**). This analysis was conducted in single subject native space.

To identify which ROIs were significantly functionally connected and construct a binary connectivity matrix, we computed t-tests on the Fischer coefficients to assess which connections were significantly different from 0 (at $p < 0.05$ corrected for multiple comparisons). The corrected p-value was calculated using a permutation test. In brief, all Fischer transformed correlations coefficients were pooled and 14 random samples were drawn to build a dataset. A two-tailed t-test was then computed. This procedure was repeated 5 million times. All t-statistics were sorted and the 95th percentile was selected as the statistical threshold (corresponding to $p = 0.00003$ uncorrected). A binary (unweighted) connectivity matrix was computed by applying the statistical threshold ($p < 0.05$ corrected for multiple comparisons) to the rs-FC data. Using this binary connectivity matrix, we first measured the connection densities within different subpart of the network. Second, we compared the modularity of the network across pre-defined parcellations of the network. Third, we inspected the topographical organization using graph visualization techniques. In addition, we analyzed the rs-FC within the local neighborhood of body representations to investigate functional interactions across body representations and across BAs. Finally, we analyzed the relationship between rs-FC and cortical distance.

3.2.5 Connection density analysis

We reported the connection densities for different subsets of nodes and connections, which can vary between 0 (if no connections are observed) and 1 (if

fully interconnected) and is calculated as the ratio between the number of observed significant connections and the total number of possible connections between the different body representations. The density of connections is reported for 1) the connections of the complete network; 2) the connections of the network formed by right and left hands (Fig.3.2B parts 1 to 3); 3) the connections of the network formed by right and left lower limbs (Fig.3.2B parts 4 to 10); 4) the connections of the networks formed by the right hand (Fig.3.2B part 1), left hand (Fig.3.2B part 2), right foot (Fig.3.2B part 4), left foot (Fig.3.2B part 5), right leg (Fig.3.2B part 6) and left leg (Fig.3.2B part 7) separately; 5) the interhemispheric connections between right and left hands (Fig.3.2B part 3); 6) the interhemispheric connections between right and left feet (Fig.3.2B part 8); 7) the interhemispheric connections between right and left legs (Fig.3.2B part 9); 8) the connections between feet and legs (Fig.3.2B part 10); 9) and the connections between hands and lower limbs (Fig.3.2B part 11).

3.2.6 Modularity analysis

To assess the modular organization of the network within primary somatosensory cortices, we compared different theoretical modular partitions of the network. The modularity of a network with nodes organized into multiple modules is measured as the difference between the fraction of connections running between nodes of the same module and the fraction of connections running between nodes of different modules (**Sporns and Zwi, 2004; Bassett and Bullmore, 2006; Van den Heuvel and Sporns, 2011**). We computed the modularity for the following possible partitions: 1) 2 modules divided into hands and lower limbs; 2) 3 modules divided into hands, feet and legs; 3) 4 modules divided into right hand, left hand, right lower limb and left lower limb; 4) 6 modules divided into right hand, left hand, right foot, left, foot, right leg, left leg; 5) 12 modules divided into right hand, left hand, right lower limb and left lower limb further divided into BAs 3b, 1 and 2; 6) 18 modules divided into right hand, left hand, right foot, left, foot, right leg, left leg further divided into BAs 3b, 1 and 2.

Additional graph theory metrics (degree distribution, "small-world" metric and "rich-club" metric) are reported in supplementary materials and in Fig.3.S1.

3.2.7 Topographical organization

The functional organization of the formed network was represented using graph visualization techniques. Such methods allow optimizing the spatial layout of the network based on the patterns of rs-FC. The resulting layout provides information about the functional organization of the considered network. We used two different types of layout to visualize the network. First with the 1D radial layout, nodes are placed on a circle and their position is optimized to minimize connections running close to the center of the circle (**Six and Tollis, 2006**). In the resulting layout, strongly inter-connected nodes are placed close to each other on the circle. Second with the 2D planar layout, each connection between pairs of nodes is simulated as a virtual spring and the position of nodes is optimized to minimize the energy the simulated springs (**Kamada and Kawai, 1989**). As for the 1D radial layout, strongly inter-connected nodes are placed close to each other. We inspected whether the clustering of nodes in the 1D radial layout and in the 2D planar layout was functionally organized with respect to interactions across hemispheres, across BAs and across body representations.

3.2.8 Functional connectivity in the local neighborhood

To quantify the local patterns of rs-FC across BAs (termed transversal axis) and across body representations (termed longitudinal axis), we carried out an additional analysis, where we considered the following connections: 1) the 1st and the 2nd neighboring representation within the same BA (denoted i+1 and i+2 respectively); 2) the homologous representation, the 1st and 2nd neighboring representations in the adjacent BA (denoted j, j+1 and j+2 respectively); 3) the homologous representation, the 1st and 2nd neighboring representations in the distal BA (denoted k, k+1 and k+2 respectively); resulting in 8 different "connection type". For each subject, we averaged the Z-scores of all connections corresponding to the same category of these 8 types of connections separately for right hand, left hand, right lower limb and left lower limb. These data were analyzed by computing a three-way repeated measures ANOVA with "connection type" (8 levels: i+1, i+2, j, j+1, j+2, k, k+1, k+2), "limb type" (2 levels: hand and lower limb), and "hemisphere" (2 levels: left and right hemispheres) as within-subject factors (resulting in a 8x2x2 ANOVA). Post-hoc

Tukey HSD tests were computed for pair-wise comparisons between the different levels of significant main effects and interactions between factors.

3.2.9 Functional connectivity and cortical distance

Finally, we analyzed the relationship between rs-FC and cortical distance by comparing different fitting function for these variables. We considered the following possibilities: a decaying linear function: $y = a*x+b$, a decaying exponential function: $y = a*e^{-x}$, or a decaying power law function: $y = a*x^{-b}$, with x and y representing respectively the 3D-euclidian distance and the strength of connectivity. The 3D-euclidian distance (in MNI space of individual subjects) between the centers of mass of each pair of representations was calculated individually and averaged across subjects. The t-values obtained from the previously described statistical analysis were used as measure of connectivity strength (the t-value is preferred to the average Z-score across subjects because it allows displaying the statistical threshold to distinguish between significant and non-significant connections). We compared the goodness of fit, R^2, between the different regressions to assess the best fitting function. As a control, we provide the same analysis between rs-FC and cortical volume in supplementary materials (the mean cortical volume between the considered pairs of nodes is calculated as a measure of cortical volume).

3.3 Results

An example of the result of the mapping procedure is presented in Fig.3.1 for a representative subject. The S1 somatotopic representations of right and left hands (thumb, index, middle, ring, little and palm), and of right and left lower limbs (big toe, small toe, heel, calf, thigh and hip) are projected on the flattened cortical surface. Corresponding maps were obtained for a total of 14 individuals. Using resting-state data, the rs-FC between the different body representations was calculated for each subject. Significant connections were established by computing one sample t-tests for each connection (with $p<0.05$ corrected for multiple comparisons). The resulting connectivity matrix is shown in Fig.3.2.
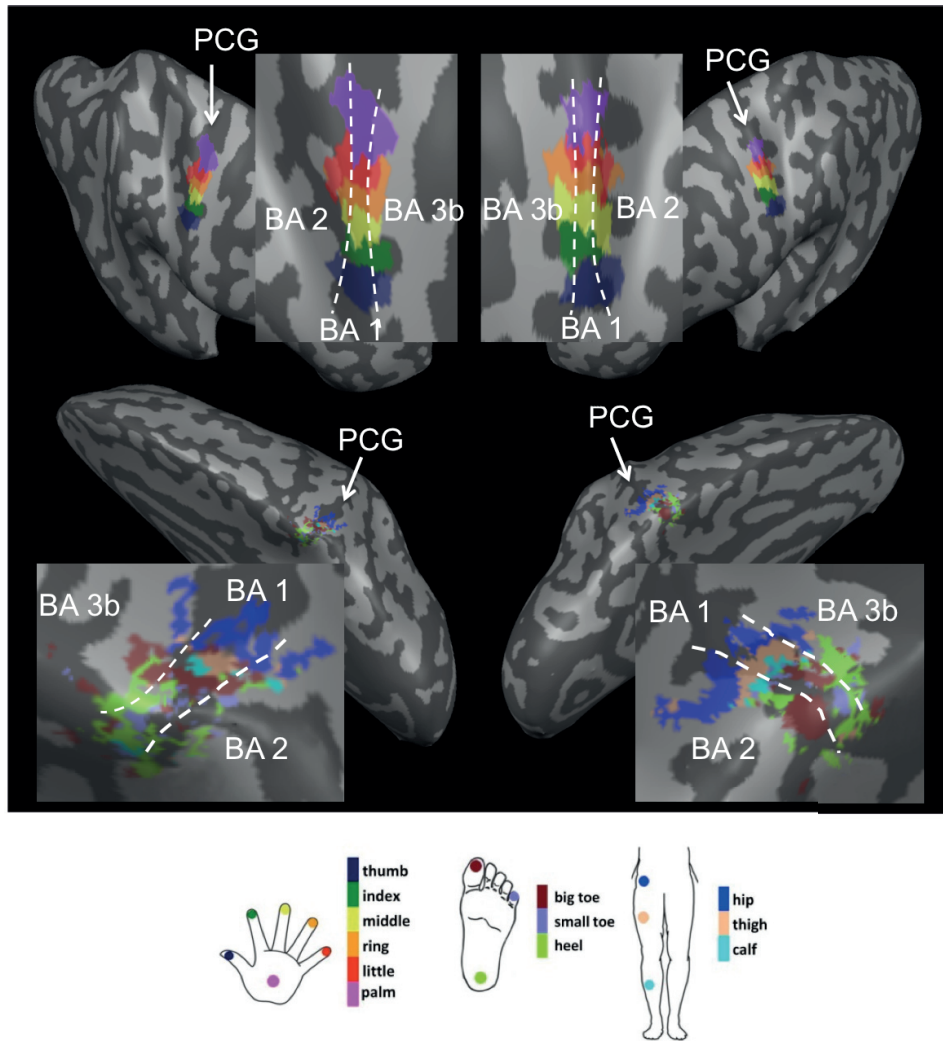
Fig.3.1 Somatotopic maps of a representative subject. The color-coded somatotopic maps are shown for a representative subjects. The representations of thumb, index, middle, ring, little, palm, big toe, small toe, heel, calf, thigh and hip are shown on a flattened surface rendering of the right hemisphere for the left hemisoma and on the left hemisphere for the right hemisoma.

3.3.1 Connection density analysis

The complete network had a connection density of 0.27, which can vary between 0 (no connections) and 1 (fully interconnected). The subnetwork composed of hand representations in S1 (Fig.3.2B parts 1-2-3) had a connection density of 0.72, and the subnetwork composed of lower limb representations in S1 (Fig.3.2B parts 4-5-6-7-8-9-10) had a connection density of 0.34. Considering separately within-foot, within-leg and within-hand connections, we found that foot and hand representations are more
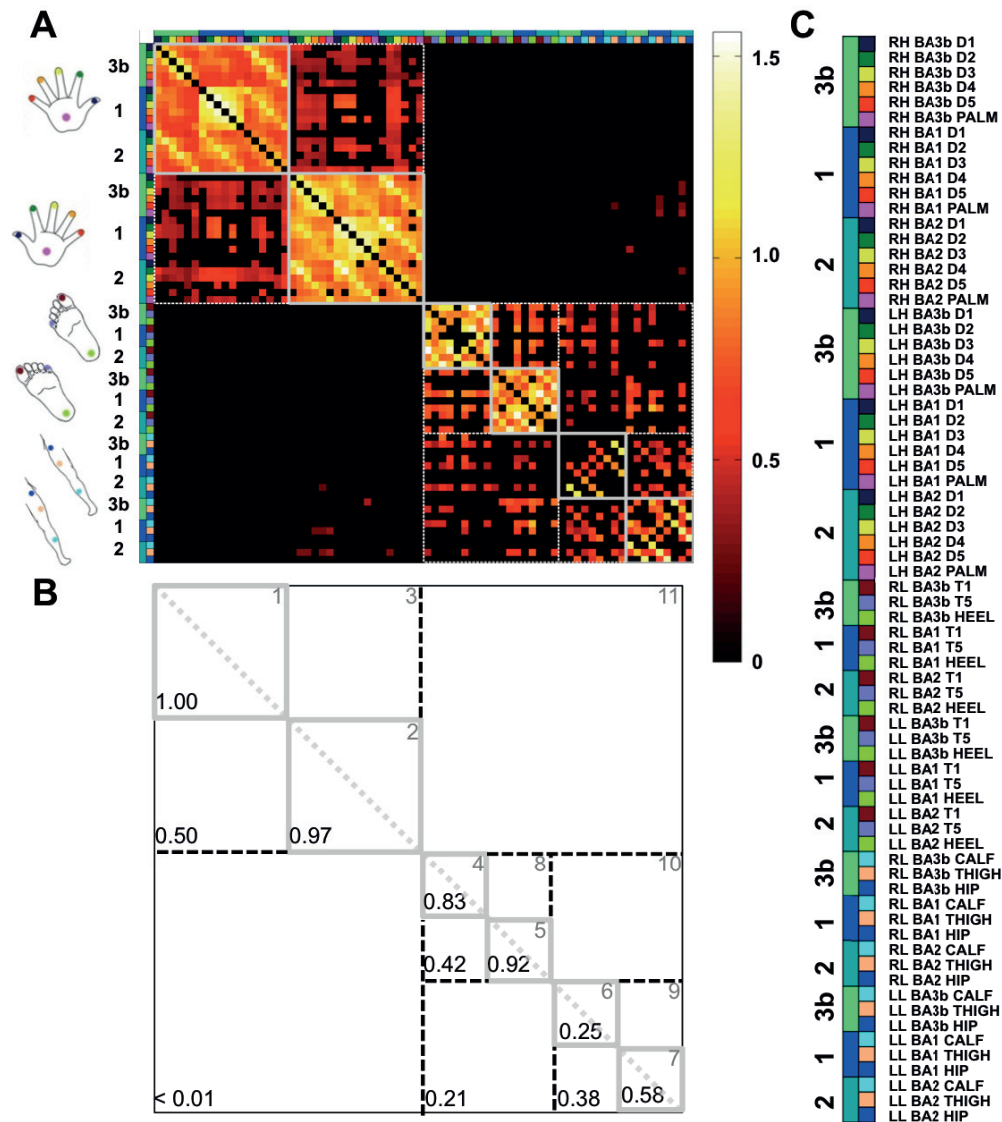
Fig.3.2 Functional connectivity matrix for all mapped body parts. A) The rs-FC matrix represents the strength of connection between each pair of representations. The average Z-scores (see Methods) are shown for significant connections (p < 0.05, corrected for multiples comparisons) with a color-code ranging from black and red for weak connections to yellow and white for strong connections. The first and second rows and lines are colorcoded to represent the different body part and BAs. **B)** The rs-FC matrix is replicated to highlight the different segments of the matrix (upper triangular part) and their respective connection density (lower triangular part). **C)** A legend with the color-code is provided (D1=thumb, D2=index, D3=middle, D4=ring, D5=little, T1=big toe, T5=small toe).

densely interconnected among themselves compared to the leg representations. Indeed, connection density was 1.00 for the right hand (Fig.2B part 1) and 0.97 for the left hand (Fig.2B part 2), 0.83 for the right foot (Fig.2B part 4), 0.92 for the left foot (Fig.2B part 5), and 0.25 for the right leg (Fig.2B part 6), 0.58 for the left leg (Fig.2B part 7). We found interhemispheric connectivity between representations of both

hands (connection density=0.50, Fig.3.2B part 3) and between representations of both feet (connection density=0.42, Fig.3.2B part 8), as well as between leg representations (connection density=0.38, Fig.3.2B part 9). This shows that interhemispheric connectivity is weaker than intrahemispheric connectivity. Finally, we found lower connection density between foot and leg representations (0.21, Fig.3.2B part 10) and almost no significant connections between hands and lower limb representations (<0.01, Fig.3.2B part 11). This extremely low connectivity between hands and lower limbs suggests that the network is composed of at least 2 sub-modules containing the representations of hands in a first cluster and the representations of feet and legs in a second cluster. In addition, we did not find a high connection density between feet and legs, suggesting a possible functional clustering between proximal and distal regions of the lower limbs.

To summarize we found that hands and feet representations are densely interconnected among themselves compared to leg representations. In addition, the low connectivity between hands and lower limbs representations suggests the presence of at least two segregated sub-networks.

3.3.2 Modularity analysis

We computed the modularity for 3 different theoretical partitions of the nodes. First, a partition into 2 modules composed of hands and lower limbs representations was tested and this architecture resulted in a modularity of 0.42. We tested a partition into 3 modules composed of hands, feet and legs representations with a modularity of 0.38. We tested a partition into 4 modules composed of right hand, left hand, right lower limb and left lower limb representations, and found a modularity of 0.36. We tested a partition into 6 modules composed of right hand, left hand, right foot, left foot, right leg and left leg, which resulted in a modularity of 0.32. Finally, the partitions into 4 and 6 modules were further divided into BAs 3b, 1 and 2 leading to partitions into 12 and 18 modules. We found a modularity of 0.09 and 0.07 respectively for the partitions into 12 and 18 modules. This result shows that a partition into two modules (hands and lower limbs representations respectively) maximizes the modularity. However, the partition considering the feet and legs separately and the partition considering the right and left body parts separately also

led to high modularity, which could suggest a further distinction into functional sub-modules.

To summarize this analysis provides a quantitative measure supporting the previously reported observation that the interactions between hand and lower limb representations are very weak leading to the segregation of these representations into two independent networks.

3.3.3 Topographical organization

We used graph visualization methods to investigate the functional organization of the network. First, we simulated the network with a 1D radial layout, which optimizes the sequence of nodes in order to form clusters of densely and strongly interconnected nodes (**Six and Tollis, 2006**). The resulting graph is presented in Fig.3.3A. As shown in our previous analyses, the most prominent segregation is between hands and lower limbs with almost no connections between the two. In addition, we observe in the sequence of nodes that representations of left hand, right hand, left foot, right foot and both leg are grouped respectively into 5 distinguishable clusters (right and left leg nodes are interleaved). We also analyzed whether S1 representations appear in the preferentially according to interareal grouping (across BAs between homologous representations) or according to intersomatic grouping (across body representations within the same BA). We measured the average distance along the sequence between the positions of homologous representations across BAs and between the positions of body representations within the same BA (Fig.3.3B). We found that within the 2 clusters formed by right and left hand representations respectively, the distances between body parts representation within the same BA were smaller compared to distances between homologous representations across BAs. This was the opposite for lower limbs. This shows that hand representations were preferentially grouped according to intersomatic interactions and lower limbs were preferentially grouped according to interareal interactions, although it was not statistically quantified. We note that the difference between interareal and intersomatic grouping was small for hand representations, showing that they are also organized according to interareal interactions. Lower limbs representations were rather strictly organized with respect to intersomatic interactions.
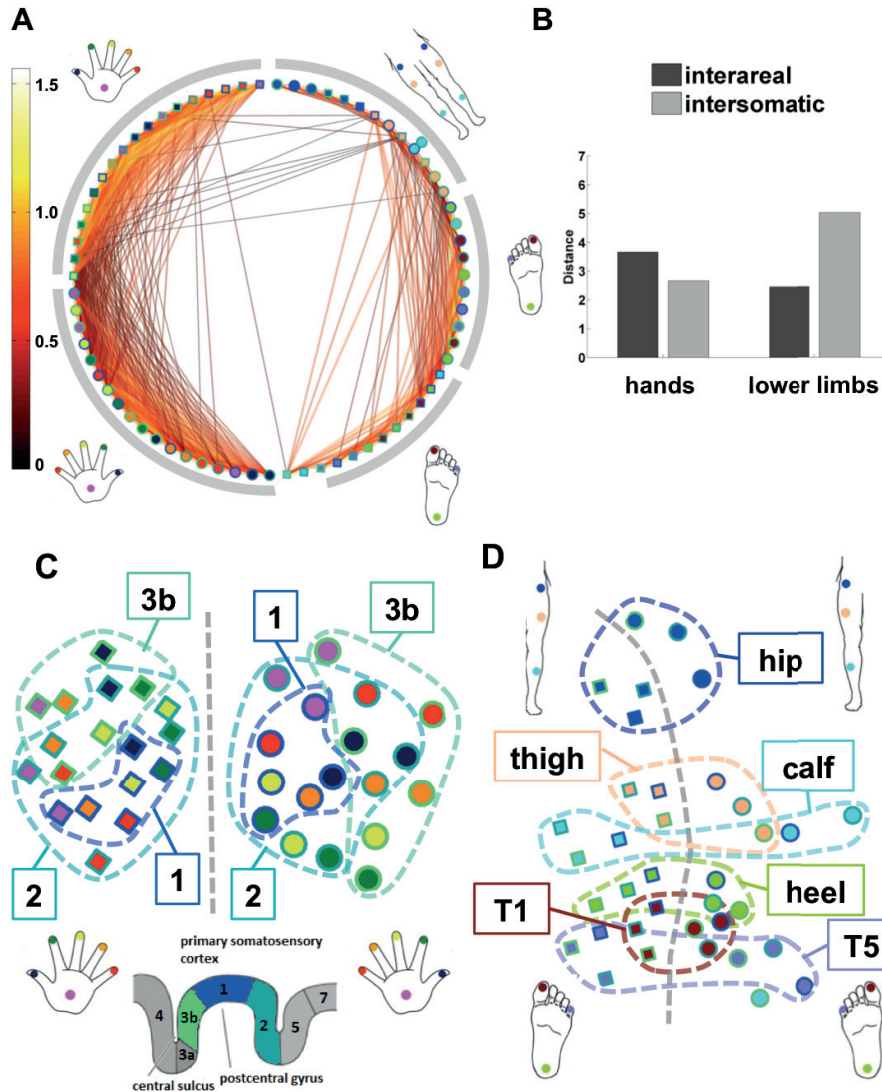
Fig.2.3 Topographical organization of S1 representations based on functional connectivity. A) The S1 network is displayed using a 1D radial layout. The position of nodes is optimized to cluster highly interconnected nodes together. Hands and lower limbs representation share almost no connection. The right hand, left hand, the right foot, the left foot and both legs appear in separate clusters. Edges are color-coded based on the strength of connection ranging from black and red for weak connections to yellow and white for strong connections. **B)** The distances in the 1D radial layout according to interareal and intersomatic grouping are shown separately for hands and lower limbs. **C-D)** The S1 network is displayed using a 2D planar layout. Each connection is simulated using a virtual spring. Strongly interconnected nodes are located closer in space. Edges are not displayed for clarity. **C)** The network formed by hands representations is presented. Nodes belonging to the same BA are highlighted by the colored dotted lines. **D)** The same graph is simulated for lower limb representations. Nodes representing the same body part are highlighted by the colored dotted lines. For graphs **A-C-D**, nodes are color-coded such that the inside of the node corresponds to the represented body part and the outline of the node corresponds to the BA. Circles and diamonds represent right and left body parts respectively.

Second, we simulated the network using a 2D planar layout, which optimizes the position of nodes such that nodes being densely and strongly interconnected among each other are placed closer to one another (**Kamada and Kawai, 1989**). We simulated 2 graphs, one for hands and one for lower limbs. The resulting graphs are presented in Fig.3.3C and in Fig.3.3D. For the hands (Fig.3.3C), we observed 2 distinct clusters formed by the representations of the right and left hands respectively. Within each of these 2 clusters, nodes belonging to the same BA appeared closer to each other (intersomatic interactions). We note that nodes representing the same body part appeared also close to each other (interareal interactions). For the foot and leg representations (Fig.3.3D), an interhemispheric separation was found similarly to the hands. However, there was no apparent clustering of nodes representing body parts within the same BA (intersomatic interactions), and there was a strong clustering between homologous representations across BAs (interareal interactions). In addition, the macroscopic arrangement of clusters formed by homologous representations was reminiscent of the somatotopic organization of these body representations (hip – thigh – calf – heel – toes appeared in an orderly manner). We note that hip representations appeared segregated from other leg representations.

To summarize, the visualization of the functional organization of the network highlighted patterns of interhemispheric, interareal and intersomatic interactions. In particular, we showed that patterns of rs-FC within hand representations were preferably organized with respect to intersomatic clustering, but also appeared clustered according to interareal interactions. Patterns of rs-FC within lower limb representations were preferably organized with respect to interareal interactions. The interhemispheric clustering was pronounced for all body parts.

3.3.4 Functional connectivity in local neighborhood

The goal of this analysis is to investigate the patterns of local rs-FC between a given somatosensory representation and the surrounding representations and how these patterns could differ across limbs (representations of hands compared to lower limbs) or across hemispheres (representations of right body parts in the left hemisphere compared to representations of left body parts in the right hemisphere). In particular, we were interested in highlighting the patterns of transversal rs-FC

between homologous representations across BAs (connections j and k) and of longitudinal rs-FC across body parts representations with the same BA (connections i+1 and i+2). The results of this analysis are presented in Fig.3.4, where the strength of connectivity in the local neighborhood of representations is shown in bar plots separately for right hand, left hand, right lower limb and left lower limb. The corresponding patterns of transversal rs-FC (across BAs) and of longitudinal rs-FC (across body parts) are graphically depicted next to the plot. Qualitatively, transversal rs-FC was strong towards the adjacent and distant BAs (connection j and k) and even stronger towards the distant BA compared to the adjacent BA for right body parts. Transversal rs-FC was similar for hands and lower limbs. Longitudinal rs-FC decreased towards more distant neighboring representations for hands and lower limbs (i+1 > i+2), although longitudinal rs-FC was stronger for hand representations compared to lower limb representations.

To statistically quantify differences within the local networks of rs-FC, we analyzed the data using a three-way repeated measures ANOVA with "connection type" (8 levels corresponding to the connectivity with the 1st and 2nd neighboring representations in the same BA, denoted i+1 and i+2; with the homologous, 1st and 2nd neighboring representations in the adjacent BA, denoted j, j+1 and j+2; and with the homologous, 1st and 2nd neighboring representations in the distal BA, denoted k, k+1, k+2), "limb type" (2 levels corresponding to hands and lower limbs) and "hemisphere" (2 levels corresponding to left and right hemispheres) as within-subject factors. Post-hoc Tukey HSD comparisons were used for pairwise comparisons between different levels of significant factors. The statistical results are summarized in Fig.3.S2.

The statistical analysis showed a significant main effect of "connection type" ($F_{7,91}=76.5$ p<0.001, Fig.3.S2A). Along the transversal axis, surprisingly we found that rs-FC between homologous representations is stronger towards the distant BA compared to the adjacent BA (i.e. k > j p<0.001). This result is further explored below regarding the presence of interactions between the main factors. Along the longitudinal axis, we found that rs-FC is stronger towards the 1st neighbor within the same BA compared to the 2nd neighbor within the same BA (i.e. i+1 > i+2, p<0.001), this was independent of "limb type" or "hemisphere".
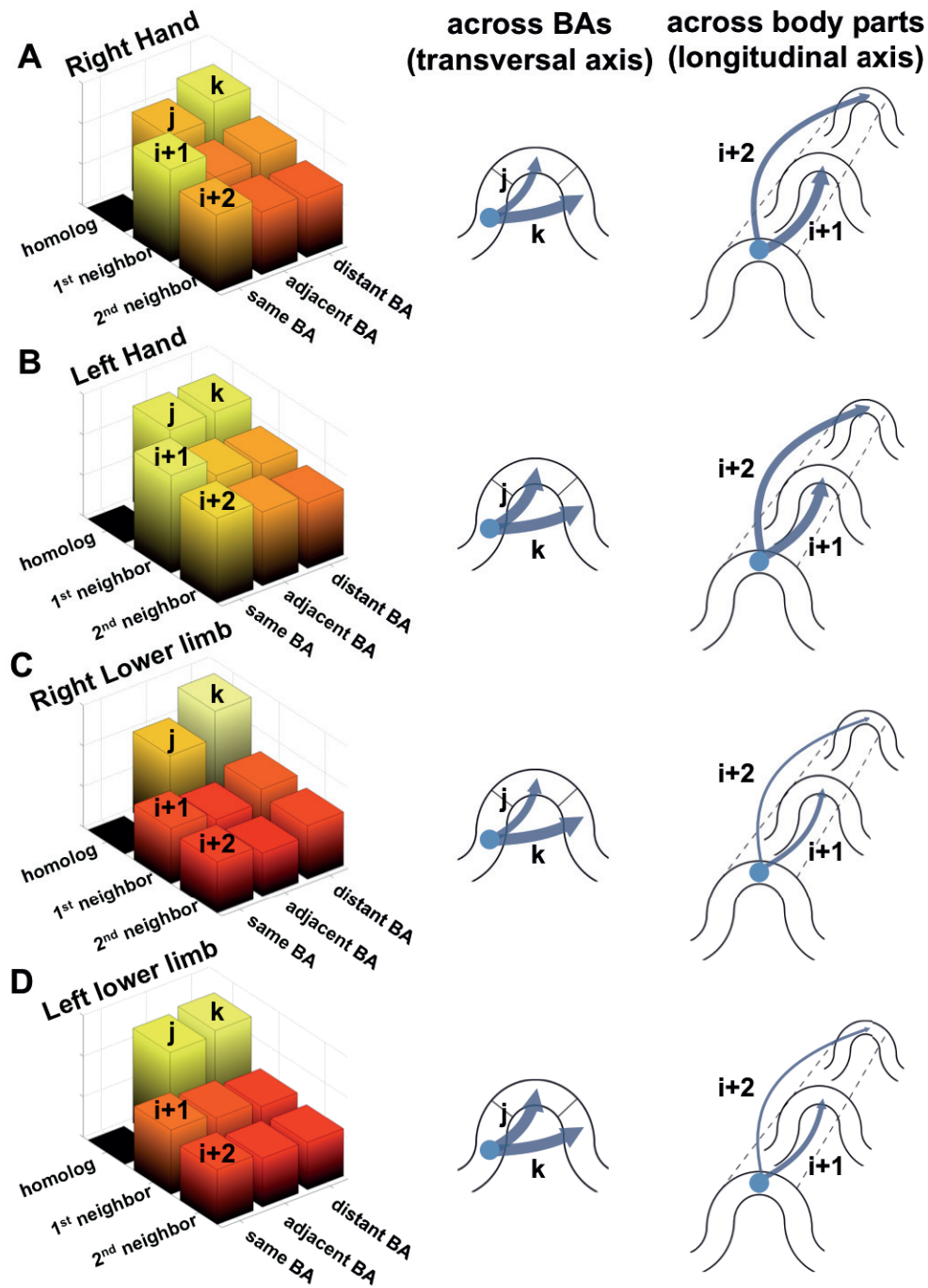
Fig.3.4 Functional connectivity in the local neighborhood of S1 representations. The connection strength (average Z-scores) within the local neighborhood of the considered representations (see Methods) is shown in the 3D bar plot separately for right hand (**A**), left hand (**B**), right lower limb (**C**), left lower limb (**D**). The connection strength is color-coded and ranges from black and red for weak connections to yellow and white for strong connections. Next to the 3D bar plots, a graphical summary of the local network organization is represented. Although rs-FC is not directional, arrows are used to represent connections for clarity. The thickness of arrows is proportional to the connection strength.

In addition, we found a main effect of "limb" ($F_{1,13}$=4.9, p=0.04, Fig.3.S2B) showing that rs-FC was stronger for hand representations compared to lower limb representations independently from "connection type" or "hemisphere" (p=0.04), which is reminiscent of the results described previously in the analysis of connection density.

Importantly, we found a significant interaction between "connection type" and "limb type" ($F_{7,91}$=14.5, p<0.001, Fig.3.S2C). Post-hoc Tukey HSD comparisons showed that rs-FC across body representations (i+1, i+2, j+1, j+2 and k+1) was stronger for hands compared to lower limbs (all p<0.01). This result indicates that rs-FC along the transversal axis is strong for hand and lower limb representations, while rs-FC along the longitudinal axis is only present for hand representations.

Finally, we found a significant interaction between "connection type" and "hemisphere" ($F_{7,91}$=8.2, p<0.001, Fig.3.S2D). Post-hoc Tukey HSD comparisons revealed that rs-FC towards the homolog and 1st neighbor in the adjacent BA (j and j+1) was stronger in the left hemisphere (right body parts) compared to the left hemisphere (left body parts) (all p<0.001). This result suggests that the pattern of rs-FC previously observed during the analysis of the main effect of "connection type", namely that rs-FC towards the distant BA is stronger compared to the adjacent BA, is different for the left and the right hemisphere. In particular, connections towards adjacent and distant BAs are similar for left body parts represented in the right hemisphere, while connections towards the distant BA are stronger compared to connections towards the adjacent BA for right body parts represented in the left hemisphere. We note that regardless of this difference, transversal rs-FC was significant both towards adjacent and distant BAs for all body parts.

Taken together this local network analysis highlighted important patterns of rs-FC along the transversal and longitudinal axes, which differed between hands and lower limbs, and differed between right and left body parts. Transversal rs-FC between homologous representations across BAs was strong and present for all body parts (right hand, left hand, right lower limb and left lower limb). Longitudinal rs-FC followed a gradient of decreased connectivity towards more distant representations for all body parts. Interestingly, transversal rs-FC was stronger towards the distant BA compared to the adjacent BA for right body parts representations, while transversal rs-

FC towards adjacent and distal BAs was similar for left body parts representations. For hand representations, rs-FC was strong along both longitudinal and transversal axes. For lower limb representations, rs-FC was only present along the transversal axis.

3.3.5 Functional connectivity and cortical distance

Finally, we investigated the overall relation between rs-FC and cortical distance. Strength of connection between each pair of representations (measured by the t-values calculated with the statistical analysis carried out on the Z-scores of all participants) is plotted as a function of the 3D-euclidian distance between each pair of representations in Fig.3.5. Qualitatively, the connectivity is decreasing with increased distance between the representations. The best fitting function describing this relationship is a power law with a negative exponent ($y = a*x^{-b}$, with a=25.48 and b=0.63, fitting: R^2=0.44, RMSE=2.14), which we compared with a decaying exponential function and a linear function (R^2=0.29 and R^2=0.13 respectively). We note that the connectivity between pairs of representations with similar cortical distance can largely vary as shown in Fig.3.5. For example, when comparing within hand connections (plotted in red in Fig.3.5) with within lower limb connections (plotted in green in Fig.3.5), one can see that connections with relatively small inter-nodes distances can have a large range of connectivity strength (up to a factor of 4 for similar cortical distance). Similarly, when inspecting between limbs connections (i.e. connections between hands and lower limbs, plotted in brown in Fig.3.5), one can see that the cortical distance between nodes with similar connectivity strength can also largely vary (up to a factor of 3 for similar connectivity strength). The connections between representations of the right and left hands are stronger than predicted by their cortical distance, as shown by the data for these connections being located above the fitting curve (plotted in orange in Fig.3.5). These results suggest that although the observed pattern of connectivity is partially related to the cortical distance between the different representations, this factor cannot entirely account for the observed patterns of rs-FC. Considering that the ROIs were not equal in size, we investigated a potential relationship between connectivity and the average volume of each pair of representations to rule out the possibility that larger ROIs may show a stronger connectivity because of the denoising effect induced by the averaging method; we

76
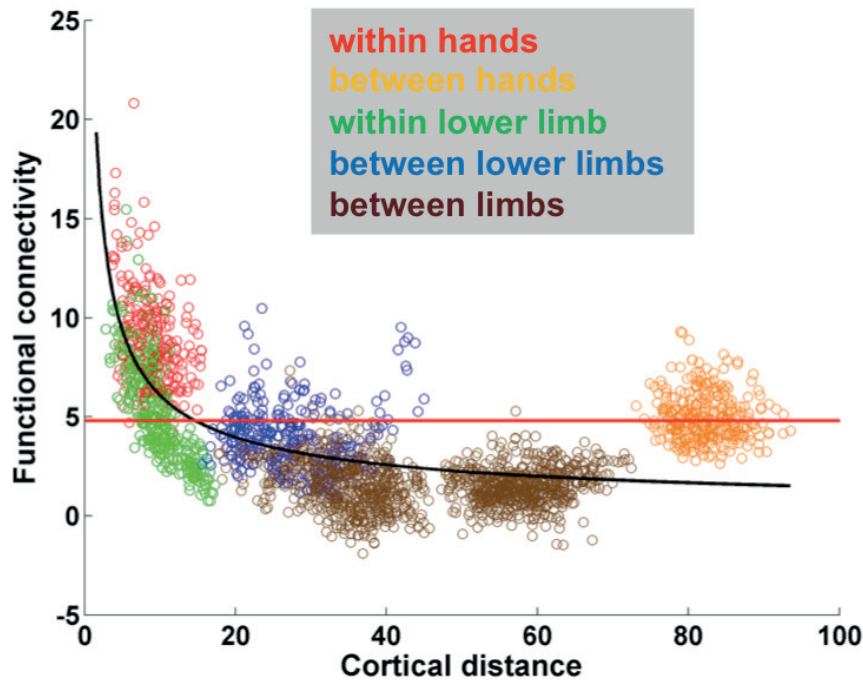
Fig.3.5 Functional connectivity and cortical distance. The overall relationship between functional connectivity (T-value) and cortical distance (3D-euclidian distance) is shown in the scatter plot. Data points corresponding to within hands connections are shown in red, within lower limbs connections are shown in green, between hands connections are shown in orange, between lower limbs connections are shown in blue, and between limbs connections are shown in brown. The best fitting function is a power law with negative exponent ($y = a*x^{-b}$, with a=25.48 and b=0.63, fitting: R^2=0.44, RMSE=2.14).

found no evidence for such a relation (all R^2<0.02 for tested fitting functions, Fig. 3.S3, see Supp. Materials).

To summarize we found a statistically strong relationship between rs-FC and cortical distance. However, this relationship does not provide a one to one mapping between rs-FC and distance, as it was shown that a large range of connectivity strength could be found between pairs of nodes with similar distance and that reciprocally pairs of nodes with varying cortical distance can have similar rs-FC.

3.4 Discussion

We applied a previously described mapping method at ultra-high field MRI (7T) (**Martuzzi et al. 2014, 2015; Akselrod et al. in revision**) to identify the maps of 24 body parts within BA 3b, 1 and 2, leading to a total of 72 separate body part representations in human S1. Using resting-state data, we investigated the functional

connectivity (rs-FC) between these representations, in order to provide a description of the network properties of human S1 maps. Our analyses revealed patterns of rs-FC across hemispheres, BAs and body representations, which differed across hands, feet and legs. To the best of our knowledge, this is the first study characterizing the functional properties of the human primary somatosensory network with respect to hand, foot and leg representations in 3 different BAs of S1.

3.4.1 Functional segregation between hands and lower limbs

Based on results from our analyses of connection density, network modularity and graph optimization, we identified an important segregation between representations of hands on one side and the representations of feet and legs on the other side, suggesting the presence of at least two functional S1 sub-networks processing tactile information independently. Our data suggests that lower limb representations could be further functionally parcellated into submodules representing feet and legs, but the most prominent segregation was between upper and lower body parts. This result is consistent with previous reports showing that based on resting-state data, S1 can be parcellated into at least two sub-networks, namely upper and lower body parts (**Li et al. 2015; Long et al. 2014**). Taken together, these results suggest a drastic dichotomy in the functional organization of S1 along the latero-medial axis and can possibly be linked to the lack of interactions between upper and lower body parts in daily life activities.

We note that such segregation was not present between representations of right and left body parts. On the contrary, our analyses highlighted the presence of interhemispheric connectivity as reported in previous studies (**Lowe et al. 1998; Salvador et al. 2005; Nir et al. 2008**). In particular, strong connectivity was found between both hands, both feet and both legs representations. However, interhemispheric connectivity was weaker compared to intrahemispheric connectivity.

3.4.2 Different functional organization between hand, foot, and leg representations

Our results provided further evidence for an important functional specialization of S1 representations with respect to the observed patterns of rs-FC across body parts.

First, we showed that within-hand and within-foot representations are highly interconnected among themselves, which was not the case for within-leg representations. Furthermore, our analysis of graph optimization showed that the network of hand representations was functionally organized according to interareal and intersomatic interactions. Contrastingly, the network of lower limb representations was mostly organized according to interareal interactions. Finally, hip representations appeared rather disconnected from the rest of the lower limbs, possibly suggesting its inclusion in a different functional network. Collectively, we believe that these results reflect different organizational principles for tactile processing within hand, foot and leg representations with respect to their respective functions.

3.4.3 Functional connections in the local neighborhood of somatosensory representations

Our graph optimization analysis showed at a macroscopic level that interareal and intersomatic interactions differed between hands and lower limbs. In addition, we analyzed and quantified the same features, but at a local scale. By investigating in detail the local connectivity across representations and across BAs, we found specific patterns of longitudinal (across representations) and transversal (across BAs) connectivity as it was reported previously in non-human primate studies (**Ashaber et al. 2014; Chen et al. 2011; Wang et al. 2013**). The longitudinal rs-FC between representations is decreasing with increased distant between representations along these body maps, with connections between neighboring representations being the strongest. In addition, longitudinal rs-FC was strong for hand representations, but weaker for lower limb representations. On the contrary, transversal rs-FC was strong and present for all body parts. To our knowledge, a single study directly quantified the connectivity across finger representations and across BAs in non-human primate somatosensory cortex (**Wang et al. 2013**). Those authors combined measures of structural, functional and BOLD-resting state connectivity and reported two axes of information flow, one across BA 3b and BA 1 for homologous representations of the same finger, and one within BA 3b across digits. In addition, they reported weaker non-finger-specific connections across BA 3b and BA 1. Our results suggest a similar local pattern of connectivity in primates and humans and extend these findings to the
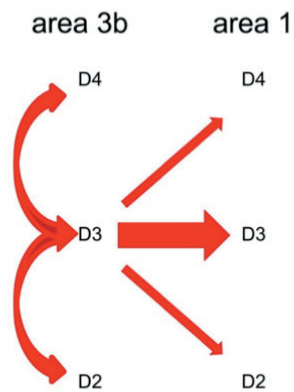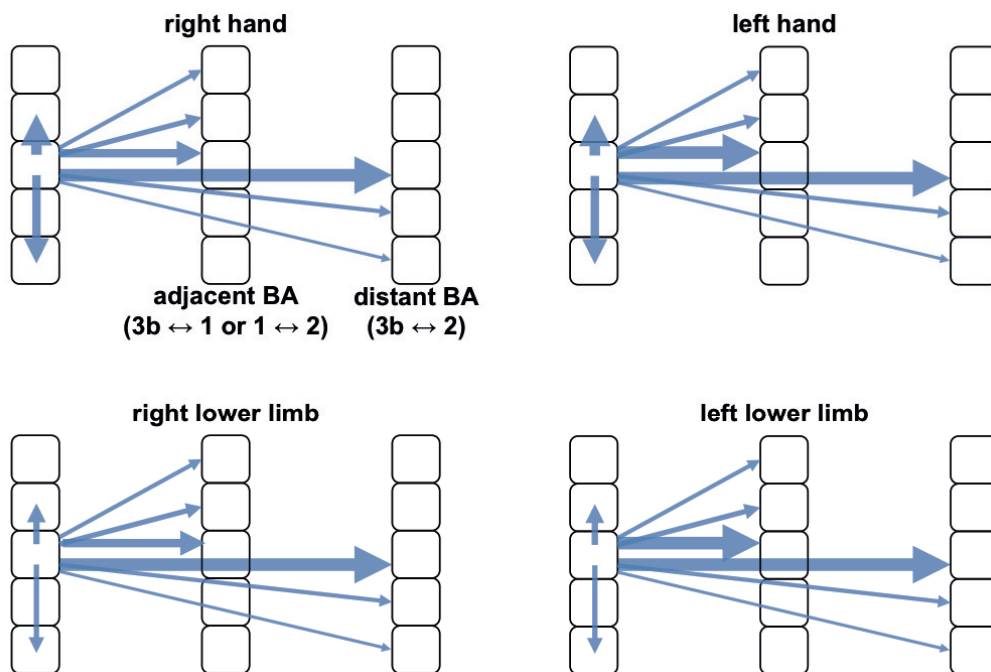
Fig.3.6 Comparison between monkeys and humans. We compared the results reported in the present study with results from the study by Wang and colleagues (**2013**). The authors investigated the local patterns of connectivity between multiple digits within BA3b and BA1 in the squirrel monkey. Our study extends these findings to humans, to the connectivity between BA 1 and BA 2, as well as to the connectivity of other body part representations, such as the lower limbs.

connectivity between BA 1 and 2, as well as to the connectivity of other body representations such as lower limbs (Fig.3.6).

3.4.4 Functional connectivity and cortical distance

Because of the somatotopic organization of S1 and the structural constrains of neuronal connections (**Shanks et al. 1985**), the cortical distance between representations is an important factor shaping the pattern of S1 connectivity. As shown in the analysis of local connectivity, it is expected that representations located more closely in space, which represents neighboring body parts, have stronger connectivity compared to distant ones. In addition, rs-FC should naturally decrease with increased distance because the noise between distant cortical areas is less correlated. Such relationship between rs-FC and cortical distance was highlighted in our analysis, showing that rs-FC decreases with greater distance between somatosensory representations following a negative power law. Previous studies reported similar relationship between these variables (**Ercsey-Ravasz et al. 2013; Alexander-Bloch et al. 2013; Salvador et al. 2005**). In particular, Ercsey-Ravasz and colleagues (**2013**) showed that in the macaque brain, the weights of connection decrease with greater distance following a decaying exponential function. In humans, Alexander-Bloch and colleagues (**2013**) found that rs-FC decreases as a function of distance following a decaying exponential law. Similarly, Salvador and colleagues (**2005**) found that the relationship between rs-FC and cortical distance was best approximated by an inverse square law. These studies investigated brain connectivity at a large scale considering whole brain data sets. We show here that such global principle is also present at shorter scales.

Importantly, we observed large differences in functional connection strength between pairs of representations with similar cortical distance (and vice versa), implying that cortical distance cannot be the only factor shaping the patterns of rs-FC and that other factors such as the functional specialization of different body parts and the nature of tactile stimulation they receive should be considered.

3.5 Conclusions

Using ultra-high field (7T) MRI, we described for the first time the finely tuned patterns of rs-FC across the multiple S1 representations of hands, feet and legs in humans. We propose that the observed patterns of connectivity reflect the finely tuned organization of somatosensory cortices to process tactile information efficiently and

differently based on the functional role of the represented body parts. In particular, the low relevance of tactile information processed from the skin on the legs in daily life results in a rather low connectivity of these regions compared to hands and feet. Furthermore, the necessity of integrating information from simultaneously used body parts, like the different parts of the feet, or from independently used body parts, like the fingers, results in different type of organization of information transfer across different representations, BAs and hemispheres. Based on the cumulated evidence we provided in this study, we propose that the patterns of rs-FC within primary somatosensory cortices are highly constrained by anatomical factors (i.e. cortical distance), but also depend on the functional role of different body parts and their functional interactions during everyday activities. Similar findings have been described for M1 connectivity (**Volz et al. 2015**), where the authors showed that the interhemispheric coupling varied a across different body parts and was related to the respective functions of these different body parts. On the opposite, patterns of rs-FC within primary visual areas follow a strict rule of spatial proximity (**Raemaekers et al. 2014**).

3.6 Supplementary Materials

3.6.1 Additional graph theory analysis

Brain networks typically exhibit "small-world" (**Sporns and Zwi, 2004; Bassett and Bullmore, 2006,**) and "rich-club" (**Van den Heuvel and Sporns, 2011**) properties. A small-world topology is characterized by densely interconnected nodes being organized into modules (as measured by the clustering coefficient), and by an efficient information transfer between the nodes of the network (as measured by the shortest path length or node-to-node distance) (**Sporns and Zwi, 2004; Bassett and Bullmore, 2006, Van den Heuvel et al. 2008**). In addition, the communication between the different modules is mediated by a set of hubs belonging to different modules and highly interconnected among them, the so-called "rich-club" (**Van den Heuvel and Sporns, 2011**).

Small-world properties can be assessed by computing the "clustering coefficient" and the "shortest path length" and by comparing these values to simulated random networks (based on the Erdös-Rényi model of random graphs, **Erdös and Rényi,**

1959) with matched edge density. The clustering coefficient is calculated as the proportion of observed connections with respect to the maximum possible number of connections in the local neighborhood of a node (i.e. the nodes connected to the considered node), this value is calculated for each node and then averaged across all nodes and denoted C. The shortest path length represents the minimal number of hopes between two nodes. This value is calculated for each pair of nodes and averaged and denoted L. The scalar small-worldness measure: $\sigma = \gamma/\lambda$ (with the scaled clustering coefficient: $\gamma = C/C_{rand}$, and the scaled shortest path length: $\lambda = L/L_{rand}$) attributes small-world properties to the considered network if larger than 1 (**Sporns and Zwi, 2004; Bassett and Bullmore, 2006**). The average clustering coefficient (C = 0.76) and average shortest path length (L = 2.31) of the network were calculated based on the binary connectivity matrix. The resulting small-world parameters (clustering coefficient scaled to matched random network: $\gamma = C/C_{rand} = 2.85$, shortest path length scaled to matched random network: $\lambda = L/L_{rand} = 1.33$, scalar small-worldness measure: $\sigma = \gamma/\lambda = 2.14$) suggest that the observed network has "small-world" properties, being characterized by a high clustering and a low shortest path length.

Rich-club organization can be measured with the rich-club coefficient $\Phi(k)$, which is the ratio between the number of observed connections and the number of possible connections within the subnetwork formed by nodes with degree larger than k (computed for each possible value of degree k, **Van den Heuvel and Sporns, 2011**). This value can be normalized to a simulated random network (**Erdös and Rényi, 1959**) and suggests a rich-club organization if larger than 1 for high values of k. The rich-club metric is shown in Fig.3.S2 and suggests a rich-club organization in our data. In fact, it seems that most nodes corresponding to hand and foot representations belong to the rich-club. This result is mostly driven by within-hands and within-feet representations being densely interconnected, forming groups of nodes with high degrees and strongly interconnected among themselves.

These results suggest that the network within somatosensory cortices share similar organizational principles with other previously studied brain networks (**Sporns and Zwi, 2004; Bassett and Bullmore, 2006; Achard et al. 2006; He et al. 2007; van den Heuvel et al. 2008; Guye et al. 2010; Van den Heuvel and Sporns, 2011).**
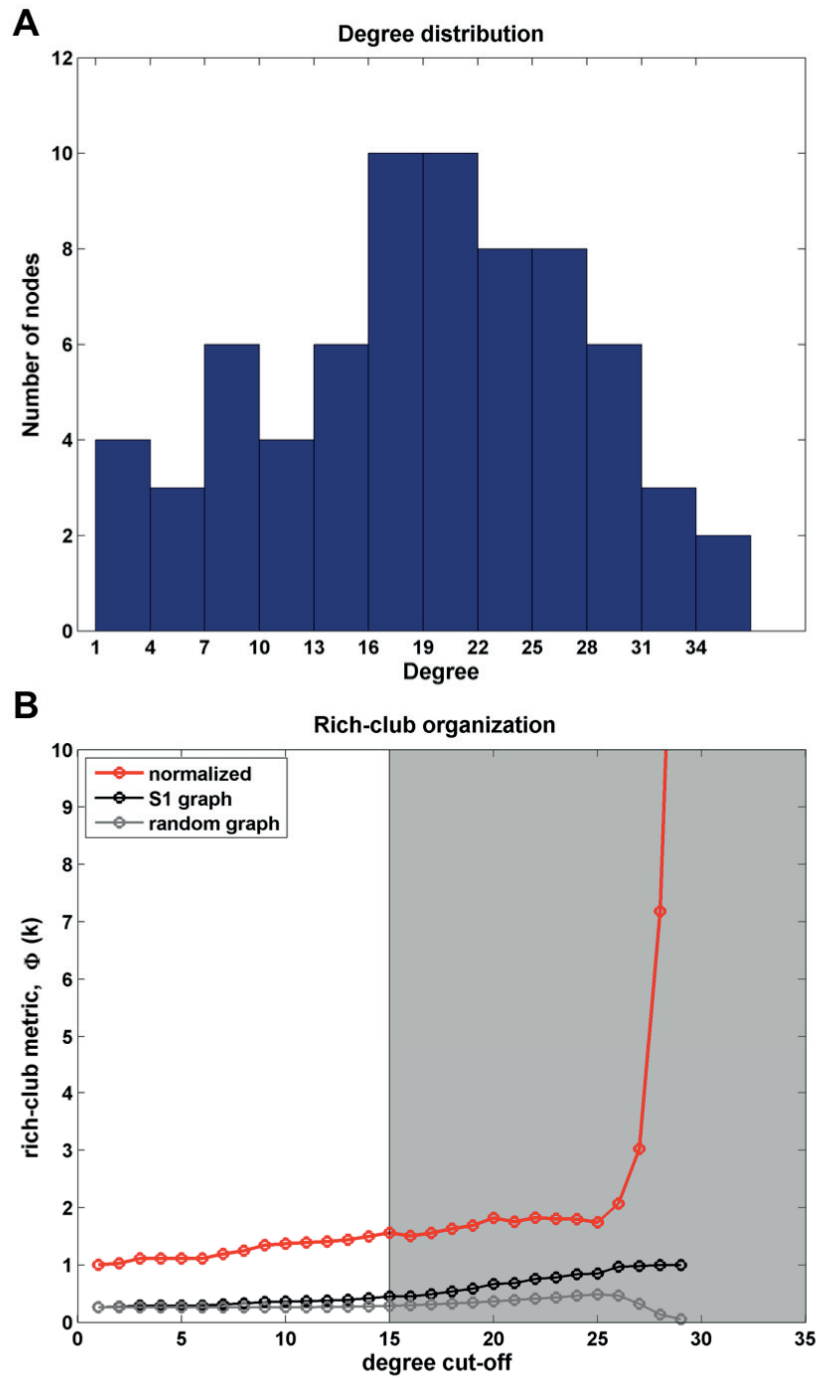
Fig.3.S1 Additional graph theory metrics. A) The degree distribution of the network formed by hands and lower limbs representations in S1. **B)** The rich club organization of the network, the grey zone highlights the rich-club regime.
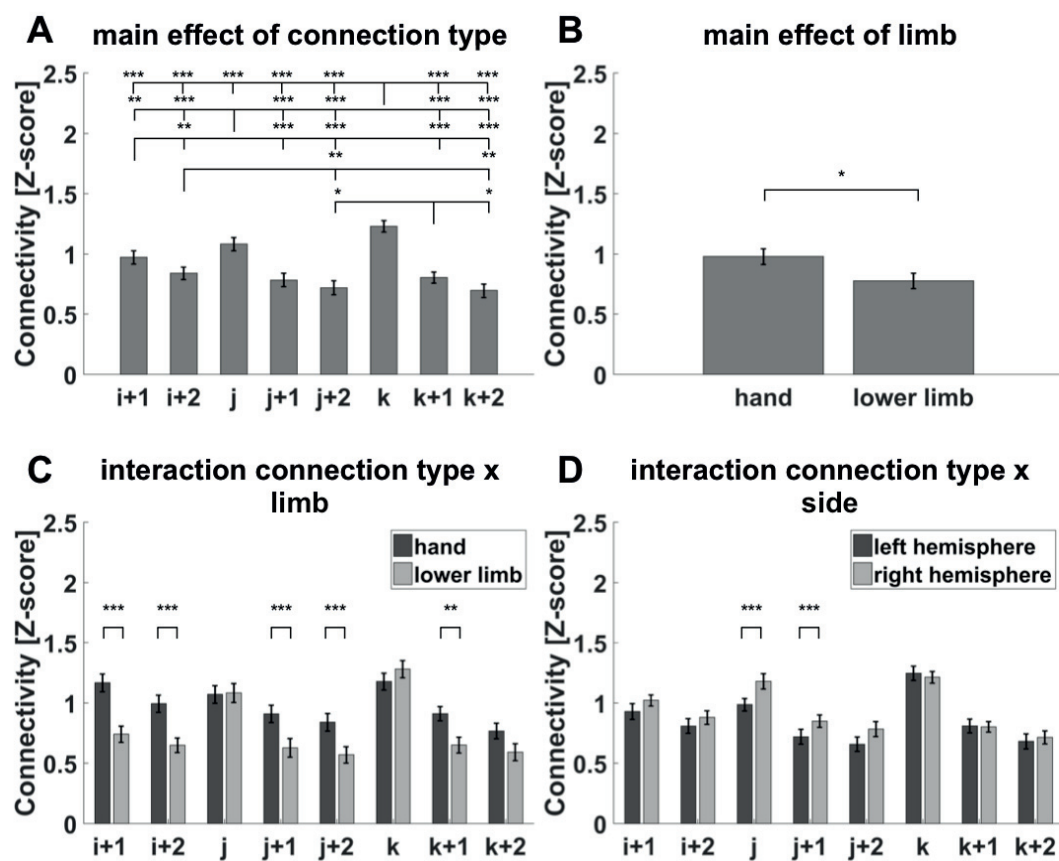
Fig.3.S2 Statistical analysis of local functional connectivity. The connection strength in the local neighborhood of representations was analyzed by means of a three-way repeated measures ANOVA. **A)** main effect of "connection type" considering the first neighbor in the same BA (i+1), the second neighbor in the same BA (i+2), the homolog in adjacent BA (j), the first neighbor in adjacent BA (j+1), the second neighbor in adjacent BA (j+2), the homolog in distant BA (k), the first neighbor in distant BA (k+1) and the second neighbor in distant BA (k+2). **B)** main effect of "limb type" (hand and lower limb). **C)** Interaction between "connection type" and "limb type". **D)** interaction between "connection type" and "hemisphere". Error bars represent the standard error of the mean. Asterisks represent the post-hoc Tukey HSD comparisons between each type of connections (* p < 0.05, ** p < 0.01, *** p < 0.001).
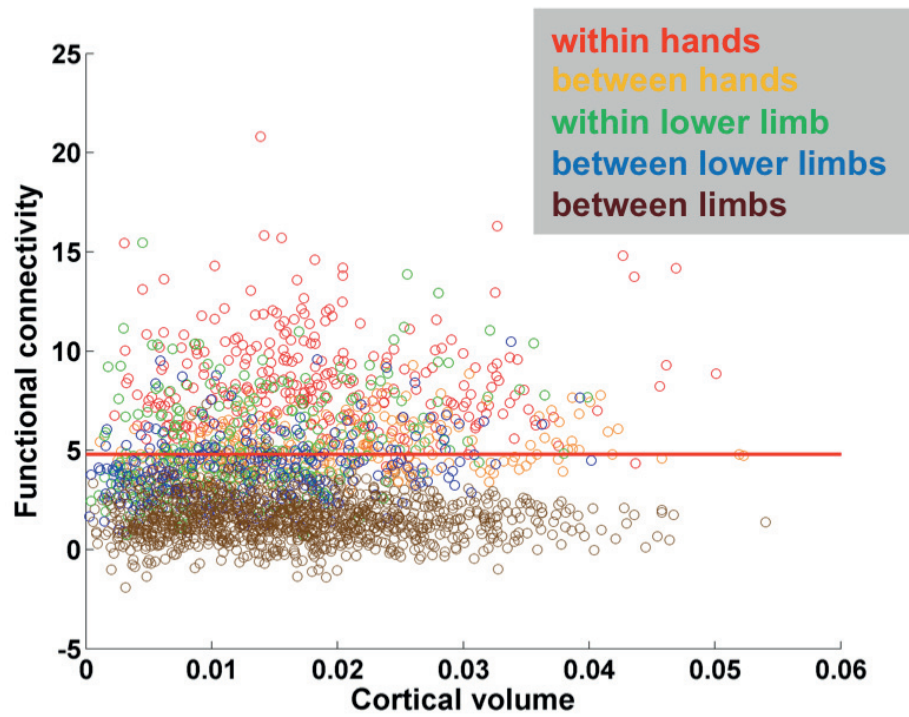
Fig.3.S3 Functional connectivity and cortical volume. The strength of functional connectivity between pairs of somatosensory representations is plotted as a function of the mean cortical volume between the same pairs. There is no specific relationship between functional connectivity and cortical volume (all $R^2 < 0.02$).

3.7 References

Achard, S., Salvador, R., Whitcher, B., Suckling, J., Bullmore, E., 2006. A resilient, low-frequency, small-world human brain functional network with highly connected association cortical hubs. The Journal of neuroscience : the official journal of the Society for Neuroscience 26, 63–72. doi:10.1523/JNEUROSCI.3874-05.2006

Alexander-Bloch, A.F., Vértes, P.E., Stidd, R., Lalonde, F., Clasen, L., Rapoport, J., Giedd, J., Bullmore, E.T., Gogtay, N., 2013. The anatomical distance of functional connections predicts brain network topology in health and schizophrenia. Cerebral cortex (New York, N.Y. : 1991) 23, 127–38. doi:10.1093/cercor/bhr388

Ashaber, M., Pálfi, E., Friedman, R.M., Palmer, C., Jákli, B., Chen, L.M., Kántor, O., Roe, A.W., Négyessy, L., 2014. Connectivity of somatosensory cortical area 1 forms an anatomical substrate for the emergence of multifinger receptive fields and complex feature selectivity in the squirrel monkey (Saimiri sciureus). The Journal of comparative neurology 522, 1769–85. doi:10.1002/cne.23499

Barone, P., Batardiere, A., Knoblauch, K., Kennedy, H., 2000. Laminar distribution of neurons in extrastriate areas projecting to visual areas V1 and V4 correlates with the hierarchical rank and indicates the operation of a distance rule. JOURNAL OF NEUROSCIENCE 20, 3263–3281.

Bassett, D.S., Bullmore, E., 2006. Small-world brain networks. The Neuroscientist : a review journal bringing neurobiology, neurology and psychiatry 12, 512–23. doi:10.1177/1073858406293182

Beckmann, C.F., DeLuca, M., Devlin, J.T., Smith, S.M., 2005. Investigations into resting-state connectivity using independent component analysis. Philos Trans R Soc Lond B Biol Sci 360, 1001–1013. doi:10.1098/rstb.2005.1634

Biswal, B., Yetkin, F.Z., Haughton, V.M., Hyde, J.S., Zerrin Yetkin, F., Haughton, V.M., Hyde, J.S., 1995. Functional connectivity in the motor cortex of resting human brain using echo-planar MRI. Magnetic resonance in medicine : official journal of the Society of Magnetic Resonance in Medicine / Society of Magnetic Resonance in Medicine 34, 537–541. doi:10.1002/mrm.1910340409

Bullmore, E., Sporns, O., 2009. Complex brain networks: graph theoretical analysis of structural and functional systems. Nature reviews. Neuroscience 10, 186–98. doi:10.1038/nrn2575

Burton, H., Wineland, A., Bhattacharya, M., Nicklaus, J., Garcia, K.S., Piccirillo, J.F., 2012. Altered networks in bothersome tinnitus: a functional connectivity study. BMC neuroscience 13, 3. doi:10.1186/1471-2202-13-3

Cha, K., Zatorre, R.J., Schönwiesner, M., 2014. Frequency Selectivity of Voxel-by-Voxel Functional Connectivity in Human Auditory Cortex. Cerebral cortex (New York, N.Y. : 1991) 26, 211–24. doi:10.1093/cercor/bhu193

Chen, L., Mishra, A., Newton, A.T., Morgan, V.L., Stringer, E.A., Rogers, B.P., Gore, J.C., 2011. Fine-scale functional connectivity in somatosensory cortex revealed by high-resolution fMRI. Magnetic resonance imaging 29, 1330–7. doi:10.1016/j.mri.2011.08.001

Craddock, R.C., Jbabdi, S., Yan, C.-G., Vogelstein, J.T., Castellanos, F.X., Di Martino, A., Kelly, C., Heberlein, K., Colcombe, S., Milham, M.P., 2013. Imaging human connectomes at the macroscale. Nature methods 10, 524–39. doi:10.1038/nmeth.2482

Damoiseaux, J.S., Rombouts, S.A.R.B., Barkhof, F., Scheltens, P., Stam, C.J., Smith, S.M., Beckmann, C.F., 2006. Consistent resting-state networks across healthy subjects. Proceedings of the National

Academy of Sciences of the United States of America 103, 13848–53. doi:10.1073/pnas.0601417103

Eckert, M.A., Kamdar, N. V, Chang, C.E., Beckmann, C.F., Greicius, M.D., Menon, V., V., K.N., Chang, C.E., Beckmann, C.F., Greicius, M.D., Menon, V., 2008. A cross-modal system linking primary auditory and visual cortices: evidence from intrinsic fMRI connectivity analysis. Human brain mapping 29, 848–857. doi:10.1002/hbm.20560

Eckert, M.A., Kamdar, N. V., Chang, C.E., Beckmann, C.F., Greicius, M.D., Menon, V., V., K.N., Chang, C.E., Beckmann, C.F., Greicius, M.D., Menon, V., 2008. A cross-modal system linking primary auditory and visual cortices: evidences from intrinsic fRMI connectivity. Human brain mapping 29, 848–857. doi:10.1002/hbm.20560.A

Ercsey-Ravasz, M., Markov, N.T., Lamy, C., Van Essen, D.C., Knoblauch, K., Toroczkai, Z., Kennedy, H., 2013. A predictive network model of cerebral cortical connectivity based on a distance rule. Neuron 80, 184–97. doi:10.1016/j.neuron.2013.07.036

Erdös, P., Rényi, a, 1959. On random graphs. Publicationes Mathematicae 6, 290–297. doi:10.2307/1999405

Felleman, D.J., Van Essen, D.C., 1991. Distributed Hierarchical Processing in the Primate Cerebral Cortex. Cerebral Cortex 1, 1–47. doi:10.1093/cercor/1.1.1

Fisher, R., 1915. Frequency distribution of the values of the correlation coefficient in samples from an indefinitely large population. Biometrika. doi:10.2307/2331838

Fox, M.D., Raichle, M.E., 2007. Spontaneous fluctuations in brain activity observed with functional magnetic resonance imaging. Nature reviews. Neuroscience 8, 700–11. doi:10.1038/nrn2201

Friston, K.J., Frith, C.D., Liddle, P.F., Frackowiak, R.S., 1993. Functional connectivity: the principal-component analysis of large (PET) data sets. Journal of Cerebral Blood Flow & Metabolism 13, 5–14. doi:10.1038/jcbfm.1993.4

Gelnar, P.A., Krauss, B.R., Szeverenyi, N.M., Apkarian, A. V, 1998. Fingertip representation in the human somatosensory cortex: an fMRI study. NeuroImage 7, 261–283. doi:10.1006/nimg.1998.0341

Geyer, S., Schleicher, a, Zilles, K., 1999. Areas 3a, 3b, and 1 of human primary somatosensory cortex. NeuroImage 10, 63–83. doi:10.1006/nimg.1999.0440

Geyer, S., Schormann, T., Mohlberg, H., Zilles, K., 2000. Areas 3a, 3b, and 1 of human primary somatosensory cortex. Part 2. Spatial normalization to standard anatomical space. NeuroImage 11, 684–96. doi:10.1006/nimg.2000.0548

Glover, G.H., Li, T.Q., Ress, D., 2000. Image-based method for retrospective correction of physiological motion effects in fMRI: RETROICOR. Magnetic Resonance in Medicine 44, 162–167. doi:10.1002/1522-2594(200007)44:1

Grefkes, C., Geyer, S., Schormann, T., Roland, P., Zilles, K., 2001. Human somatosensory area 2: observer-independent cytoarchitectonic mapping, interindividual variability, and population map. NeuroImage 14, 617–31. doi:10.1006/nimg.2001.0858

Greicius, M.D., Krasnow, B., Reiss, A.L., Menon, V., 2003. Functional connectivity in the resting brain: a network analysis of the default mode hypothesis. Proceedings of the National Academy of Sciences of the United States of America 100, 253–8. doi:10.1073/pnas.0135058100

Guye, M., Bettus, G., Bartolomei, F., Cozzone, P.J., 2010. Graph theoretical analysis of structural and functional connectivity MRI in normal and pathological brain networks. Magma (New York, N.Y.) 23, 409–21. doi:10.1007/s10334-010-0205-z

Harrison, S.J., Woolrich, M.W., Robinson, E.C., Glasser, M.F., Beckmann, C.F., Jenkinson, M., Smith, S.M., 2015. Large-scale probabilistic functional modes from resting state fMRI. NeuroImage 109, 217–31. doi:10.1016/j.neuroimage.2015.01.013

He, Y., Chen, Z.J., Evans, A.C., 2007. Small-world anatomical networks in the human brain revealed by cortical thickness from MRI. Cerebral cortex (New York, N.Y. : 1991) 17, 2407–19. doi:10.1093/cercor/bhl149

Iwamura, Y., 1998. Hierarchical somatosensory processing. Current opinion in neurobiology 8, 522–8.

Jones, E.G., Coulter, J.D., Hendry, S.H., 1978. Intracortical connectivity of architectonic fields in the somatic sensory, motor and parietal cortex of monkeys. The Journal of comparative neurology 181, 291–347. doi:10.1002/cne.901810206

Kaas, J., Nelson, R., Sur, M., Lin, C., Merzenich, M., 1979. Multiple representations of the body within the primary somatosensory cortex of primates. Science 204, 1977–1979.

Kamada, T., Kawai, S., 1989. An algorithm for drawing general undirected graphs. Information Processing Letters 31, 7–15. doi:10.1016/0020-0190(89)90102-6

Li, Q., Song, M., Fan, L., Liu, Y., Jiang, T., 2015. Parcellation of the primary cerebral cortices based on local connectivity profiles. Frontiers in neuroanatomy 9, 50. doi:10.3389/fnana.2015.00050

Long, X., Goltz, D., Margulies, D.S., Nierhaus, T., Villringer, A., 2014. Functional connectivity-based parcellation of the human sensorimotor cortex. The European journal of neuroscience 39, 1332–42. doi:10.1111/ejn.12473

Lowe, M.J., Mock, B.J., Sorenson, J.A., 1998. Functional connectivity in single and multislice echoplanar imaging using resting-state fluctuations. NeuroImage 7, 119–132. doi:10.1006/nimg.1997.0315

Marques, J., Kober, T., van der Zwaag, W., Kruegger, G., Gruetter, R., 2008. MP2RAGE, a self-bias field corrected sequence for improved segmentation at high field. Proceedings 16th Scientific Meeting, International Society for Magnetic Resonance in Medicine Toronto, 1393.

Martuzzi, R., van der Zwaag, W., Dieguez, S., Serino, a., Gruetter, R., Blanke, O., 2015. Distinct contributions of Brodmann areas 1 and 2 to body ownership. Social Cognitive and Affective Neuroscience 1–11. doi:10.1093/scan/nsv031

Martuzzi, R., van der Zwaag, W., Farthouat, J., Gruetter, R., Blanke, O., 2014. Human finger somatotopy in areas 3b, 1, and 2: A 7T fMRI study using a natural stimulus. Human brain mapping 35, 213–226. doi:10.1002/hbm.22172

Maudoux, A., Lefebvre, P., Cabay, J.-E., Demertzi, A., Vanhaudenhuyse, A., Laureys, S., Soddu, A., 2012. Connectivity graph analysis of the auditory resting state network in tinnitus. Brain research 1485, 10–21. doi:10.1016/j.brainres.2012.05.006

Merzenich, M.M., Kaas, J.H., Sur, M., Lin, C.S., 1978. Double representation of the body surface within cytoarchitectonic areas 3b and 1 in "SI" in the owl monkey (Aotus trivirgatus). The Journal of comparative neurology 181, 41–73. doi:10.1002/cne.901810104

Nelson, R.J., Sur, M., Felleman, D.J., Kaas, J.H., 1980. Representations of the body surface in postcentral parietal cortex of Macaca fascicularis. The Journal of comparative neurology 192, 611–43. doi:10.1002/cne.901920402

Nir, Y., Mukamel, R., Dinstein, I., Privman, E., Harel, M., Fisch, L., Gelbard-Sagiv, H., Kipervasser, S., Andelman, F., Neufeld, M.Y., Kramer, U., Arieli, A., Fried, I., Malach, R., 2008. Interhemispheric correlations of slow spontaneous neuronal fluctuations revealed in human sensory cortex. Nature Neuroscience 11, 1100–1108. doi:10.1038/nn.2177

Oldfield, R.C., 1971. The assessment and analysis of handedness: The Edinburgh inventory. Neuropsychologia 9, 97–113. doi:10.1016/0028-3932(71)90067-4

Powell, T.P.S., Mountcastle, V.B., 1959. The cytoarchitecture of the postcentral gyrus of the monkey macaca mulatta. Bulletin Johns Hopkins Hospital 105, 108–130.

Raemaekers, M., Schellekens, W., van Wezel, R.J. a, Petridou, N., Kristo, G., Ramsey, N.F., 2014. Patterns of resting state connectivity in human primary visual cortical areas: a 7T fMRI study. NeuroImage 84, 911–21. doi:10.1016/j.neuroimage.2013.09.060

Salvador, R., Suckling, J., Coleman, M.R., Pickard, J.D., Menon, D., Bullmore, E., 2005. Neurophysiological architecture of functional magnetic resonance images of human brain. Cerebral Cortex 15, 1332–2342. doi:10.1093/cercor/bhi016

Sanchez-Panchuelo, R.M., Besle, J., Beckett, A., Bowtell, R., Schluppeck, D., Francis, S., 2012. Within-digit functional parcellation of Brodmann areas of the human primary somatosensory cortex using functional magnetic resonance imaging at 7 tesla. Journal of Neuroscience 32, 15815–22. doi:10.1523/JNEUROSCI.2501-12.2012

Sanchez-Panchuelo, R.M., Francis, S., Bowtell, R., Schluppeck, D., 2010. Mapping Human Somatosensory Cortex in Individual Subjects With 7T Functional MRI. J. neurophysiol 2544–2556. doi:10.1152/jn.01017.2009.

Sanchez-Panchuelo, R.-M., Besle, J., Mougin, O., Gowland, P., Bowtell, R., Schluppeck, D., Francis, S., 2014. Regional structural differences across functionally parcellated Brodmann areas of human primary somatosensory cortex. NeuroImage 93 Pt 2, 221–30. doi:10.1016/j.neuroimage.2013.03.044

Shanks, M., Pearson, R., Powell, T., 1985. The ipsilateral cortico-cortical connexions between the cytoarchitectonic subdivisions of the primary somatic sensory cortex in the monkey. Brain Research Reviews 9, 67–88. doi:10.1016/0165-0173(85)90019-0

Six, J.M., Tollis, I.G., 2006. A framework and algorithms for circular drawings of graphs. Journal of Discrete Algorithms 4, 25–50. doi:10.1016/j.jda.2005.01.009

Speck, O., Stadler, J., Zaitsev, M., 2008. High resolution single-shot EPI at 7T. Magnetic Resonance Materials in Physics, Biology and Medicine 21, 73–86. doi:10.1007/s10334-007-0087-x

Sporns, O., Zwi, J.D., 2004. The small world of the cerebral cortex. Neuroinformatics 2, 145–62. doi:10.1385/NI:2:2:145

Striem-Amit, E., Ovadia-Caro, S., Caramazza, A., Margulies, D.S., Villringer, A., Amedi, A., 2015. Functional connectivity of visual cortex in the blind follows retinotopic organization principles. Brain : a journal of neurology 138, 1679–95. doi:10.1093/brain/awv083

Stringer, E.A., Chen, L.M., Friedman, R.M., Gatenby, C., Gore, J.C., 2011. Differentiation of somatosensory cortices by high-resolution fMRI at 7 T. NeuroImage 54, 1012–20. doi:10.1016/j.neuroimage.2010.09.058

Stringer, E., Qiao, P.-G., Friedman, R.M., Holroyd, L., Newton, A.T., Gore, J.C., Min Chen, L., 2014. Distinct fine-scale fMRI activation patterns of contra- and ipsilateral somatosensory areas 3b and 1 in humans. Human Brain Mapping 35, 4841–4857. doi:10.1002/hbm.22517

Van De Ven, V.G., Formisano, E., Prvulovic, D., Roeder, C.H., Linden, D.E.J., 2004. Functional connectivity as revealed by spatial independent component analysis of fMRI measurements during rest. Human Brain Mapping 22, 165–178. doi:10.1002/hbm.20022

van den Heuvel, M.P., Stam, C.J., Boersma, M., Hulshoff Pol, H.E., 2008. Small-world and scale-free organization of voxel-based resting-state functional connectivity in the human brain. NeuroImage 43, 528–39. doi:10.1016/j.neuroimage.2008.08.010

van den Heuvel, M.P., Sporns, O., 2011. Rich-Club Organization of the Human Connectome. Journal of Neuroscience 31, 15775–15786. doi:10.1523/JNEUROSCI.3539-11.2011

Volz, L.J., Eickhoff, S.B., Pool, E.-M., Fink, G.R., Grefkes, C., 2015. Differential modulation of motor network connectivity during movements of the upper and lower limbs. NeuroImage 119, 44–53. doi:10.1016/j.neuroimage.2015.05.101

Wang, Z., Chen, L.M., Négyessy, L., Friedman, R.M., Mishra, A., Gore, J.C., Roe, A.W., 2013. The relationship of anatomical and functional connectivity to resting-state connectivity in primate somatosensory cortex. Neuron 78, 1116–26. doi:10.1016/j.neuron.2013.04.023

Whitfield-Gabrieli, S., Nieto-Castanon, A., 2012. Conn: A Functional Connectivity Toolbox for Correlated and Anticorrelated Brain Networks. Brain Connectivity 2, 125–141. doi:10.1089/brain.2012.0073

Yeo, B.T.T., Krienen, F.M., Sepulcre, J., Sabuncu, M.R., Lashkari, D., Hollinshead, M., Roffman, J.L., Smoller, J.W., Zöllei, L., Polimeni, J.R., Fischl, B., Liu, H., Buckner, R.L., 2011. The organization of the human cerebral cortex estimated by intrinsic functional connectivity. Journal of neurophysiology 106, 1125–65. doi:10.1152/jn.00338.2011

4 - Study III: upper limb cortical maps in amputees with targeted muscle and sensory reinnervation: a 7T fMRI study

Andrea Serino*, Michel Akselrod*, Roy Salomon, Roberto Martuzzi, Maria Laura Blefari, Elisa Canzoneri, Giulio Rognini, Wietske van der Zwaag, Maria Iakova, François Luthi, Amedeo Amoresano, Todd Kuiken, Olaf Blanke

these authors contributed equally

Abstract

Neuroprosthetics research in amputee patients aims at developing new prostheses that move and feel like real limbs. Targeted muscle and sensory reinnervation (TMSR) is such an approach and consists in rerouting motor and sensory nerves from the residual limb towards intact muscles and skin regions. Movement of the myoelectric prosthesis is enabled via decoded EMG activity from reinnervated muscles and touch sensation on the missing limb is enabled by stimulation of the reinnervated skin areas. Here we ask whether and how motor control and redirected somatosensory stimulation provided via TMSR affected the maps of the upper limb in primary motor (M1) and primary somatosensory (S1) cortex, as well as its functional connections. To this aim, we tested three TMSR patients and investigated the extent, strength, and topographical organization of the missing limb and several control body regions in M1 and S1 at ultra high-field (7T) fMRI. Additionally, we analyzed functional connectivity between M1 and S1 and of both these regions with posterior parietal cortex, important for multisensory upper limb processing. These data were compared with those of control amputee patients (non-TMSR patients) and healthy controls. We found that M1 maps of the amputated limb in TMSR patients were similar in terms of extent, strength, and topography to healthy controls and different from non-TMSR patients. S1 maps of TMSR patients were also more preserved in terms of topographical organization and extent, as compared to non-TMSR patients, but weaker in activation strength compared to healthy controls. Functional connectivity in TMSR patients between upper limb maps in M1 and S1 was normal and comparable with healthy controls, while being reduced in non-TMSR patients. However, connectivity was reduced between M1 and between S1 and multisensory posterior parietal regions, in both the TMSR and non-TMSR patients with respect to

healthy controls; this was associated with the absence of a well-established multisensory effect (visual enhancement of touch) in TMSR patients. Collectively, these results show how S1 and M1 process signals related to movement and touch enabled by TMSR. Moreover, they suggest that TMSR may counteract maladaptive cortical plasticity typically found after limb loss, in M1, partially in S1, and for their mutual connectivity. The decreased connectivity with posterior parietal cortex and the lack of multisensory interaction in the present data suggests that further engineering advances are necessary (e.g., the integration of somatosensory feedback into current prostheses) to enable prostheses that move and feel as real limbs.

Detailed contributions: I shared most responsibilities of this project with Dr. Serino (first co-authors). I prepared the paradigms, collected and analyzed the data (in collaboration with other authors), participated in writing the manuscript and created the figures.

4.1 Introduction

The loss of an upper limb results in functional reorganization of primate primary motor (M1) and somatosensory (S1) areas as originally demonstrated in non-human primates (**Pons, 1991; Kaas et al. 1983; Merzenich et al. 1983; Kaas, 1991**). In humans, such reorganization after limb amputation has also been observed and considered a form of maladaptive plasticity, linked to the phantom limb syndrome and associated chronic pain (**Flor et al. 1995; Lotze et al. 2001; Foell et al. 2013, Makin et al. 2015b**). Subsequently, it has been proposed that motor activity and usage of the missing limb, as well as related sensory feedback, may in principle counteract maladaptive reorganization of sensory-motor cortices in amputees, thus inspiring several rehabilitation techniques, based on motor imagery and mirror box therapy (**Chan et al. 2007, Rothgangel et al. 2011**). These approaches, however, require long sessions of training and are unrelated to true ecological limb usage. Thus, optimal sensory-motor training should consist in naturalistic control of a prosthetic limb.

The fields of neuroprosthetics pursue various approaches for the development of bidirectional interfaces allowing amputees to feel and control a prosthetic limb in the most intuitive and natural fashion. A key example of these techniques is the so-called Targeted Muscle and Sensory Reinnervation (TMSR; **Kuiken, et al. 2004; Kuiken et al. 2007b**). It consists in de-innervating spare muscle groups in the residual limb or the chest of the amputee (i.e. target muscles) and in reinnervating them with the residual arm nerves of the amputated limb. This way, motor commands generated to control the arm or hand are decoded from electromyographical signals of the target muscles and used to control a prosthetic limb (**Kuiken, et al. 2004; Kuiken et al. 2007b**). In some patients the approach may also include targeted sensory reinnervation, for which deinnervated skin regions near or over the target muscle are reinnervated with afferent fibers of the residual somatosensory nerves of the amputated limb (**Kuiken et al. 2007a, Hebert et al. 2014**). As a consequence, stimuli applied to the reinnervated skin regions evoke somatosensory sensations as if the missing limb were stimulated. Thus, amputees may use such TSMR systems to control their prosthetic limb by recruiting central motor representations of the missing limb and may perceive sensory feedback as arising from the missing limb, likely activating central somatosensory representations. However, while there exist

evidences of motor and sensory cortical plasticity in patients who underwent the TMSR procedure (**Chen et al. 2013; Yao et al. 2015**), it is yet not clearly demonstrated to which extent TMSR-based prostheses recruit and reinstate cortical representations of the missing limb. A way to answer this question would be testing whether and how TMSR procedure affects cortical body representations in primary motor and somatosensory cortices, potentially impacting current trends to improve motor control and tactile perception as well as phantom limb pain due to maladaptive plasticity (**Flor et al. 1995, Lotze et al. 2001**).

In the present study, we first investigated whether movement and somatosensory feedback linked to TMSR prosthesis is associated with preserved somatotopic maps in M1 and S1 in TMRS patients, predicting that, compared to amputee patients without TMSR, M1 and S1 organization would be more similar to the normal organization in healthy participants. To this aim, we used ultra high-field functional magnetic resonance imaging (fMRI, 7T) paradigms to map upper limb representations (and neighboring regions) in M1 and S1 in TMSR patients as described previously in healthy subjects (**Martuzzi et al. 2014, 2015; Siero et al. 2014; Ejaz et al. 2015**). In particular, we examined M1 activity induced by movements of different parts of the upper limb (**Alkadhi et al. 2002; Lotze et al. 2000; Porro et al. 1996; Zeharia et al. 2012**). Moreover, by applying touch cues to re-innervated skin regions resulting in clear tactile percepts on the missing limb, we also mapped the somatosensory representation of the upper limb in S1, at the level of single fingers (e.g. **Martuzzi et al. 2014, 2015; Sanchez-Panchuelo et al. 2010; Stringer et al. 2011**). Specifically, we studied the extent, strength, location, and topographical sequence of upper limb representations in M1 and S1 using 7T fMRI in TMSR patients.

In addition, it is well known that perception of body parts does not rely only on unimodal representations in M1 and S1, but also on multimodal body representations, especially in the posterior parietal cortex, as well as on distributed processing between unimodal and multimodal brain regions (**Serino & Haggard, 2010, Blanke et al. 2015**). In fact, key rehabilitative approaches for phantom limb pain, such as the mirror box treatment, are based on integration of multimodal visual, somatosensory, and motor cues (**Chan et al. 2007; Ramachandran & Altschuler, 2009**). Therefore, we also applied resting state functional connectivity (rs fc fMRI) (**Fox and Raichle,**

2007) to study the functional organization between maps of the different body parts (including the amputated limb) in M1, S1 and in multisensory arm regions in the parietal cortex (**Graziano et al. 2006, Dijkerman & De Haan, 2007; Berlucchi & Aglioti, 2010**). This analysis was complemented by a psychophysical investigation of the Visual Enhancement of Touch (VET) in TMSR patients, testing how vision of the missing limb affects somatosensory perception on the targeted skin region. The presence of VET in TMSR patients would demonstrate existing interactions between visual and somatosensory representations of the missing limb, pointing to preserved multisensory representations. Three patients, who received TMSR to control a prosthetic arm, were studied and their fMRI and behavioral results were compared with those from three non-TMSR control amputees, suffering from comparable upper limb amputation (without any TMSR), and with healthy control subjects.

4.2 Methods

4.2.1 Participants

Three TMSR patients that have been previously extensively tested (**Kuiken et al. 2004, Kuiken et al. 2007b; Marasco et al. 2009**) were enrolled in the present study. Patient TMSR-01 was a 45 year-old woman, who suffered transhumeral amputation due to car accident. Fifteen months after injury and 7 years before the current investigation, her residual median and distal radial nerves were transferred to the medial biceps and lateral triceps muscles, respectively. Her intercostobrachial nerve was cut to facilitate sensory reinnervation of her arm. Patient TMSR-02 was a 33 years-old woman, who suffered left shoulder disarticulation following a motor vehicle collision. Fifteen months after amputation and 8 years before the current investigation, the median, ulnar and radial nerves on the left side were transferred to different segments of her ipsilateral pectoralis major and serratus anterior muscles. In addition, the supraclavicular cutaneous and the intercostobrachial cutaneous nerves were cut and their distal portions were coapted to the ulnar and median nerves respectively. TMSR-03 was a 66 years-old man, who lost both his arms at the shoulder due to electrical burns. Nine months after injury and 16 years before the current testing, his remaining median, ulnar, radial, and musculocutaneous nerves were transferred to different segments of his left pectoralis major and minor muscles. For all patients, more detailed clinical information about the surgical procedures and

96

outcomes is reported in previous papers (**Dumanian et al. 2009; Hijjawi et al. 2006; Kuiken et al. 2004; Kuiken et al. 2007a; Kuiken et al. 2007b; O'Shaughnessy et al. 2008**).

Three amputated patients who did not receive TMSR surgery (non-TMSR amputees) were recruited to approximately match the amputation site of the three TMRS patients (see supplementary materials). A group of eight healthy controls performed fMRI scanning (mean age=31.7 years, SD=±15.1 years, 2 females) and another group of 12 healthy participants took part as a control group in the experiment on Visual Enhancement of touch (mean age=22 years, SD=±2.3 years, all female).

All participants were originally right-handed, as confirmed by the Edinburgh Oldfield Handedness Inventory (**Oldfield, 1971**). The study was approved by the Ethics Committee of the University of Lausanne (Reference number: 113/2013) and conducted in accordance with the Declaration of Helsinki. All participants provided written informed consent to participate to the study.

4.2.2 Assessment of somatosensory sensation from the missing limb

All amputee patients were interviewed (semi-structured interview; adapted from Giummara & Moseley, **2011**; see supplementary materials) about residual sensations, phantom limb experiences and pain. All TMRS patients reported a clear sensation of the presence of a phantom limb, in a natural and comfortable posture. At the time of testing none of the patients reported phantom pain, except TMSR-03. All TMSR patients claimed to be able to move their phantom limbs. All patients reported well-defined tactile sensation following tactile stimulation of different skin regions from the re-innervated residual limb (see supplementary material).

In order to quantify these referred sensations to the amputated limb and to precisely localize the regions over the reinnervated skin inducing reliable tactile percepts on different parts of the missing limb, we conducted a detailed psychophysical assessments on the first day of testing, and a second shorter assessment at the beginning of later sessions to confirm the reliability of stimulation (for details about mapping of referred sensations on the reinnervated skin see supplementary materials). Results are reported in Fig.4.1, showing that all TMSR

**stimulation sites on   corresponding
reinnervated skin   referred sensations**

TMSR-01

TMSR-02

TMSR-03
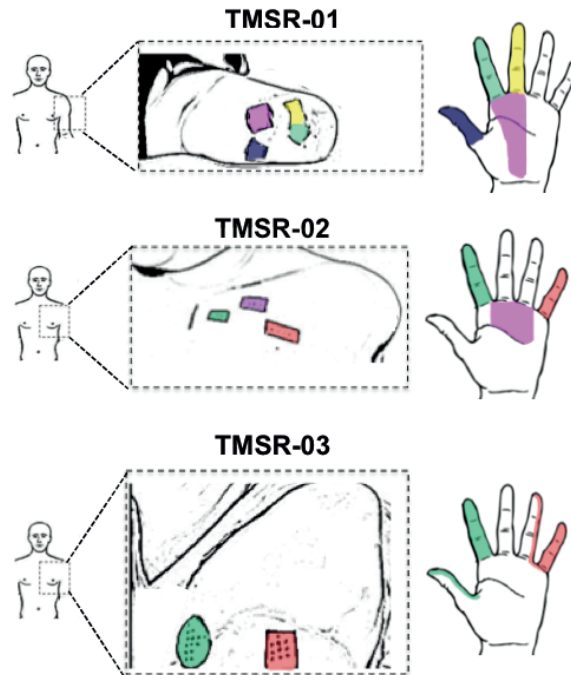
Fig.4.1 Mapping of referred tactile sensations. The stimulation of reinnervated skin regions induced specific phantom sensations in each of the three TMRS patients.

participants perceived reliable sensations from the amputated limb, mostly localized on the palm, thumb, index, middle and little finger. A similar mapping procedure was used with non-TMSR patients to identify possible areas of tactile sensations refereed to the amputated limb from stimulation of the skin over the residual limb. These examinations were used to select the skin regions that were used for S1 mapping using 7T fMRI and the VET experiment in TMRS patients.

4.2.3 fMRI data acquisition

Images were acquired on a short-bore head-only 7T scanner (Siemens Medical, Germany) with a 32-channel Tx/Rx rf-coil (Rapid Biomedical, Germany) (**Salomon et al. 2013**). Functional images were acquired using a sinusoidal readout EPI sequence (**Speck et al. 2008**) and comprised 28 axial slices. Slices were placed over the postcentral gyrus (approximately orthogonal to the central sulcus) in order to cover the primary somatosensory and motor cortices (in-plane resolution 1.3×1.3mm^2; slice thickness 1.3mm; gap 0.13mm; matrix size 160×160, TR= 2s, FOV=210mm, TE=27ms, GRAPPA=2). Two fMRI sessions were performed on different days, to

map motor and somatosensory representations, respectively. A 5-minute resting-state acquisition was also performed and participants were asked to lay relaxed and still with the eyes closed and to retain from any goal-oriented thinking.

Motor representations were mapped using a block design (participants performed in each run three types of movements of one out of six body parts (see below) for 20 times, 1 movement per second, followed by 10s of rest). One run per body side (i.e. left and right) was performed and each block was repeated eight times. Movements were selected based on prosthesis movements (**Zhou et al. 2007**) and included: hand closure and opening, wrist pronation/supination and elbow extension/flexion for left and right hands. Blocks of tongue, chest and finger movements on both sides were also included. All participants were trained on the movements before entering the magnet and successfully execute the requested movements on the healthy and amputated side.

Somatosensory representations were mapped by adapting the procedure described in (**Martuzzi et al. 2014, 2015**): each mapped body regions was manually stroked by the experimenter positioned at the entrance of the bore, with a Q-tip probe (mounted on a stick if necessary). Each area was stroked for 20s, followed by 10s of rest (no stroking); the stroking sequence was repeated four times, keeping the order of the body-parts being stroked fixed. Participants were instructed to pay attention to the body region being stroked. For TMSR and non-TMSR patients, tactile stimulations were delivered on skin regions inducing well-defined referred sensations of the missing limb. Additionally, we mapped the lips and the big toe bilaterally, in order to identify the full extent of the somatotopic homunculus in S1. The stimulation protocol used in amputees was adapted in healthy controls in order to map the comparable body parts in non-amputated individuals. Mapped body parts included: right and left fingers, palm, arm, chest, lips and big toe (supplementary materials).

4.2.4 fMRI data analysis

Statistical analyses were conducted using SPM8 (Wellcome Department of Cognitive Neurology, London, UK), Brainvoyager QX 2.4 (Brain Innovation, Maastricht, The Netherlands), and custom routines running in MATLAB (Mathworks, Boston). Functional volumes were spatially realigned to the first volume. For M1

mapping in which somatotopy is more variable (**Alkadhi et al. 2002; Beisteiner et al. 2001**), no smoothing was applied to M1 images in order to retain the highest level of spatial specificity. For S1 mapping, images were smoothed with an isotropic Gaussian kernel (FWHM=2mm) following the procedure presented in Martuzzi et al. (**2014**).

For M1 and S1 mapping, separate statistical analyses were performed using a General Linear Model (GLM), where each different movement / tactile stimulation was modeled as boxcar regressor and convolved with the canonical hemodynamic response function (HRF) as basis function and six motion parameters were added as nuisance regressors.

Motor mapping of the hand, wrist, elbow, chest, fingers and tongue movements were calculated for each body side by contrasting each movement to rest epochs (e.g. Hand> Rest). Regions-Of-Interest (ROI) for each body part were collected using False Detection Rate $q < 0.05$ (FDR, **Genovese et al. 2002**) to correct for multiple comparisons. However, in one participant (non-TMSR-01) we had to use a threshold of $p < 0.00001$ FDR corrected because no voxels were activated otherwise (for movements of the elbow on the amputated side).

S1 mapping was performed by computing an F-contrast ($p < 0.001$ uncorrected) including HRF regressors of all the body regions stimulated during the same run, to identify all voxels responding to the stimulation of at least one body region. The result was used as an S1 mask. Maps of single region responses were computed by means of a t-contrast ($p < 0.001$ uncorrected). Within the S1 mask, each voxel was independently labeled as representing the region demonstrating the highest t-value for that particular voxel leading to a "winner takes all" competition between the stimulated body regions. This procedure was applied independently for the regions of the reinnervated skin for TMSR patients and of the residual limb for non-TMSR patients, for the chest and arm on the intact limb (bilaterally for controls), for the palm and fingers on the intact limb (bilaterally for controls), for right and left big toes, and for right and left lips.

The following functional connections (when available) were investigated in all TMSR patients, non-TMSR patients and healthy controls: left M1-left S1, left M1-left SPL, left S1-left SPL, right M1-right S1, right M1-right SPL, right S1-right SPL. To

account for inter-subject variability in average brain connectivity (**Goncalves et al. 2006**), the functional connectivity between the investigated pairs of ROIs was normalized by the individual average seed-to-whole brain functional connectivity of the 6 seed regions. Further details about this analysis are provided in supplementary materials.

4.2.5 Visual enhancement of touch (VET)

Visual enhancement of touch was studied by comparing two-point discrimination thresholds (2PDT) when subjects saw either the stimulated body part (without viewing the actual tactile stimuli) or another body part (see **Serino et al. 2009; Serino & Haggard, 2010**; see supplementary materials). TMSR patients, comfortably lying down on a bed in a prone position, were presented with tactile stimulation delivered by four mechanical solenoids (M & E Solve, Estelle Close, Rochester, Kent ME1 2BP), on the target area (non-TMSR or TMSR region), in different experimental blocks. In each trial, subjects were lightly tapped either by a single stimulus or by two simultaneous spatially separated stimuli. Patients were requested to discriminate between single and double taps, by verbally responding "one" (32 trials) or ''two'' (45 trials). Patients performed the tactile task in two visual conditions, while viewing their hand ("View Hand") or the chest/arm ("View Chest"/"View Arm"), filmed trough a video camera. In the "View Hand" condition patients saw their preserved hand, flipped as to resemble the amputated one (a video of a man's hand was used for the TMSR03).

A control group of healthy participants performed the task with the same procedure as for TMSR patients. They performed the tactile task either on the chest ("Touch Chest") or the hand ("Touch Hand"), while viewing their chest ("View Chest") or their Hand ("View Hand"). Signal-detection measures were used to quantify tactile performance. Double taps were defined as the to-be-detected signal. D prime (d') was calculated as measure of perceptual sensitivity (**Green & Swets, 1966; Krantz, 1969**).

4.3 Results

4.3.1 M1 mapping

All three TMSR patients showed a normal somatotopic location and order of body-part activations in contralateral M1 for different movements of the amputated hand, which were similar to regions activated by the movements made by their intact hand. The same movements-related activations in non-TMSR amputees were reduced or even absent. Moreover, in the two unilateral TMSR patients, activation in the M1 hand area contralateral to the amputated hand was stronger than that induced by movements of the healthy hand; this was not found for any of the non-TMSR patients. In the bilateral TMSR patient, consistently with these findings, activation in the M1 hand area contralateral to the reinnervated side was higher than that induced by movements of the non-reinnervated side. The regions of M1 associated with specific movements of the hand and upper limb in TMSR, non-TMSR amputees, and healthy controls are shown in Fig.4.2A.

In order to quantify M1 activations between TMSR patients, non-TMSR patients, and healthy controls we analyzed three main parameters: 1) the *extent* of the activation for each mapped movement was given by the number of active voxels; 2) the *strength* of each activation was quantified by determining the peak activity (max t-value); 3) the topographical order of these activations was described by calculating the *distance* of center of mass of activation clusters for different movements.

Extent. We first extracted the number of voxels active during movements of the amputated and healthy hand in the contralateral M1 regions as a measure of the extent of the hand representation. For each patient, we then calculated an index of activation extent, as the difference between the number of active voxels in the right (contralateral to amputation) and the left hemisphere. The index of activation extent was positive in the two unilateral TMSR amputees, indicating more widespread activation in the contralateral M1 during movements of the amputated limb, as compared to the intact limb. The index was positive also in TMRS-03, meaning in this case, that more voxels were activated when he moved his reinnervated amputated hand as compared to the non-reinnervated amputated hand. For each TMSR patient, the index of activation extent voxel was equivalent to that recorded in healthy controls (Fig.4.2B; t=1.18; p=.27 and t=.86, p=.42; t=.69, p=.51, for TMSR-01, TMSR-02,

TMSR-03 respectively, as compared to controls using Crawford test). In contrast, this index was negative for the non-TMSR amputees and significantly different from healthy controls in two out of the three tested patients (Non-TMSR-01:t=-2-26, p=.05; Non-TMSR-03: t=-3.06, p<.02; Non-TMSR-02=-1.737, p=.10 one-tailed, Crawford test). This shows that in non re-innervated patients, contralateral M1 activity is significantly weaker when performing movements with the amputated arm as compared to the healthy arm. This analysis therefore suggests that the extent of activations during hand movements in the M1 contralateral to amputation is more preserved and similar to normal conditions in TMSR patients as compared to non-TMSR patients. This observation at the single patient level was corroborated at the group level, as non-parametric Wilcoxon comparisons showed that the index of activation extent is not significant different between TMSR patients and healthy controls (p=0.16), whereas it is significantly more negative in non-TMRS patients as compared to controls (p=0.02).

Strength. Similar analyses were performed on the peak t-values, taken as an index of activation strength of the representations in M1 concerning *hand movements* (i.e. the maximal t-value on the side representing the amputated limb minus the maximal t-value representing the healthy limb). These results mimic those of the index of activation extent: the index of activation strength in TMSR patients was positive and not significantly different from healthy controls (t=.78, p=.46; t=1.09, p=.31; t=-.32, p=.75 for TMSR-01, -02 and -03), whereas it was negative in two non-TMSR patients (non-TMSR-01 and non-TMSR-02) and significantly different from controls for one for them (non-TMSR-01, t= 1.91, p=.04 one-tailed; see Fig.4.2C). Similar analyses were performed for wrist and elbow movements, and led to findings similar to hand activations (supplementary materials; Fig.4.S2).

Distance. To study whether in addition to the preserved extent and strength of M1 activations, patients with TMSR also have a preserved location and topographical sequence of activations of the different movements in M1, we localized the centers of mass of activation clusters for hand movements and tongue movements in each hemisphere and calculated their distance (measured as the 3D-euclidian distance) as a proxy of reorganization due to amputation (see supplementary materials and Fig.4.S3). This distance index was calculated by subtracting the hand-to-tongue center
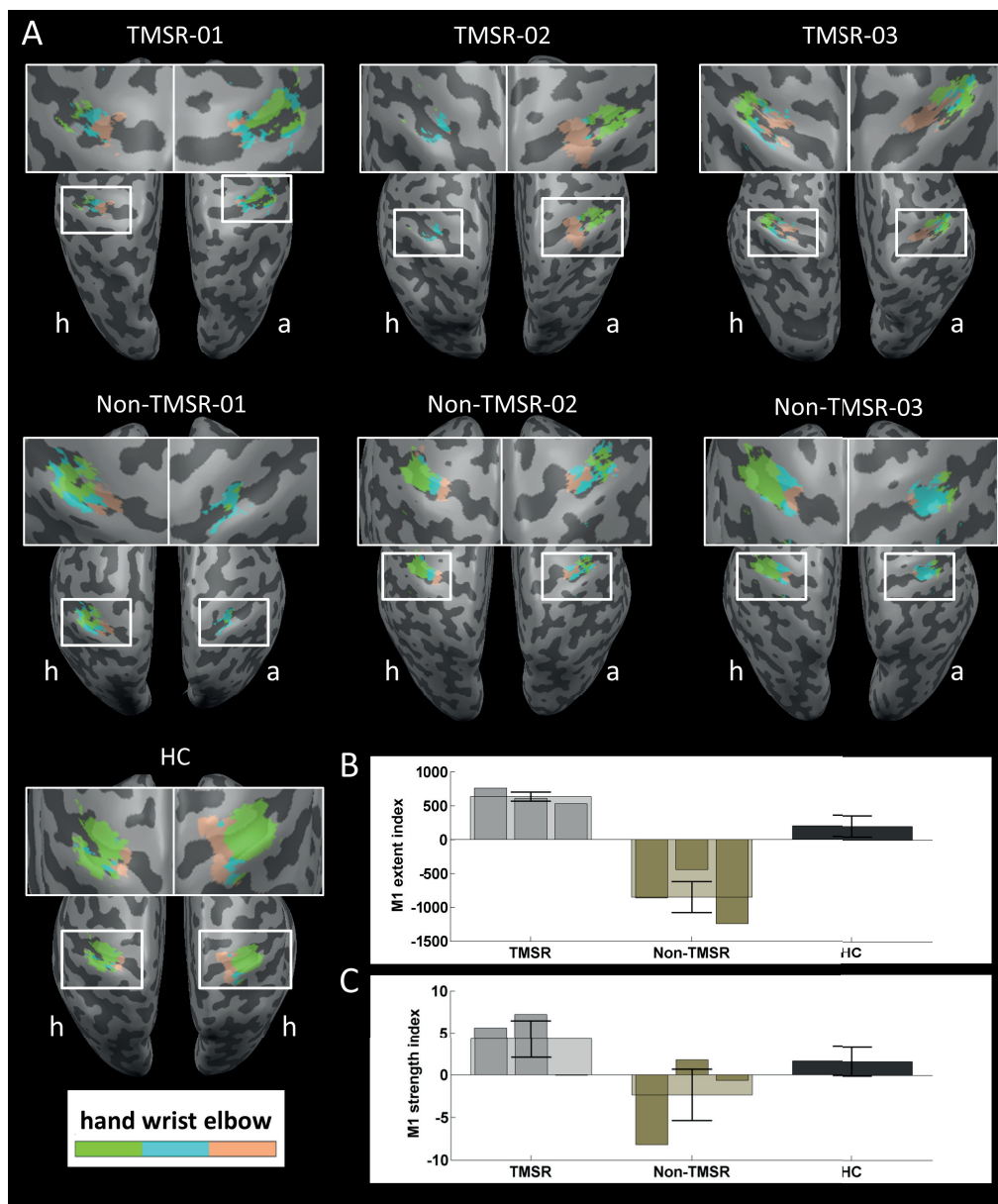
Fig.4.2 Representations of upper limb movements in M1. A) M1 regions activated by movements of the contralateral hand in each TMSR and non-TMRS patient and on average in healthy controls. **B)** Indices of differential M1 activations for the right (i.e. contralateral to amputation in unilateral amputees) and left M1 for number of activated voxels, analyzed as a measure of the extent of M1 hand representations. **C)** Indices of differential M1 activations for the right (i.e. contralateral to amputation in unilateral amputees) and left M1 for maximal t-values, analyzed as a measure of the strength of M1 hand representations. Error bars represent the standard error of the mean.

of mass distance in the right hemisphere (contralateral to amputation in unilateral amputees) and in the left hemisphere (see Supplementary Fig.4.S3). The distance index was close to zero in healthy controls, confirming a symmetrically large distance between the representations of the hand and tongue in both hemispheres and the same

was found for both patient groups. In none of the TMRS and non-TMSR patients these indices were significantly different from healthy controls at the single-subjects level, as shown by non-significant Crawford tests (all p>0.18). Thus, in terms of distance in M1 between body representations, both patient groups (TMSR; non-TMSR amputees) did not differ from healthy controls (see discussion).

These analyses of M1 activity induced by movements of the amputated limb suggest that TMSR results in an almost normal representation of hand movements in contralateral M1 in extent and strength, which were reduced in non-TMSR patients. The location of these different body part representations did not differ between TMSR, non-TMSR patients, and healthy controls.

4.3.2 S1 Mapping

Activation maps in S1 induced by tactile stimulation of the different body regions are shown in Fig.4.3A. For TMSR-01, we observed significant activations within the right S1 (contralateral to the amputated limb) in response to the stimulation of all the three skin areas of the residual limb that elicited hand sensations (i.e. the index, the middle finger, and the palm on the left reinnervated residual limb). The representations of the amputated hand were located in corresponding portions of right S1 (i.e. compared to those representing the right healthy hand in left S1). For TMSR-02 we observed a significant activation within right S1 (small in size though) in response to the stimulation of the regions of the left chest resulting in sensations on the amputated left index finger and on the amputated left little finger. These activations in were contralateral and at a corresponding location within S1 with respect to the representation of the fingers of the non-amputated hand. For TMSR-03, (who suffered bilateral amputation) the stimulation of the different body-parts did not yield any significant response within S1 on either side of the body. TMSR-03 and his respective control patient (Non-TMSR-03) were then excluded from further S1 analyses. For patient non-TMSR-01, only the stimulation of a residual limb region inducing referred sensations on the missing thumb elicited small activation in contralateral S1. For patient non-TMSR-02, only the stimulation of a residual limb region inducing referred sensations on the missing little finger elicited a rather dispersed activity in the contralateral S1. Stimulation of other portions of the residual limb did not elicit activation in the S1 hand areas. These S1 maps suggest that
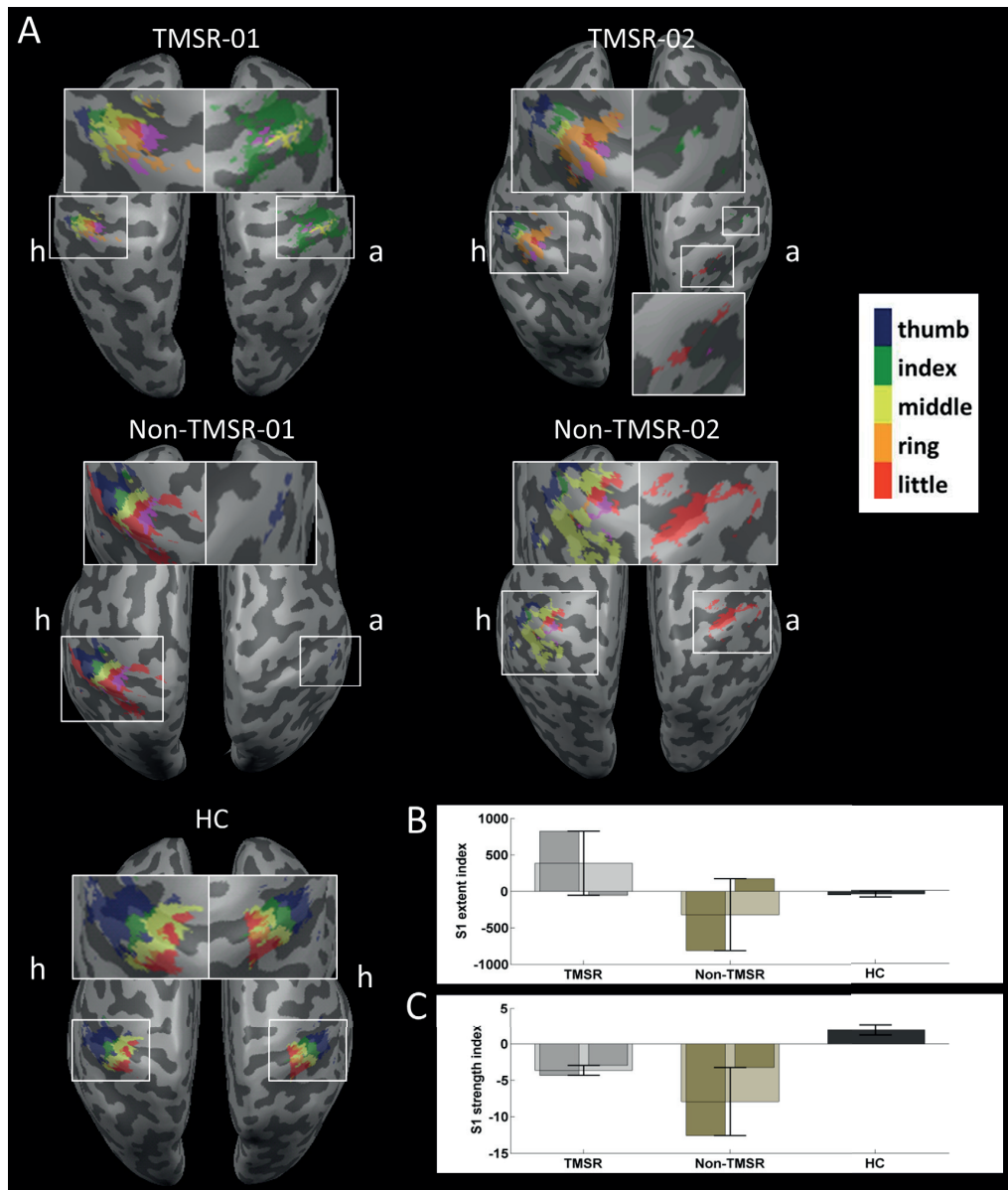
Fig.4.3 Representations of upper limb tactile processing in S1. A) S1 regions activated by stimulation of different intact body parts of the reinnervated skin regions inducing well-localized referred tactile sensations on the missing limb in TMSR amputees and of regions of the residual limb inducing referred tactile sensations in non-TMSR patients. **B)** Indices of differential S1 activations for the right (i.e. contralateral to amputation in unilateral amputees) and left S1 for number of activated voxels, analyzed as a measure of the extent of S1 hand representations. **C)** Indices of differential S1 activations for the right (i.e. contralateral to amputation in unilateral amputees) and left S1 for maximal t-values, analyzed as a measure of the strength of S1 hand representations. Error bars represent the standard error of the mean.

multiple and reliable finger-specific S1 representations of the missing hand are accessible in TMSR patients. Activations evoked by stimulation of the healthy side of the body resulted in well-defined somatotopically organized activity in the contralateral S1 in both TMRS and non-TMRS amputee groups.

In order to compare statistically the S1 representations for the amputated and the healthy limb we performed the same analyses as performed for M1 (extent, strength, distance). Thus, also for S1 we computed the difference between contralateral S1 activity when stimulating the amputated versus the healthy limb. For each patient, these values were compared to the homologous indices computed in healthy controls (i.e. as the difference between activity evoked by left and right upper limb stimulation in the contralateral S1).

Extent. Concerning the number of voxels in TMSR patients, the index of activation extent was close to 0 and not significantly different to healthy controls in TMSR-02 (t=-0.06, p=.48) and was even positive in TMRS-01 (t=6.89, p<.001). Thus, S1 activity evoked by applying touch to reinnervated skin regions that induces tactile sensation on the missing hand and fingers was comparable (or even enhanced) in extent with respect to S1 activations induced by stimulation of the contralateral healthy limb. This was different in control amputee patients, in whom the index of activation extent was negative and significantly lower than in controls (t=-6.05, p<.001), in patient non-TMRS-01, thus showing reduced S1 activation when stimulation was administered to residual limb regions evoking referred tactile sensations on the missing thumb. In Non-TMRS-02, the index of activation extent was not significantly different compared to healthy controls (t=1.75, p=.12) (see Fig.4.3B).

Strength. S1 activity evoked by stimulation of reinnervated skin regions was lower in intensity, as compared to stimulation of the healthy limb and this was found in all amputees, independently on whether they received TMSR surgery or not. Indeed, activation indices for t-max values were negative in all amputee patients and different from those in healthy controls (all p-value<.05) (see Fig.4.3C).

Distance. In order to study whether TMSR also resulted in a differential reorganization of S1 as compared to non-TMSR amputees, for each participant we calculated the 3D-euclidian distance between the centers of mass of the representations of the index finger and the lips in each hemisphere (see Fig.4.4A). The distance index in S1 was calculated by subtracting the lip-to-hand distance in the right hemisphere (contralateral to amputation) and in the left hemisphere (see Fig.4.4B). This index was close to 0 for the TMSR amputees, where hands and lips

107
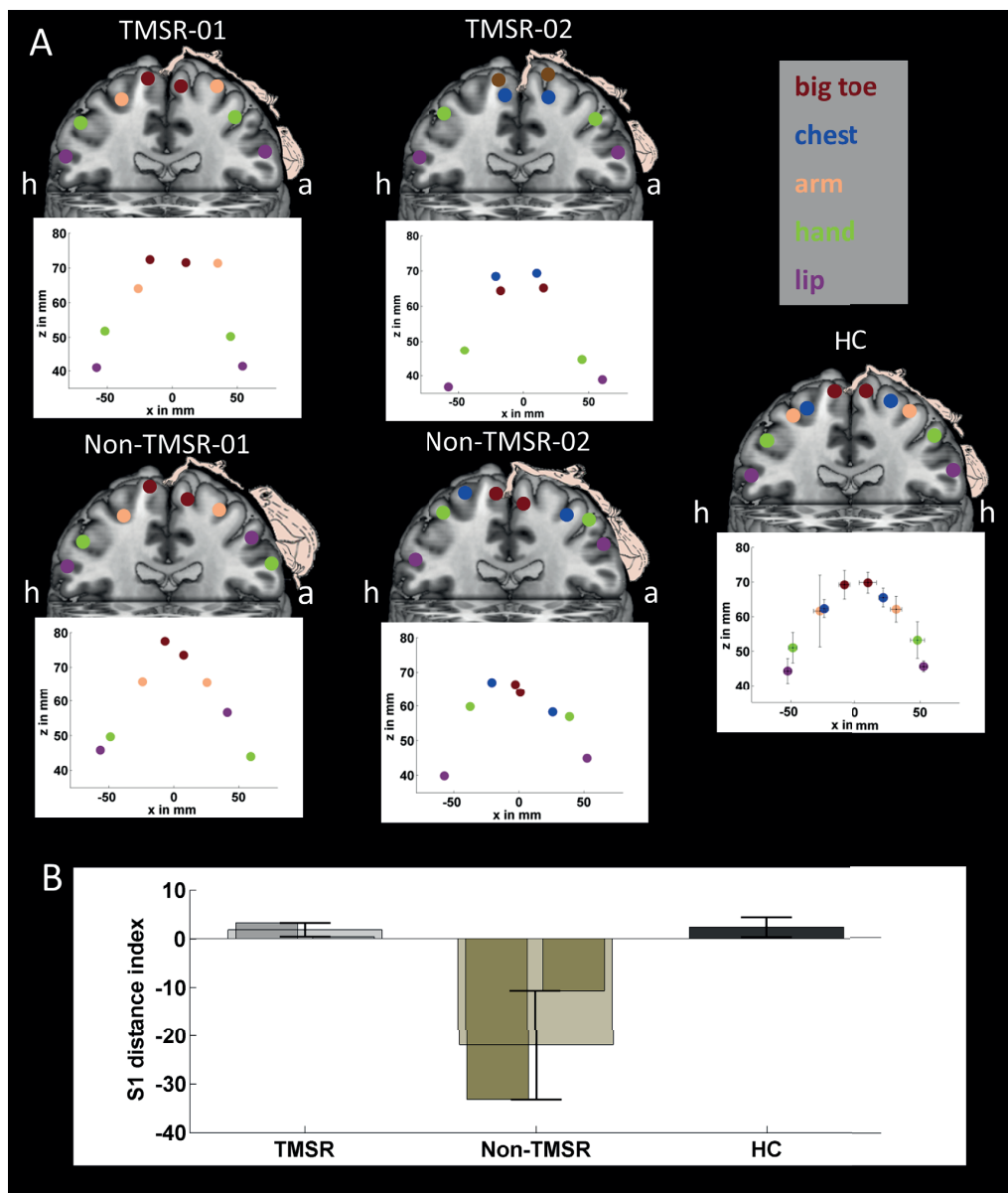
Fig.4.4 Localization and plasticity in S1 body parts representations. A) Centers of mass for the representations of different body parts mapped in S1 and their correspondence in S1 homunculus. **B)** Index of organization of S1 representations in the two hemispheres computed as the difference in the right (i.e. contralateral to amputation in unilateral amputees) and left S1 of the distance between the center of mass for activity evoked by lip and by index finger stimulation.

representation were symmetrical and not significantly different than those in healthy controls (t=.12, p=.89, and t=-.33, p=.75, respectively). For non-TMSR amputees, this index was negative and significantly different from healthy controls for both non-TMSR patients (Crawford test: t=5.87, p=.001 and t=-2.16, p=.03, one-tailed in non-TMSR-01 and Non-TMSR-02 respectively), compatible with S1 reorganization, with invasion of face areas into the hand areas for the hemisphere contralateral to

amputation. These findings were confirmed also by non-parametric comparisons between groups, whereby no difference was found for TMSR patients as compared to healthy controls (Wilcoxon test, p=.22), whereas values for Non-TMSR patients were significantly lower than those for healthy controls (p=.03) (Fig.4.4B).

To summarize, the TMSR procedure is associated with a preserved somatotopic representation in S1 for the regions of the missing limb whose peripheral nerves were re-targeted to different skin regions and whose stimulation leads to tactile sensation on the missing hand and fingers. The extent of those representations was similar to those of homologous body parts in the contralateral hemisphere, as in healthy controls. However, the strength of these representations was weaker as compared to those for the intact body parts on the healthy limb and to healthy controls.

4.3.3 Functional connectivity between M1 and S1 and functional connectivity between M1 and S1 with posterior parietal cortex

In order to study how M1 and S1 limb representations were interconnected functionally and how each area was connected with multisensory limb representations in posterior parietal cortex, we analysed resting state functional connectivity between (1) the hand maps in M1 and in S1, (2) between the hand maps in M1 and SPL, (3) and between the hand maps in S1 and SPL. The results are presented in Fig.4.5.

For the M1-S1 analysis, we compared the strength of functional connectivity in the hemisphere contralateral and ipsilateral to amputation by computing an index of M1-S1 connectivity as the difference between the normalized Z-scores for the right and the left hemisphere. This index was positive in TMSR-01, close to zero in TMSR-02, and in both cases within the normal limits obtained in healthy controls (p=.65 and p=.85 respectively), indicating a symmetric pattern of connectivity between the primary motor and somatosensory cortices. The same index was negative in both non-TMSR patients, and significantly different from controls in patient non-TMSR-01 (t=-4.52, p=.001; patient non-TMSR-02: t=-1.19, p=.07 one-tailed). Statistical analysis at the group level showed a significant difference in connectivity indices between non-TMSR and healthy controls (Wilcoxon test, p=.01), but not between TMSR patients and healthy controls (p=.5). Thus, connectivity between primary somatosensory and

motor maps of the missing hand is preserved in the present TMSR patients, but is reduced in non-TMSR amputees (see Fig.4.5).

For the SPL functional connectivity analysis, we first identified a seed region in the superior parietal lobule (SPL) showing high connectivity with M1 and S1 in healthy controls (see Methods and supplementary materials). We then analysed the functional connectivity between the SPL-M1 and between the SPL-S1 hand representations in TMSR and non-TMSR patients (connectivity indices were computed as the difference in normalized Z-scores for M1-SPL and S1-SPL connectivity in the right minus the left hemisphere). Concerning M1-SPL connectivity, in both TMSR and non-TMSR patients, M1-SPL indices were negative, indicating stronger M1-SPL connectivity for the healthy limb region compared to the amputated limb region, whereas they were close to 0 in healthy controls. Although at the single patient level these data did not differ statistically from controls (p-values TMSR01: 0.23; TMSR02: 0.19; TMSR03: 0.25; non-TMSR-01: 0.12; non-TMSR02: 0.22; non-TMSR03: 0.06), group level analysis showed that the indices were significantly lower than controls in TMSR (p= 0.03) and non-TMSR (p= 0.01) patients (Fig.4.5).

For S1-SPL indices, functional connectivity indices were negative in all amputees and close to zero in healthy controls (with marginally significant differences for patients TMSR01, p =0.09; TMSR02, p=0.14; and significant differences for patients non-TMSR01; t=-2.33, p= 0.02 and non-TMSR02, t=-2.29, p=0.02). At the group level, connectivity was significantly lower than controls in the hemisphere contralateral to amputation both in TMSR (p=0.018) and non-TMSR (p=0.018) patients.

Taken together, these results suggest that TMSR is associated with preserved connectivity between S1 and M1, but with abnormally low M1-SPL and S1-SPL connectivity, that is between the M1 and S1 hand regions with multimodal parietal regions (Fig.4.5). These results suggest that in TMSR the local connectivity within primary somatosensory and motor areas is comparable to healthy controls; however, more distributed connectivity, i.e., connectivity between somatosensory and motor maps with parietal multisensory areas, is reduced and similar to what is observed in non-TMSR patients.
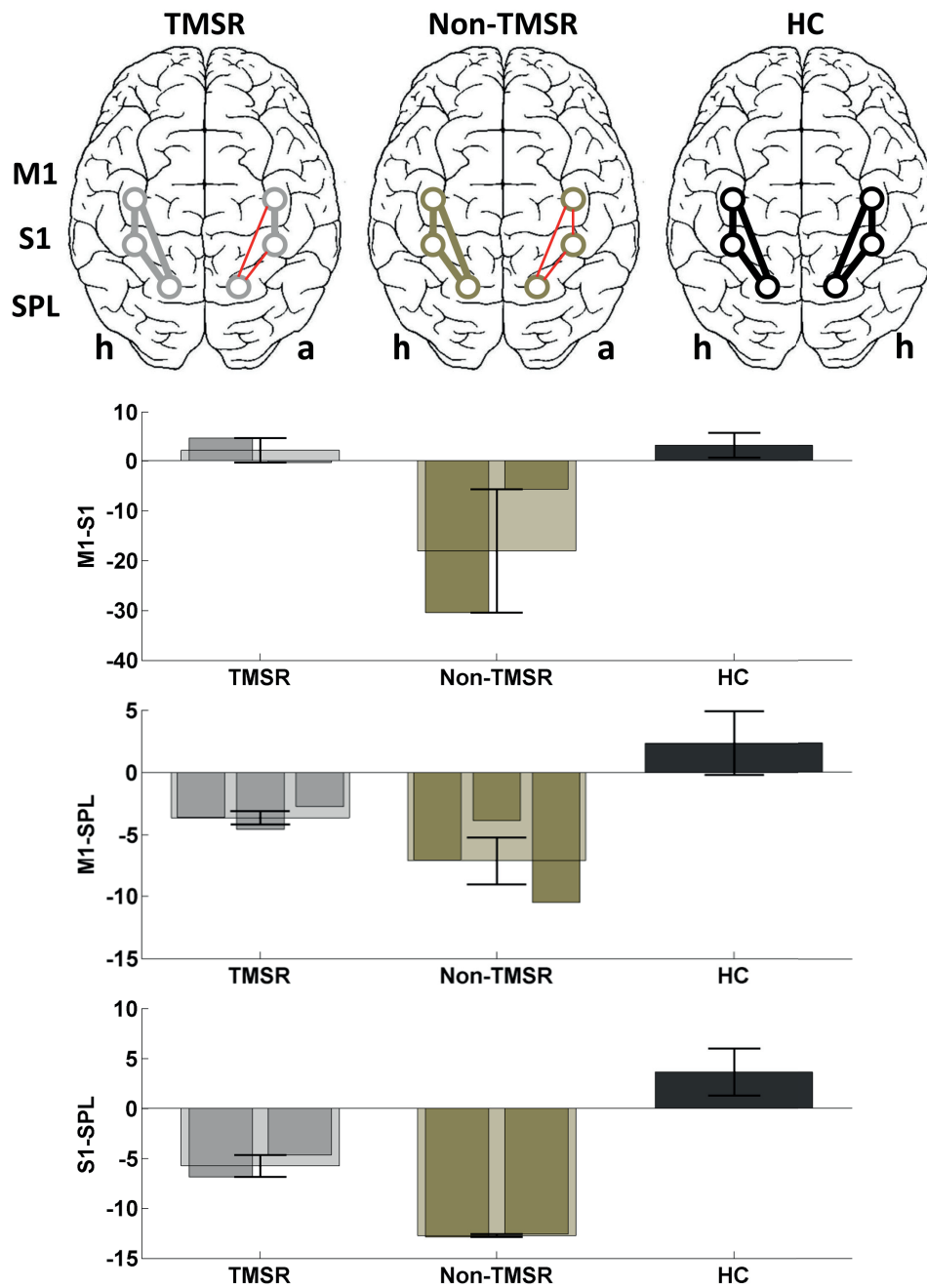
Fig.4.5 Connectivity between M1, S1 and multisensory areas in the superior parietal cortex (SPL). A) Schematic representation of the pattern of resting-state connectivity between M1, S1 and SPL in the right and left hemisphere. The thickness of the connecting lines represents the connectivity strength and weak connections are shown in red. B) Index of differential connectivity between the right (contralesional to amputation) and the left hemisphere for M1-S1, M1-SPL and S1-SPL regions.

4.3.4 Visual enhancement of touch (VET)

Based on the previous results, one might predict that primary sensory functions of the TMSR skin region are preserved and acquire some of the tactile properties of the missing hand before amputation, as shown by previous studies demonstrating enhanced tactile acuity on TMSR regions as compared to homologous non-reinnervated skin regions (see **Marasco et al. 2009**). However, because of the functional disconnection between M1/S1 and SPL, TMSR patients should not show visuo-tactile integrative behavioral effects, typically present for intact body representations, as these might rely on the interaction between unisensory and multisensory areas in the posterior parietal cortex (**Ro et al. 2004, Konen et al. 2014, Taylor-Clarke et al. 2002**). To test this hypothesis, we studied VET in TMSR amputees, as an index of visuo-tactile interaction (**Kennett et al. 2001; Serino & Haggard, 2010**). VET consists in a facilitation of tactile acuity if subjects simultaneously see the stimulated body part (without seeing the actual tactile stimulation), as compared to conditions of no visual stimulation, vision of a non-bodily stimulus, or vision of a non-homologous body part (**Serino et al. 2009**). Here, we compared the effectiveness of the VET effect for reinnervated and non-reinnervated body parts by measuring tactile acuity on TMSR and non-TMSR regions of the residual limb or chest, while patients were either viewing the body part to which tactile sensations were referred to (i.e., the hand or the physically stimulated body part, i.e. the arm in TMRS01 or chest in TMSR02 and TMSR03). These results were compared to the VET effect in healthy participants on the hand and the chest (see Methods for details).

In line with previous reports (**Serino et al. 2009, Haggard et al. 2007, Kennett et al. 2001**), in healthy participants, tactile acuity (d' scores) was higher when visual information matched the stimulated body part (see Fig.4.6). The ANOVA run on d' scores with Visual condition ("View Hand", "View Chest") and Touch ("Touch Hand", "Touch Chest") as within subjects factors, showed a significant two-way interaction ($F_{(1,11)}=10.99$, $p< 0.01$). Post hoc analysis (Fisher test) confirmed that viewing the chest improved tactile performance on the chest (d'=0.92), as compared to the hand (d'=0.57, $p<0.05$), and complementarily, viewing the hand improved tactile performance on the hand (d'=0.98) as compared to viewing the chest (d'=0.59,
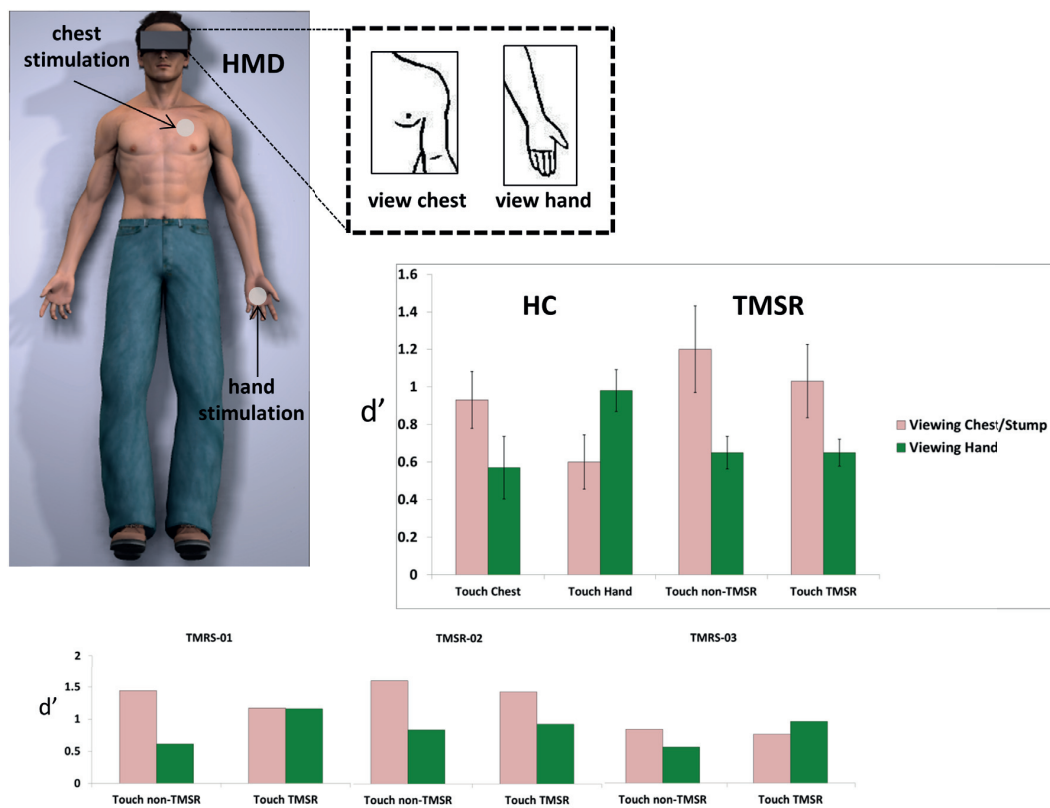
Fig.4.6 Visual enhancement of touch. Schematic representation of the VET set-up, showing the participants' posture during the experiment and visual stimulation provided via head-mounted displays. Accuracy in two-point discrimination task (measured as d' score) for tactile stimuli administered to the each of two target body parts (hand-chest in healthy controls (HC); TMRS or non-TMSR skin regions in TMSR patients), while participants viewed either stimulated or the non-stimulated body part. Average data for TMSR patients and healthy controls are shown in the top graphs. Individual data for TMSR patients are shown in the bottom graphs.

$p<0.04$). Thus, in healthy participants, a clear somatotopic pattern in the VET effect was found (**Serino et al. 2009**), both for the hand and the chest.

As shown in Fig.4.6, in all TMSR patients, an amelioration of tactile acuity was found when tactile stimulation was administered on the non-TMSR skin region when patients were looking at the same body part (chest or arm), as compared to when they were looking at a hand, thus showing a somatotopically determined VET effect. However, crucially, for the present study, this effect was absent when tactile stimulation was provided to the TMSR region (chest or residual limb) evoking tactile perception on the hand while patients were looking at the hand, as compared to when looking at their chest or arm. In order to provide statistical support to these observations, we calculated an index of the VET effect for the TMSR and the non-

113

TMSR region as the difference in d-prime scores when viewing the body part stimulated or when viewing the other body part. Those values were compared to the analogues indices computed in healthy controls for VET effect on the hand and on the chest. For the non-TMSR regions, the VET index was equivalent in the three TMSR patients to the VET index for chest stimulation in healthy controls (Crawford test: TMSR01: t = 1.075, p=0.30; TMSR02: t= 0.366, p = 0.72; TMSR03: t = -0.183, p=0.85). In contrast, in all of the three TMSR patients, the VET index for the TMSR region was significantly lower than that for the hand in controls (TMSR01: t = -2.355, p= 0.038; TMSR02: t = -3.936, p = 0.002; TMSR03: t = -3.006, p= 0.012). These findings were confirmed by group-level analyses, showing equivalent VET indices for non-TMSR regions in patients and chest stimulation in controls (Wilcoxon test: p=.48), and significantly lower indices for TMSR regions in patients compared to hand stimulation in controls (p<.001). Thus, these psychophysical data reveal an absence of visuo-tactile interaction for TMSR body regions.

4.4 Discussion

This study is the first systematic investigation of how a bionic prosthesis for upper limb amputees based on TMSR impacts the functional organization of the missing limb in M1 and S1, their mutual connectivity, and their connectivity with posterior parietal cortex (SPL). We report that, first, the M1 maps for hand and arm movements controlling the prosthetic limb are well preserved in TMSR patients: they are similar in extent and strength compared to healthy individuals performing the same actions with physically existing limbs and are stronger than those in non-TMSR amputees. Second, S1 activity evoked by applying touch to reinnervated skin regions on the chest or residual limb (inducing tactile sensation on the missing hand) activated well-defined portions in locations that were comparable to the normal hand region in S1, although these activations were weaker compared to healthy controls. Third, TMSR is associated with preserved local functional connectivity between M1-S1 upper limb regions, whereas this was not the case for non-TMSR amputees. Finally, functional connectivity with SPL was reduced in both amputee groups for M1 as well as S1 and associated with the absence of the VET, shown previously to depend on projections from SPL to S1. Although these findings are based on a relatively limited sample of patients, primarily due to the fact that TMSR patients are rare, we were able to exploit

114

the high spatial resolution of ultra high-field 7T fMRI and single case analysis. Here, we discuss what these findings reveal about plasticity of body maps in S1 and in M1 and discuss the relevance of our findings for current and future approaches in bionic limbs.

4.4.1 TMSR preserves M1 upper limb representation

In order to map motor cortex in amputees, we used a paradigm employed by previous investigators, consisting in asking patients to perform movements with their amputated limb or movements with their mouth and studied the associated fMRI activity in M1 (**Lotze et al. 1999; Makin et al. 2013, 2015b; van den Heiligenberg et al. 2015**). Because of the lower spatial resolution of earlier work using 1.5T or 3T fMRI (and because of somatosensory-related processing associated with the tested movements), previous reports were not able to distinguish between motor versus somatosensory evoked activity or whether activity was in the anterior and posterior banks of the central sulcus. Accordingly, it was not separately investigated how M1 and S1 contributed to the reported activation patterns in amputees. Across these studies it was found that, as compared to healthy participants, sensorimotor activations in upper limb amputees differ in terms of strength, extent and location (see **Reilly & Sirigu, 2008** for a review). Extending our previous work on human S1 using ultra-high field fMRI in healthy subjects (**Martuzzi et al. 2014, 2015**) we were here able to separately investigate S1 and M1 in TMSR patients. We found that the M1 activations during movements of the phantom limb in non-TMSR amputees were reduced in terms of extension and strength as compared to healthy controls, in line with previous findings (reporting activations in M1 and S1). This was different in the three tested TMSR patients in whom M1 activations were comparable to controls. Thus, M1 activity related to the control of the prosthetic limb (via decoded EMG signals recorded from muscles re-innervated by residual arm nerves) is associated with preserved upper limb activations in TMSR amputees. This suggests that the functional solicitation of M1 upper limb areas associated with the use of a prosthetic limb is potentially able to re-instate normal M1 maps. In all participants (TMSR, Non-TMSR and healthy controls), the mapped motor activations were located on the precentral gyrus corresponding to M1, and showed the normal somatotopic organization within M1, compatible with a recent 7T study reporting finger

somatotopy in M1 in healthy participants (**Siero et al. 2014**). We note that although the somatotopic organization was observed in all participants, the exact location of motor maps differed across participants, highlighting the importance of single subject analysis at ultra-high field strength to study the organization of M1.

We also measured the degree of cortical reorganization within M1 following amputation, by quantifying the displacement of lip activations towards the missing hand activations as used by previous authors using 1.5 or 3 T fMRI (**Lotze et al. 1999, 2001**; see **Mercier et al. 2006; Reilly et al. 2006; Reilly & Sirigu, 2008** for evidence from TMS). The present 7T fMRI investigation, however, did not reveal any evidence for cortical reorganization (i.e. changes in the location of the lip M1 representation with respect to the hand M1 representation in either group of amputees). Recent reports are in accordance with our results and showed that the displacement of lip representation, considered as a marker of cortical reorganization and previously related to phantom limb symptoms (e.g., Flor et al. 1995), is not always present or detectable (**Makin et al. 2015b**). Considering these controversial reports, currently the existence and nature of the relationship between the phenomenology of phantom limbs and cortical reorganization following limb loss remains unclear. In particular, cortical reorganization within M1 and S1 may not go hand in hand and should be investigated separately (further discussed below).

4.4.2 TMSR allows accessing S1 upper limb representation

Mapping somatosensory activations of the missing limb in S1 in amputees has been more challenging than mapping movements in M1 (**Yang et al. 1994; Ramachandran et al. 1995; Flor et al. 1995, Björkman et al. 2012**). Influential MEG studies assessed the maps of the missing limb in S1 by stimulating the patient's lip region and revealed evidence for a distorted somatotopic organization in S1 after amputation, suggesting that the face area shifted medially towards or into the hand area (**Yang et al. 1994; Ramachandran et al. 1995; Flor et al. 1995**). A more recent 3T fMRI study investigated the maps of the missing limb in S1 by stimulating specific residual limb regions that evoked referred tactile sensations on the missing hand (**Björkman et al. 2012**). These authors found that activity in several S1 regions that were activated by stimulation of the residual limb showed differences in location and extent depending on whether stimulation induced referred tactile sensation on the

missing hand or not (**Björkman et al. 2012**). In the present study we used 7T fMRI and extended this approach to TMSR patients, in whom specific tactile referred sensations can be induced by stimulating reinnervated skin regions on the chest or the residual arm. Such surgically reinnervated skin regions have the advantage of covering larger portions of skin and of being spatially well segregated, offering a high resolution tactile interface to induce controlled, reliable and specific phantom limb sensations in TMSR patients (**Kuiken et al. 2007a, Hebert et al. 2014**). Thus, we asked whether spontaneous S1 reorganization as occurring in non-TMSR-amputees differs from S1 reorganization associated with the surgical redirection of somatosensory nerve fibers in the TMSR procedure. Our data reveal two findings. First, S1 tactile activations concerning the missing limb of TMSR patients were located at a position corresponding to the S1 hand activations in healthy controls, although they were weaker in terms of strength of activation. Second, TMSR-related S1 activations were somatotopically organized and comparable to those in healthy controls (based on the distance between hand and lip representations); this was not the case for non-TMSR patients, who showed larger shifts of maps in S1. The displacement of the lip map has been proposed as a marker of maladaptive plasticity in amputee patients, due to lack of hand-related sensory inputs in amputation (**Flor et al. 1995**). Moreover, the degree of such maladaptive changes has been related to the level of phantom pain in amputees (but see **Makin et al. 2013, 2015b**) and has been shown to be reversible after an extensive tactile training over the residual limb region, which also decreased pain ratings (**Flor et al. 2001**). Based on these earlier findings and on the normal topographical S1 organization and smaller degree of maladaptive plasticity found in TMSR patients, we speculate that TMSR might prevent maladaptive plasticity in S1 (in addition to M1) maps and may potentially prevent or diminish phantom limb related symptoms. However, we note that the present investigation, based on data from three TMSR, was not aimed at and does not allow establishing a direct link between S1 organization and phantom limb pain.

4.4.3 TMSR preserves functional connectivity between M1-S1 upper limb maps

The interaction between motor and somatosensory maps is crucial during action execution and studies in healthy subjects have revealed strong functional connectivity within a network formed by the motor and somatosensory cortex and other higher-tier

sensorimotor areas (e.g. premotor cortex, **Yeo et al. 2011**), as well as with association cortex (e.g., the superior parietal lobe **Markov et al. 2013** and **Rizzolatti and Matelli, 2003**), i.e. the so-called "sensorimotor" network (**Beckman et al. 2005; Biswal et. al, 1995; Cordes et al. 2000, 2001; Lowe et al. 1998; Xiong et al. 1999; Fox et al. 2006; De Luca et al. 2005**). This sensorimotor functional connectivity has been shown to be altered in many clinical conditions, such as stroke or schizophrenia (**Gerloff et al. 2006; Helmich et al. 2010; Meyer-Lindenberg et al. 2001; Mostofsky et al. 2009; Wang et al. 2010**). Recently, it has been observed in amputees that the functional connectivity between the representation of the missing limb and the rest of the sensorimotor network is decreased (**Makin et al. 2015**). Based on the present high-resolution and functionally specific mapping approach, we were able to directly test M1-S1 connectivity and found that the M1 hand map was normally connected with the S1 hand map in TMSR patients, while M1-S1 functional connectivity was significantly reduced in non-TMSR amputees. Together M1-S1 connectivity data and M1 and S1 mapping data suggest therefore that the TMRS procedure is associated with preserved upper limb sensorimotor maps and preserved mutual interconnections.

4.4.4 M1 and S1 are functionally disconnected from multisensory parietal regions in TMSR patients

Upper limb control and perception depends not only on neural processing within motor and unisensory cortices, but on a more widely distributed network of areas integrating multisensory and motor signals that involve higher-level motor regions and multisensory regions in posterior parietal cortex. The posterior parietal cortex, in particular, is a key region for the integration of multisensory bodily signals (**Berlucchi & Aglioti, 2010; Graziano & Botvinick, 2002; Serino & Haggard, 2010, Blanke et al. 2015**). Moreover, posterior parietal cortex (and its connection with premotor areas) has been linked to multisensory visuo-tactile stimulation and the sense of hand ownership (**Ehrsson et al. 2004, 2005; Gentile et al. 2015**). Prominent functional and structural connectivity exist between posterior parietal and sensorimotor cortex (**Mars et al. 2011; Yeo et al. 2011; Rushworth et al. 2006; Uddin et al. 2010; Tomassini et al. 2007**) underlying motor execution and motor imagery (**Gao et al. 2011; Solodkin et al. 2004**). Therapeutically, paradigms used to treat phantom limb syndrome (such as the mirror box therapy) directly exploit the

multisensory nature of limb representation and likely rely on multimodal (i.e. visuo-somatosensory-motor) maps of the upper limb within an extended multisensory-motor network (**Chan et al. 2007; Ramachandran & Altschuler, 2009; Ehrsson et al. 2008**). When we investigated the integrity of functional connectivity of M1 and of S1 with the multisensory regions of the posterior parietal cortex, namely SPL, known to integrate cues from different sensory modalities, we found that M1 and S1 were less functionally connected with the SPL. Importantly, this appeared to be the case both for non-TMSR and TMSR patients, suggesting reduced connectivity between unimodal and multimodal limb maps also in TMSR patients. These results extend recent reports by Makin et al. (**2015a**) showing that in amputees, the combined S1-M1 map of the missing limb is less connected with the sensorimotor network, as defined by Beckmann et al. (**2005**). Importantly, our results show that only distant, but not local, connectivity of the upper limb is impaired in TMSR patients. Thus, although the repetitive movements of the EMG-driven myoelectric prosthesis in TMSR patients seems to re-instate M1 (and partially S1) representations and their mutual local functional connectivity, current TMSR systems does not normalize connectivity with more distant parietal multisensory regions, as reflected in the decreased connectivity of M1 and of S1 with SPL.

The latter finding was further supported by the behavioral data on VET, showing that - although touch sensation on the missing limb can be reliably evoked in TMSR patients, this information is not integrated with visual bodily cues. Indeed, viewing a hand, while performing a tactile spatial discrimination task on the re-innervated skin region, did not improve tactile perception in TMRS patients: the VET effect that occurs in healthy participants (**Haggard et al. 2003; Kennett et al. 2001; Serino & Haggard, 2010**) is absent in TMSR patients. The VET effect depends on the integration of visual cues related to the body with tactile inputs, based on projections from multimodal areas in posterior parietal cortex to S1 (**Cardini et al. 2011; Konen & Haggard, 2014; Ro et al. 2004; Serino et al. 2009; Taylor-Clarke et al. 2002**). The lack of hand-related VET in TMSR patients therefore corroborates the reduction of functional interactions between SPL-S1 hand maps. We speculate that this is due to the fact that current TMRS interfaces do not utilize somatosensory inputs (via the reinnervated skin regions) in current prostheses. Such integrated tactile input seems important for the development of future TMSR devices as under normal conditions,

when we move our hands and touch different objects, we normally receive coherent visual, auditory, tactile, and proprioceptive cues that the brains integrates for optimal control (**Maravita et al. 2003**). However, in current TMSR-prostheses (and most other bionic limbs), motor commands generated to drive the prosthesis are controlled only with visual information related to the prosthetic limb, without integrated somatosensory feedback. Our behavioral and imaging data suggest that current procedures are not able to reinstate multimodal upper limb representations that are based on interactions between unimodal and multimodal hand maps.

4.5 Conclusions

"Closing the loop" between motor control and sensory feedback is a key target for the next generation of bidirectional neuroprosthetic devices. Recent advances have been made with peripheral implants (**Raspopovic et al. 2014**) and likely target the brain and S1 in particular (i.e. **Bensmaia, 2015; Bensmaia & Miller, 2014**) to inject tactile information sensed by the prosthetic device directly into the nervous system. These advancements may not only improve prosthesis control during hand-object interaction, but may also minimize abnormal cortical reorganization, boost prostheses acceptance and somatosensory experiences. Indeed, current models in neuroscience propose that complex bodily experiences such as the experience of the body as one's own (body ownership) normally arise through the integration of multisensory body-related cues, within a distributed network of unisensory and multisensory fronto-parietal areas (**Blanke, 2012; Blanke et al. 2015; Ehrsson, 2012; Tsakiris, 2010**). A prosthesis - being able not only to transform the patient's motor commands into movements of the prosthesis, but also to interface motor control with integrated multisensory signals from the robotic hand and objects, it is in contact with, may be felt like a real limb (**Bensmaia, 2015; De Preester & Tsakiris, 2014**). Such an embodied prosthetic limb would become "part of the patient's body" and have less maladaptive plasticity through full functional integration within and beyond sensorimotor cortex. Recent experiments with bidirectional signal flow including somatosensory feedback to the reinnervated skin regions (**Marasco et al. 2011)** or the peripheral nervous system **(Raspopovic et al. 2014**) suggest that this is feasible and potentially effective.

4.6 Supplementary materials

4.6.1 Non-TMSR patients

Non-TMSR-01 was a 46 years old male who suffered left transhumeral amputation 28 months from the present testing. Non-TMSR-02 was a 31 years old male with a left shoulder disarticulation amputation (14 months prior to present testing). Non-TMSR-03 was a 35 years old male with a left transradial amputation (18 months prior to present testing). Three healthy age-matched control participants also took part in the study (HC-01:03; 3 males). They were aged 30, 41, and 65 years old. None of them had history of psychological or neurological disease. Other five non age-matched controls were also included in the healthy controls group (mean age 22.6, SD=±4.5, 3 males).

4.6.2 Oral interview with amputee patients (TMSR and Non-TMSR)

Before the experiments, all amputee patients were interviewed by means of a semi-structured interview, The first part of the interview included the Edinburgh Handedness Inventory (Oldfield, 1971) to determine hand preferences. The second part of the interview included a questionnaire with 21 items (adapted from Giummara & Moseley, 2011) aimed at interviewing about residual sensations, phantom limb experiences and phantom limb pain. Items 1 to 14 investigated specifically phantom limb sensations. Items 15 to 18 aimed at collecting information about the use of an artificial limb. Finally items 19 to 21 investigated referred touch sensations. It appeared that when wearing their prosthetic device, none of them reported to feel discomfort or conflict between the phantom limb and the prosthesis; however, none of them claimed that their prosthetic limb was perceive as if it were their phantom limb, rather, the two coexisted and moved together, but were perceptually clearly distinguishable for all TMSR patients.

4.6.3 Sensory mapping of referred sensations

In terms of tactile sensation evoked by touching the re-targeted skin regions, TMSR-01 reported well-defined tactile sensations (described as pressure with touch) referred to the missing palm, thumb and index-middle fingers arising from tactile stimulation of different skin regions from the re-innervated residual limb, originating several weeks after surgical reinnervation. TMSR-02 reported that within 4 months

after surgical re-innervation, the numb area in front of her chest developed touch sensation (described as tingling) referred to regions of the missing hand and wrist. TMSR-03 reported referred sensations (described as pressure with touch) to his missing limb, when he touched on his chest, starting within 5 months from operation.

From the interview, it also emerged that in terms of tactile sensation evoked by touching the re-targeted skin regions, TMSR-01 reported well-defined tactile sensations (described as pressure with touch) referred to the missing palm, the thumb and the index-middle fingers arising from tactile stimulation of different skin regions from the re-innervated residual limb, originating several weeks after surgical reinnervation. TMSR-02 reported that within 4 months after surgical re-innervation, the numb area in front of her chest developed touch sensation (described as tingling) referred to regions of the missing hand and wrist. TMSR-03 reported referred sensations (described as pressure with touch) to his missing limb, when he touched on his chest, starting within 5 months from operation.

Von Frey filaments (**Fruhstorfer et al. 2001**) were used to apply a controlled force of 300g over selected skin regions and an orthogonal grid was employed to localize the stimulation site. The grid consisted of a plastic sheet with small holes (spacing between the holes 2mm). The grid was placed on the arm for patient TMSR-01 and on the chest for patients TMSR-02 and TMSR-03, and fixed on the skin with medical tape. The experimenter mapped the area by gently touching each point of the grid with the Von Frey filament. At each stimulation site, the patient was asked whether he/she felt any tactile sensation. If patients responded positively, they were asked whether they felt the stimulus as administered either on the residual limb, on the chest, on the phantom limb, or on both, and to localize as precisely as possible the referred sensation by pointing at an image of a left hand, arm and chest, placed in front of them. The experimenter recorded participants' answers and gently marked on the skin with different color the sensations referred to different fingers and different parts of the missing limb. The mapping procedure was repeated three times, in order to localize portion of the skin where participants had coherent and stable referred sensations.

4.6.4 fMRI mapping of referred sensations

For TMSR patients, the different portions of the reinnervated skin region inducing reliable sensation on the missing limb as well as neighboring regions inducing local sensation on the residual limb were selected, individually for each patients, based on the results of the perceptual assessment described above. Specifically, for TMSR-01, three locations of the residual left upper arm, whose stimulation induced reliable sensations on the left thumb, index-middle-finger and palm, were stimulated to map the representations in S1 of these body parts from the missing limb (see Fig.4.1). Another portion of the residual limb was stimulated to map the representation of the residual arm. Her normal right arm and the right hand, including the five fingers and the palm, were stimulated to map the representation of the healthy limb. For patient TMSR-02, in different blocks we stimulated three portions of the chest, inducing reliable sensations on the left missing index finger, little finger and palm, a region of the left chest with no referred sensation, the homologues region of the right chest, right arm, palm and fingers. For TMSR-03, we stimulated two regions of the reinnervated left chest, inducing referred sensation to the missing left index and little finger, a portion of the left chest inducing no referred sensation and homologues regions of the right chest.

In order to identify somatosensory representation of the missing limb in non-TMSR patients, we stimulated regions of the residual limb inducing reliable referred tactile sensation. For patient non-TMSR-01, we stimulated 4 regions on the residual limb, which led to referred tactile sensations on the missing thumb, index, pinky and whole hand respectively, as well as a region on the residual limb inducing no referred sensation, and the regions of the right chest, arm, palm and fingers. For patient non-TMSR-02, we stimulated 2 regions on the residual limb leading to referred tactile sensations on the missing thumb and little fingers, as well as a region on the residual limb inducing no referred sensations, and the regions of the right chest, arm, palm and fingers. For patient non-TMSR-03, a single region on the residual limb was stimulated, which led to referred tactile sensations on the missing thumb, index and middle fingers together, as well as a region on the residual limb inducing no referred sensations, and the regions of the right chest, arm, palm and fingers.

4.6.5 Functional connectivity analysis

Functional connectivity including 6 predefined seed regions, i.e. bilateral S1, M1, superior parietal lobule (SPL), was performed. The S1 regions were defined based on the somatosensory mapping of the index finger (or the most comparable available representation, see below). The M1 regions were defined based on the motor mapping of hand movement. The SPL ROIs were defined as the regions in posterior parietal cortex exhibiting the highest functional connectivity with the M1 and S1 hand ROIs in the group of 8 controls (see below).

First, the individual functional connectivity statistical maps (beta estimates) of seed-to-whole brain analysis with left M1, right M1, left S1, right S1 as seed regions were normalized into the MNI stereotaxic space. Second, a group-level analysis (one sample t-test, $p < 0.05$ FDR-corrected) using SPM8 was carried out using the previously mentioned normalized maps leading to two symmetrical clusters in left and right superior parietal lobules (see Fig.4.S1). These clusters were back-transformed into the native space of all participants and used in the seed based functional connectivity analysis.

Functional connectivity was analyzed using the Conn SPM toolbox (**Whitfield-Gabrieli & Nieto-Castanon, 2012**). Images were first preprocessed using SPM8 by applying realignment and coregistration with the functional images of the previous runs and at each voxel the BOLD signal was band-pass filtered (0.008-0.09 Hz). The cardiac and respiratory-related components of the BOLD signal were estimated using the RETROICOR algorithm (**Glover et al. 2000**) and regressed out from the data. The average BOLD signal of white matter and cerebrospinal fluid (CSF) and the six estimated motion parameters were also included as nuisance regressors in the model. The global signal (i.e. the mean BOLD signal in grey matter regions was not removed, **Hahamy et al. 2014**). The bivariate temporal correlations between all combinations of pairs of ROIs were calculated from the preprocessed BOLD time-courses of the resting state run. The obtained correlation coefficients were transformed into Gaussian values by applying the Fischer transform (**Fisher, 1915**).

For all participants (TMSR patients, non-TMSR patients and controls), the activation clusters in M1 induced by movements of the contralateral hand (or by
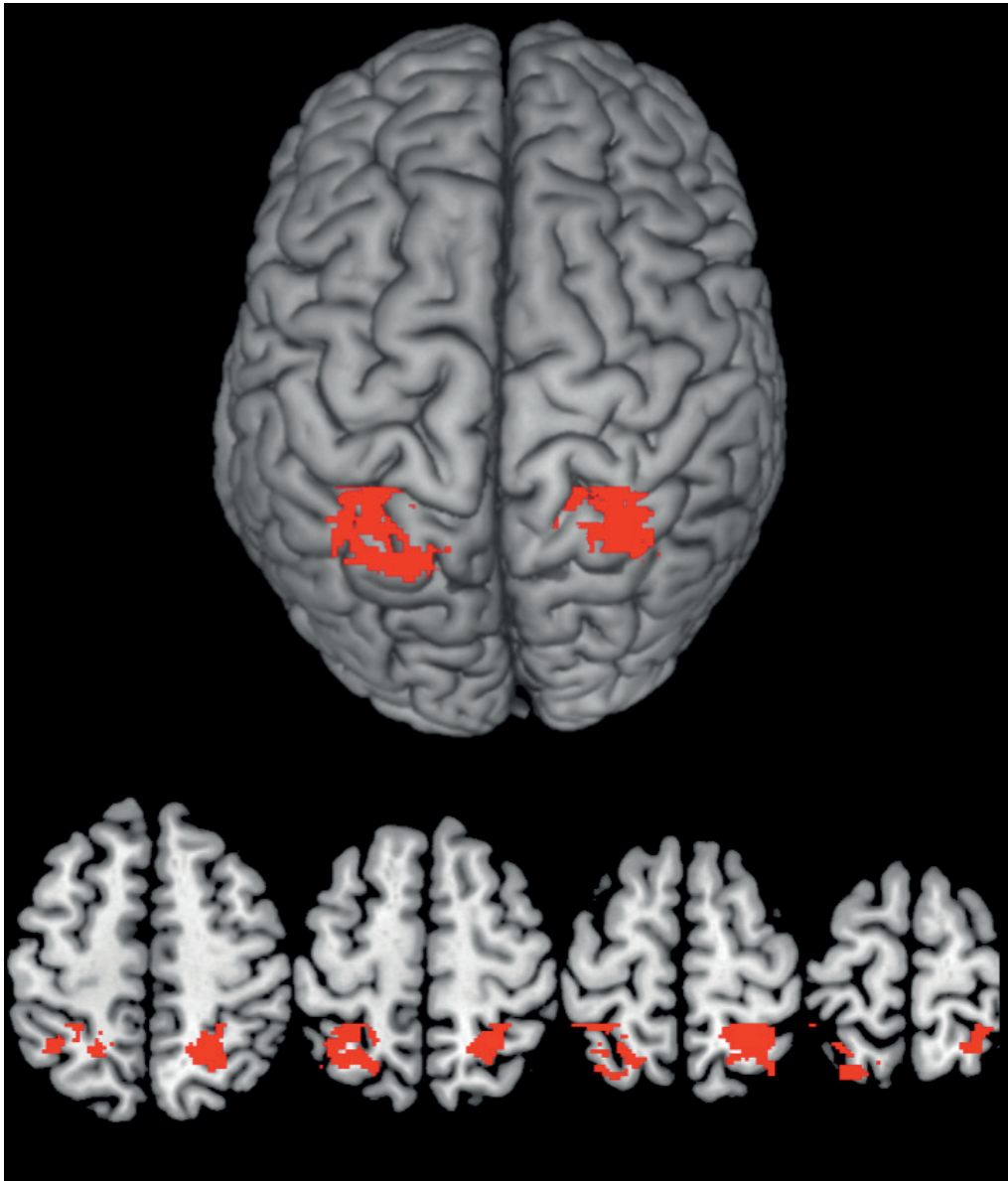
Fig.4.S1 Clusters in SPL for functional connectivity analysis. The MNI positions of the SPL clusters are x=25, y=-52, z=57 in the right hemisphere and x=-27, y=-53, z=58 in the left hemisphere.

movements of the contralateral phantom hand) were selected for both hemispheres. For TMSR patients and controls, the activation clusters in S1 induced by the tactile stimulation of the contralateral index (or the reinnervated skin region inducing referred sensations on the missing index for the amputated side in TMSR patients) were selected for both hemispheres. For non-TMSR patients, activation clusters in S1 corresponding to the stimulation of a region of the residual limb leading to referred sensations on the missing index were not available. Therefore, for non-TMSR-01, activation clusters in S1 induced by the tactile stimulation of the contralateral thumb

and of the residual limb region inducing referred sensations on the missing thumb were selected. For non-TMSR-02, activation clusters in S1 induced by the tactile stimulation of the contralateral little finger and of the residual limb region inducing referred sensations on the missing little finger were selected.

4.6.6 2DPT evaluation for VET

Prior to the VET experiment, we measured tactile spatial acuity on the chest (for TMSR-02 and TMSR-03) or on the arm (for TMSR-01), both on the areas generating only chest sensation or arm sensation (non-TMSR region) and on the skin regions generating hand-referred sensation (TMSR region) by means of 2PDT assessment. A staircase procedure was used as follows (**Taylor et al. 1983; Weinstein, 1968**). Blindfolded participants were tactilely stimulated with needles (diameter 1 mm) mounted on a caliper. Either double (67%) or single posts (33%) were administered at random. Only double posts were used to compute the staircase. The starting double posts separation was larger than 40 mm, clearly above the 2PDT. The separation was then reduced progressively by 50% after each set of three successive correct responses. When participants made an error, the separation was subsequently increased to midpoint of the current (erroneous) trial and the immediately preceding (correct) trial. This procedure was terminated at the shortest separation at which participants clearly perceived two posts. We then confirmed this 2PDT estimate by delivering five double posts at this separation randomly intermixed with five single posts. If participants scored between 7/10 and 9/10 correct, the threshold estimate was accepted for experimental testing. Otherwise, the procedure was repeated.

4.6.7 Statistical analysis for wrist and elbow movements in M1

The analyses performed on M1 hand representations were also conducted for wrist and elbow M1 representations. These results are shown in Fig.4.S2 and partially replicate the findings presented for hand movements representations in M1.

For the wrist, the indices of activated voxels were positive in all TMSR patients and not different from controls (all $p>0.11$). For patients Non-TMSR-01 and Non-TMSR-02, the indices of activate voxels were negative and significantly different from controls ($p=0.01$ and $p=0.02$ respectively). For patient TMSR-03, the index of activated voxel was close to 0 and not different from controls ($p=0.33$). At the group
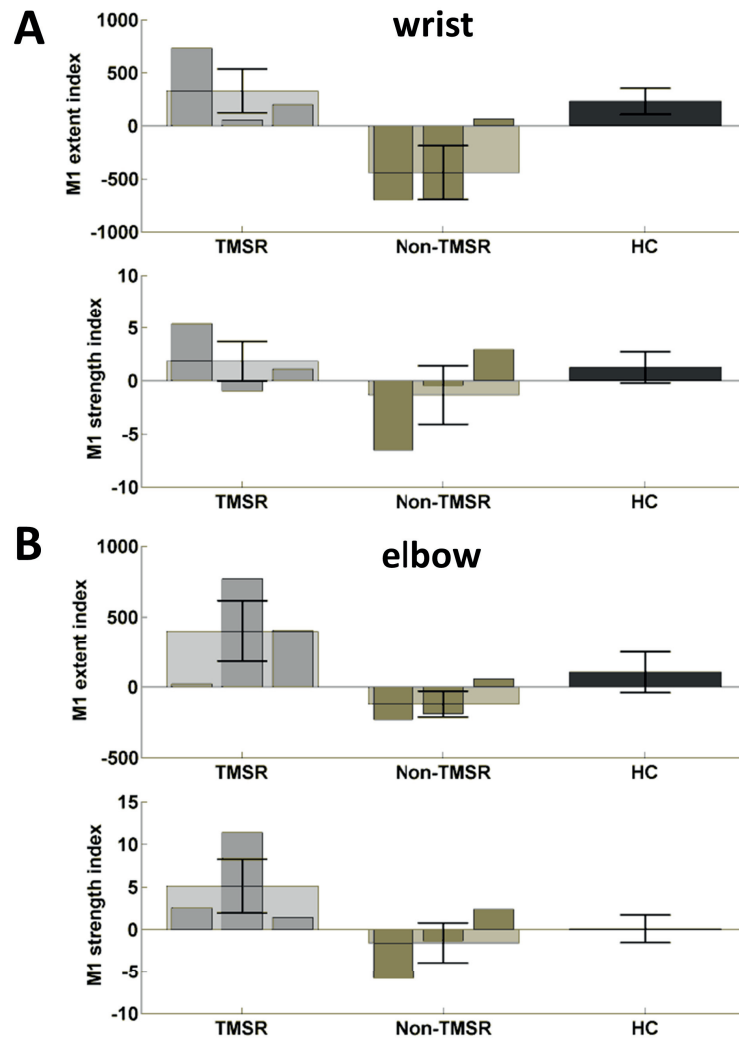
Fig.4.S2 Indices of extent and strength of activation in M1 for wrist and elbow movements.

level (using non-parametric Wilcoxon tests), indices of activated voxels for TMSR patients were not different from controls (p=0.34), and for Non-TMSR patients, these indices were significantly lower than for controls (p=0.03). We also analyzed the indices of activation strength. These indices did not differ between TMSR patients and controls (all p>0.17). For patient Non-TMSR-01, the index of activation strength was strongly negative and significantly lower than in controls (p=0.04). For patients Non-TMSR-02 and Non-TMSR-03, the indices of activation strength did not differ from controls (all p>0.34). At the group level (using non-parametric Wilcoxon tests), the indices of activation strength were not different between TMSR patients and controls (p=0.42), and not different between Non-TMSR-patients and controls (p=0.15).
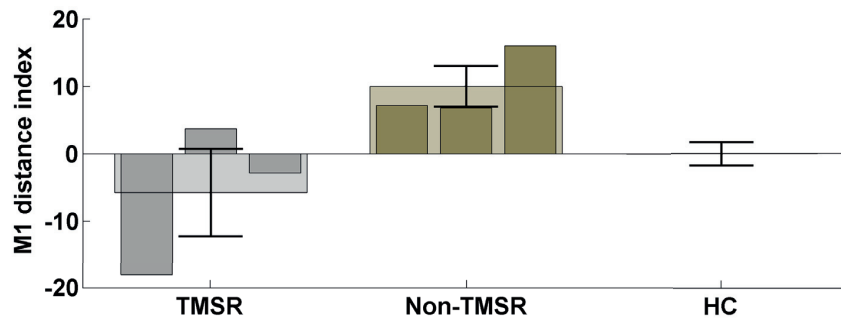
Fig.4.S3 3D-Euclidean distances between tongue and hand representations in M1.

For the elbow, the indices of activated voxels were positive in all TMSR patients and not different from controls (all p>0.08). For Non-TMSR patients, the indices of activate voxels were also not significantly different from controls (all p>0.23), although these indices were negative for Non-TMSR-01 and Non-TMSR-02. At the group level (using non-parametric Wilcoxon tests), indices of activated voxels for TMSR patients were not different from controls, neither for Non-TMSR patients compared to controls (all p>0.15). We then analyzed the indices of activation strength. These indices were positive in all TMSR patients. They did not differ from controls for patients TMSR-01 and TMSR-03 (p=0.31 and p=0.38 respectively), and the index of activation strength was even greater for TMSR-02 compared to controls (p=0.01). For Non-TMSR patients, the index of activation strength was not different than for controls (all p>0.12). At the group level (using non-parametric Wilcoxon tests), the indices of activation strength were not different between TMSR patients and controls and not different between Non-TMSR-patients and controls (all p>0.20).

4.6.8 Hand to tongue cortical distances in M1

The cortical distances between hand and tongue representations in M1 was measured as the 3D-Euclidian distance between their centers of mass to investigate cortical reorganization as previously described in the literature (**Flor et al. 1995; Makin et al. 2015**). We found no evidence for reorganization at the level of M1 representations, as there was no difference between TMSR patients, Non-TMSR patients and controls (all p>0.15). The results are presented in Fig.4.S3.

4.7 References

Alkadhi, H., Crelier, G.R., Boendermaker, S.H., Golay, X., Hepp-Reymond, M.C., Kollias, S.S., 2002. Reproducibility of primary motor cortex somatotopy under controlled conditions. American Journal of Neuroradiology 23, 1524–1532.

Beckmann, C.F., DeLuca, M., Devlin, J.T., Smith, S.M., 2005. Investigations into resting-state connectivity using independent component analysis. Philos Trans R Soc Lond B Biol Sci 360, 1001–1013. doi:10.1098/rstb.2005.1634

Beisteiner, R., Windischberger, C., Lanzenberger, R., Edward, V., Cunnington, R., Erdler, M., Gartus, A., Streibl, B., Moser, E., Deecke, L., 2001. Finger somatotopy in human motor cortex. NeuroImage 13, 1016–26. doi:10.1006/nimg.2000.0737

Bensmaia, S.J., 2015. Biological and bionic hands : natural neural coding and artificial perception. Philosophical Transactions Royal Society, B 370, 20140209. doi:10.1098/rstb.2014.0209

Bensmaia, S.J., Miller, L.E., 2014. Restoring sensorimotor function through intracortical interfaces: progress and looming challenges. Nature Reviews Neuroscience 15, 313–325. doi:10.1038/nrn3724

Berlucchi, G., Aglioti, S.M., 2010. The body in the brain revisited. Experimental Brain Research 200, 25–35. doi:10.1007/s00221-009-1970-7

Biswal, B., Yetkin, F.Z., Haughton, V.M., Hyde, J.S., Zerrin Yetkin, F., Haughton, V.M., Hyde, J.S., 1995. Functional connectivity in the motor cortex of resting human brain using echo-planar MRI. Magnetic resonance in medicine : official journal of the Society of Magnetic Resonance in Medicine / Society of Magnetic Resonance in Medicine 34, 537–541. doi:10.1002/mrm.1910340409

Björkman, A., Weibull, A., Olsrud, J., Henrik Ehrsson, H., Rosén, B., Björkman-Burtscher, I.M., 2012. Phantom digit somatotopy: A functional magnetic resonance imaging study in forearm amputees. European Journal of Neuroscience 36, 2098–2106. doi:10.1111/j.1460-9568.2012.08099.x

Blanke, O., 2012. Multisensory brain mechanisms of bodily self-consciousness. Nature reviews. Neuroscience 13, 556–71. doi:10.1038/nrn3292

Blanke, O., Slater, M., Serino, A., 2015. Behavioral, Neural, and Computational Principles of Bodily Self-Consciousness. Neuron. doi:10.1016/j.neuron.2015.09.029

Brozzoli, C., Makin, T.R., Cardinali, L., Holmes, N.P., Farnè, A., 2012. Peripersonal Space: A Multisensory Interface for Body–Object Interactions. The Neural Bases of Multisensory Processes 1–13.

Cardini, F., Longo, M.R., Haggard, P., 2011. Vision of the body modulates somatosensory intracortical inhibition. Cerebral Cortex 21, 2014–2022. doi:10.1093/cercor/bhq267

Chan, B.L., Witt, R., Charrow, A.P., Magee, A., Howard, R., Pasquina, P.F., Heilman, K.M., Tsao, J.W., 2007. Mirror therapy for phantom limb pain. The New England journal of medicine 357, 2206–2207. doi:10.1056/NEJMc071927

Chen, A., Yao, J., Kuiken, T., Dewald, J.P. a. A., 2013. Cortical motor activity and reorganization following upper-limb amputation and subsequent targeted reinnervation. NeuroImage: Clinical 3, 498–506. doi:10.1016/j.nicl.2013.10.001

Cléry, J., Guipponi, O., Wardak, C., Ben Hamed, S., 2015. Neuronal bases of peripersonal and extrapersonal spaces, their plasticity and their dynamics: Knowns and unknowns. Neuropsychologia 70, 313–326. doi:10.1016/j.neuropsychologia.2014.10.022

Cordes, D., Haughton, V.M., Arfanakis, K., Carew, J.D., Turski, P.A., Moritz, C.H., Quigley, M.A., Meyerand, M.E., 2001. Frequencies contributing to functional connectivity in the cerebral cortex in "resting-state" data. American Journal of Neuroradiology 22, 1326–1333.

Cordes, D., Haughton, V.M., Arfanakis, K., Wendt, G.J., Turski, P.A., Moritz, C.H., Quigley, M.A., Meyerand, M.E., 2000. Mapping functionally related regions of brain with functional connectivity MR imaging. American Journal of Neuroradiology 21, 1636–1644.

De Luca, M., Smith, S., De Stefano, N., Federico, A., Matthews, P.M., 2005. Blood oxygenation level dependent contrast resting state networks are relevant to functional activity in the neocortical sensorimotor system. Experimental Brain Research 167, 587–594. doi:10.1007/s00221-005-0059-1

De Preester, H., Tsakiris, M., 2014. Sensitivity to differences in the motor origin of drawings: From human to robot. PLoS ONE 9. doi:10.1371/journal.pone.0102318

Dijkerman, H.C., de Haan, E.H.F., 2007. Somatosensory processes subserving perception and action. The Behavioral and brain sciences 30, 189-201–39. doi:10.1017/S0140525X07001392

Dumanian, G. a, Ko, J.H., O'Shaughnessy, K.D., Kim, P.S., Wilson, C.J., Kuiken, T. a, 2009. Targeted reinnervation for transhumeral amputees: current surgical technique and update on results. Plastic and reconstructive surgery 124, 863–869. doi:10.1097/PRS.0b013e3181b038c9

Ehrsson, H.H., Holmes, N.P., Passingham, R.E., 2005. Touching a rubber hand: feeling of body ownership is associated with activity in multisensory brain areas. The Journal of neuroscience : the official journal of the Society for Neuroscience 25, 10564–73. doi:10.1523/JNEUROSCI.0800-05.2005

Ehrsson, H.H., Rosén, B., Stockselius, A., Ragnö, C., Köhler, P., Lundborg, G., 2008. Upper limb amputees can be induced to experience a rubber hand as their own. Brain : a journal of neurology 131, 3443–52. doi:10.1093/brain/awn297

Ehrsson, H.H., Spence, C., Passingham, R.E., 2004. That's my hand! Activity in premotor cortex reflects feeling of ownership of a limb. Science (New York, N.Y.) 305, 875–7. doi:10.1126/science.1097011

Ehrsson, H., 2012. The Concept of Body Ownership and Its Relation to Multisensory Integration, in: B.E. Stein (Ed.), The New Handbook of Multisensory Processes. MIT Press, Cambridge, pp. 775–792.

Ejaz, N., Hamada, M., Diedrichsen, J.O.R., 2015. Hand use predicts the structure of representations in sensorimotor cortex. Nature Neuroscience 103, 1–10. doi:10.1038/nn.4038

Fisher, R., 1915. Frequency distribution of the values of the correlation coefficient in samples from an indefinitely large population. Biometrika. doi:10.2307/2331838

Flor, H., Elbert, T., Knecht, S., Wienbruch, C., 1995. Phantom-limb pain as a perceptual correlate of cortical reorganization following arm amputation. Science 375, 482–484.

Flor, H., Denke, C., Schaefer, M., Grüsser, S., 2001. Effect of sensory discrimination training on cortical reorganisation and phantom limb pain. Lancet 357, 1763–1764. doi:10.1016/S0140-6736(00)04890-X

Foell, J., Bekrater-Bodmann, R., Diers, M., Flor, H., 2014. Mirror therapy for phantom limb pain: Brain changes and the role of body representation. European Journal of Pain (United Kingdom) 18, 729–739. doi:10.1002/j.1532-2149.2013.00433.x

Fox, M.D., Raichle, M.E., 2007. Spontaneous fluctuations in brain activity observed with functional magnetic resonance imaging. Nature reviews. Neuroscience 8, 700–11. doi:10.1038/nrn2201

Fox, M.D., Snyder, A.Z., Zacks, J.M., Raichle, M.E., 2006. Coherent spontaneous activity accounts for trial-to-trial variability in human evoked brain responses. Nature neuroscience 9, 23–5. doi:10.1038/nn1616

Fruhstorfer, H., Gross, W., Selbmann, O., 2001. Von Frey hairs: New materials for a new design. European Journal of Pain 5, 341–342. doi:10.1053/eujp.2001.0250

Gao, Q., Duan, X., Chen, H., 2011. Evaluation of effective connectivity of motor areas during motor imagery and execution using conditional Granger causality. NeuroImage 54, 1280–8. doi:10.1016/j.neuroimage.2010.08.071

Genovese, C.R., Lazar, N.A., Nichols, T., 2002. Thresholding of statistical maps in functional neuroimaging using the false discovery rate. NeuroImage 15, 870–878. doi:10.1006/nimg.2001.1037$\$rS1053811901910377

Gentile, G., Björnsdotter, M., Petkova, V.I., Abdulkarim, Z., Ehrsson, H.H., 2015. Patterns of neural activity in the human ventral premotor cortex reflect a whole-body multisensory percept. NeuroImage 109, 328–340. doi:10.1016/j.neuroimage.2015.01.008

Gerloff, C., Bushara, K., Sailer, A., Wassermann, E.M., Chen, R., Matsuoka, T., Waldvogel, D., Wittenberg, G.F., Ishii, K., Cohen, L.G., Hallett, M., 2006. Multimodal imaging of brain reorganization in motor areas of the contralesional hemisphere of well recovered patients after capsular stroke. Brain 129, 791–808. doi:10.1093/brain/awh713

Giummarra, M.J.M., Moseley, G.L., MJ., G., GL., M., Giummarra, M.J.M., Moseley, G.L., 2011. Phantom limb pain and bodily awareness: current concepts and future directions. Current opinion in anaesthesiology 24, 524–531. doi:10.1097/ACO.0b013e32834a105f

Glover, G.H., Li, T.Q., Ress, D., 2000. Image-based method for retrospective correction of physiological motion effects in fMRI: RETROICOR. Magnetic Resonance in Medicine 44, 162–167. doi:10.1002/1522-2594(200007)44:1

Gonçalves, S.I., De Munck, J.C., Pouwels, P.J.W., Schoonhoven, R., Kuijer, J.P.A., Maurits, N.M., Hoogduin, J.M., Van Someren, E.J.W., Heethaar, R.M., Lopes Da Silva, F.H., Goncalves, S.I., De Munck, J.C., Pouwels, P.J.W., Schoonhoven, R., Kuijer, J.P.A., Maurits, N.M., Hoogduin, J.M., Van Someren, E.J.W., Heethaar, R.M., Lopes Da Silva, F.H., 2006. Correlating the alpha rhythm to BOLD using simultaneous EEG/fMRI: Inter-subject variability. NeuroImage 30, 203–213. doi:10.1016/j.neuroimage.2005.09.062

Graziano, M.S.A., Cooke, D.F., 2006. Parieto-frontal interactions, personal space, and defensive behavior (DOI:10.1016/j.neuropsychologia.2005.09.009). Neuropsychologia. doi:10.1016/j.neuropsychologia.2005.09.011

Graziano, M., Botvinick, M., 2002. How the brain represents the body: insights from neurophysiology and psychology, in: Common Mechanisms in Perception and Action: Attention and Performance. pp. 136–157.

Green, D.M., Swets, J.A., 1966. Signal detection theory and psychophysics. Society 1, 521. doi:10.1901/jeab.1969.12-475

Haggard, P., Taylor-Clarke, M., Kennett, S., 2003. Tactile perception, cortical representation and the bodily self. Current biology : CB 13, R170–R173. doi:10.1016/S0960-9822(03)00115-5

Hahamy, A., Calhoun, V., Pearlson, G., Harel, M., Stern, N., Attar, F., Malach, R., Salomon, R., 2014. Save the global: global signal connectivity as a tool for studying clinical populations with functional magnetic resonance imaging. Brain connectivity 4, 395–403. doi:10.1089/brain.2014.0244

Hebert, J.S., Olson, J.L., Morhart, M.J., Dawson, M.R., Marasco, P.D., Kuiken, T. a., Chan, K.M., 2014. Novel Targeted Sensory Reinnervation Technique to Restore Functional Hand Sensation after Transhumeral Amputation. IEEE Transactions on Neural Systems and Rehabilitation Engineering 22, 765–773. doi:10.1109/TNSRE.2013.2294907

Helmich, R.C., Derikx, L.C., Bakker, M., Scheeringa, R., Bloem, B.R., Toni, I., 2010. Spatial remapping of cortico-striatal connectivity in Parkinson's disease. Cerebral cortex (New York, N.Y. : 1991) 20, 1175–86. doi:10.1093/cercor/bhp178

Hijjawi, J.B., Kuiken, T. a, Lipschutz, R.D., Miller, L. a, Stubblefield, K. a, Dumanian, G. a, 2006. Improved myoelectric prosthesis control accomplished using multiple nerve transfers. Plastic and reconstructive surgery 118, 1573–1578. doi:10.1097/01.prs.0000242487.62487.fb

Kaas, J.H., 1991. Plasticity of sensory and motor maps in adult mammals. Annual review of neuroscience 14, 137–67. doi:10.1146/annurev.ne.14.030191.001033

Kaas, J.H., Merzenich, M.M., Killackey, H.P., 1983. The reorganization of somatosensory cortex following peripheral nerve damage in adult and developing mammals. Annual review of neuroscience 6, 325–56. doi:10.1146/annurev.ne.06.030183.001545

Kennett, S., Taylor-Clarke, M., Haggard, P., 2001. Noninformative vision improves the spatial resolution of touch in humans. Current Biology 11, 1188–1191. doi:10.1016/S0960-9822(01)00327-X

Konen, C.S., Haggard, P., 2014. Multisensory parietal cortex contributes to visual enhancement of touch in humans: A single-pulse TMS study. Cerebral Cortex 24, 501–507. doi:10.1093/cercor/bhs331

Krantz, D.H., 1969. Threshold theories of signal detection. Psychological review 76, 308–24.

Kuiken, T.A., Dumanian, G.A., Lipschutz, R.D., Miller, L.A., Stubblefield, K.A., 2004. The use of targeted muscle reinnervation for improved myoelectric prosthesis control in a bilateral shoulder disarticulation amputee. Prosthetics and orthotics international 28, 245–53.

Kuiken, T.A., Marasco, P.D., Lock, B.A., Harden, R.N., Dewald, J.P.A., 2007. Redirection of cutaneous sensation from the hand to the chest skin of human amputees with targeted reinnervation. Proceedings of the National Academy of Sciences of the United States of America 104, 20061–20066. doi:10.1073/pnas.0706525104

Kuiken, T.A., Miller, L.A., Lipschutz, R.D., Lock, B.A., Stubblefield, K., Marasco, P.D., Zhou, P., Dumanian, G.A., 2007. Targeted reinnervation for enhanced prosthetic arm function in a woman with a proximal amputation: a case study. Lancet (London, England) 369, 371–80. doi:10.1016/S0140-6736(07)60193-7

Ladavas, E., Serino, A., 2008. Action-dependent plasticity in peripersonal space representations. Cognitive neuropsychology 25, 1099–1113. doi:10.1080/02643290802359113

Longo, M.R., Pernigo, S., Haggard, P., 2011. Vision of the body modulates processing in primary somatosensory cortex. Neuroscience letters 489, 159–63. doi:10.1016/j.neulet.2010.12.007

Lotze, M., Erb, M., Flor, H., Huelsmann, E., Godde, B., Grodd, W., 2000. fMRI evaluation of somatotopic representation in human primary motor cortex. NeuroImage 11, 473–481. doi:10.1006/nimg.2000.0556

Lotze, M., Flor, H., Grodd, W., Larbig, W., Birbaumer, N., 2001. Phantom movements and pain. An fMRI study in upper limb amputees. Brain : a journal of neurology 124, 2268–2277. doi:10.1093/brain/124.11.2268

Lotze, M., Grodd, W., Birbaumer, N., Erb, M., Huse, E., Flor, H., 1999. Does use of a myoelectric prosthesis prevent cortical reorganization and phantom limb pain? Nature neuroscience 2, 501–502. doi:10.1038/9145

Lowe, M.J., Mock, B.J., Sorenson, J.A., 1998. Functional connectivity in single and multislice echoplanar imaging using resting-state fluctuations. NeuroImage 7, 119–132. doi:10.1006/nimg.1997.0315

Makin, T.R., Scholz, J., Filippini, N., Slater, D.H., Tracey, I., Johansen-berg, H., Henderson Slater, D., 2013. Phantom pain is associated with preserved structure and function in the former hand area. Nature communications 4, 1570. doi:10.1038/ncomms2571

Makin, T.R., Cramer, A.O., Scholz, J., Hahamy, A., Slater, D.H., Tracey, I., Johansen-Berg, H., 2013. Deprivation-related and use-dependent plasticity go hand in hand. eLife 2, 1–15. doi:10.7554/eLife.01273

Makin, T.R., Filippini, N., Duff, E.P., Henderson Slater, D., Tracey, I., Johansen-Berg, H., 2015. Network-level reorganisation of functional connectivity following arm amputation. NeuroImage 114, 217–225. doi:10.1016/j.neuroimage.2015.02.067

Makin, T.R., Scholz, J., Henderson Slater, D., Johansen-Berg, H., Tracey, I., 2015. Reassessing cortical reorganization in the primary sensorimotor cortex following arm amputation. Brain 138, 2140–2146. doi:10.1093/brain/awv161

Marasco, P.D., Kim, K., Colgate, J.E., Peshkin, M.A., Kuiken, T.A., 2011. Robotic touch shifts perception of embodiment to a prosthesis in targeted reinnervation amputees. Brain 134, 747–758. doi:10.1093/brain/awq361

Marasco, P.D., Schultz, A.E., Kuiken, T.A., 2009. Sensory capacity of reinnervated skin after redirection of amputated upper limb nerves to the chest. Brain 132, 1441–1448. doi:10.1093/brain/awp082

Maravita, A., Spence, C., Driver, J., 2003. Multisensory integration and the body schema: Close to hand and within reach. Current Biology. doi:10.1016/S0960-9822(03)00449-4

Markov, N.T., Ercsey-Ravasz, M., Lamy, C., Ribeiro Gomes, A.R., Magrou, L., Misery, P., Giroud, P., Barone, P., Dehay, C., Toroczkai, Z., Knoblauch, K., Van Essen, D.C., Kennedy, H., 2013. The role of long-range connections on the specificity of the macaque interareal cortical network. Proceedings of the National Academy of Sciences of the United States of America 110, 5187–92. doi:10.1073/pnas.1218972110

Mars, R.B., Jbabdi, S., Sallet, J., O'Reilly, J.X., Croxson, P.L., Olivier, E., Noonan, M.P., Bergmann, C., Mitchell, A.S., Baxter, M.G., Behrens, T.E.J., Johansen-Berg, H., Tomassini, V., Miller, K.L., Rushworth, M.F.S., 2011. Diffusion-weighted imaging tractography-based parcellation of the human parietal cortex and comparison with human and macaque resting-state functional connectivity. The Journal of neuroscience : the official journal of the Society for Neuroscience 31, 4087–4100. doi:10.1523/JNEUROSCI.5102-10.2011

Martuzzi, R., van der Zwaag, W., Dieguez, S., Serino, a., Gruetter, R., Blanke, O., 2015. Distinct contributions of Brodmann areas 1 and 2 to body ownership. Social Cognitive and Affective Neuroscience 1–11. doi:10.1093/scan/nsv031

Martuzzi, R., van der Zwaag, W., Farthouat, J., Gruetter, R., Blanke, O., 2014. Human finger somatotopy in areas 3b, 1, and 2: A 7T fMRI study using a natural stimulus. Human brain mapping 35, 213–226. doi:10.1002/hbm.22172

Mercier, C., Reilly, K.T., Vargas, C.D., Aballea, A., Sirigu, A., 2006. Mapping phantom movement representations in the motor cortex of amputees. Brain 129, 2202–2210. doi:10.1093/brain/awl180

Merzenich, M.M., Kaas, J.H., Wall, J.T., Sur, M., Nelson, R.J., Felleman, D.J., 1983. Progression of change following median nerve section in the cortical representation of the hand in areas 3b and 1 in adult owl and squirrel monkeys. Neuroscience 10, 639–65. doi:10.1016/0306-4522(83)90208-7

Meyer-Lindenberg, A., Poline, J.B., Kohn, P.D., Holt, J.L., Egan, M.F., Weinberger, D.R., Berman, K.F., 2001. Evidence for abnormal cortical functional connectivity during working memory in schizophrenia. The American journal of psychiatry 158, 1809–17. doi:10.1176/appi.ajp.158.11.1809

Mostofsky, S.H., Powell, S.K., Simmonds, D.J., Goldberg, M.C., Caffo, B., Pekar, J.J., 2009. Decreased connectivity and cerebellar activity in autism during motor task performance. Brain : a journal of neurology 132, 2413–25. doi:10.1093/brain/awp088

O'Shaughnessy, K.D., Dumanian, G.A., Lipschutz, R.D., Miller, L.A., Stubblefield, K., Kuiken, T.A., 2008. Targeted reinnervation to improve prosthesis control in transhumeral amputees. A report of three cases. The Journal of bone and joint surgery. American volume 90, 393–400. doi:10.2106/JBJS.G.00268

Oldfield, R.C., 1971. The assessment and analysis of handedness: The Edinburgh inventory. Neuropsychologia 9, 97–113. doi:10.1016/0028-3932(71)90067-4

Pons, T.P., Garraghty, P.E., Ommaya, A.K., Kaas, J.H., Taub, E., Mishkin, M., 1991. Massive cortical reorganization after sensory deafferentation in adult macaques. Science (New York, N.Y.) 252, 1857–60.

Porro, C.A., Francescato, M.P., Cettolo, V., Diamond, M.E., Baraldi, P., Zuiani, C., Bazzocchi, M., di Prampero, P.E., 1996. Primary motor and sensory cortex activation during motor performance and motor imagery: a functional magnetic resonance imaging study. J Neurosci. 16, 7688–7698.

Ramachandran, V.S., Altschuler, E.L., 2009. The use of visual feedback, in particular mirror visual feedback, in restoring brain function. Brain. doi:10.1093/brain/awp135

Ramachandran, V.S., Rogers-Ramachandran, D., Cobb, S., 1995. Touching the phantom limb. Nature 489–490. doi:10.1038/377489a0

Raspopovic, S., Capogrosso, M., Petrini, F.M., Bonizzato, M., Rigosa, J., Di Pino, G., Carpaneto, J., Controzzi, M., Boretius, T., Fernandez, E., Granata, G., Oddo, C.M., Citi, L., Ciancio, A.L., Cipriani, C., Carrozza, M.C., Jensen, W., Guglielmelli, E., Stieglitz, T., Rossini, P.M., Micera, S., 2014. Restoring Natural Sensory Feedback in Real-Time Bidirectional Hand Prostheses. Science Translational Medicine 6.

Reilly, K.T., Sirigu, A., 2008. Neuroscientist The Motor Cortex and Its Role in Phantom Limb Phenomena Phantom Limb Phenomena. The Neuroscientist 14, 195–202. doi:10.1177/1073858407309466

Reilly, K.T., Mercier, C., Schieber, M.H., Sirigu, A., 2006. Persistent hand motor commands in the amputees' brain. Brain 129, 2211–2223. doi:10.1093/brain/awl154

Rizzolatti, G., Matelli, M., 2003. Two different streams form the dorsal visual system: anatomy and functions. Experimental brain research 153, 146–57. doi:10.1007/s00221-003-1588-0

Ro, T., Wallace, R., Hagedorn, J., Farnè, A., Pienkos, E., Farne, A., Pienkos, E., 2004. Visual enhancing of tactile perception in the posterior parietal cortex. Journal of cognitive neuroscience 16, 24–30. doi:10.1162/089892904322755520

Rothgangel, A.S., Braun, S.M., Beurskens, A.J., Seitz, R.J., Wade, D.T., 2011. The clinical aspects of mirror therapy in rehabilitation: a systematic review of the literature. International journal of rehabilitation research. Internationale Zeitschrift für Rehabilitationsforschung. Revue internationale de recherches de réadaptation 34, 1–13. doi:10.1097/MRR.0b013e3283441e98

Rushworth, M.F.S., Behrens, T.E.J., Johansen-Berg, H., 2006. Connection patterns distinguish 3 regions of human parietal cortex. Cerebral Cortex 16, 1418–1430. doi:10.1093/cercor/bhj079

Salomon, R., Darulova, J., Narsude, M., van der Zwaag, W., 2014. Comparison of an 8-channel and a 32-channel coil for high-resolution FMRI at 7 T. Brain topography 27, 209–12. doi:10.1007/s10548-013-0298-6

Sanchez-Panchuelo, R.M., Francis, S., Bowtell, R., Schluppeck, D., 2010. Mapping Human Somatosensory Cortex in Individual Subjects With 7T Functional MRI. J. neurophysiol 2544–2556. doi:10.1152/jn.01017.2009.

Serino, A., Haggard, P., 2010. Touch and the body. Neuroscience and Biobehavioral Reviews. doi:10.1016/j.neubiorev.2009.04.004

Serino, A., Padiglioni, S., Haggard, P., Làdavas, E., 2009. Seeing the hand boosts feeling on the cheek. Cortex 45, 602–609. doi:10.1016/j.cortex.2008.03.008

Siero, J.C.W., Hermes, D., Hoogduin, H., Luijten, P.R., Ramsey, N.F., Petridou, N., 2014. BOLD matches neuronal activity at the mm scale: A combined 7T fMRI and ECoG study in human sensorimotor cortex. NeuroImage 101, 177–84. doi:10.1016/j.neuroimage.2014.07.002

Solodkin, A., Hlustik, P., Chen, E.E., Small, S.L., 2004. Fine modulation in network activation during motor execution and motor imagery. Cerebral cortex (New York, N.Y. : 1991) 14, 1246–55. doi:10.1093/cercor/bhh086

Speck, O., Stadler, J., Zaitsev, M., 2008. High resolution single-shot EPI at 7T. Magnetic Resonance Materials in Physics, Biology and Medicine 21, 73–86. doi:10.1007/s10334-007-0087-x

Stringer, E.A., Chen, L.M., Friedman, R.M., Gatenby, C., Gore, J.C., 2011. Differentiation of somatosensory cortices by high-resolution fMRI at 7 T. NeuroImage 54, 1012–20. doi:10.1016/j.neuroimage.2010.09.058

Taylor-Clarke, M., Kennett, S., Haggard, P., 2002. Vision modulates somatosensory cortical processing. Current Biology 12, 233–236. doi:10.1016/S0960-9822(01)00681-9

Taylor, M.M., Forbes, S.M., Creelman, C.D., 1983. PEST reduces bias in forced choice psychophysics. The Journal of the Acoustical Society of America 74, 1367–74. doi:10.1121/1.390161

Tomassini, V., Jbabdi, S., Klein, J.C., Behrens, T.E.J., Pozzilli, C., Matthews, P.M., Rushworth, M.F.S., Johansen-Berg, H., 2007. Diffusion-weighted imaging tractography-based parcellation of the human lateral premotor cortex identifies dorsal and ventral subregions with anatomical and

functional specializations. The Journal of neuroscience : the official journal of the Society for Neuroscience 27, 10259–69. doi:10.1523/JNEUROSCI.2144-07.2007

Tsakiris, M., 2010. My body in the brain: a neurocognitive model of body-ownership. Neuropsychologia 48, 703–12. doi:10.1016/j.neuropsychologia.2009.09.034

Uddin, L.Q., Supekar, K., Amin, H., Rykhlevskaia, E., Nguyen, D.A., Greicius, M.D., Menon, V., 2010. Dissociable connectivity within human angular gyrus and intraparietal sulcus: Evidence from functional and structural connectivity. Cerebral Cortex 20, 2636–2646. doi:10.1093/cercor/bhq011

van den Heiligenberg, F., Macdonald, S., Duff, E., Henderson Slater, D., Johansen-Berg, H., Culham, J., Makin, T., 2015. Activity in hand- and tool-selective regions for prosthetic limbs in amputees is associated with prosthesis usage in everyday life. Journal of vision 15, 983. doi:10.1167/15.12.983

Wang, L., Yu, C., Chen, H., Qin, W., He, Y., Fan, F., Zhang, Y., Wang, M., Li, K., Zang, Y., Woodward, T.S., Zhu, C., 2010. Dynamic functional reorganization of the motor execution network after stroke. Brain : a journal of neurology 133, 1224–38. doi:10.1093/brain/awq043

Weinstein, S., 1968. Intensive and extensive aspects of tactile sensitivity as a function of body part, sex and laterality, in: First International Symposium on Skin Senses. pp. 195–222.

Whitfield-Gabrieli, S., Nieto-Castanon, A., 2012. Conn: A Functional Connectivity Toolbox for Correlated and Anticorrelated Brain Networks. Brain Connectivity 2, 125–141. doi:10.1089/brain.2012.0073

Wolpert, D.M., Ghahramani, Z., Jordan, M.I., 1995. An internal model for sensorimotor integration. Science 269, 1880–1882. doi:10.1126/science.7569931

Xiong, J., Parsons, L.M., Gao, J.H., Fox, P.T., 1999. Interregional connectivity to primary motor cortex revealed using MRI resting state images. Human brain mapping 8, 151–6. doi:10.1002/(SICI)1097-0193(1999)8:2/3

Yang, T.T., Gallen, C., Schwartz, B., Bloom, F.E., Ramachandran, V.S., Cobb, S., 1994. Sensory maps in the human brain. Nature 368, 592–593. doi:10.1038/368592b0

Yao, J., Carmona, C., Chen, A., Kuiken, T., Dewald, J., Carmona, C., Dewald, J., 2015. Sensory cortical re-mapping following upper-limb amputation and subsequent targeted reinnervation: A case report. NeuroImage. Clinical 8, 329–36. doi:10.1016/j.nicl.2015.01.010

Yeo, B.T.T., Krienen, F.M., Sepulcre, J., Sabuncu, M.R., Lashkari, D., Hollinshead, M., Roffman, J.L., Smoller, J.W., Zöllei, L., Polimeni, J.R., Fischl, B., Liu, H., Buckner, R.L., 2011. The organization of the human cerebral cortex estimated by intrinsic functional connectivity. Journal of neurophysiology 106, 1125–65. doi:10.1152/jn.00338.2011

Zeharia, N., Hertz, U., Flash, T., Amedi, A., 2012. Negative blood oxygenation level dependent homunculus and somatotopic information in primary motor cortex and supplementary motor area. Proceedings of the National Academy of Sciences of the United States of America 109, 18565–70. doi:10.1073/pnas.1119125109

Zhou, P., Lowery, M.M., Englehart, K.B., Huang, H., Li, G., Hargrove, L., Dewald, J.P.A., Kuiken, T.A., 2007. Decoding a new neural machine interface for control of artificial limbs. Journal of neurophysiology 98, 2974–82. doi:10.1152/jn.00178.2007

5 - Study IV: temporal cortex contributes to the senses of hand ownership and of hand agency

Michel Akselrod, Julio Duenas, Roberto Martuzzi, James Sulzer, Philipp Stampfli, Erich Seifritz, Olaf Blanke, Gassert Roger

Abstract

We normally experience our hands as part of our body and feel in control of their actions. Under specific conditions, it is possible to extend these subjective experiences towards external objects such as a fake rubber hand or a virtual hand. Studying such altered states of the sense of hand ownership and the sense of hand agency can offer insights into their underlying brain mechanisms. Using a novel setup combining MR-compatible robotics and virtual reality, we manipulated the sensorimotor and visual information to induce altered states of the sense of hand ownership and the sense of hand agency. On a trial-by-trial basis, participants reported their subjective feeling of ownership and of agency towards the seen virtual hand. Using Representational Similarity Analysis, we compared the ongoing BOLD activity with participant's subjective reports to identify brain regions associated wit the sense of hand ownership and agency. We report two partially overlapping networks including occipital, temporal, parietal, frontal, insular, cingulate and cerebellar regions. In particular, we report the implication of posterior and anterior temporal regions, which have been rarely highlighted in previous literature. This study extends previous reports by highlighting the interplay between the sense of hand ownership and the sense of hand agency both at the level of behavior and brain mechanisms.

Detailed contributions: I was in charge of the project. I prepared the paradigms, collected and analyzed the data, wrote the initial manuscript and created the figures.

5.1 Introduction

The illusory feeling of ownership towards a fake hand can be induced by the well known "rubber hand illusion" (**Botvinick and Cohen, 1998**). In this setup, the participant sees a fake rubber hand being stroked, while his hidden hand receives a spatially and temporally congruent touch. Only when the visual and tactile stimulations are delivered in synchrony, as opposed to asynchronous stimulations, participants report experiencing the fake hand as their own. Since then, the manipulation of multisensory signals has been extensively used to alter and study the subjective experience of one's hand. With the advent of virtual reality, it has been possible to manipulate visual information in unprecedented ways allowing replacing fake hands by virtual one's. Studies investigating the "virtual hand illusion" showed that illusory ownership could be induced for virtual objects similarly to real objects (**Berkater-Bodman et al. 2012, 2014; Ma and Hommel, 2013, 2015; Ma et al. 2013; Padilla-Castaneda et al. 2014; Perez-Marco et al. 2009, 2012; Sanchez-Vives et al. 2010; Shibuya et al. 2016; Slater et al. 2008; Zhang et al. 2015**). Most importantly, the combination of virtual reality and robotics allows manipulating the visual and sensorimotor (i.e. tactile, proprioceptive and motor) information in a controlled and reproducible manner. In particular, the manipulation of visuo-motor signals allows studying the interplay between the sense of hand ownership (SO) and the sense of hand agency (SA). SO refers to the subjective experience that the hand is identified with the self ("this is my hand"), while SA refers to the subjective experience that the self is identified as the agent of the hand's actions ("I am controlling this hand") (**Schwabe and Blanke, 2007; Haggard and Chambon, 2012; Tsakiris et al. 2007**).

Previous studies have investigated the experimental alteration of SO and SA, as well as their interplay. SO can manipulated by the factor of temporal synchrony between sensorimotor signals and by the factor of congruent structure (shape or position of the owned object). Considering that SO can be altered under static conditions as in the "Rubber Hand Illusion", the presence of movements is not strictly necessary. Contrastingly, SA is strongly altered by the factor of temporal synchrony between sensorimotor signals and by the factor of agentivity (active or passive movements) (**Braun et al. 2014; Caspar et al. 2015; Jenkinson and Preston, 2015;**

Klackert and Ehrsson, 2012, 2014; Shibuya et al. 2016). This suggests a partial dissociation between SO and SA. In addition, some of these studies also report a correlation between SO and SA suggesting a certain degree of interaction between the two (**Caspar et al. 2015; Klackert and Ehrsson, 2012, 2014**). Other studies suggested that SA boosts and extends SO, thus further supporting the presence of interactions between SO and SA (**Asai et al. 2016; Dummer et al. 2009; Hara et al. 2016; Ma and Hommel, 2015; Tsakiris et al. 2006**).

Neuroimaging studies have successfully induced altered states of SO while monitoring brain activity and identified the premotor cortex, the posterior parietal cortex, extra-striate visual areas, the insula, the cingulate cortex and the cerebellum as key regions underlying the mechanisms of SO (**Berkater-Bodman et al. 2012, 2014; Brozzoli et al. 2012; Ehrsson et al. 2004, 2005; Gentile et al. 2013; Guterstam et al. 2013; Limanowski et al. 2014, 2015, 2016; Petkova et al. 2011; Tsakiris et al. 2007**). Similarly, the neural correlates of SA have been identified as the premotor cortex, supplementary motor areas, the dorsolateral prefrontal cortex, the posterior parietal cortex, extra-striate visual areas, the superior temporal gyrus/sulcus, the insula, and the cerebellum (**David et al. 2006; Farrer and Frith 2002; Farrer et al. 2003, 2008; Fink et al. 1999; Leube et al. 2003**). Other neuroimaging studies investigated the sense of agency for non-bodily object (such as computer game actions) and reported the implication of the same brain regions suggesting that the mechanisms underlying the sense of agency for bodily and non-bodily objects might be comparable (**Kühn et al. 2013; Lee and Reeve 2013; Miele et al. 2011; Renes et al. 2015; Yomogida et al. 2010**).

Studying the interplay between SO and SA is more difficult in MR-environment due to the challenge of developing an MR-compatible setup allowing controlled and repeatable movements. Remarkably, Tsakiris and colleagues (**2010**) investigated specifically the link between SO and SA and studied their neural correlates. They manipulated the synchrony of the visual feedback during active and passive finger lifts. This allowed dissociating SO and SA and their respective brain activations. The authors reported the absence of overlapping activations between SO and SA and found two specific networks for SO and SA respectively, suggesting their independence. Regions specific for SO included the inferior and middle temporal

gyri, fusiform gyrus, superior medial gyrus, posterior cingulate cortex, postcentral gyrus, precuneus and cuneus. Regions associated with SA were the cerebellum, precentral gyrus (premotor), anterior insula, inferior and superior parietal lobule, postcentral gyrus, inferior and middle occipital gyrus, supplementary motor areas, middle and superior frontal gyrus, superior temporal gyrus and the thalamus. This study provided important information regarding the neural correlates of SO and SA. However, the authors compared the relative activations elicited by specific experimental conditions assumed to affect specifically SO and SA, rather than directly comparing subjective measures of SO and SA from the participants. Up to now, not a single study has attempted to associate ongoing brain activity with changes in the subjective experience of SO and SA.

Representational similarity analysis (RSA, **Kriegeskorte et al. 2008**) is a powerful neuroimaging method allowing comparing and associating the similarity structure between behavioral/computational data and patterns of brain activations. Conceptually, RSA allows associating brain activations with almost any type of measure, but requires a condition-rich design to create a representational signature across many experimental conditions and their associated brain activations. However, it has not yet been applied to study cognitive and subjective processes.

SO and SA are classically measured with subjective reports from the participants who indicate on a likert scale whether they experience the fake hand as their own (SO) or whether they feel in control of the fake hand (SA). These subjective measures have been largely validated in the literature. However, to avoid relying on subjective judgments, researchers have used more objective measures to quantify the strength of an illusion. For example, during the "rubber hand illusion", participants localize the perceived position of their real hand shifted towards the fake hand, indicating that a proprioceptive drift has occurred (**Botvinick and Cohen, 1998**). The proprioceptive drift has been proposed as a proxy of the strength of the illusion, however the association between subjective reports and objective measures has not always been reproduced (**Fiorio et al. 2011; Holle et al. 2011; Riemer et al. 2015; Rohde et al. 2011**), suggesting that these measures are capturing different aspects of the illusion.

The goal of the present study is to investigate the brain networks associated with SO and SA. To this end, we developed a novel setup combining MR-compatible

robotics and virtual reality allowing to induce altered states of SO and SA. While participants performed pinching movements and watched a virtual avatar also performing pinching movements, we manipulated the type of movements produced (active or passive), the synchrony between the real and virtual movements (synchronous or asynchronous), as well as the congruency of the moving virtual hand (right or left virtual hand moving). Using RSA and an explorative approach, we identified brain regions in which BOLD patterns across experimental trials were modulated similarly as participant's levels of SO and SA towards the virtual hand on a trial-by-trial basis. We expect to replicate previous reports by highlighting the key regions proposed so far in the available literature. Considering the increased sensitivity of our approach accounting for intra-subject variability, we hypothesize that our analysis will also extend previous results by highlighting additional brain regions that could not be revealed by classical designs. We discuss these results with respect to previous neuroimaging studies investigating SO and SA, as well as their implication for future investigations in this field.

5.2 Materials and Methods

5.2.1 Behavioral experiment

To confirm that our manipulations could reliably induce altered states of SO and SA, we first conducted a behavioral experiment.

5.2.1.1 Participants

A group of 27 naive and right-handed healthy participants (5 females) aged between 18 and 39 years old (mean ± std: 24.3 ± 5.2 years) were recruited for the study. All subjects gave written informed consent. All procedures were approved by the Ethics Committee of the Federal Institute of Technology of Zurich, and the study was conducted in accordance with the Declaration of Helsinki.

5.2.1.2 Robotic manipulandum

The robotic device was composed of a fixed thumb socket and a mobile index socket attached to a linear rail (1 degree of freedom) and connected to a DC motor (maxon DC motor RE40 150 Watt, Maxon motor AG) via a cable/pulley transmission

(Fig.5.1A). An optical encoder (HEDM-5500, Agilent Technologies) was used to count the rotations of the shaft. A force sensor (CentoNewton, Institute of production and robotic EPFL) placed below the end effector allowed monitoring the interaction force applied by the subject. The rest of the hardware consisted of a data acquisition card (DAQ M Series NI USB-621x, National Instruments Corporation) and a linear amplifier (ESCON 50/5 Servo Controller P/N 409510, Maxon motor AG). The controller software was designed with Labview (National Instruments Corporation). The virtual environment was designed using Poser9 software (SmithMicro, Inc.) and rendered using an OPEN-GL based software (ExpyVR, http://lnco.epfl.ch/expyvr). A UDP connection was implemented to communicate between the controller and the rendering software.

The robotic system was designed to allow the user to perform active and passive pinching movements. During active movements, a virtual spring was rendered (position control, stiffness and damping: k=0.0065 [V/m] and c=0.0005 [V*s/m]) to simulate a compressible object and the user could perform pinching movements by actively approaching the index towards the opposing thumb. The simulation of a virtual spring was preferred over a transparent movement to better mimic the ecological sensation of pinching a compressible object (as displayed in the virtual environment). During passive movements, a preplanned sequence was imposed to the user's index using a PD controller (position control, K_p=0.04, K_d=0.00074). The sequence consisted of successive pinching movements towards the fixed thumb following a sinusoidal trajectory with variable frequencies, amplitudes and interstimulus intervals (ISI) between two successive pinching movements (frequency ranged between 0.5 and 0.9 Hz, amplitude ranged between 66% and 100% of maximum aperture, ISI ranged between 75 and 125 ms). During passive stimulation, each trial consisted of 12 pinching movements. During active movements, the number of pinching movements was 12.2 ± 6.1 (mean $\pm$ std).

5.2.1.3 Experimental Setup

Participants were laid in supine position on a bed with a head-mounted display (HMD, manufacturer: Oculus VR, LLC, Menlo Park, CA, USA; resolution: 1280x800 pixels at 60 Hz) fixed on the head. The right hand, fixed to the robot, was positioned

15cm to the right from body midline. The robot was placed over the abdomen on a support structure. The right arm was supported by foam pads to guarantee the participant's comfort. The left arm was rested on the bed along the body and the left hand was used to control response buttons. In the HMD, a virtual environment was displayed and showed a first person perspective with a direct view on the right hand and the body of the avatar. The virtual hand was positioned at the body midline of the avatar and was holding a compressible piston (Fig.5.1B). The spatial offset between the real and virtual hands was introduced to measure a potential proprioceptive drift towards the virtual hand. The avatar was matched according to participant's gender and skin color.

5.2.1.4 Experimental conditions

During each experimental trial, participants performed pinching movements during 30 sec with their right hand while watching the virtual hand also performing pinching movements. There were a total of 8 experimental conditions with 3 factors being manipulated (2x2x2 design). First, the type of movement produced by the participant's hand could be active or passive (factor of "movement type"). Second, the virtual movements were either synchronous or asynchronous with the movements of the participants (factor of "synchrony"). During asynchronous trials, the virtual avatar performed a different preplanned sequence of pinching movements leading to both spatial and temporal mismatch between the movements of the participant's hand and of the avatar's hand. Finally, the virtual moving hand was either the right or the left hand of the avatar, while participants always performed the movement with their right hand (factor of "congruency"). Each condition was repeated 8 times leading to a total of 64 trials divided into 4 runs of approximately 15min. The 4 runs were divided into 2 runs with active movements and 2 runs with passive movements. The order of the runs was pseudo-randomized across participants and the order of condition presentations within the same run was randomized across participants.

5.2.1.5 Experimental measures

To measure a potential proprioceptive drift induced by the stimulation, participants reported the perceived position of their right hand using a digital horizontal ruler displayed in the HDM. This localization task was performed right before and after

143

each period of stimulation, and consisted in aligning the ruler with the perceived position of the participant's right hand. The proprioceptive drift was measured as the difference in localization before and after the stimulation.

Following each stimulation period (and after the localization task), participants rated 3 statements aiming at evaluating their subjective SO towards the virtual hand and SA over the virtual movement, as well as a control statement.

- ownership rating: "I felt as if the virtual hand was my own hand"
- agency rating: "I felt as if I was producing the virtual hand movements"
- control rating: "I felt as if my real hand was disappearing"

A virtual ruler was used by the participants to rate these items on a likert scale ranging from 1 to 7 (1 corresponding to "totally disagree" and 7 corresponding to "totally agree").

After the subjective ratings and before starting the next stimulation period, a rest period of 3 sec was included to allow the subject to be prepared to interact with the robot. During the localization task, subjective ratings and rest period, the robot was set in stand-by mode preventing movements of the participant's right hand.

5.2.1.6 Experimental procedure

Participants were first given an explanatory session to familiarize with the robotic device and the HMD. A demonstration of active and passive movements with the robotic manipulandum was presented. Subjects received instructions regarding the type of pinching movements to be performed during the experiments. For active movements, participants were trained to perform smooth and uninterrupted pinching movements from start to end (a complete closing and opening movement). In particular, they were asked to mark a pause between each successive pinching and to try, as best as possible, to maintain a regular pace similar to the one previously demonstrated with passive movements (between 0.5 and 0.9 Hz approximately). For passive movements, participants were trained to relax their fingers and avoid exerting any force on the robot.

After the familiarization with the setup, the experimenter introduced the different

experimental measures to ensure the participant's understanding and demonstrated how to use the response buttons. For the localization task, participants could practice with the digital ruler to align it with the perceived position of their hand.

Participants were instructed to fixate and maintain their attention on the virtual hand during the 30 sec of stimulation. Rather than including an attentional control task, we considered that the proprioceptive task and the rating of items every 30 sec were sufficient to ensure the participant's arousal and attention. An experimenter was monitoring whether participants were indeed conducting the tasks. Before the beginning of the experiments, participants were fitted with black clothes (pants, socks and a t-shirt) to match the one's of the avatar displayed in the HMD.

5.2.1.7 Statistical analysis

By measuring the precise distance between the participant's right hand and body midline, the results of the localization task were transformed into physical distances in cm. Before the statistical analysis, the subjective ratings were normalized using the ipsatization method (**Broughton and Wasel, 1990; Cunningham et al. 1967**) to reduce between-subject biases, which consist in normalizing separately for each subject the ratings by subtracting the mean and dividing by the standard deviation of all ratings.

Normalized subjective ratings and proprioceptive drift were analyzed separately using linear mixed effects models, with "movement type", "synchrony" and "congruency" as fixed effects. The following models were selected respectively for each analysis: 1) intercepts for subjects as random effects, and a by-subject random slope for the effect of "movement type", "synchrony" and "congruency" for ratings of SO; 2) intercepts for subjects as random effects, and a by-subject random slope for the effect of "movement type" and "synchrony" for ratings of SA; 3) intercepts for subjects as random effects, and a by-subject random slope for the effect of "movement type", "synchrony" and "congruency" for control ratings; 4) intercepts for subjects as random effects, and a by-subject random slope for the effect of "synchrony" and "congruency" for proprioceptive drift. In all models, p-values were obtained by likelihood ratio tests, and degrees of freedom were approximated using the Kenward-Roger method. In addition, we investigated the correlation between the

different experimental measures (subjective ratings and proprioceptive drift).

5.2.2 fMRI experiment

In a second experiment, we replicated the setup in MR-environment and conducted the same experiment while recording the whole brain BOLD activity of our participants.

5.2.2.1 Participants

A group of 26 naive and right-handed healthy participants (14 females) aged between 18 and 35 years old (mean ± std: 25.5 ± 4.3 years) were recruited for the study. All subjects gave written informed consent. All procedures were approved by the Cantonal Ethics Committee, Department of Health of the Canton Zurich, Switzerland, and the study was conducted in accordance with the Declaration of Helsinki.

Four participants were excluded due to excessive motion during the fMRI acquisition (more than 4 mm of motion during at least one of the fMRI sessions).

5.2.2.2 MR-compatible robotic manipulandum

The robotic device was an MR-compatible homolog of the device used in the behavioral experiment. It was also composed of a fixed thumb socket and a mobile index socket. A DC motor actuated a linear drive through a spindle, to which a hydraulic piston was fixed and remotely controlled the slave module inside the scanner room through a hydrostatic transmission (**Gassert et al. 2006**). Interaction forces during movements were measured with an MR-compatible optical fiber force sensor (Baumer, Switzerland). This setup was tested and used during a previous study (**Sulzer et al. 2013**). The controller software was designed with Labview (National Instruments Corporation). The virtual environment was designed using Poser9 software (SmithMicro, Inc.) and rendered using an OPEN-GL based software (ExpyVR, http://lnco.epfl.ch/expyvr). A UDP connection was implemented to communicate between the controller and the rendering software.

Similarly to the behavioral experiment, the robotic system allowed the user to

perform active and passive pinching movements. During active movements, a virtual spring was rendered (position control, stiffness: k=3 [V/m]) to simulate a compressible object and the user could perform pinching movements by actively approaching the index towards the opposing thumb. During passive movements, a preplanned sequence was imposed to the user's index using a PID controller (position control, K_p=80, K_i=1.2, K_d=1.4). The same preplanned trajectories were used as in the behavioral experiment. During passive stimulation, each trial consisted of 12 pinching movements. During active movements, the number of pinching movements was 10.8±3.5 (mean ± std).

5.2.2.3 Experimental Setup

Participants were laid in supine position on the scanner bed. The right hand was fixed to the robot, which was mounted on an aluminum structure (Fig.5.2A). The right arm was supported by foam pads to guarantee the participant's comfort. The left arm was rested on the scanner bed along the body and the left hand was used to control MR-compatible response buttons. MR-compatible goggles (manufacturer: Resonance Technology, Inc., Northridge, CA, USA; resolution: 800x600 pixels at 60 Hz) were used to display a virtual environment showing a first person perspective with a direct view on the right hand and the body of the avatar. The virtual hand was positioned at the body midline of the avatar and was holding a compressible piston (Fig.5.2B). The avatar was matched according to participant's gender and skin color.

5.2.2.4 Experimental conditions

The same experimental conditions were used as in the behavioral experiment. There were a total of 8 experimental conditions with 3 factors being manipulated (2x2x2 design): "movement type" with active or passive movements of the participant's right hand, "synchrony" with synchronous or asynchronous movements between the hands of the participant and of the avatar, and "congruency" with the right or the left virtual hand moving (participants always moved their right hand). Each condition was repeated 8 times leading to a total of 64 trials divided into 4 runs of approximately 12min. The 4 runs were divided into 2 runs with active movements and 2 runs with passive movements. The order of the runs was pseudo-randomized across participants and the order of condition presentations within the same run was

randomized across runs and participants.

5.2.2.5 Experimental measures

The proprioceptive drift was not measured during the fMRI experiment due to time constraints. Following each stimulation period, participants rated the 3 same statements as in the behavioral experiment:

- ownership rating: "I felt as if the virtual hand was my own hand"
- agency rating: "I felt as if I was producing the virtual hand movements"
- control rating: "I felt as if my real hand was disappearing"

As in the previous experiment, a virtual ruler was used by the participants to rate these items on a likert scale ranging from 1 to 7 (1 corresponding to "totally disagree" and 7 corresponding to "totally agree"). After the items rating and before starting the next stimulation period, a rest period of 3 sec was included to allow the subject to be prepared to interact with the robot. During the subjective ratings and rest period, the robot was set in stand-by mode preventing movements of the participant's right hand.

5.2.2.6 Experimental procedure

As in the behavioral part of the study, the participants were given an explanatory session to familiarize with the robotic setup and the subjective ratings. Before the beginning of the experiments, participants were fitted with black clothes (pants, socks and a t-shirt) to match the one's of the avatar displayed in the virtual environment.

5.2.2.7 fMRI acquisition

All data were acquired on a Philips Achieva 3T magnetic resonance (MR) scanner with a 32 channel receive head coil (Philips, Best, The Netherlands). Functional volumes were acquired using a gradient-echo planar imaging (EPI) sequence over the whole brain (TR: 2000 ms; TE: 35 ms; slice thickness: 3 mm; 35 axial slices; 1.1mm slice gap; FOV: 240×240 mm^2; in-plane resolution: 3×3 mm^2; sensitivity-encoding reduction factor: 2.0). Four functional runs were acquired with the presentation of the experimental conditions, each with 384 volumes. Furthermore, T1-weighted structural images (FOV: 256x256x180 mm^3, sagittal orientation, resolution: 1x1x1 mm^3, TR:

6.9 ms, TE: 3.1 ms, flip angle: 8°) were recorded before the acquisition of functional images.

5.2.2.8 Analysis of behavioral data

As in the behavioral experiment, the subjective ratings were normalized using the ipsatization method before the statistical analysis (**Broughton and Wasel, 1990; Cunningham et al. 1967**).

Normalized subjective ratings were analyzed separately using linear mixed effects models, with "movement type", "synchrony" and "congruency" as fixed effects. The following models were selected respectively for each analysis: 1) intercepts for subjects as random effects, and a by-subject random slope for the effect of "movement type", "synchrony" and "congruency" for ratings of SO; 2) intercepts for subjects as random effects, and a by-subject random slope for the effect of "movement type" and "synchrony" for ratings of SA; 3) intercepts for subjects as random effects, and a by-subject random slope for the effect of "movement type" and "synchrony" for control ratings. In all models, p-values were obtained by likelihood ratio tests, and degrees of freedom were approximated using the Kenward-Roger method. In addition, we investigated the correlation between the different experimental measures (subjective ratings).

5.2.2.9 fMRI data processing

All images were preprocessed using the SPM8 software (Wellcome Department of Cognitive Neurology, London, UK). Preprocessing steps included slice-timing correction, realignment, smoothing (FWHM=8mm) and normalization to MNI space. A GLM analysis, including the 4 experimental runs, was carried out to estimate the BOLD responses (beta estimates) induced by the different experimental trials. The model included 65 regressors, one for each experimental trial and one for all the periods of item ratings, convoluted with the hemodynamic response, as well as the 6 rigid-body motion parameters as nuisance regressors. The software Carret5 was used for surface visualization (Van Hessen Laboratory, Washington University, Saint-Louis, Missouri, USA).

5.2.2.10 Representational similarity analysis (RSA)

RSA (**Kriegeskorte et al. 2008**) is a multi-voxel pattern analysis method that relies on the similarity structure between classes of externals objects/measures and their brain representations to establish their respective associations. The goal of the RSA was to identify brain regions associated with changes in participant's subjective ratings of SO and SA. To this end, we adopted a searchlight approach (**Kriegeskorte et al. 2006**) and computed a representational dissimilarity matrix based on the BOLD responses associated with the 64 experimental trials (brain-RDMs) for each considered voxel. We compared the calculated brain-RDMs with behavioral models (model-RDMs), which were derived from participant's subjective ratings of SO and SA. The analysis was restricted to voxels located within the grey matter, as identified by the segmentation procedure implemented in SPM8.

To apply RSA it is necessary to obtain a large range of subjective ratings (from low to high) to capture their modulation with respect to BOLD activity. For this reason, we considered only participants which experienced the largest modulation of SO and SA. For this reason, we selected 15 participants which showed the strongest and most reliable modulation of SO and SA to conduct the RSA.

Separately for each participant, the BOLD response pattern across all voxels located within a sphere (radius of 9 mm) around the considered voxel was extracted for each experimental trial. Using 1-correlation as measure of dissimilarity, we computed the dissimilarity between the BOLD response patterns associated with each of the 64 experimental trials, leading to a 64x64 symmetrical matrix. Such brain-RDM was calculated for each voxel of the grey matter.

Separately for each participant, we computed two model-RDMs, one based on the subjective ratings of SO and another based on the subjective ratings of SA. The absolute difference between subjective ratings across all trials was used as measure of distance, leading to two 64x64 symmetrical matrices per subject.

To compare the brain-RDMs with the model-RDMs and assess which brain regions are associated with subjective changes in SO and SA, we calculated the correlation between each voxel's brain-RDM and the two model-RDMs of SO and SA

(values from the upper triangular matrix excluding the diagonal were used for the correlation). This led to two correlation-maps for each participant, one associated with SO and another with SA. The correlation-maps were transformed into normal values using Fisher's transformation (**Fisher, 1915**). At each voxel, we computed a t-test across participants. The statistical significance was assessed using spatial permutations (n=1000) across voxels and participants. The 95th percentile of the distribution of t-values was selected as statistical threshold. This procedure was computed separately for SO and SA. Brain regions with significant Fischer transformed correlations and more than 200 contiguous voxels were retained.

5.3 Results

5.3.1 Behavioral experiment

While participants performed pinching movements with their right hand and observed a virtual avatar also performing pinching movements, we manipulated the visual and sensorimotor information to induce altered states of SO and SA. In particular, we manipulated the factor of "movement type" (active or passive movements), of synchrony (synchronous or asynchronous movements of the virtual hand with respect to the real hand) and of congruency (right or left virtual hand moving). After each trial, participants reported subjective ratings of SO and SA towards the virtual hand, as well as a control rating. In addition, we measured the proprioceptive drift.

5.3.1.1 Subjective ratings and proprioceptive drift

Results regarding subjective ratings and proprioceptive drift are presented in Fig.5.1C. For the statistical analysis, the data were normalized to minimize between-subject biases. Separately for each variable, the data were analyzed using linear mixed effects models (see Methods). The statistical analysis is summarized in Tab.5.S1A.

For the ratings of SO, we found a main effect of "synchrony" ($F_{1,26}=103.99$, $p<0.0001$) with greater SO ratings during synchronous trials compared to asynchronous trials. We also found a main effect of "congruency" ($F_{1,26}=80.02$, $p<0.0001$) showing greater SO ratings during congruent trials compared to incongruent ones. In addition, there was a 2-way interaction between "movement
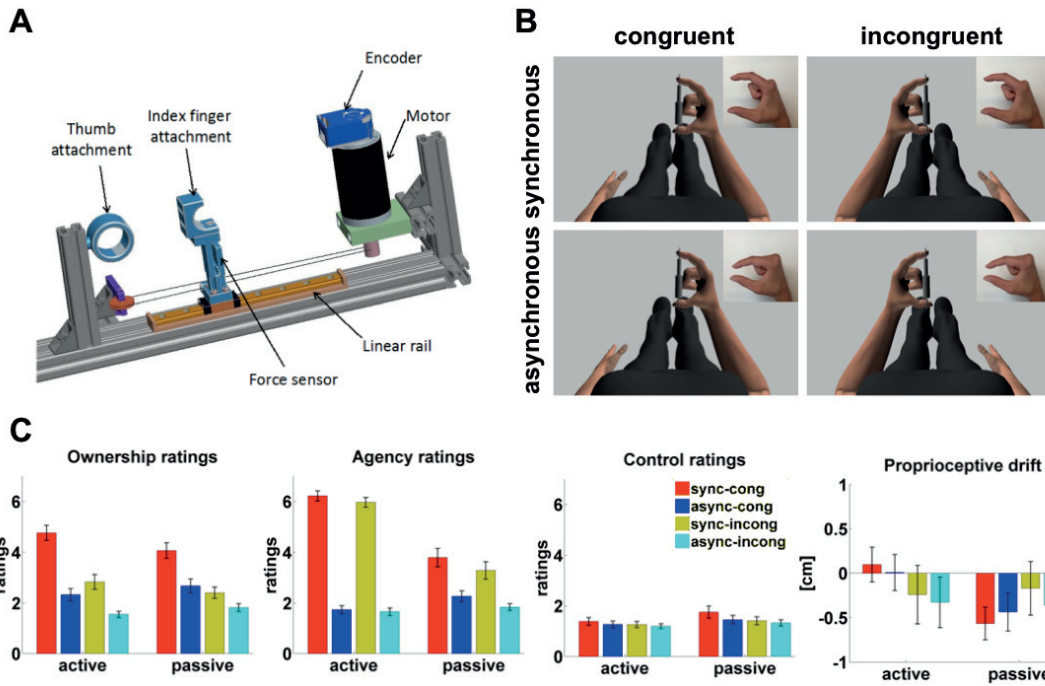
Fig.5.1 Behavioral experiment. A) The robotic finger manipulandum allows performing a pinching movement either actively or passively while recording hand aperture (moving index against fixed thumb) and interaction force. Control is achieved via cable transmission from a direct-drive torque motor holding an optical encoder as well as a force transducer integrated into the moving finger module. **B)** A virtual environment displays an avatar performing a pinching action. The synchrony and congruency (left vs right hand of the avatar) can be manipulated through computer control. **C)** Subjective ratings and proprioceptive drift associated with the 8 experimental conditions. Subjective ratings ranged from 1 to 6 on a likert scale. For the proprioceptive drift, a negative value represents a drift towards the virtual hand. Conditions are grouped into active and passive conditions. In addition, synchronous and congruent conditions are shown in red, asynchronous and congruent conditions are shown in blue, synchronous and incongruent conditions are shown in yellow, asynchronous and incongruent conditions are shown in cyan. Statistical results concerning the ratings are shown in Tab.5.S1A.

type" and "synchrony" ($F_{1,1616}$=67.31, p<0.0001) showing that the drop in SO due to asynchrony was greater during active trials compared to passive trials. Finally, the analysis also revealed a 2-way interaction between "synchrony" and "congruency" ($F_{1,1616}$=86.86, p<0.0001) showing that the drop in SO due to asynchrony was greater during congruent trials compared to incongruent trials. We note that there was no main effect of movement type, suggesting that SO is similarly affected by active and passive movements.

For the ratings of SA, there was a main effect of "movement type" ($F_{1,26}$=22.51, p<0.0001) with greater SA ratings during active conditions compared to passive ones. There was also a main effect of "synchrony" ($F_{1,26}$=375.31, p<0.0001) showing greater SA ratings during synchronous trials compared to asynchronous trials. We

152

also found a main effect of congruency ($F_{1,1642}$=36.89, p<0.0001) with greater SA ratings during congruent trials compared to incongruent ones. In addition, the analysis revealed a 2-way interaction between "movement type" and "synchrony" ($F_{1,1642}$=747.10, p<0.0001) showing that the drop in SA due to asynchrony was greater during active trials compared to passive trials. Finally, we found a 2-way interaction between "movement type" and "congruency" ($F_{1,1642}$=8.22, p=0.004) revealing that the drop in SA due to incongruency was greater during passive trials compared to active ones.

Unexpectedly, we also found significant effects for control ratings (3 main effects and 3 2-way interactions, see Tab.5.S1A). However, the magnitude of these effects were very small in comparison to the effects observed for SO and SA ratings. There was no significant effect associated with the proprioceptive drift.

We also found a significant correlation between SO and SA ratings (r=0.49, p<0.0001, see Fig.5.S1A).

To summarize, we found that the factors of "synchrony" and "congruency" strongly modulated SO. In addition, we report that for SO the factor of synchrony had interactions with the factors of "movement type" and "congruency". SA ratings were strongly modulated by the factors of "movement type", "synchrony" and "congruency". In addition, the factor of "movement type" had interactions with the factors of "synchrony" and "congruency" for SA. This shows that both SO and SA are modulated by our experimental factors, but in different ways. Control ratings were weakly modulated by the experimental factors and we found no effect for the proprioceptive drift. There was a significant correlation between SO and SA ratings. Overall these results suggest that our experimental design is able to induce altered states of SO and SA.

5.3.2 fMRI experiment

The previous experiment was replicated in MR-environment to measure the ongoing BOLD activity while participants experienced altered states of SO and SA. The same experimental conditions and measures were used as in the behavioral experiment, except we did not measure the proprioceptive drift.
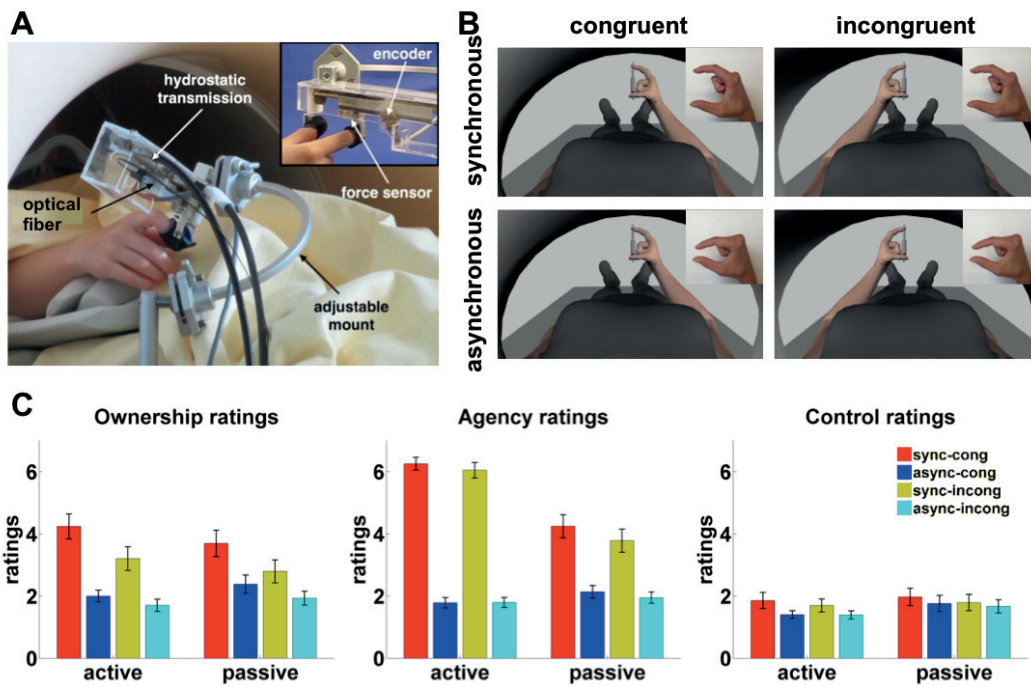
Fig.5.2 fMRI experiment. A) The MR-compatible finger manipulandum is attached to the scanner bed with an adjustable mount allowing performing a pinching movement either actively or passively while recording hand aperture (moving index against fixed thumb) and interaction force. Control is achieved via a hydrostatic transmission actuated by a motor located in the control room, as well as a position and a force transducer integrated into the moving finger module on the slave interface. **B)** A virtual environment displays an avatar performing a pinching action. The synchrony and congruency (left vs right hand of the avatar) can be manipulated through computer control. **C)** Subjective ratings associated with the 8 experimental conditions. Subjective ratings ranged from 1 to 6 on a likert scale. Conditions are grouped into active and passive conditions. In addition, synchronous and congruent conditions are shown in red, asynchronous and congruent conditions are shown in blue, synchronous and incongruent conditions are shown in yellow, asynchronous and incongruent conditions are shown in cyan. Statistical results concerning the ratings are shown in Tab.5.S1B.

5.3.2.1 Subjective ratings

Subjective ratings are reported in Fig.5.2C. For the statistical analysis, the data were normalized to minimize between-subject biases. Separately for each variable, the data were analyzed using linear mixed effects models (see Methods). The statistical analysis is summarized in Tab.5.S1B.

For the ratings of SO, there was a main effect of "synchrony" ($F_{1,21}$=60.38, p<0.0001) showing greater SO ratings during synchronous trials compared to asynchronous trials. We also found a main effect of "congruency" ($F_{1,21}$=15.34, p=0.001) with greater SO ratings during congruent trials compared to incongruent

ones. In addition, there was a 2-way interaction between "movement type" and "synchrony" ($F_{1,1316}$=49.79, p<0.0001) showing that the drop in SO due to asynchrony was greater during active trials compared to passive trials. Finally, the analysis also revealed a 2-way interaction between "synchrony" and "congruency" ($F_{1,1316}$=22.79, p<0.0001) showing that the drop in SO due to asynchrony was greater during congruent trials compared to incongruent trials.

For the ratings of SA, we found a main effect of "movement type" ($F_{1,21}$=15.62, p=0.001) with greater SA ratings during active conditions compared to passive ones. There was also a main effect of "synchrony" ($F_{1,21}$=288.18, p<0.0001) showing greater SA ratings during synchronous trials compared to asynchronous trials. We also found a main effect of congruency ($F_{1,1337}$=12.13, p=0.001) with greater SA ratings during congruent trials compared to incongruent ones. In addition, the analysis revealed a 2-way interaction between "movement type" and "synchrony" ($F_{1,1337}$=334.58, p<0.0001) showing that the drop in SA due to asynchrony was greater during active trials compared to passive trials. Finally, we found a weak 2-way interaction between "synchrony" and "congruency" ($F_{1,1337}$=3.99, p=0.046) revealing that the drop in SA due to asynchrony was greater during congruent trials compared to incongruent ones.

Unexpectedly, we also found significant effects for control ratings (main effects of "synchrony" and "congruency" and a 2-way interaction between "movement type" and "synchrony", see Tab.5.S1B). However, the magnitude of these effects were very small in comparison to the effects observed for SO and SA ratings.

We also investigated the correlation between the different experimental measures and found a significant correlation between SO and SA (r=0.44, p<0.0001, see Fig.5.S1B).

To summarize, we strongly replicated the findings from the previous experiment. We found that the factors of "synchrony" and "congruency" strongly modulated SO. In addition, we report that for SO the factor of synchrony had interactions with the factors of "movement type" and "congruency". SA ratings were strongly modulated by the factors of "movement type", "synchrony" and "congruency". In addition, the factor of "synchrony" had interactions with the factors of "movement type" and

"congruency" for SA. Control ratings were weakly modulated by the experimental factors. There was a significant correlation between SO and SA ratings.

5.3.2.2 Representational similarity analysis (RSA)

We applied RSA to identify brain regions associated with changes in subjective ratings of SO and SA respectively. To this end, we computed model-RDMS for SO and SA based on participant's subjective ratings. The average model-RDMs for SO and SA are shown in Fig.5.S2. Then, we identified brain regions exhibiting BOLD patterns with the same similarity structures as the model-RDMs of SO and of SA respectively.

RSA identified brain regions in which the similarity of BOLD patterns across experimental conditions was associated with the modulation of SO. The brain regions associated with SO are listed in Tab.5.1 and displayed in Fig.5.3 (top panel). We identified a large-scale network including occipital, parietal, temporal, frontal, insular, medial and cerebellar cortices. In the left hemisphere, we found the superior occipital gyrus (SOG), the superior parietal lobule (SPL), the posterior superior temporal sulcus (pSTS, which extends into the posterior middle temporal gyrus), the anterior superior temporal sulcus (aSTS), the precentral gyrus (vPMC), the middle and superior frontal gyri (DLPFC), the anterior and posterior insula (aIns and pIns, which extends into the parietal operculum, S2), the anterior cingulate cortex and the cerebellum. Brain regions in the right hemisphere corresponded to the inferior occipital gyrus (LOC), the posterior superior temporal sulcus (pSTS, extending into the posterior middle gyrus), the anterior superior temporal sulcus (aSTS) and, the precentral gyrus (dPMC), the posterior middle and superior frontal gyi (DLPFC), the inferior and middle anterior frontal gyri (VLPFC), the posterior insula (pIns, extending into the parietal operculum, S2), the anterior cingulate cortex (ACC) and the precuneus (Pre).

Similarly, RSA highlighted brain regions in which the similarity of BOLD patterns across experimental conditions was associated with the modulation of SA. The brain regions associated with SA are presented in Tab.5.2 and displayed in Fig.5.3 (middle panel) and included occipital, parietal, temporal, frontal, insular and cerebellar cortices. In details, we found in the left hemisphere the superior occipital gyrus
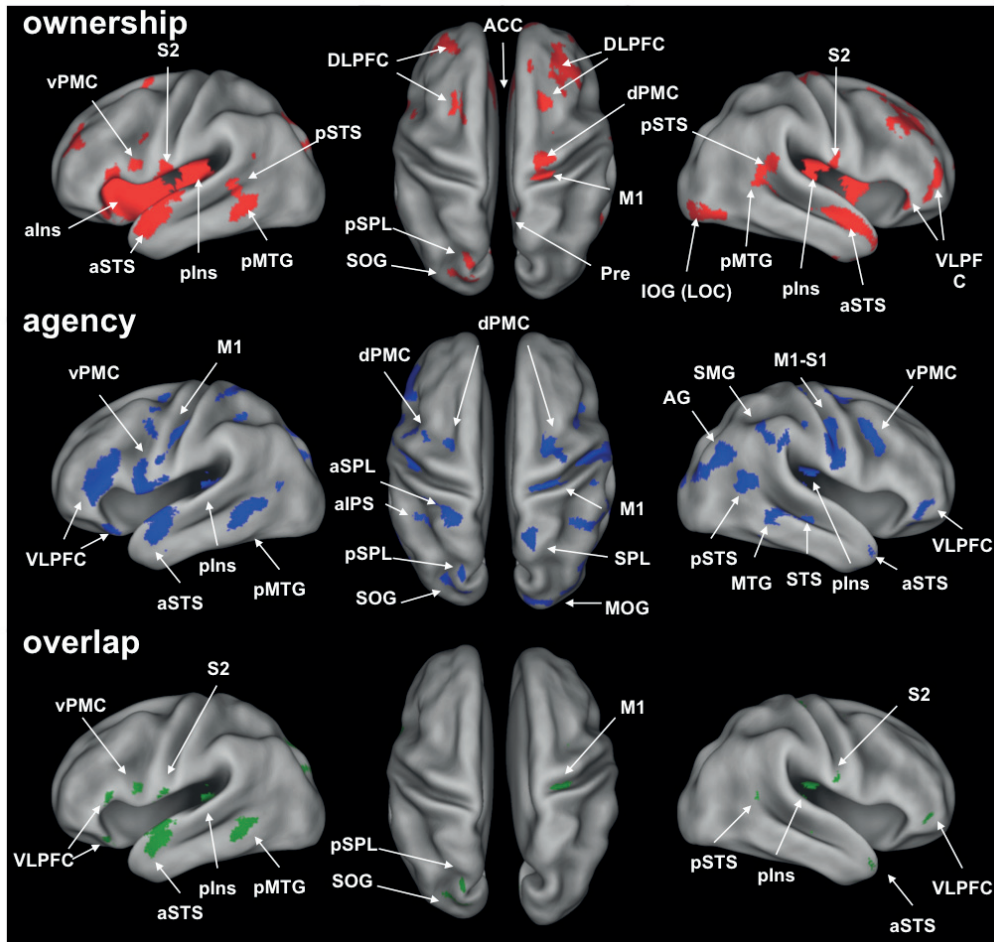
Fig.5.3 Brain Regions associated with the sense of hand ownership and the sense of hand agency. Brain regions associated with ownership are shown in red in the top panel, brain regions associated with agency are shown in blue in the middle panel, and brain regions common to ownership and agency (overlap) are shown in green in the bottom panel. (a=anterior, p=posterior, d=dorsal, v=ventral, AAC=anterior cingulate cortex, AG=angular gyrus, DLPFC = dorsolateral prefrontal cortex, IOG=inferior occipital gyrus, Ins=insula, IPS=intraparietal sulcus, M1=primary motor cortex, MOG=middle occipital gyrus, MTG=middle temporal gyrus, LOC=lateral occipital complex, PMC=premotor cortex, Pre=precuneus, S1=primary somatosensory cortex, S2=secondary somatosensory cortex, SOG=superior occipital gyrus, SMG=supramarginal gyrus, SPL=superior parietal lobule, STS=superior temporal sulcus, VLPFC=ventrolateral prefrontal cortex)

(SOG), the posterior superior parietal lobule (pSPL), the anterior intraparietal sulcus (aIPS), the anterior superior parietal lobule (aSPL, extending into the postcentral gyrus), the posterior middle temporal gyrus (pMTG), the anterior superior temporal sulcus (aSTS), the precentral gyrus (3 clusters: M1, which extends into the postcentral gyrus, S1; dPMC; and vPMC, which extends into the parietal operculum, S2), the posterior superior frontal gyrus (dPMC), the anterior inferior frontal gyrus (VLPFC) and the posterior insula (pIns). Brain regions in the right hemisphere corresponded to the middle occipital gyrus (MOG), the angular gyrus (AG), the superior parietal

Left hemisphere	BA	x	y	z	t-peak	Right hemishere	BA	x	y	z	t-peak
L sup occipital gyrus (SOG)	19	-15	-89	33	24.0	R inf occipital gyrus (IOG, LOC)	19	38	-84	11	27.6
L post sup parietal lobule (pSPL)	7	-17	-75	44	18.4						
L post sup temporal sulcus (pSTS)	21, 22	-62	-56	-8	25.5	R post sup temporal sulcus (pSTS)	22	59	-44	17	27.3
L post mid temporal gyrus (pMTG)	21	-56	-42	6	19.4	R post mid temporal gyrus (pMTG)	21	51	-42	0	20.3
L ant sup temporal gyrus (aSTS)	22, 38	-48	2	-15	43.7	R ant sup temporal sulcus (aSTS)	22, 38	54	3	-20	31.9
L precentral gyrus (vPMC)	6	-47	4	19	17.6	R precentral gyrus (dPMC)	6	23	-23	71	17.3
L post sup frontal gyrus (DLPFC)	8	-20	5	63	19.1	R post sup frontal gyrus (DLPFC)	8	23	27	35	25.2
L ant mid frontal gyrus (DLPFC)	9, 46	-29	48	36	21.0	R post mid frontal gyrus (DLPFC)	9, 46	23	12	50	34.1
L ant sup frontal gyrus	9	-24	60	24	17.6						
						R ant mid frontal gyrus (VLPFC)	46	42	54	6	19.8
						R ant inf frontal gyrus (VLPFC)	47	48	32	-9	19.5
L ant insula (aIns)	48	-27	20	6	35.4	R post insula (pIns)	48	36	2	8	33.7
L post insula (pIns)	48	-38	-9	-12	31.4	R parietal operculum (S2)	48				
L parietal operculum (S2)	48										
L ant cingulate cortex (ACC)	24, 32	-2	29	32	21.3	R ant cingulate cortex (ACC)	24, 32	14	26	29	21.7
						R sup medial gyrus	10	15	48	11	22.5
						R precuneus (Pre)	7	6	-45	51	20.2
L cerebellum (lobule VIIa)		-35	-63	-32	25.7						
L cerebellum (lobule X)		-29	-42	-38	17.9						

Tab.5.1 **Brain regions associated with subjective changes in the sense of body ownership .** The anatomical name, the functional abbreviation, the Brodmann area, the MNI location and the peak t-value are reported for each cluster. (L=left, R=right, post=posterior, ant=anterior, inf=inferior, mid=middle, sup=superior)

lobule (SPL), the supramarginal gyrus (SMG, 2 clusters), the posterior superior temporal sulcus (pSTS), the superior temporal sulcus (STS, which extends into the middle temporal gyrus), the anterior superior temporal sulcus (aSTS), the precentral gyrus (2 clusters: dorsal M1 and ventral M1, which extends into the postcentral gyrus, S1), the posterior middle (vPMC) and posterior superior (dPMC) frontal gyri, the anterior inferior frontal gyrus (VLPFC), the posterior insula (pIns) and the cerebellum.

In addition, we found several brain regions common to SO and SA (Tab.5.S2). Brain regions common to SO and SA in the left hemisphere included the superior occipital gyrus (SOG), the posterior superior parietal lobule (pSPL), the parietal operculum (S2), the posterior middle temporal gyrus (pMTG), the anterior superior temporal sulcus (aSTS), the precentral gyrus (vPMC), the anterior inferior frontal gyrus (VLPFC) and the posterior insula (pIns). In the right hemisphere, brain regions common to SO and SA were the parietal operculum (S2), the posterior superior

Left hemisphere	BA	x	y	z	t-peak	Right hemisphere	BA	x	y	z	t-peak
L sup occipital gyrus (SOG)	19	-15	-86	26	20.8	R mid occipital gyrus (MOG)	19	47	-78	21	26.5
L post sup parietal lobule (pSPL)	7	-18	-77	48	18.7	R angular gyrus (AG)	39	44	-63	30	25.8
L ant sup parietal lobule (aSPL)	5	-35	-35	59	17.9	R sup parietal lobule (SPL)	5	17	-54	66	21.9
L postcentral gyrus	2	-23	-44	63	23.8						
						R supramarginal gyrus (SMG)	40	45	-44	45	21.1
L ant intraparietal sulcus (aIPS)	40	-39	-45	48	18.0			60	-33	41	19.5
L post mid temporal gyrus (pMTG)	21	-57	-48	-5	26.8	R post sup temporal sulcus (pSTS)	21	51	-51	15	19.5
L ant sup temporal sulcus (aSTS)	22, 38	-56	6	-2	28.0	R sup temporal sulcus (STS)	21	57	-36	-6	20.5
						R mid temporal gyrus (MTG)	20	57	-38	-14	25.2
						R ant sup temporal gyrus (aSTS)	38	39	9	-35	22.9
L precentral gyrus (M1)	4	-45	-9	35	24.3	R precentral (M1)	4	45	-11	38	30.9
						R postcentral (S1)	3	66	-5	20	21.4
L precentral gyrus (dPMC)	6	-45	2	39	20.4						
						R precentral gyrus (M1)	4	35	-23	57	19.4
L precentral gyrus (vPMC)	6	-48	3	21	22.2						
L parietal operculum (S2)	48					R post sup frontal gyrus (dPMC)	6	21	11	47	18.7
L post sup frontal gyrus (dPMC)	6	-23	-6	56	19.6	R post mid frontal gyrus (vPMC)	6	35	8	38	25.3
L ant inf frontal gyrus (VLPFC)	45	-51	38	6	24.0	R ant inf frontal gyrus (VLPFC)	46	42	44	-11	22.4
	47	-41	62	-18	20.7						
L post Insula (pIns)	48	-35	-30	12	18.8	R post insula (pIns)	48	36	-21	23	22.2
						R cerebellum (lobule VI)		0	-77	-2	42.6
						R lingual gyrus		12	-72	-3	23.2

Tab.5.2 Tab.2 **Brain regions associated with subjective changes in the sense of hand agency.** The anatomical name, the functional abbreviation, the Brodmann area, the MNI location and the peak t-value are reported for each cluster. (L=left, R=right, post=posterior, ant=anterior, inf=inferior, mid=middle, sup=superior)

temporal sulcus (pSTS), the anterior superior temporal sulcus (aSTS), the precentral gyrus (M1), the anterior inferior frontal gyrus (VLPFC), and the posterior insula (pIns).

To summarize, we used RSA to identify two partially overlapping networks associated with SO and SA respectively. These networks included occipital, parietal, temporal, frontal, insular, cingulate and cerebellar regions.

5.4 Discussion

In the present study, we developed a novel setup combining MR-compatible robotics and virtual reality to induce altered states of SO and SA. We manipulated 3 experimental factors: 1) the "type of movement" performed by the participants (active or passive); 2) the "synchrony" between the movements of the participant's hand and of the seen virtual hand (synchronous or asynchronous); 3) the "congruency" between the participant's hand and the seen virtual hand (right or left virtual hand moving).

These experimental conditions led to a fine-grained modulation of participant's SO and SA towards the virtual hand on a trial-by-trial basis, which we associated to two brain networks, one for SO and another for SA, using RSA.

5.4.1 Alterations of SO and SA

As shown and replicated by our behavioral and fMRI experiments, subjective reports of SO were strongly modulated by the factor of "synchrony" and by the factor of "congruency", but to a lesser extent by the factor of "type of movement". Classically, SO has been manipulated under static conditions, suggesting that active movements are not necessary. Nevertheless, several studies reported that SO is increased during active movements compared to passive movements (**Asai et al. 2016; Dummer et al. 2009; Ma and Hommel, 2015; Tsakiris et al. 2006**). On the other hand, subjective reports of SA were modulated by the factors of "type of movement", "synchrony" and "congruency". The importance of the congruent structure for SA seems counterintuitive considering that it is possible to experience agency over non-bodily objects (**David, 2008**) such as in computer games. The present data replicate previous findings by showing that the congruent structure of the controlled object also affects SA when manipulated concomitantly with SO (**Braun et al. 2014; Klackert et al. 2012; Jenkinson and Preston, 2015**). Overall, the effects associated with our experimental factors are replicating the results from previous literature (**Asai et al. 2016; Braun et al. 2014; Caspar et al. 2015; Dummer et al. 2009; Hara et al. 2016; Jenkinson and Preston, 2015; Klackert and Ehrsson, 2012, 2014; Ma and Hommel, 2015; Shibuya et al. 2016; Tsakiris et al. 2006**).

The present behavioral data suggest that SO and SA are tightly linked components of the experience that we have of our hands and that they can be modulated by the same experimental factors. This is additionally supported by the presence of a statistical correlation between subjective reports of SO and SA (present study and **Caspar et al. 2015; Klackert and Ehrsson, 2012, 2014**). These results further support the view that both SO and SA are components of self-consciousness generated by low-level sensorimotor processing (**Schwabe and Blanke, 2007; Tsakiris et al. 2007**). However, there is accumulating evidence that SO and SA are preferably modulated by different types of low-level sensorimotor signals. For example, SO is less affected by the type of movement compared to SA (present study

and **Asai et al. 2016; Braun et al. 2014; Ma and Hommel, 2015; Tsakiris et al. 2006**). Contrastingly SA is less affected by the congruent structure of the owned hand compared to SO (present study and **Braun et al. 2014; Klackert et al. 2012; Jenkinson and Preston, 2015**). In addition, the amount of temporal asynchrony affects differently SO and SA (**Imaizumi et al. 2015; Ismail and Shimada, 2016**). Cumulatively, These results suggest that SO and SA are distinct neural processes with a certain degree of interplay.

Unexpectedly, our experimental factors also modulated our control subjective rating ("I felt as if my real hand was disappearing"). However, the associated effect sizes were much smaller compared to SO and SA subjective ratings. Anecdotally, several participants spontaneously reported "experiencing" more vividly the virtual hand than their own, which can be interpreted as a disembodiment of their real hand. This can explain the observed effects.

The absence of effects associated with the proprioceptive drift in our behavioral experiment was mostly due to a large inter-trial and inter-subject variability. This can be attributed to the rather difficult and uncommon setup of the task, which required participants to establish a mapping between a virtual and the real space.

5.4.2 Brain regions associated with SO

In the present study, we associated the alteration of SO with a brain network including the premotor cortex, the posterior parietal cortex, the insula, the anterior cingulate cortex and the cerebellum, which are the brain regions most consistently reported in previous studies (**Berkater-Bodman et al. 2012, 2014; Brozzoli et al. 2012; Ehrsson et al. 2004, 2005; Gentile et al. 2013; Guterstam et al. 2013; Limanowski et al. 2014, 2015, 2016; Petkova et al. 2011; Tsakiris et al. 2007;** see **Blanke et al. 2015** for a review), thus confirming the validity of our approach. In addition, our analysis highlighted an association between SO and areas processing somatosensory information (S2; as in **Limanowski et al. 2015; Petkova et al. 2011; Tsakiris et al. 2010**), as well as areas processing visual information (SOG and LOC; as in **Gentile et al. 2013; Limanowski et al. 2015; Petkova et al. 2011**). We note that we did not find any association between SO and changes in BOLD patterns within primary somatosensory areas or within primary visual areas, suggesting that

activity in primary sensory areas is not directly associated with subjective changes in SO. Furthermore, we report the implication of frontal areas (DLPFC, VLPFC; as in **Limanowski et al. 2016; Petkova et al. 2011; Tsakiris et al. 2010)**, which have been linked to self-recognition and self-other distinction (**Apps and Tsakiris, 2014; Sugiura et al. 2015**). These regions could be involved in the recognition of the virtual hand as part of the self and a corresponding change in relevance of the virtual hand. We also found that SO was associated with the posterior middle temporal gyrus (pMTG), which processes visual motion (**Maus et al. 2013; Tootel et al. 1995**) and with the posterior superior temporal sulcus (pSTS), which is important for biological motion (**Grossman et al. 2000; Servos et al. 2002; Gilaie-Dotan et al. 2013**) and action representation (**Vander Wyk et al. 2012**). Finally, anterior temporal areas (aSTS) were also associated with the alteration of SO, which could be linked to working memory and access to conceptual hand representations (**Peelen and Caramazza, 2012; Simmons and Barsalou, 2003**). We note that several studies also found an implication of temporal regions for SO, although these aspects were not emphasized (**Limanowski et al. 2016; Petkova et al. 2011; Tsakiris et al. 2010**). Temporal contributions have been so far neglected in previous studies investigating SO.

5.4.3 Brain regions associated with SA

We report an association between the alteration of SA and the brain network including the premotor cortex, the posterior parietal cortex (superior parietal lobule, the intraparietal sulcus, the angular gyrus and the supramarginal gyrus), the frontal cortex (VLPFC), the middle and superior temporal gyri, the insula and the cerebellum. In addition, our analysis highlighted an association between SA and areas processing sensorimotor information (M1, S1 and S2), as well as areas processing visual information (SOG and MOC). As for SO, we link the implication of posterior temporal regions with processing of motion and action representations, and we link the implication of the anterior temporal regions with working memory and conceptual representations. These results are in accordance with previous literature on agency (**David et al. 2006; Farrer and Frith 2002; Farrer et al. 2003, 2008; Fink et al. 1999; Leube et al. 2003;** see **David, 2008** for a review), although our analysis did not reveal an association with supplementary motor areas. In particular, our results

replicate strongly the ones presented by Tsakiris and colleagues **(2010)**, who investigated SA in a very similar framework and reported also a link between SA and a comparable network of premotor, parietal, temporal, insular, frontal and cerebellar areas.

5.4.4 Brain mechanisms common to SO and SA

Our analysis revealed brain regions that were commonly associated with SO and SA. They included occipital, parietal, temporal, frontal and insular regions, showing that SO and SA share common substrates in most of the fundamental brain areas highlighted in the literature and in the present study. In particular, the largest overlap was found in the left posterior and anterior temporal cortices, suggesting that the contributions of these regions for SO and SA should not be neglected. However, the extent of overlap between SO and SA networks is rather small compared to the extent of non-overlapping regions associated with SO and SA, suggesting that they rely on structurally and functionally similar brain networks, but spatially distinct. Most prominently, SO was associated with extended insular regions and with midline structures (cingulate and precuneus), but not SA, which could be linked to the processing of interoceptive signals contributing to SO (**Park and Tallon-Baudry, 2014; Park et al. 2016**). Similarly, SA was associated with extended sensorimotor, premotor and parietal areas compared to SO reflecting the increased motor contributions to SA.

Conceptually and computationally, SO and SA must rely on a number of common brain mechanisms starting with visual processing in occipital areas and sensorimotor processing in precentral and postcentral areas. In addition, multimodal neurons and multisensory integration are key features of SO and SA (**Blanke et al. 2015**). Our experimental manipulations induced 3 different types of multisensory conflicts, which altered SO and SA. The first multisensory conflict is the temporal and spatial match/mismatch between the felt and seen hand movements. The second conflict is the congruency between the structures of the seen hand and of the felt hand. The last conflict is the comparison between the predicted outcomes of motor commands (the so-called motor efferent copy) and the actual perceived outcome. In the absence of conflicts, the multisensory information is integrated to generate the stable and coherent experience of owning and controlling the perceived hand. In particular,
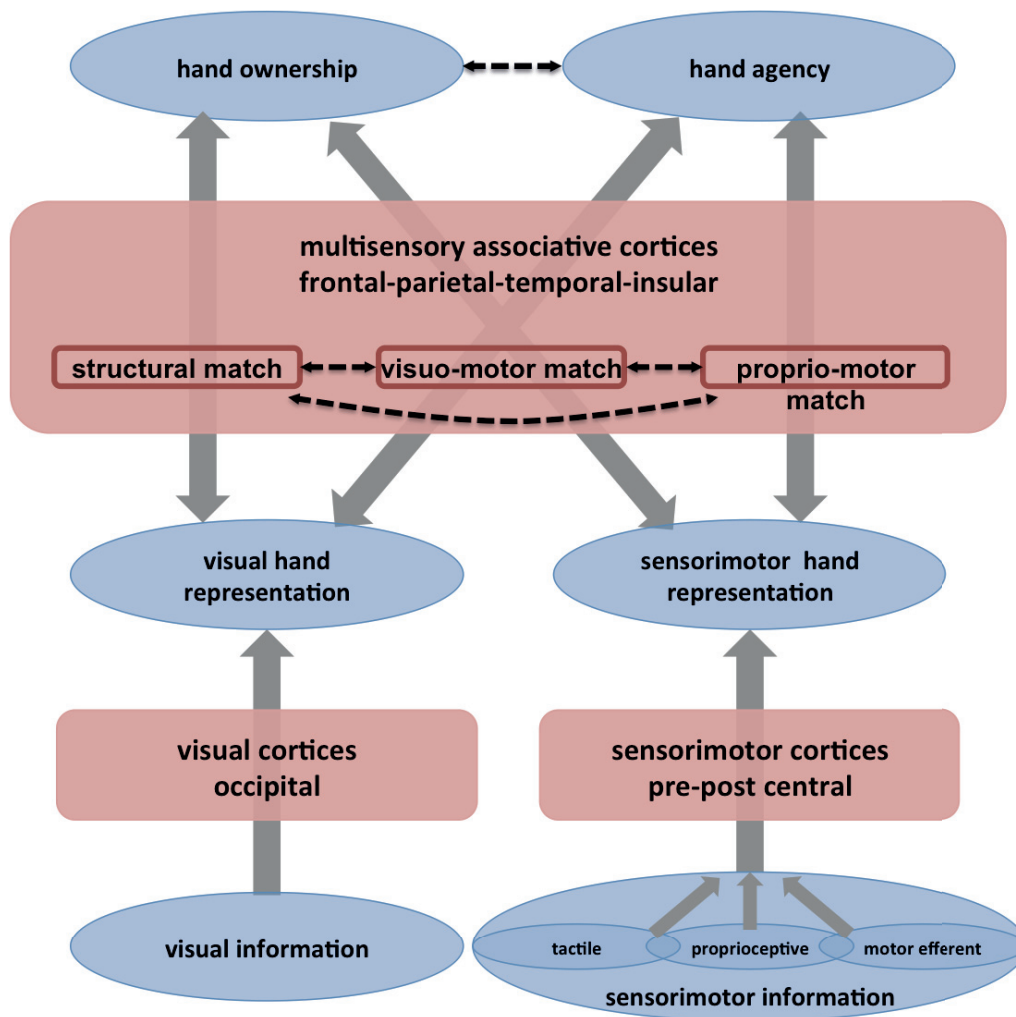
Fig.5.4 **Sumarrizing model.** Visual information is processed in occipital areas to create a visual representation of the hand. Tactile, proprioceptive and motor efferent information are processed in precentral and postcentral areas to create a representation of the sensorimotor hand. The multisensory information is integrated in multisensory frontal, parietal, temporal and insular areas (non-exhaustively). If a certain number of constraints are satisfied (those constraints are different for SO and SA) SO and SA are generated towards the perceived hand. The dashed arrows represent potential interactions between different types of inter-sensory conflicts (as shown by the interactions highlighted in our statistical analysis) and between SO and SA directly (as sown by the correlation between ratings of SO and SA).

parietal, frontal, temporal and insular multisensory brain areas are strong candidates to process these multimodal conflicts. A simple model summarizing these aspects is depicted in Fig.5.4.

5.5 Conclusions

Our behavioral and neuroimaging results support the view that SO and SA are distinct processes both relying on the integration of multisensory and motor

information. Two partially overlapping networks including parietal, temporal, frontal and insular areas have been associated with SO and SA. In particular, we highlighted the important contribution of posterior and anterior temporal cortices for SO and SA, which have been so far neglected in the literature.

The identified networks represent the set of brain regions in which BOLD patterns co-varied with subjective reports of SO and SA. They do not necessarily represents the neural substrates of SO and SA, but rather highlight the complex and broad mechanisms involved in SO and SA. These investigations have been carried out specifically in the context of hand self-consciousness. It remains unclear whether these processes for other body parts such as face or trunk rely on the same networks or whether there exist body-part specific mechanisms of SO and SA.

We believe that studying the subjective experience of our body has critical applications in the fields of robotics and neuroprosthetics. An important challenge in these fields is to develop devices that can be interfaced with the user's nervous system, allowing them to feel and control the prosthesis as their own limb. The understanding of altered states of SO and SA are critical steps to reach this achievement.

5.6 Supplementary materials

A. behavioral experiment

		SO ratings				SA ratings				control ratings				proprioceptive drift		
		d.o.f.	F-statistic	p-value		d.o.f.	F-statistic	p-value		d.o.f.	F-statistic	p-value		d.o.f.	F-statistic	p-value
AP	1	26.000	1.190	0.285	1	26.000	22.508	<0.0001	1	26.003	6.668	0.016	1	1668.000	3.223	0.073
SYNC	1	26.000	103.985	<0.0001	1	26.000	375.313	<0.0001	1	26.302	5.250	0.030	1	54.097	0.123	0.727
CONG	1	26.000	88.020	<0.0001	1	1642.000	36.888	<0.0001	1	26.337	6.302	0.019	1	26.132	0.057	0.813
AP*SYNC	1	1616.000	67.306	<0.0001	1	1642.000	747.098	<0.0001	1	1641.999	5.175	0.023	1	1668.000	0.037	0.847
AP*CONG	1	1616.000	1.251	0.263	1	1642.000	8.224	0.004	1	1641.999	9.392	0.002	1	1668.000	3.736	0.053
SYNC*CONG	1	1616.000	86.858	<0.0001	1	1642.000	0.856	0.355	1	1641.999	5.993	0.014	1	1668.000	0.283	0.595
AP*SYNC*CONG	1	1616.000	3.176	0.075	1	1642.000	0.182	0.670	1	1641.999	3.242	0.072	1	1668.000	0.293	0.588

B. fMRI experiment

		SO ratings				SA ratings				control ratings		
		d.o.f.	F-statistic	p-value		d.o.f.	F-statistic	p-value		d.o.f.	F-statistic	p-value
AP	1	21.000	1.373	0.254	1	21.000	15.617	0.001	1	21.000	2.140	0.158
SYNC	1	21.000	60.375	<0.0001	1	21.000	288.175	<0.0001	1	21.000	6.078	0.022
CONG	1	21.000	15.341	0.001	1	1337.000	12.131	0.001	1	1337.000	6.625	0.010
AP*SYNC	1	1316.001	49.792	<0.0001	1	1337.000	334.583	<0.0001	1	1337.000	7.708	0.006
AP*CONG	1	1316.001	0.151	0.698	1	1337.000	2.084	0.149	1	1337.000	0.220	0.639
SYNC*CONG	1	1316.001	22.794	<0.0001	1	1337.000	3.994	0.046	1	1337.000	1.689	0.194
AP*SYNC*CONG	1	1316.001	2.145	0.143	1	1337.000	0.003	0.954	1	1337.000	0.096	0.756

Tab.5.S1 Statistical analysis of subjective ratings. A) Subjective ratings and proprioceptive drift from the behavioral experiment were analyzed using linear mixed effects models. **B)** Subjective ratings from the fMRI experiment were analyzed using linear mixed effects models (significant effects are shown in red (p<0.005) and in green (p<0.05). Main effects and interactions were investigated for factors of "movement type" (active or passice, AP), "synchrony" (synchronous or asynchronous, SYNC) and "congruency" (congruent or incongruent), CONG.

Left hemisphere	BA	Right hemisphere	BA
L sup occipital gyrus (SOG)	19		
L post sup parietal lobule (pSPL)	7	R parietal operculum (S2)	48
L parietal operculum (S2)	48		
L post mid temporal gyrus (pMTG)	21	R post sup temporal sulcus (pSTS)	21
L ant sup temporal sulcus (aSTS)	22, 38	R ant sup temporal sulcus (aSTS)	38
L precentral gyrus (vPMC)	6	R precentral (M1)	4
L ant inferior frontal gyrus (VLPFC)	45, 47	R ant inf frontal gyrus (VLPFC)	46
L post insula (pIns)	48	R post insula (pIns)	48

Tab.5.S2 Brain regions common to the sense of hand ownership and the sense of hand agency. The anatomical name, the functional abbreviation and the Brodmann area are reported for each cluster. (L=left, R=right, post=posterior, ant=anterior, inf=inferior, mid=middle, sup=superior)

A. behavioral experiment

Correlation between SO and SA

r=0.49

B. fMRI experiment

Correlation between SO and SA

r=0.44
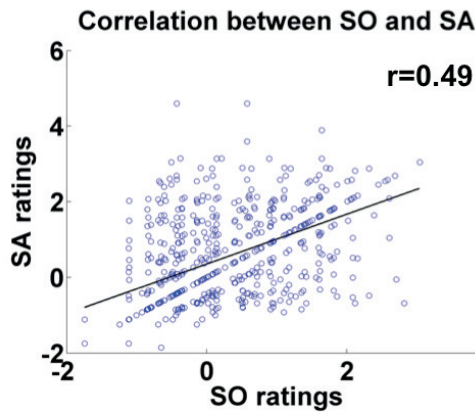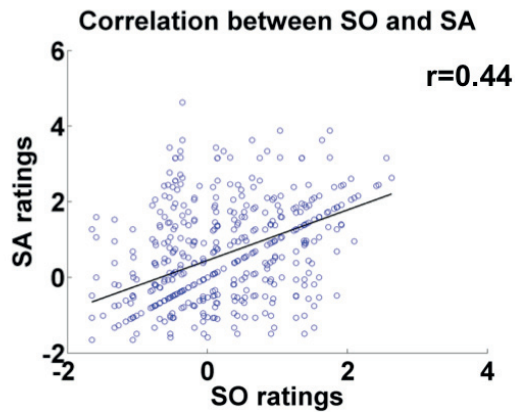
Fig.5.S1 Correlation between SO and SA. A) Subjective ratings of SO and SA from the behavioral experiment were significantly correlated (r=0.49, p<0.0001, regression: SA=0.66*SO+0.35, R^2=0.24). **B)** Subjective ratings of SO and SA from the fMRI experiment were significantly correlated (r=0.44, p<0.0001, regression: SA=0.66*SO+0.47, R^2=0.19).

average RDM for SO

average RDM for SA

1 active sync cong
2 active async cong
3 active sync incong
4 active async incong
5 passive sync cong
6 passive async cong
7 passive sync incong
8 passive async incong

Fig.5.S2 Average representational dissimilarity matrix (RDM) for SO and SA. The individual RDMs for SO and SA were averaged across repetitions (64x64 -> 8x8) and across participants. The correlation between SO and SA RDMs ranged between 0.17 and 0.98 (mean ± std: 0.59 ± 0.3). The matrix is symmetrical and the distances on the diagonal are zeros.

5.7 References

Apps, M.A.J., Tsakiris, M., 2014. The free-energy self: A predictive coding account of self-recognition. Neuroscience and Biobehavioral Reviews. doi:10.1016/j.neubiorev.2013.01.029

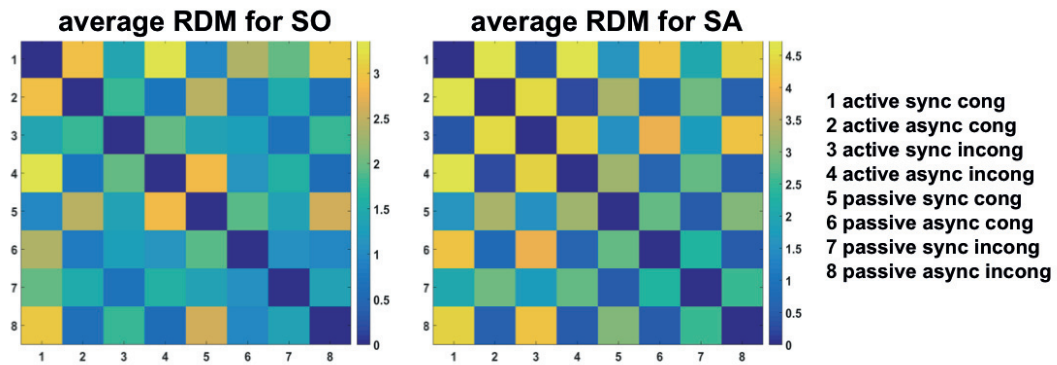Asai, T., 2016. Agency elicits body-ownership: proprioceptive drift toward a synchronously acting external proxy. Experimental Brain Research 234, 1163–1174. doi:10.1007/s00221-015-4231-y

Bekrater-Bodmann, R., Foell, J., Diers, M., Flor, H., 2012. The perceptual and neuronal stability of the rubber hand illusion across contexts and over time. Brain research 1452, 130–9. doi:10.1016/j.brainres.2012.03.001

Bekrater-Bodmann, R., Foell, J., Diers, M., Kamping, S., Rance, M., Kirsch, P., Trojan, J., Fuchs, X., Bach, F., Çakmak, H.K., Maaß, H., Flor, H., 2014. The importance of synchrony and temporal order of visual and tactile input for illusory limb ownership experiences - an FMRI study applying virtual reality. PloS one 9, e87013. doi:10.1371/journal.pone.0087013

Blanke, O., Slater, M., Serino, A., 2015. Behavioral, Neural, and Computational Principles of Bodily Self-Consciousness. Neuron. doi:10.1016/j.neuron.2015.09.029

Botvinick, M., Cohen, J.D., 1998. Rubber hand "feels" what eyes see. Nature 391, 756.

Braun, N., Thorne, J.D., Hildebrandt, H., Debener, S., 2014. Interplay of agency and ownership: The intentional binding and rubber hand illusion Paradigm Combined. PLoS ONE 9. doi:10.1371/journal.pone.0111967

Broughton, R., Wasel, N., 1990. A text-stimuli presentation manager for the IBM PC with ipsatization correction for response set and reaction times 22, 421–423.

Brozzoli, C., Gentile, G., Ehrsson, H.H., 2012. That's near my hand! Parietal and premotor coding of hand-centered space contributes to localization and self-attribution of the hand. The Journal of Neuroscience 32, 14573–82. doi:10.1523/JNEUROSCI.2660-12.2012

Caspar, E.A., Cleeremans, A., Haggard, P., 2015. The relationship between human agency and embodiment. Consciousness and Cognition 33, 226–236. doi:10.1016/j.concog.2015.01.007

Caspar, E.A., De Beir, A., Magalhaes De Saldanha Da Gama, P.A., Yernaux, F., Cleeremans, A., Vanderborght, B., 2015. New frontiers in the rubber hand experiment: When a robotic hand becomes one's own. Behavior Research 47, 744–755. doi:10.3758/s13428-014-0498-3

Cnaan, A., Laird, N.M., Slasor, P., 1997. Using the general linear mixed model to analyse unbalanced repeated measures and longitudinal data. Statistics in Medicine 16, 2349–2380. doi:10.1002/(SICI)1097-0258(19971030)16:20

Cunningham, W.H., Cunningham, I.C.M., Green, R.T., 1977. The Ipsative Process to Reduce Response Set Bias 41, 379–384.

David, N., Bewernick, B.H., Cohen, M.X., Newen, A., Lux, S., Fink, G.R., Shah, N.J., Vogeley, K., 2006. Neural representations of self versus other: visual-spatial perspective taking and agency in a virtual ball-tossing game. Journal of cognitive neuroscience 18, 898–910. doi:10.1162/jocn.2006.18.6.898

David, N., Newen, A., Vogeley, K., 2008. The "sense of agency" and its underlying cognitive and neural mechanisms. Consciousness and Cognition 17, 523–534. doi:10.1016/j.concog.2008.03.004

Dummer, T., Picot-Annand, A., Neal, T., Moore, C., 2009. Movement and the rubber hand illusion. Perception 38, 271–280. doi:10.1068/p5921

Ehrsson, H.H., Holmes, N.P., Passingham, R.E., 2005. Touching a rubber hand: feeling of body ownership is associated with activity in multisensory brain areas. The Journal of neuroscience : the official journal of the Society for Neuroscience 25, 10564–73. doi:10.1523/JNEUROSCI.0800-05.2005

Ehrsson, H.H., Spence, C., Passingham, R.E., 2004. That's my hand! Activity in premotor cortex reflects feeling of ownership of a limb. Science (New York, N.Y.) 305, 875–7. doi:10.1126/science.1097011

Farrer, C., Franck, N., Georgieff, N., Frith, C.D., Decety, J., Jeannerod, M., 2003. Modulating the experience of agency: A positron emission tomography study. NeuroImage 18, 324–333. doi:10.1016/S1053-8119(02)00041-1

Farrer, C., Frith, C.D., 2002. Experiencing oneself vs another person as being the cause of an action: The neural correlates of the experience of agency. NeuroImage 15, 596–603. doi:10.1006/nimg.2001.1009

Farrer, C., Frey, S.H., Van Horn, J.D., Tunik, E., Turk, D., Inati, S., Grafton, S.T., 2008. The angular gyrus computes action awareness representations. Cerebral Cortex 18, 254–261. doi:10.1093/cercor/bhm050

Fink, G.R., Marshall, J.C., Halligan, P.W., Frith, C.D., Driver, J., Frackowiak, R.S.J., Dolan, R.J., 1999. The neural consequences of conflict between intention and the senses. Brain 122, 497–512. doi:10.1093/brain/122.3.497

Fiorio, M., Weise, D., Önal-Hartmann, C., Zeller, D., Tinazzi, M., Classen, J., 2011. Impairment of the rubber hand illusion in focal hand dystonia. Brain 134, 1428–1437. doi:10.1093/brain/awr026

Fisher, R., 1915. Frequency distribution of the values of the correlation coefficient in samples from an indefinitely large population. Biometrika. doi:10.2307/2331838

Gassert, R., Moser, R., Burdet, E., Bleuler, H., 2006. MRI/fMRI-compatible robotic system with force feedback for interaction with human motion. IEEE/ASME Transactions on Mechatronics 11, 216–224. doi:10.1109/TMECH.2006.871897

Gentile, G., Guterstam, A., Brozzoli, C., Ehrsson, H.H., 2013. Disintegration of multisensory signals from the real hand reduces default limb self-attribution: an fMRI study. The Journal of neuroscience : the official journal of the Society for Neuroscience 33, 13350–66. doi:10.1523/JNEUROSCI.1363-13.2013

Gilaie-Dotan, S., Kanai, R., Bahrami, B., Rees, G., Saygin, A.P., 2013. Neuroanatomical correlates of biological motion detection. Neuropsychologia 51, 457–463. doi:10.1016/j.neuropsychologia.2012.11.027

Grossman, E., Donnelly, M., Price, R., Pickens, D., Morgan, V., Neighbor, G., Blake, R., 2000. Brain areas involved in perception of biological motion. Journal of cognitive neuroscience 12, 711–20. doi:10.1162/089892900562417

Guterstam, A., Gentile, G., Ehrsson, H.H., 2013. The invisible hand illusion: multisensory integration leads to the embodiment of a discrete volume of empty space. Journal of cognitive neuroscience 25, 1078–99. doi:10.1162/jocn_a_00393

Haggard, P., Chambon, V., 2012. Sense of agency. Current Biology. doi:10.1016/j.cub.2012.02.040

Hara, M., Pozeg, P., Rognini, G., Higuchi, T., Fukuhara, K., Yamamoto, A., Higuchi, T., Blanke, O., Salomon, R., 2015. Voluntary self-touch increases body ownership. Frontiers in Psychology 6, 1509. doi:10.3389/fpsyg.2015.01509

Holle, H., McLatchie, N., Maurer, S., Ward, J., 2011. Proprioceptive Drift without Illusions of Ownership for Rotated Hands in the "Rubber Hand Illusion" Paradigm. Cognitive Neuroscience 2, 37–41. doi:10.1080/17588928.2011.603828

Imaizumi, S., Asai, T., 2015. Dissociation of agency and body ownership following visuomotor temporal recalibration. Frontiers in integrative neuroscience 9, 35. doi:10.3389/fnint.2015.00035

Ismail, M.A.F., Shimada, S., 2016. "Robot" hand illusion under delayed visual feedback: Relationship between the senses of ownership and agency. PLoS ONE 11. doi:10.1371/journal.pone.0159619

Jenkinson, P.M., Preston, C., 2015. New reflections on agency and body ownership: The moving rubber hand illusion in the mirror. Consciousness and Cognition 33, 432–442. doi:10.1016/j.concog.2015.02.020

Kalckert, A., Ehrsson, H.H., 2012. Moving a Rubber Hand that Feels Like Your Own: A Dissociation of Ownership and Agency. Frontiers in human neuroscience 6, 40. doi:10.3389/fnhum.2012.00040

Kalckert, A., Ehrsson, H.H., 2014. The moving rubber hand illusion revisited: comparing movements and visuotactile stimulation to induce illusory ownership. Consciousness and cognition 26, 117–32. doi:10.1016/j.concog.2014.02.003

Kriegeskorte, N., Goebel, R., Bandettini, P., 2006. Information-based functional brain mapping. Proceedings of the National Academy of Sciences of the United States of America 103, 3863–3868. doi:10.1073/pnas.0600244103

Kriegeskorte, N., Mur, M., Bandettini, P. a., 2008. Representational similarity analysis – connecting the branches of systems neuroscience. frontiers in systems neuroscience 2, 1–28. doi:10.3389/neuro.06.004.2008

Kühn, S., Brass, M., Haggard, P., 2013. Feeling in control: Neural correlates of experience of agency. Cortex 49, 1935–1942. doi:10.1016/j.cortex.2012.09.002

Lee, W., Reeve, J., 2013. Self-determined, but not non-self-determined, motivation predicts activations in the anterior insular cortex: An fMRI study of personal agency. Social Cognitive and Affective Neuroscience 8, 538–545. doi:10.1093/scan/nss029

Leube, D.T., Knoblich, G., Erb, M., Grodd, W., Bartels, M., Kircher, T.T.J., 2003. The neural correlates of perceiving one's own movements. NeuroImage 20, 2084–2090. doi:10.1016/j.neuroimage.2003.07.033

Limanowski, J., Blankenburg, F., 2016. That's not quite me: limb ownership encoding in the brain. Social Cognitive and Affective Neuroscience nsv079. doi:10.1093/scan/nsv079

Limanowski, J., Blankenburg, F., 2015. Network activity underlying the illusory self-attribution of a dummy arm. Human Brain Mapping 36, 2284–2304. doi:10.1002/hbm.22770

Limanowski, J., Lutti, A., Blankenburg, F., 2014. The extrastriate body area is involved in illusory limb ownership. NeuroImage 86, 514–524. doi:10.1016/j.neuroimage.2013.10.035

Ma, K., Hommel, B., 2013. The virtual-hand illusion: Effects of impact and threat on perceived ownership and affective resonance. Frontiers in Psychology 4. doi:10.3389/fpsyg.2013.00604

Ma, K., Hommel, B., 2015. Body-ownership for actively operated non-corporeal objects. Consciousness and Cognition 36, 75–86. doi:10.1016/j.concog.2015.06.003

Ma, K., Hommel, B., 2015. The role of agency for perceived ownership in the virtual hand illusion. Consciousness and Cognition 36, 277–288. doi:10.1016/j.concog.2015.07.008

Maus, G.W., Fischer, J., Whitney, D., 2013. Motion-dependent representation of space in area MT+. Neuron 78, 554–562. doi:10.1016/j.neuron.2013.03.010

Miele, D.B., Wager, T.D., Mitchell, J.P., Metcalfe, J., 2011. Dissociating neural correlates of action monitoring and metacognition of agency. Journal of cognitive neuroscience 23, 3620–36. doi:10.1162/jocn_a_00052

Padilla-Castañeda, M.A., Frisoli, A., Pabon, S., Bergamasco, M., 2014. The Modulation of Ownership and Agency in the Virtual Hand Illusion under Visuotactile and Visuomotor Sensory Feedback. Presence: Teleoperators and Virtual Environments 23, 209–225. doi:10.1162/PRES_a_00181

Park, H.-D., Bernasconi, F., Bello-Ruiz, J., Pfeiffer, C., Salomon, R., Blanke, O., 2016. Transient Modulations of Neural Responses to Heartbeats Covary with Bodily Self-Consciousness. Journal of Neuroscience 36, 8453–8460. doi:10.1523/JNEUROSCI.0311-16.2016

Park, H.-D., Tallon-Baudry, C., 2014. The neural subjective frame: from bodily signals to perceptual consciousness. Philosophical transactions of the Royal Society of London 369, 20130208. doi:10.1098/rstb.2013.0208

Peelen, M. V., Caramazza, A., 2012. Conceptual object representations in human anterior temporal cortex. The Journal of neuroscience 32, 15728–36. doi:10.1523/JNEUROSCI.1953-12.2012

Perez-Marcos, D., Sanchez-Vives, M. V, Slater, M., 2012. Is my hand connected to my body? The impact of body continuity and arm alignment on the virtual hand illusion. Cognitive Neurodynamics 6, 295–305. doi:10.1007/s11571-011-9178-5

Perez-Marcos, D., Slater, M., Sanchez-Vives, M. V, 2009. Inducing a virtual hand ownership illusion through a brain-computer interface. Neuroreport 20, 589–594. doi:10.1097/WNR.0b013e32832a0a2a

Petkova, V.I., Bjo, M., Gentile, G., Jonsson, T., Li, T.Q., Ehrsson, H.H., Björnsdotter, M., Gentile, G., Jonsson, T., Li, T.Q., Ehrsson, H.H., 2011. From part- to whole-body ownership in the multisensory brain. Current Biology 21, 1118–1122. doi:10.1016/j.cub.2011.05.022

Renes, R.A., van Haren, N.E.M., Aarts, H., Vink, M., 2015. An exploratory fMRI study into inferences of self-agency. Social cognitive and affective neuroscience 10, 708–712. doi:10.1093/scan/nsu106

Riemer, M., Bublatzky, F., Trojan, J., Alpers, G.W., 2015. Defensive activation during the rubber hand illusion: Ownership versus proprioceptive drift. Biological Psychology 109, 86–92. doi:10.1016/j.biopsycho.2015.04.011

Rohde, M., Luca, M. Di, Ernst, M.O., Greenlee, M.W., Di Luca, M., 2011. The Rubber Hand Illusion: feeling of ownership and proprioceptive drift do not go hand in hand. PLoS ONE 6, e21659. doi:10.1371/journal.pone.0021659

Sanchez-Vives, M. V., Spanlang, B., Frisoli, A., Bergamasco, M., Slater, M., 2010. Virtual Hand Illusion Induced by Visuomotor Correlations. PLoS ONE 5, e10381. doi:10.1371/journal.pone.0010381

Schwabe, L., Blanke, O., 2007. Cognitive neuroscience of ownership and agency. Consciousness and cognition 16, 661–6. doi:10.1016/j.concog.2007.07.007

Servos, P., Osu, R., Santi, A., Kawato, M., 2002. The neural substrates of biological motion perception: an fMRI study. Cerebral cortex (New York, N.Y. : 1991) 12, 772–782. doi:10.1093/cercor/12.7.772

Shibuya, S., Unenaka, S., Ohki, Y., 2016. Body ownership and agency: task-dependent effects of the virtual hand illusion on proprioceptive drift. Experimental Brain Research epub. doi:10.1007/s00221-016-4777-3

Simmons, W.K., Barsalou, L.W., 2003. The similarity-in-topography principle: reconciling theories of conceptual deficits. Cognitive neuropsychology 20, 451–486. doi:10.1080/02643290342000032

Slater, M., Perez-Marcos, D., Ehrsson, H.H., Sanchez-Vives, M. V, 2008. Towards a digital body: the virtual arm illusion. Frontiers in human neuroscience 2, 6. doi:10.3389/neuro.09.006.2008

Sugiura, M., Miyauchi, C.M., Kotozaki, Y., Akimoto, Y., Nozawa, T., Yomogida, Y., Hanawa, S., Yamamoto, Y., Sakuma, A., Nakagawa, S., Kawashima, R., 2015. Neural mechanism for mirrored self-face recognition. Cerebral Cortex 25, 2806–2814. doi:10.1093/cercor/bhu077

Sulzer, J., Duenas, J., Stampili, P., Hepp-Reymond, M.C., Kollias, S., Seifritz, E., Gassert, R., 2013. Delineating the whole brain BOLD response to passive movement kinematics, in: IEEE International Conference on Rehabilitation Robotics. IEEE, pp. 1–5. doi:10.1109/ICORR.2013.6650474

Tootell, R.B.H., Reppas, J., Kwong, K., Malach, R., Born, R., Brady, T., Rosen, B., Belliveau, J., 1995. Functional analysis of human MT and related visual cortical areas using magnetic resonance imaging. Journal of Neuroscience 15, 3215–3230.

Tsakiris, M., Hesse, M.D., Boy, C., Haggard, P., Fink, G.R., 2007. Neural signatures of body ownership: A sensory network for bodily self-consciousness. Cerebral Cortex 17, 2235–2244. doi:10.1093/cercor/bhl131

Tsakiris, M., Longo, M.R., Haggard, P., 2010. Having a body versus moving your body: neural signatures of agency and body-ownership. Neuropsychologia 48, 2740–9. doi:10.1016/j.neuropsychologia.2010.05.021

Tsakiris, M., Prabhu, G., Haggard, P., 2006. Having a body versus moving your body : How agency structures body-ownership 15, 423–432. doi:10.1016/j.concog.2005.09.004

Tsakiris, M., Schütz-Bosbach, S., Gallagher, S., 2007. On agency and body-ownership: phenomenological and neurocognitive reflections. Consciousness and cognition 16, 645–60. doi:10.1016/j.concog.2007.05.012

Vander Wyk, B.C., Voos, A., Pelphrey, K.A., 2012. Action representation in the superior temporal sulcus in children and adults: An fMRI study. Developmental Cognitive Neuroscience 2, 409–416. doi:10.1016/j.dcn.2012.04.004

Yomogida, Y., Sugiura, M., Sassa, Y., Wakusawa, K., Sekiguchi, A., Fukushima, A., Takeuchi, H., Horie, K., Sato, S., Kawashima, R., 2010. The neural basis of agency: An fMRI study. NeuroImage 50, 198–207. doi:10.1016/j.neuroimage.2009.12.054

Zhang, J., Ma, K., Hommel, B., 2015. The virtual hand illusion is moderated by context-induced spatial reference frames. Frontiers in Psychology 6, 1659. doi:10.3389/fpsyg.2015.01659

6 - General Discussion

6.1 Summary of scientific contributions

The present thesis provided important findings regarding the organization of brain areas processing bodily information. In particular, I proposed a series of fMRI experiments investigating the brain representations of body parts such as hands, feet and legs both at the level of primary somatosensory and motor representations and at the level of higher-tier body representations.

First, I extended previous 7T fMRI results regarding the non-invasive mapping of body parts representations within primary somatosensory areas. Previous research strongly focused on hand and finger representations (**Martuzzi et al. 2014, 2015; Sanchez-Panchuelo et al. 2010, 2012, 2014; Stringer et al. 2011, 2014**), thus neglecting other body parts such as feet and legs. I mapped the somatosensory representations of big toe, small toe, heel, calf, thigh and hip within 3 subregions of S1 bilaterally. I highlighted the somatotopic organization of leg representations, the importance of big toe representations and a lack of stimulus-driven interactions between feet and legs representations. This study complements previous 7T fMRI research about primary somatosensory representations and shows that high-resolution fMRI is a promising tool to further study somatosensory representations associated with small neuronal populations, such as the legs or the trunk. Importantly, this study shows that somatosensory representations of lower limbs within subregions of S1 can be retrieved in individual subjects. Such individualized approaches are important to understand the link between the functional specialization of somatosensory representations and the respective behavioral functions of different body parts such as hands, feet and legs. In addition, these results might have implications for studies investigating plasticity in lower limb representations following different experimental manipulations (**Abrahamse et al. 2009; Godde et al. 1996**), as well as for clinical research focusing on pathologies affecting the lower limbs, such as amputation, vascular disease or spinal cord injury (**Freund et al. 2013; Henderson et al. 2014**).

Second, I used 7T fMRI and resting-state functional connectivity (rs-FC) to investigate the functional interactions between body representations within subregions of S1. Similar investigations have been carried out in non-human primates for finger

representations (**Ashaber et al. 2014; Chen et al. 2011; Wang et al. 2013**). Here, I extend this research to study the rs-FC across multiple S1 representations of 24 body parts in humans including hands, feet and legs. The data suggested a functional segregation between hand and lower limb representations. In addition, I showed that patterns of rs-FC reflected interhemispheric, interareal and intersomatic interactions, which differed across hands, feet and legs. This study shows that within the large-scale functional network, termed the "sensorimotor" network (**Beckman et al. 2005**), there are smaller short-scale networks corresponding to functional clusters formed by the representations of different body parts. In particular, these data suggest the presence of fundamental differences with respect to the finely tuned functional organization of S1 cortices across hand, foot and leg representations, which could be linked to their behavioral role in everyday activities.

Third, I studied cortical plasticity associated with the use of a neuroprosthetic arm in primary somatosensory and motor cortices. After targeted muscle and sensory reinnervation (TMSR), patients use phantom movements of their missing limb to control a robotic device and have a precise map of referred touch on the reinnervated skin to induce phantom sensations. Unlike normal amputees, TMSR patients recruit the motor representations of the missing limb in a functionally relevant manner and can experience precise phantom sensations controlled by touch. I applied and extended the previously presented methods to investigate whether the TMSR procedure is associated with preserved somatosensory and motor representations. I showed that motor representations of the missing limb in TMSR were very similar to healthy participants, and that somatosensory representations of the missing limb had no trace of topographical reorganization as observed in normal amputees. In addition, I showed that although the local rs-FC between somatosensory and motor representations was intact, interactions between primary and parietal multisensory areas were impaired. These results demonstrate that the repetitive and functionally relevant recruitment of sensorimotor representations of a missing limb have the potential to reduce abnormal reorganization and support the importance of a closed-loop between motor commands and sensory feedback. Importantly, these data support the major role of inputs from different body regions during activities of daily living for the establishment and persistence of body maps in somatosensory and motor areas (**Buonomano et al. 1998; Serino and Haggard 2010**).

Finally, I studied more integrated forms of body representations, such as the sense of hand ownership (SO) and the sense of hand agency (SA). Using a novel MR-compatible system and modern neuroimaging methods, I identified brain regions associated with subjective changes of SO and SA. I replicated and extended previous results by showing the implication of parietal, frontal, temporal, insular, cingulate and cerebellar areas. I showed that SO and SA are associated with partially overlapping, but distinct brain networks. In particular, I highlighted the greater contributions of insular and cingulate areas for SO compared to SA and the greater contributions of sensorimotor and posterior parietal areas for SA compared to SO. Importantly, I emphasized the contribution of temporal posterior and anterior areas for both SO and SA, so far quite neglected in the literature. In addition, I showed that during the alteration of SO and SA, the activity in primary somatosensory and motor areas is modulated by visual factors (see Annexes). This suggests top-down modulations in S1 and M1 from upstream areas and extends the implication of primary sensorimotor cortices in BSC. This technically challenging study shows that controlled and repeatable multisensory stimulation is able to quasi- parametrically alter different components of BSC. This achievement allowed considering inter-subject and intra-subject variability to identify brain regions in which multivoxel BOLD patterns co-varied with subjective reports of SO and SA. In addition, this study establishes the first step towards the thorough mapping and comparison of brain networks associated with distinct components of BSC.

Collectively, the presented neuroimaging studies demonstrated the non-invasive mapping and characterization of the functional organization of primary somatosensory and motor representations in individual subjects using ultra high-field 7T fMRI. These methods were applied to study the relationship between sensorimotor training and cortical plasticity in a rare population of amputees (TMSR). The proposed individualized approaches will enable future research to investigate how inter-subject differences in brain organization relate to individual perceptual and cognitive functions. In addition, the mapping methods demonstrated for primary somatosensory representations could be extended towards higher-tier body representations to investigate the functional organization of networks involved in BSC. The present work also establishes a first step towards this goal.

6.2 Comparison between visual and somatosensory systems

The visual system is one of the most well studied systems of the human brain. Using fMRI, the hierarchy and retinotopic organization of visual occipital areas has been thoroughly described up to the level of cortical columns (**Grill-Spector and Malach, 2004; Yacoub et al. 2008**). In addition, the organization of specialized visual areas is also well understood, as for example the areas specialized in the visual recognition of faces or specific categories of objects (**Grill-Spector and Malach, 2004**). These aspects are still poorly understood for other sensory modalities, in particular for the somatosensory system despite its importance for bodily processing. Until recently, most studies still considered the multiple and distinct somatosensory and motor representations as a unique sensorimotor representation.

It remains unknown to which extent the visual and somatosensory systems share common organizational principles. For example, cortical magnification in the visual system as a function of eccentricity is a well-known principle (with hugely enlarged cortical representations for the fovea) (**Tootell et al. 1982, 1988**). Visual cortical magnification has been parametrically characterized showing that it decreases monotonically with increased eccentricity in several occipital visual areas (**Harvey and Dumoulin, 2011**). For the somatosensory system, cortical magnification is more complicated. A broad description of cortical magnification in S1 was proposed in the work of Penfield and Rasmussen (**1947**). They showed that the hands and the face have larger somatosensory representations, while other body representations such as the legs and the trunk are smaller. More recently, 7T fMRI research focusing on somatosensory representations of fingers suggested a cortical magnification of thumb representation compared to other fingers consistently across BAs 3b, 1 and 2 of S1 (**Martuzzi et al. 2014**), and the present work showed a similar result for big toe representation compared to small toe representation (study 1, Fig.2.4). This suggests a homology between hand and foot representation, which is observed across individuals. In addition, observing consistent differences in cortical size between representations of very similar body parts such as 2 fingers or 2 toes suggests the presence of a fine pattern of cortical magnification common to most individuals. There seems to be a canonical functional layout of body maps in S1, but it remains unknown whether this is genetically programmed or whether this common functional

organization could be the result of cortical plasticity induced by very similar daily life somatosensory stimulation. More importantly, inter-subject differences between individual S1 maps are observed and remain unexplained. Further studies investigating the possible functional link between inter-individual differences at the level of S1 maps and at the level of behavioral performance are necessary. For example, the thorough comparison of somatosensory representations of 5 fingers and 5 toes between right and left handers has never been conducted and could potentially offer answers with respect to the respective specialization of these body parts.

An important distinction between the visual and somatosensory system is the structure of their representational space. Visual space is linearly structured and natural stimulation follows spatial rules of proximity. The somatosensory space is dynamic and 2 cortically distant representations such as right and left hands can often be stimulated together as during bimanual exploration for example. In addition, the function of different portions of the visual field remains very similar, while different body parts might need to preferentially process different features of touch to achieve their respective functions. As a result, the functional coupling (rs-FC) across body parts representations, as shown in the present work (study II), is more complex than the linear and spatial coupling of segments of the visual space. Indeed, it was shown that rs-FC across early visual areas also reflects interhemispheric, interareal and iso-eccentric (across close retinotopic locations) interactions, similarly to what was proposed in the present work for somatosensory areas (**Raemaekers et al. 2014**). However, iso-eccentric interactions followed regular radial and tangential patterns. Contrastingly, the present results showed that rs-FC across subregions of S1 reflected the functional grouping of different body parts rather than following a strict rule of proximity (study II, Fig.3.3). This suggests that future research could potentially rely on the fine patterns of rs-FC across primary somatosensory areas to identify body part specific portions of S1.

Finally, the distinction between different features processed in primary somatosensory areas and how they are represented in S1 need to be further investigated. Although recent progress has been made in the understanding of neuronal encoding of touch (**Graczyk et al. 2016; Pack and Bensmaia, 2015; Saal et al. 2015; Weber et al. 2013**), other important features of S1 such as temperature,

pain and proprioception are less studied. In addition, how the maps of different features are arranged in human S1 is also unknown, although the columnar organization of somatosensory areas has been suggested by work in non-human primates (**Chen et al. 2001; Friedman et al. 2004**).

6.3 Studying higher-tier body representations

Behavioral and neuroimaging studies investigating altered states of BSC showed that its different components (body ownership for body parts, agency for bodily actions, self-identification with the full-body and self-location in space) share many common properties. Indeed, components of BSC rely on and can be manipulated by similar types of multisensory signals. Depending on the type of multisensory stimulations and where they are delivered, different components of BSC can be specifically targeted (**Blanke et al. 2015**). Moreover, studies focusing on different components of BSC consistently report the implications of often overlapping fronto-parietal and temporo-parietal areas, suggesting that these mechanisms share common neuronal substrates (**Ehrsson et al. 2004, 2005; Ionta et al. 2011; Petkova et al. 2011; Serino et al. 2011; Tsakiris et al. 2008, 2010**, and the present work, study IV, Fig.5.3).

Inducing altered states of BSC is technically challenging (especially in MR-environment), and most studies are limited to the investigation of isolated components of BSC. For this reason, the functional organization of BSC networks is not well understood. For example, the presence of body maps in primary somatosensory and multisensory areas involved in BSC (**Hong et al. 2011; Huang et al. 2012; Kiss et al. 1994; Saadon-Grosman et al. 2015; Sereno and Huang, 2014; Zeharia et al. 2015**) could suggest that BSC components, such as body part ownership, are also organized into body maps. Recent studies provided evidence for body part specific processes in premotor and posterior parietal cortex, and a body gradient between hands and trunk in parietal cortex (**Gentile et al. 2015; Petkova et al. 2011**), but strong evidence of the presence of a body map for body ownership is still missing. Further studies focusing on the direct comparison of BSC components for different body parts such as hands, legs, face and trunk are required. Second, an important distinction has been made between partial aspects of BSC for body parts, such as hand ownership and hand agency, and global aspects of BSC for the full-body and the self,

such as self-identification and self-location, which might rely on different mechanisms (**Blanke et al. 2015**). What is the link between partial and global aspects of BSC? Does global BSC rely on the integration of partial aspects of BSC or do they correspond to distinct processes? This is still debated and undemonstrated (**Blanke et al. 2015, Gentille et al. 2015**). Third, how are organized the different networks underlying the distinct components of BSC and to which extent do they overlap? Neuroimaging studies directly comparing different components of BSC are rare and often limited to the comparison between few BSC components (**Guterstam et al. 2015; Tsakiris et al. 2010** and present work, study IV). Additional fMRI research is needed to describe in details the functional organization of brain networks underlying the multiple components of BSC.

6.4 Future research goals

Beyond improving our understanding of primary and higher-tier body representations, we need to investigate their combined mechanisms. The implication of primary sensory areas in higher cognitive functions has been proposed for V1 (**Muckli, 2010**), and the present work suggested top-down modulations in S1. Future neuroimaging studies should combine unisensory and multisensory mapping approaches with the alteration of BSC for multiple body parts. This would allow investigating whether body part specific modulations are found in S1 or M1 and would highlight the presence of body maps for components of BSC. Furthermore, functional and structural connectivity measures between body part specific areas in unisensory and multisensory areas could be informative about the functional organization of BSC networks.

More importantly, the computational mechanisms underlying the processing of bodily information from primary areas to multisensory areas involved in BSC are unknown. Research focusing on modeling approaches is still poorly explored in this field.

6.5 Clinical considerations

Recent major advances have been made in research for sensory prostheses and bidirectional neuroprosthetics (**Bensmaia, 2015; Bensmaia and Miller, 2014; Graczyk et al. 2016; Hebert et al. 2014; Raspopovic et al. 2014**). The

understanding of BSC mechanisms can potentially have major applications for the fields of rehabilitation and limb replacement to create neuroprosthetic limbs that move and feel like real limbs. Possible therapies based on BSC alteration can be considered in order to incorporate artificial limbs into the representation of the body in the brain.

Beyond the replacement of limbs, this research could also lead to applications in human-machine interactions and enhancement of human capabilities. It remains unknown whether the brain is capable of representing extra-numerous effectors such as a third arm or a drone. Tools are represented in the brain to be manipulated mostly by our hands, but what would be the possibilities if tools were directly interfaced with the nervous system to be felt and controlled as real limbs.

Although it seems closer to fiction than reality, it is possible that the tools necessary to conduct this research will be available earlier than can be expected. The advances of the industry of video games and virtual reality might propose in a near future the technology required to investigate in detail the features, the parameters, and the mechanisms involved in BSC. Systems interfacing with multiple senses of users and providing fully immersive experiences are being currently developed and will become major tools for researchers.

Finally, the establishment of mapping methods identifying multiscale body representations in individual subject could become an important tool to monitor short-term and long-term plasticity in areas processing bodily information. These methods could become clinical tools to assess the effects on bodily networks of various rehabilitative therapies associated with clinical conditions such as amputation, spinal cord injury, stroke and many others.

7 - Annexes

7.1 Top-down modulations in primary somatosensory and motor areas

I present here an additional analysis conducted with the data from study IV (see study IV of the thesis). In this fMRI study, we manipulated three experimental factors to modulate our participant's senses of hand ownership and of hand agency towards a virtual hand. The following factors were manipulated: the "movement type" produced (active or passive), the "synchrony" between the movements of the participant's hand and of the virtual hand, and the "congruency" between the moving hand of participants (right hand) and the moving virtual hand (right or left hand). Using these data, I conducted a Region of Interest (ROI) analysis within primary somatosensory (S1) and motor (M1) areas.

First, I used published cytoarchitectonic probabilistic maps to separate S1 and M1 into 6 ROIs corresponding to BAs 3a, 3b, 1 and 2 for S1, and to BAs 4a and 4p for M1 (**Geyer et al. 1996, 1997, 1999; Grefkes et al. 2001**). This analysis was conducted in both hemispheres (contralateral and ipsilateral with respect to the participant's moving hand). Within the different BAs, I extracted the mean BOLD activity (betas estimates of the GLM) associated with each of the 8 experimental conditions (Fig.7.1). Using 3-way repeated measures ANOVAs, I analyzed whether BOLD activity was modulated by our experimental factors in the considered BAs. I expected that the factor of "movement type", whose manipulation directly affects the signals processed in S1 and M1, would modulate the BOLD activity. However, I wonderer whether the factors of "synchrony" and "congruency", whose manipulation also relies on visual processing, would also be associated with changes in BOLD activity.

The statistical analysis is summarized in Tab.7.1. In the contralateral hemisphere, there was a main effect of "movement type" in all BAs. In addition, there was a main effect of "synchrony" in all BAs, except in BA 4a. In the ipsilateral hemisphere, there was a main effect of "movement type" in all BAs, except in BA 4a. Furthermore, there was also a main effect of "synchrony" in BAs 1 and 2.
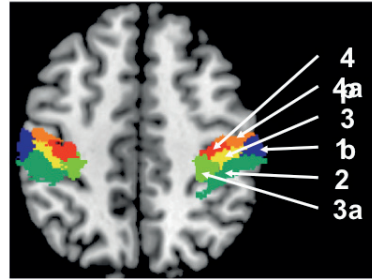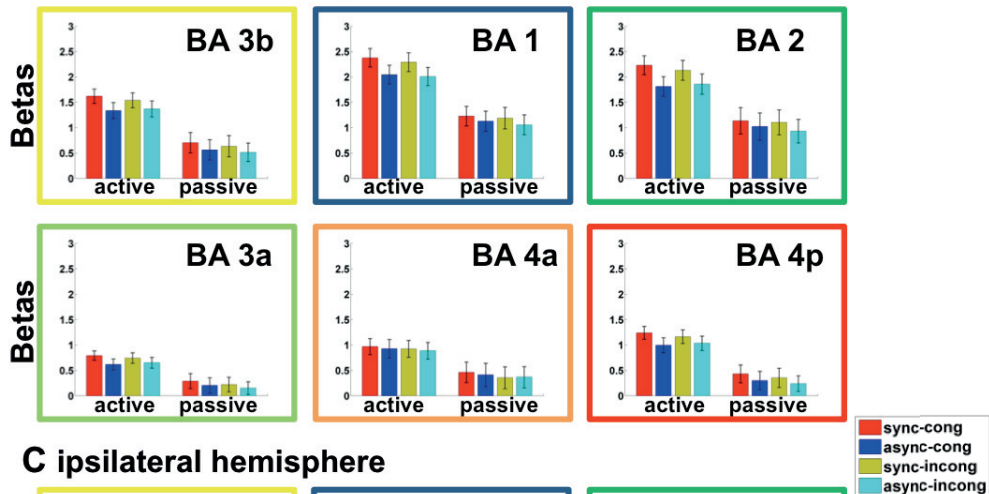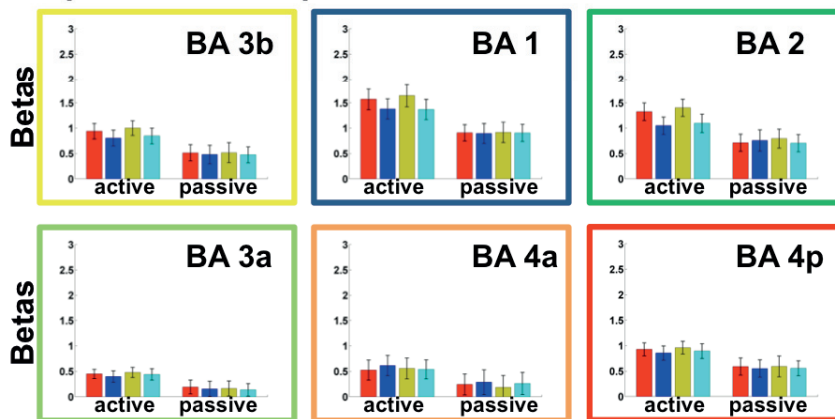
Fig.7.1 Top-down modulations in primary somatosensory and motor areas. A) Primary somatosensory and motor cortices were divided into BAs 3b, 1, 2, 3a, 4a, 4p. **B)** The BOLD activity (betas estimates) associated with the 8 experimental conditions are shown in the bar plots for each BA. Conditions are grouped into active and passive conditions. In addition, synchronous and congruent conditions are shown in red, asynchronous and congruent conditions are shown in blue, synchronous and incongruent conditions are shown in yellow, asynchronous and incongruent conditions are shown in cyan. Statistical results concerning the betas estimates are shown in Tab.7.1.

As expected, these results show that the factor of "movement type" modulated BOLD activity in all BAs of both hemispheres (except for BA 4a in the right hemisphere). In addition, our analysis shows that several BAs were also modulated by

A

	3a		3b		1		2		4a		4p	
	F-statistic	p-value	F-statistic	p-value	F-statistic	p-value	F-statistic	p-value	F-statistic	p-value	F-statistic	p-value
AP	24.585	<0.0001	40.205	<0.0001	29.954	<0.0001	27.899	<0.0001	11.688	0.002	36.005	<0.0001
SYNC	4.812	0.039	9.251	0.006	9.999	0.004	7.291	0.013	0.095	n.s.	7.183	0.014
CONG	0.956	n.s.	1.398	n.s.	2.538	n.s.	1.156	n.s.	1.600	n.s.	1.215	n.s.
AP*SYNC	0.856	n.s.	1.144	n.s.	3.619	n.s.	3.229	n.s.	0.041	n.s.	0.812	n.s.
AP*CONG	0.466	n.s.	0.121	n.s.	0.003	n.s.	0.051	n.s.	0.079	n.s.	0.321	n.s.
SYNC*CONG	0.522	n.s.	0.476	n.s.	0.005	n.s.	0.117	n.s.	0.074	n.s.	0.542	n.s.
AP*SYNC*CONG	0.261	n.s.	0.385	n.s.	0.216	n.s.	1.351	n.s.	0.045	n.s.	0.391	n.s.

contralateral hemisphere

B

	3a		3b		1		2		4a		4p	
	F-statistic	p-value	F-statistic	p-value	F-statistic	p-value	F-statistic	p-value	F-statistic	p-value	F-statistic	p-value
AP	6.384	0.019	8.466	0.008	10.966	0.003	8.041	0.009	3.491	n.s.	8.242	0.009
SYNC	0.466	n.s.	2.225	n.s.	4.648	0.042	5.558	0.028	0.175	n.s.	0.631	n.s.
CONG	0.023	n.s.	0.434	n.s.	0.203	n.s.	0.791	n.s.	0.375	n.s.	0.230	n.s.
AP*SYNC	0.042	n.s.	1.134	n.s.	0.027	n.s.	6.036	0.022	0.041	n.s.	0.095	n.s.
AP*CONG	0.492	n.s.	0.273	n.s.	3.784	n.s.	0.163	n.s.	0.025	n.s.	0.108	n.s.
SYNC*CONG	0.023	n.s.	0.021	n.s.	0.143	n.s.	0.702	n.s.	0.075	n.s.	0.002	n.s.
AP*SYNC*CONG	0.001	n.s.	0.008	n.s.	0.341	n.s.	0.329	n.s.	0.242	n.s.	0.001	n.s.

ipsilateral hemisphere

Tab.7.1 Statistical analysis of BOLD activity in primary somatosensory and motor areas. Beta estimates were analyzed using repeated-measures ANOVA with « movement type » (active or passive movements of the participant, AP), « synchrony » (synchronous or asynchronous movements of the virtual hand with respect to the participant's hand, SYNC) and « congruency » (congruent or incongruent virtual hand moving with respect to participant's hand, CONG) as within subjects factors. Significant effects are highlitghed in red. BAs in the contralateral hemisphere are shown in **A** and BAs in the ipsilateral hemisphere are shown in **B**.

the factor of "synchrony" (preferentially in the contralateral hemisphere). Detecting the synchrony between felt and seen movements requires the integration of multisensory information. Therefore our result shows that subregions of S1 and M1 receive top-down modulations from upstream areas. Our data also suggest that this effect is stronger in the contralateral hemisphere compared to the ipsilateral hemisphere. We note that this analysis was carried-out without considering the somatotopic organization of S1 and M1. It would be interesting to investigate whether this effect is body part specific or whether this effect is global across body representations.

7.2 Additional contributions

I am also involved in three additional ongoing studies. First, I am investigating cortical reorganization of somatosensory representations after lower limb amputation. I am applying the methods developed during my thesis to identify in patients the somatosensory representations of the healthy and amputated lower limbs, in particular of the most distal part of the residual limb. The topography, extent and strength of activations associated with the stimulation of the residual limb will be used to assess the extent of cortical reorganization, how it might differ across BAs and how it could relate to phantom sensations of the missing limb. Second, I am conducting a case study about an extremely rare case of polydactylism. A 7T fMRI somatosensory and motor mapping procedure was conducted with a subject having 6 fully functional fingers on each hand. I am investigating the relationship between the representations of the 6th finger within primary somatosensory and motor areas and the functional characteristics of the 6th finger in various sensory and motor tasks in this individual. Finally, I am also collaborating in a 7T fMRI study investigating the neural correlates of the peripersonal space (PPS) of the face. PPS is the multisensory space immediately surrounding the body and has been proposed as a key mechanism for BSC. I will also be involved in a series of fMRI studies currently in development focusing on the direct comparison of brain correlates of distinct BSC components for multiple body parts, such as hands, face and trunk.

8 - References

Abrahamse, E.L., Van Der Lubbe, R.H.J., Verwey, W.B., 2009. Sensory information in perceptual-motor sequence learning: Visual and/or tactile stimuli. Experimental Brain Research 197, 175–183. doi:10.1007/s00221-009-1903-5

Asai, T., 2016. Agency elicits body-ownership: proprioceptive drift toward a synchronously acting external proxy. Experimental Brain Research 234, 1163–1174. doi:10.1007/s00221-015-4231-y

Ashaber, M., Pálfi, E., Friedman, R.M., Palmer, C., Jákli, B., Chen, L.M., Kántor, O., Roe, A.W., Négyessy, L., 2014. Connectivity of somatosensory cortical area 1 forms an anatomical substrate for the emergence of multifinger receptive fields and complex feature selectivity in the squirrel monkey (Saimiri sciureus). Journal of Comparative Neurology 522, 1769–1785. doi:10.1002/cne.23499

Aspell, J.E., Heydrich, L., Marillier, G., Lavanchy, T., Herbelin, B., Blanke, O., 2013. Turning Body and Self Inside Out: Visualized Heartbeats Alter Bodily Self-Consciousness and Tactile Perception. Psychological Science 24, 2445–2453. doi:10.1177/0956797613498395

Beckmann, C.F., DeLuca, M., Devlin, J.T., Smith, S.M., 2005. Investigations into resting-state connectivity using independent component analysis. Philosophical Transactions of the Royal Society of London. Series B: Biological Sciences 360, 1001–1013. doi:10.1098/rstb.2005.1634

Bekrater-Bodmann, R., Foell, J., Diers, M., Flor, H., 2012. The perceptual and neuronal stability of the rubber hand illusion across contexts and over time. Brain Research 1452, 130–139. doi:10.1016/j.brainres.2012.03.001

Bekrater-Bodmann, R., Foell, J., Diers, M., Kamping, S., Rance, M., Kirsch, P., Trojan, J., Fuchs, X., Bach, F., Çakmak, H.K., Maaß, H., Flor, H., 2014. The importance of synchrony and temporal order of visual and tactile input for illusory limb ownership experiences - An fMRI study applying virtual reality. PLoS ONE 9, e87013. doi:10.1371/journal.pone.0087013

Bensmaia, S.J., 2015. Biological and bionic hands : natural neural coding and artificial perception. Philosophical Transactions Royal Society, B 370, 20140209. doi:10.1098/rstb.2014.0209

Bensmaia, S.J., Miller, L.E., 2014. Restoring sensorimotor function through intracortical interfaces: progress and looming challenges. Nature Reviews Neuroscience 15, 313–325. doi:10.1038/nrn3724

Biran, I., Chatterjee, A., 2004. Alien Hand Syndrome. Archives of Neurology 61, 292. doi:10.1001/archneur.61.2.292

Biswal, B., Zerrin Yetkin, F., Haughton, V.M., Hyde, J.S., 1995. Functional connectivity in the motor cortex of resting human brain using echo-planar mri. Magnetic Resonance in Medicine 34, 537–541. doi:10.1002/mrm.1910340409

Blanke, O., 2012. Multisensory brain mechanisms of bodily self-consciousness. Nature reviews. Neuroscience 13, 556–71. doi:10.1038/nrn3292

Blanke, O., Landis, T., Spinelli, L., Seeck, M., 2004. Out-of-body experience and autoscopy of neurological origin. Brain. doi:10.1093/brain/awh040

Blanke, O., Metzinger, T., 2009. Full-body illusions and minimal phenomenal selfhood. Trends in Cognitive Sciences 13, 7–13. doi:10.1016/j.tics.2008.10.003

Blanke, O., Slater, M., Serino, A., 2015. Behavioral, Neural, and Computational Principles of Bodily Self-Consciousness. Neuron. doi:10.1016/j.neuron.2015.09.029

Botvinick, M., Cohen, J., 1998. Rubber hands "feel" touch that eyes see. Nature 391, 756. doi:10.1038/35784

Braun, N., Thorne, J.D., Hildebrandt, H., Debener, S., 2014. Interplay of agency and ownership: The intentional binding and rubber hand illusion Paradigm Combined. PLoS ONE 9. doi:10.1371/journal.pone.0111967

Brozzoli, C., Gentile, G., Ehrsson, H.H., 2012. That's near my hand! Parietal and premotor coding of hand-centered space contributes to localization and self-attribution of the hand. The Journal of Neuroscience 32, 14573–82. doi:10.1523/JNEUROSCI.2660-12.2012

Bullmore, E.T., Sporns, O., 2009. Complex brain networks: graph theoretical analysis of structural and functional systems. Nature reviews. Neuroscience 10, 186–98. doi:10.1038/nrn2575

Buonomano, D. V, Merzenich, M.M., 1998. {CORTICAL PLASITICITY}: {F}rom {S}ynapses to {M}aps. Annual Review of Neuroscience 21, 149–186. doi:10.1146/annurev.neuro.21.1.149

Caspar, E.A., De Beir, A., Magalhaes De Saldanha Da Gama, P.A., Yernaux, F., Cleeremans, A., Vanderborght, B., 2015. New frontiers in the rubber hand experiment: When a robotic hand becomes one's own. Behavior Research 47, 744–755. doi:10.3758/s13428-014-0498-3

Chen, L.M., Friedman, R.M., Ramsden, B.M., Lamotte, R.H., Roe, A.W., 2001. Fine-scale organization of SI (Area 3b) in the squirrel monkey revealed with intrinsic optical imaging. Journal of Neurophysiology 86, 3011–3029.

Chen, L., Mishra, A., Newton, A.T., Morgan, V.L., Stringer, E.A., Rogers, B.P., Gore, J.C., 2011. Fine-scale functional connectivity in somatosensory cortex revealed by high-resolution fMRI. Magnetic Resonance Imaging 29, 1330–1337. doi:10.1016/j.mri.2011.08.001

Da Costa, S., Saenz, M., Clarke, S., van der Zwaag, W., 2014. Tonotopic Gradients in Human Primary Auditory Cortex: Concurring Evidence From High-Resolution 7 T and 3 T fMRI. Brain Topography 66–69. doi:10.1007/s10548-014-0388-0

Damoiseaux, J.S., Rombouts, S. a R.B., Barkhof, F., Scheltens, P., Stam, C.J., Smith, S.M., Beckmann, C.F., 2006. Consistent resting-state networks across healthy subjects. Proceedings of the National Academy of Sciences of the United States of America 103, 13848–53. doi:10.1073/pnas.0601417103

David, N., Bewernick, B.H., Cohen, M.X., Newen, A., Lux, S., Fink, G.R., Shah, N.J., Vogeley, K., 2006. Neural representations of self versus other: visual-spatial perspective taking and agency in a virtual ball-tossing game. Journal of cognitive neuroscience 18, 898–910. doi:10.1162/jocn.2006.18.6.898

Dummer, T., Picot-Annand, A., Neal, T., Moore, C., 2009. Movement and the rubber hand illusion. Perception 38, 271–280. doi:10.1068/p5921

Eckert, M.A., Kamdar, N. V., Chang, C.E., Beckmann, C.F., Greicius, M.D., Menon, V., 2008. A cross-modal system linking primary auditory and visual cortices: Evidence from intrinsic fMRI connectivity analysis. Human Brain Mapping 29, 848–857. doi:10.1002/hbm.20560

Ehrsson, H.H., 2005. Touching a Rubber Hand: Feeling of Body Ownership Is Associated with Activity in Multisensory Brain Areas. Journal of Neuroscience 25, 10564–10573. doi:10.1523/JNEUROSCI.0800-05.2005

186

Ehrsson, H.H., 2004. That's My Hand! Activity in Premotor Cortex Reflects Feeling of Ownership of a Limb. Science 305, 875–877. doi:10.1126/science.1097011

Farrer, C., Franck, N., Georgieff, N., Frith, C.D., Decety, J., Jeannerod, M., 2003. Modulating the experience of agency: A positron emission tomography study. NeuroImage 18, 324–333. doi:10.1016/S1053-8119(02)00041-1

Farrer, C., Frith, C.D., 2002. Experiencing oneself vs another person as being the cause of an action: The neural correlates of the experience of agency. NeuroImage 15, 596–603. doi:10.1006/nimg.2001.1009

Fink, G.R., Marshall, J.C., Halligan, P.W., Frith, C.D., Driver, J., Frackowiak, R.S.J., Dolan, R.J., 1999. The neural consequences of conflict between intention and the senses. Brain 122, 497–512. doi:10.1093/brain/122.3.497

Fox, M.D., Raichle, M.E., 2007. Spontaneous fluctuations in brain activity observed with functional magnetic resonance imaging. Nat Rev Neurosci 8, 700–711. doi:10.1038/nrn2201

Freund, P., Weiskopf, N., Ashburner, J., Wolf, K., Sutter, R., Altmann, D.R., Friston, K., Thompson, A., Curt, A., 2013. MRI investigation of the sensorimotor cortex and the corticospinal tract after acute spinal cord injury: A prospective longitudinal study. The Lancet Neurology 12, 873–881. doi:10.1016/S1474-4422(13)70146-7

Friedman, R.M., Chen, L.M., Roe, A.W., 2004. Modality maps within primate somatosensory cortex. Proceedings of the National Academy of Sciences of the United States of America 101, 12724–9. doi:10.1073/pnas.0404884101

Gallace, A., Spence, C., 2010. Touch and the Body : The Role of the Somatosensory Cortex in Tactile Awareness. Psyche 16, 30–67.

Gentile, G., Björnsdotter, M., Petkova, V.I., Abdulkarim, Z., Ehrsson, H.H., 2015. Patterns of neural activity in the human ventral premotor cortex reflect a whole-body multisensory percept. NeuroImage 109, 328–340. doi:10.1016/j.neuroimage.2015.01.008

Gentile, G., Guterstam, A., Brozzoli, C., Ehrsson, H.H., 2013. Disintegration of multisensory signals from the real hand reduces default limb self-attribution: an fMRI study. The Journal of neuroscience : the official journal of the Society for Neuroscience 33, 13350–66. doi:10.1523/JNEUROSCI.1363-13.2013

Geyer, S., Ledberg, A., Schleicher, A., Kinomura, S., Schormann, T., Bürgel, U., Klingberg, T., Larsson, J., Zilles, K., Roland, P.E., 1996. Two different areas within the primary motor cortex of man. Nature 382, 805–7. doi:10.1038/382805a0

Geyer, S., Schormann, T., Mohlberg, H., Zilles, K., Schleicher, A., Zilles, K., 1999. Areas 3a, 3b, and 1 of human primary somatosensory cortex. NeuroImage 10, 63–83. doi:10.1006/nimg.1999.0440

Geyer, S., Schleicher, A., Zilles, K., 1997. The Somatosensory Cortex of Human : Cytoarchitecture and Regional Distributions of Receptor-Binding Sites. NeuroImage 45, 27–45. doi:10.1006/nimg.1997.0271

Glover, G.H., 2011. Overview of functional magnetic resonance imaging. Neurosurgery Clinics of North America. doi:10.1016/j.nec.2010.11.001

Godde, B., Spengler, F., Dinse, H., 1996. Associative pairing of tactile stimulation induces somatosensory cortical reorganization in rats and humans. Neuroreport.

Graczyk, E.L., Schiefer, M.A., Saal, H.P., Delaye, B.P., Bensmaia, S.J., Tyler, D.J., 2016. The neural basis of perceived intensity in natural and artificial touch (accepted). Science Translational Medicine 8, 362ra142-362ra142. doi:10.1126/scitranslmed.aaf5187

Grefkes, C., Geyer, S., Schormann, T., Roland, P., Zilles, K., 2001. Human somatosensory area 2: observer-independent cytoarchitectonic mapping, interindividual variability, and population map. NeuroImage 14, 617–631. doi:10.1006/nimg.2001.0858

Grill-Spector, K., Malach, R., 2004. the Human Visual Cortex. Annual Review of Neuroscience 27, 649–677. doi:10.1146/annurev.neuro.27.070203.144220

Guterstam, A., Björnsdotter, M., Gentile, G., Ehrsson, H.H., 2015. Supplementary material - Posterior Cingulate Cortex Integrates the Senses of Self - Location and Body Ownership. Current Biology 25, 1416–1425. doi:10.1016/j.cub.2015.03.059

Guterstam, A., Gentile, G., Ehrsson, H.H., 2013. The invisible hand illusion: multisensory integration leads to the embodiment of a discrete volume of empty space. Journal of cognitive neuroscience 25, 1078–99. doi:10.1162/jocn_a_00393

Haggard, P., Chambon, V., 2012. Sense of agency. Current Biology. doi:10.1016/j.cub.2012.02.040

Hara, M., Pozeg, P., Rognini, G., Higuchi, T., Fukuhara, K., Yamamoto, A., Higuchi, T., Blanke, O., Salomon, R., 2015. Voluntary self-touch increases body ownership. Frontiers in Psychology 6, 1509. doi:10.3389/fpsyg.2015.01509

Harvey, B.M., Dumoulin, S.O., 2011. The relationship between cortical magnification factor and population receptive field size in human visual cortex: constancies in cortical architecture. J Neurosci 31, 13604–13612. doi:10.1523/JNEUROSCI.2572-11.2011

Hassan, A., Josephs, K.A., 2016. Alien Hand Syndrome. Current Neurology and Neuroscience Reports 16, 292. doi:10.1007/s11910-016-0676-z

Hebert, J.S., Olson, J.L., Morhart, M.J., Dawson, M.R., Marasco, P.D., Kuiken, T.A., Chan, K.M., 2014. Novel targeted sensory reinnervation technique to restore functional hand sensation after transhumeral amputation. IEEE Transactions on Neural Systems and Rehabilitation Engineering 22, 765–773. doi:10.1109/TNSRE.2013.2294907

Henderson, L.A., Gustin, S.M., Macey, P.M., Wrigley, P.J., Siddall, P.J., 2011. Functional Reorganization of the Brain in Humans Following Spinal Cord Injury: Evidence for Underlying Changes in Cortical Anatomy. Journal of Neuroscience 31, 2630–2637. doi:10.1523/JNEUROSCI.2717-10.2011

Hong, J.H., Kwon, H.G., Jang, S.H., 2011. Probabilistic somatotopy of the spinothalamic pathway at the ventroposterolateral nucleus of the thalamus in the human brain. American Journal of Neuroradiology 32, 1358–1362. doi:10.3174/ajnr.A2497

Huang, R.-S., Chen, C., Tran, A.T., Holstein, K.L., Sereno, M.I., 2012. Mapping multisensory parietal face and body areas in humans. Proceedings of the National Academy of Sciences of the United States of America 109, 18114–9. doi:10.1073/pnas.1207946109

Ionta, S., Heydrich, L., Lenggenhager, B., Mouthon, M., Fornari, E., Chapuis, D., Gassert, R., Blanke, O., 2011. Multisensory Mechanisms in Temporo-Parietal Cortex Support Self-Location and First-Person Perspective. Neuron 70, 363–374. doi:10.1016/j.neuron.2011.03.009

Iwamura, Y., 1998. Hierarchical somatosensory processing. Current Opinion in Neurobiology 8, 522–528. doi:10.1016/S0959-4388(98)80041-X

Jenkinson, P.M., Preston, C., 2015. New reflections on agency and body ownership: The moving rubber hand illusion in the mirror. Consciousness and Cognition 33, 432–442. doi:10.1016/j.concog.2015.02.020

Kaas, J.H., Nelson, R.J., Sur, M., Lin, C.S., Merzenich, M.M., 1979. Multiple representations of the body within the primary somatosensory cortex of primates. Science (New York, N.Y.) 204, 521–523. doi:10.1126/science.107591

Kalckert, A., Ehrsson, H.H., 2012. Moving a Rubber Hand that Feels Like Your Own: A Dissociation of Ownership and Agency. Frontiers in human neuroscience 6, 40. doi:10.3389/fnhum.2012.00040

Kalckert, A., Ehrsson, H.H., 2014. The moving rubber hand illusion revisited: Comparing movements and visuotactile stimulation to induce illusory ownership. Consciousness and Cognition 26, 117–132. doi:10.1016/j.concog.2014.02.003

Kannape, O.A., Schwabe, L., Tadi, T., Blanke, O., 2010. The limits of agency in walking humans. Neuropsychologia 48, 1628–1636. doi:10.1016/j.neuropsychologia.2010.02.005

Kiss, Z.H., Dostrovsky, J.O., Tasker, R.R., 1994. Plasticity in human somatosensory thalamus as a result of deafferentation. Stereotactic and functional neurosurgery 62, 153–63.

Kriegeskorte, N., Mur, M., Bandettini, P., 2008. Representational similarity analysis - connecting the branches of systems neuroscience. Frontiers in systems neuroscience 2, 4. doi:10.3389/neuro.06.004.2008

Kuiken, T.A., Dumanian, G.A., Lipschutz, R.D., Miller, L.A., Stubblefield, K.A., 2005. Targeted muscle reinnervation for improved myoelectric prosthesis control. 2nd International IEEE EMBS Conference on Neural Engineering 2005, 396–399. doi:10.1109/CNE.2005.1419642

Kuiken, T. a, Marasco, P.D., Lock, B. a, Harden, R.N., Dewald, J.P. a, 2007. Redirection of cutaneous sensation from the hand to the chest skin of human amputees with targeted reinnervation. Proceedings of the National Academy of Sciences of the United States of America 104, 20061–20066. doi:10.1073/pnas.0706525104

Lee, M.H., Smyser, C.D., Shimony, J.S., 2013. Resting-state fMRI: A review of methods and clinical applications. American Journal of Neuroradiology 34, 1866–1872. doi:10.3174/ajnr.A3263

Lenggenhager, B., Tadi, T., Metzinger, T., Blanke, O., 2007. Video Ergo Sum: Manipulating BodilySelf-Consciousness. Science 1096, 1–5. doi:10.1126/science.1143439

Leube, D.T., Knoblich, G., Erb, M., Grodd, W., Bartels, M., Kircher, T.T.J., 2003. The neural correlates of perceiving one's own movements. NeuroImage 20, 2084–2090. doi:10.1016/j.neuroimage.2003.07.033

Li, Q., Song, M., Fan, L., Liu, Y., Jiang, T., 2015. Parcellation of the primary cerebral cortices based on local connectivity profiles. Frontiers in neuroanatomy 9, 50. doi:10.3389/fnana.2015.00050

Limanowski, J., Blankenburg, F., 2015. That's not quite me: limb ownership encoding in the brain. Social Cognitive and Affective Neuroscience nsv079. doi:10.1093/scan/nsv079

Limanowski, J., Blankenburg, F., 2015. Network activity underlying the illusory self-attribution of a dummy arm. Human Brain Mapping 36, 2284–2304. doi:10.1002/hbm.22770

Limanowski, J., Lutti, A., Blankenburg, F., 2014. The extrastriate body area is involved in illusory limb ownership. NeuroImage 86, 514–524. doi:10.1016/j.neuroimage.2013.10.035

Ma, K., Hommel, B., 2015. The role of agency for perceived ownership in the virtual hand illusion. Consciousness and Cognition 36, 277–288. doi:10.1016/j.concog.2015.07.008

Martin, A., 2007. The Representation of Object Concepts in the Brain. Annual Review of Psychology 58, 25–45. doi:10.1146/annurev.psych.57.102904.190143

Martuzzi, R., van der Zwaag, W., Dieguez, S., Serino, A., Gruetter, R., Blanke, O., 2015. Distinct contributions of Brodmann areas 1 and 2 to body ownership. Social Cognitive and Affective Neuroscience 10, 1449–1459. doi:10.1093/scan/nsv031

Martuzzi, R., van der Zwaag, W., Farthouat, J., Gruetter, R., Blanke, O., 2014. Human finger somatotopy in areas 3b, 1, and 2: A 7T fMRI study using a natural stimulus. Human Brain Mapping 35, 213–226. doi:10.1002/hbm.22172

Muckli, L., 2010. What are we missing here? Brain imaging evidence for higher cognitive functions in primary visual cortex V1. International Journal of Imaging Systems and Technology 20, 131–139. doi:10.1002/ima.20236

Olman, C.A., Van de Moortele, P.F., Schumacher, J.F., Guy, J.R., Uğurbil, K., Yacoub, E., 2010. Retinotopic mapping with spin echo BOLD at 7T. Magnetic Resonance Imaging 28, 1258–1269. doi:10.1016/j.mri.2010.06.001

Pack, C.C., Bensmaia, S.J., 2015. Seeing and Feeling Motion: Canonical Computations in Vision and Touch. PLoS Biology 13, e1002271. doi:10.1371/journal.pbio.1002271

Petkova, V.I., Björnsdotter, M., Gentile, G., Jonsson, T., Li, T.Q., Ehrsson, H.H., 2011. From part- to whole-body ownership in the multisensory brain. Current Biology 21, 1118–1122. doi:10.1016/j.cub.2011.05.022

Raemaekers, M., Schellekens, W., van Wezel, R.J.A., Petridou, N., Kristo, G., Ramsey, N.F., 2014. Patterns of resting state connectivity in human primary visual cortical areas: A 7T fMRI study. NeuroImage 84, 911–921. doi:10.1016/j.neuroimage.2013.09.060

Rasmussen, T., Penfield, W., 1947. Further studies of the sensory and motor cerebral cortex of man. Federation proceedings 6, 452–460.

Raspopovic, S., Capogrosso, M., Petrini, F.M., Bonizzato, M., Rigosa, J., Di Pino, G., Carpaneto, J., Controzzi, M., Boretius, T., Fernandez, E., Granata, G., Oddo, C.M., Citi, L., Ciancio, A.L., Cipriani, C., Carrozza, M.C., Jensen, W., Guglielmelli, E., Stieglitz, T., Rossini, P.M., Micera, S., 2014. Restoring Natural Sensory Feedback in Real-Time Bidirectional Hand Prostheses. Science Translational Medicine 6, 222ra19-222ra19. doi:10.1126/scitranslmed.3006820

Saadon-Grosman, N., Tal, Z., Itshayek, E., Amedi, A., Arzy, S., 2015. Discontinuity of cortical gradients reflects sensory impairment. Proceedings of the National Academy of Sciences 112, 16024–16029. doi:10.1073/pnas.1506214112

Saal, H.P., Harvey, M.A., Bensmaia, S.J., 2015. Rate and timing of cortical responses driven by separate sensory channels. eLife 4, e10450. doi:10.7554/eLife.10450

Sanchez-Panchuelo, R.M., Besle, J., Beckett, A., Bowtell, R., Schluppeck, D., Francis, S., 2012. Within-digit functional parcellation of Brodmann areas of the human primary somatosensory cortex using functional magnetic resonance imaging at 7 tesla. The Journal of Neuroscience 32, 15815–15822. doi:10.1523/jneurosci.2501-12.2012

Sanchez-Panchuelo, R.M., Francis, S., Bowtell, R., Schluppeck, D., 2010. Mapping human somatosensory cortex in individual subjects with 7T functional MRI. Journal of neurophysiology 103, 2544–2556. doi:10.1152/jn.01017.2009

Sánchez-Panchuelo, R.M., Besle, J., Mougin, O., Gowland, P., Bowtell, R., Schluppeck, D., Francis, S., 2014. Regional structural differences across functionally parcellated Brodmann areas of human primary somatosensory cortex. NeuroImage 93, 221–230. doi:10.1016/j.neuroimage.2013.03.044

Schwabe, L., Blanke, O., 2007. Cognitive neuroscience of ownership and agency. Consciousness and Cognition 16, 661–666. doi:10.1016/j.concog.2007.07.007

Sereno, M.I., Huang, R.S., 2014. Multisensory maps in parietal cortex. Current Opinion in Neurobiology. doi:10.1016/j.conb.2013.08.014

Serino, A., Canzoneri, E., Avenanti, A., 2011. Fronto-parietal areas necessary for a multisensory representation of peripersonal space in humans: an rTMS study. Journal of cognitive neuroscience 23, 2956–67. doi:10.1162/jocn_a_00006

Serino, A., Haggard, P., 2010. Touch and the body. Neuroscience and Biobehavioral Reviews. doi:10.1016/j.neubiorev.2009.04.004

Shibuya, S., Unenaka, S., Ohki, Y., 2016. Body ownership and agency: task-dependent effects of the virtual hand illusion on proprioceptive drift. Experimental Brain Research epub. doi:10.1007/s00221-016-4777-3

Siero, J.C.W., Hermes, D., Hoogduin, H., Luijten, P.R., Ramsey, N.F., Petridou, N., 2014. BOLD matches neuronal activity at the mm scale: A combined 7T fMRI and ECoG study in human sensorimotor cortex. NeuroImage 101, 177–184. doi:10.1016/j.neuroimage.2014.07.002

Stringer, E.A., Chen, L.M., Friedman, R.M., Gatenby, C., Gore, J.C., 2011. Differentiation of somatosensory cortices by high-resolution fMRI at 7T. NeuroImage 54, 1012–1020. doi:10.1016/j.neuroimage.2010.09.058

Stringer, E.A., Qiao, P.G., Friedman, R.M., Holroyd, L., Newton, A.T., Gore, J.C., Chen, L.M., 2014. Distinct fine-scale fMRI activation patterns of contra- and ipsilateral somatosensory areas 3b and 1 in humans. Human Brain Mapping 35, 4841–4857. doi:10.1002/hbm.22517

Tootell, R.B.H., Silverman, M.S., Switkes, E., De Valois, R.L., 1982. Deoxyglucose Analysis of Retinotopic Organization in Primate Striate Cortex. Science 218, 902–904. doi:10.1126/science.7134981

Tootell, R.B.H., Switkes, E., Silverman, M.S., Hamilton, S.L., 1988. Functional anatomy of macaque striate cortex. II. Retinotopic organization. J Neurosci 8, 1531–1568.

Tsakiris, M., 2008. Looking for myself: Current multisensory input alters self-face recognition. PLoS ONE 3, e4040. doi:10.1371/journal.pone.0004040

Tsakiris, M., 2010. My body in the brain: A neurocognitive model of body-ownership. Neuropsychologia 48, 703–712. doi:10.1016/j.neuropsychologia.2009.09.034

Tsakiris, M., Hesse, M.D., Boy, C., Haggard, P., Fink, G.R., 2007. Neural signatures of body ownership: A sensory network for bodily self-consciousness. Cerebral Cortex 17, 2235–2244. doi:10.1093/cercor/bhl131

Tsakiris, M., Longo, M.R., Haggard, P., 2010. Having a body versus moving your body: Neural signatures of agency and body-ownership. Neuropsychologia 48, 2740–2749. doi:10.1016/j.neuropsychologia.2010.05.021

Tsakiris, M., Prabhu, G., Haggard, P., 2006. Having a body versus moving your body: How agency structures body-ownership. Consciousness and cognition 15, 423–32. doi:10.1016/j.concog.2005.09.004

Tsakiris, M., Schütz-Bosbach, S., Gallagher, S., 2007. On agency and body-ownership: Phenomenological and neurocognitive reflections. Consciousness and Cognition 16, 645–660. doi:10.1016/j.concog.2007.05.012

Vallar, G., Ronchi, R., 2009. Somatoparaphrenia: A body delusion. A review of the neuropsychological literature, in: Experimental Brain Research. pp. 533–551. doi:10.1007/s00221-008-1562-y

van den Heuvel, M.P., Hulshoff Pol, H.E., 2010. Exploring the brain network: A review on resting-state fMRI functional connectivity. European Neuropsychopharmacology. doi:10.1016/j.euroneuro.2010.03.008

van der Zwaag, W., Francis, S., Head, K., Peters, A., Gowland, P., Morris, P., Bowtell, R., 2009. fMRI at 1.5, 3 and 7 T: Characterising BOLD signal changes. NeuroImage 47, 1425–1434. doi:10.1016/j.neuroimage.2009.05.015

Wang, Z., Chen, L., Négyessy, L., Friedman, R., Mishra, A., Gore, J., Roe, A., 2013. The Relationship of Anatomical and Functional Connectivity to Resting-State Connectivity in Primate Somatosensory Cortex. Neuron 78, 1116–1126. doi:10.1016/j.neuron.2013.04.023

Weber, A.I., Saal, H.P., Lieber, J.D., Cheng, J.-W., Manfredi, L.R., Dammann, J.F., Bensmaia, S.J., 2013. Spatial and temporal codes mediate the tactile perception of natural textures. Proceedings of the National Academy of Sciences of the United States of America 110, 17107–17112. doi:10.1073/pnas.1305509110

Yacoub, E., Harel, N., Ugurbil, K., 2008. High-field fMRI unveils orientation columns in humans. Proceedings of the National Academy of Sciences of the United States of America 105, 10607–12. doi:10.1073/pnas.0804110105

Zeharia, N., Hertz, U., Flash, T., Amedi, A., 2015. New Whole - Body Sensory - Motor Gradients Revealed Using Phase - Locked Analysis and Verified Using Multivoxel Pattern Analysis and Functional Connectivity. The Journal of neuroscience : the official journal of the Society for Neuroscience 35, 2845–59. doi:10.1523/JNEUROSCI.4246-14.2015

192

9 - Curriculum Vitae

Michel Akselrod

Contact address: Laboratory of Cognitive Neuroscience (LNCO), EPFL
EPFL-SV-BMI-LNCO
Campus Biotech H4
Chemin des Mines 9
CH-1202 Genève (Switzerland)

Phone: +4178 866 09 88

Email: michel.akselrod@gmail.com

Current position: doctoral assistant at the Laboratory of Cognitive Neuroscience, Swiss Federal Institute of Technology of Lausanne (EPFL)

EDUCATION

Gymnasium Emilie-Gourd Geneva, Switzerland
Scientific Maturity   **June 2006**

Swiss Federal Institute of Technology of Lausanne (EPFL) Lausanne, Switzerland
Bachelor's Degree in Life Sciences & Technology   **July 2010**
Average grade: 5.09 / 6

Swiss Federal Institute of Technology of Lausanne (EPFL) Lausanne, Switzerland
Master's Degree in Life Sciences & Technology   **July 2012**
Specialization in Neurosciences
Average grade: 5.72 / 6

University of Houston Houston, USA
Master's Project during academic exchange   **2011 - 2012**
At the laboratory of Cognitive and Perceptual Dynamics
Thesis title "*Neural Correlates Of Path Guided Apparent Motion Perception Using Functional Magnetic Resonance Imaging*"

Swiss Federal Institute of Technology of Lausanne (EPFL) Lausanne, Switzerland
PhD student   **(anticipated date) April 2017**
Laboratory of Cognitive Neuroscience, Chair Fundation Bertarelli of Cogntive Neuroprosthetics
Rehabilitation Engineering Laboratory, Institute of Robotics and Intelligent Systems

PROFESSIONAL EXPERIENCE

Bank *"Banque Privée Edmond de Rothschild"*, Geneva Summer 2009
Computing Department Intern

- Learned basic knowledge of batch processing, database design, data query systems, javascript programming

Swiss Federal Institute of Technology of Lausanne (EPFL), since 2011 (ongoing)
Teaching Assistant

- Supervised a group of 10 students during practical sessions in the course *"General Physics "* (Bachelor)

- Supervised lectures, prepared and supervised practical sessions in the course *"Neuroscience for engineers"* (Bachelor)

Swiss Federal Institute of Technology of Lausanne (EPFL), since 2012 (ongoing)
Research Engineer
- Design of behavioral and neuroimaging studies
- Acquisition and analysis behavioral and neuroimaging data
- Scientific writing for academic publication
- Supervision of student projects

SKILLS
Language
Fluent in French and English, proficient in Russian (orally), basic conversational ability in German

Computing
Windows, MacOS, Linux

Programming
C++, matlab, latex, dot, python, javascript, html, labview

Laboratory
Behavioral data acquisition, neuroimaging data acquisition, basic knowledge in histology, immunohistochemistry, cell cultures, PCR, DNA analysis

Experimental design
Design of behavioral and neuroimaging experiments, basic knowledge in robotics and virtual reality

Data analysis
Neuroimaging data analysis, statistical analysis, graph analysis, machine learning

JOURNAL PUBLICATIONS
- **Akselrod M**, Herzog MH, Ogmen H. (2013) Tracing path-guided apparent motion in human primary visual cortex V1, *Sci. Rep.*, vol. 4, p. 6063
- Favrod J, Brana A, Gavillet A, **Akselrod M**, Nguyen A, Palix J (2014) [Training to cope with workplace stress for people with mild intellectual disability: a pilot study] *J. Thérapie Comport. Cogn.*, vol. 25, no. 3, pp. 132–141
- Palix J, **Akselrod M**, Cungi C, Giuliani F, Favrod J. (2016) Changes in heart-rate variability recorded in natural situation with t-shirt integrated sensors and level of observed behavioral excitation: a pilot study of patients with intellectual disabilities and psychiatric disorders. *Frontiers in Psychiatry*
- **Akselrod M**, Martuzzi R, Serino A, van der Zwaag W, Gassert R, Blanke O. Anatomical and functional properties of the foot and leg representations in areas 3b, 1 and 2 of primary somatosensory cortex in humans: a 7T fMRI study, in revision for *Neuroimage*
- Serino A*, **Akselrod M***, Salomon R, Martuzzi R, Blefari ML, Canzoneri E, Rognini G, van der Zwaag W, Iakova M, Luthi F, Amoresano A, Kuiken T, Blanke O. Upper limb cortical maps in amputees with targeted muscle and sensory reinnervation: a 7T fMRI study, in revision for *Brain* (* are first co-authors)
- **Akselrod M**, Martuzzi R, Serino A, van der Zwaag W, Gassert R, Blanke O. Properties of the functional connectivity network of hands, feet and legs representations in three areas of primary somatosensory cortex in humans: a 7T study, in preparation
- **Akselrod M**, Duenas J, Martuzzi R, Sulzer J, Stampfli P, Seifritz E, Blanke O, Gassert R. Temporal cortex contributes to the senses of hand ownership and of hand agency, in preparation

194